

Distribution Agreement

In presenting this thesis or dissertation as a partial fulfillment of the requirements for an advanced degree from Emory University, I hereby grant to Emory University and its agents the non-exclusive license to archive, make accessible, and display my thesis or dissertation in whole or in part in all forms of media, now or hereafter known, including display on the world wide web. I understand that I may select some access restrictions as part of the online submission of this thesis or dissertation. I retain all ownership rights to the copyright of the thesis or dissertation. I also retain the right to use in future works (such as articles or books) all or part of this thesis or dissertation.

Signature:

Cassandra L. Zaremba

Date

Membranes & Metals: Bacterial Targets to Fight Antibiotic Resistance

By

Cassandra Lynn Zaremba

Doctor of Philosophy

Chemistry

Advisor

William M. Wuest, Ph.D.

Committee Member

Simon B. Blakey, Ph.D.

Committee Member

Christine Dunham, Ph.D.

Accepted:

Kimberly Jacob Arriola, Ph.D, MPH

Dean of the James T. Laney School of Graduate Studies

Date

Membranes & Metals: Bacterial Targets to Fight Antibiotic Resistance

By

Cassandra Lynn Zaremba

B.S. Xavier University, 2016

Advisor: William M. Wuest, PhD

An abstract of

A dissertation submitted to the Faculty of the

James T. Laney School of Graduate Studies of Emory University

in partial fulfillment of the requirements for the degree of

Doctor of Philosophy in Chemistry

2022

Abstract

Membranes & Metals: Bacterial Targets to Fight Antibiotic Resistance

By Cassandra L. Zaremba

The need for antibiotics with novel mechanisms of action has been a mounting problem for over a decade. In 2014, O'Neill released a mathematical analysis that predicted that antibiotic resistant infections may be the leading cause of death by 2050 if the situation remains unrectified. Although academic research in the analysis of novel antibiotic compounds has increased, there has been a lack of translation to commercialization in part due to strenuous approval processes from the Food and Drug Administration and lack of financial support from pharmaceutical companies. The larger antagonist in this story, however, is the constantly evolving bacteria. Bacteria have developed several mechanisms to evade the killing power of antibiotics: resistance and persistence. Resistance is a genetic alteration whereas persistence is phenotype change. To combat both issues, novel mechanisms of action need to be explored. Discussed herein, I analyze three small molecule scaffolds that serve as tool compounds to explore novel mechanisms of action: membrane perturbation and disruption of metal homeostasis.

Membranes & Metals: Bacterial Targets to Fight Antibiotic Resistance

By

Cassandra L Zaremba

B.S. Xavier University, 2016

Advisor: William M. Wuest, PhD

A dissertation submitted to the Faculty of the
James T. Laney School of Graduate Studies of Emory University
in partial fulfillment of the requirements for the degree of
Doctor of Philosophy in Chemistry

2022

Acknowledgements

They whispered to her, “You cannot withstand the storm.”

“I am the storm.” She whispered back.

I’d like to dedicate this dissertation to my dad. Growing up he always told me that I was a smartass, but it turns out you can make being a smartass a career. He challenged me from day one, and I hope that he’s smiling down on me as I present this to my committee. I know he would be so dang proud to see me accomplish this goal.

Now this wouldn’t be possible, really, without Mama, PhD. She has been my rock my entire life. She was the first one who encouraged my chemistry brain from summer at-home activities to allowing me to mix her expensive perfumes for my “experiments.” She always pushed me to do more and believed I was capable of anything. Her motto of “I can do hard things well” kept me going when things got tough. She is everything I hope to be.

I can’t, however, forget about my wonderful step-Dan. Thank you for supporting me and becoming a father figure I was desperately missing in my life. You stepped into this role not knowing what you were getting into and loved me from the start. I am so thankful you are a part of our family.

Confidence and refusing to back down are both skills my brothers, Zak and Alex, made sure I learned quickly. Growing up with two older brothers really toughens your skin quickly, but it also gives you two best friends who will always have your back. Luckily, they also gave me the sisters I always wanted in Lindsay and Evan. Together, the Zaremba Youths keep me from falling. They are my pillars.

Beyond my family, I am lucky to have amazing friends who have become my chosen family. My chemistry twin, Emily, who inspires me to see beyond my work and shows me that I have a bigger purpose in this world. My ride-or-die Wuest Lab Ladies and Midwest Mom Friends: Savannah, Amber, Martina, and Maddie. These women have shown me what true friendship is and have supported me in my darkest moments. I think with them I am not only able to complete this dissertation, but also, I believe I am still alive because of them. I hope to be half as good of a friend as they have been to me.

Lastly, I’d like to thank two advisors and mentors that have both had to put up with me. Firstly, my undergraduate PI, Rick. If it wasn’t for you, I don’t think I ever would have pursued graduate school. You called it from day one that I would one day get my PhD. Thank you for never letting me quit, even when I so desperately wanted to. Finally, Bill. You’ve said that it bums you out when you’re not acknowledged in a student’s dissertation. Welp don’t worry. I didn’t forget about you. Thank you for putting up with me for the past 4 or so years. You have been an extremely supportive advisor. You pushed me when I needed it and backed off when I needed a break. I am so appreciative of the guidance you have given me throughout this whole process and am thankful you never fired me (even though I’m sure you wanted to). You always said you are our advisor first and only a mentor if earned. Welp, I think you earned that title. Thank you.

Table of Contents

Chapter 1 – Introduction	1
Chapter 2 – Structure-Activity-Relationship Campaign of the synthetic retinoid, CD437	72
Chapter 3 – Synthetic and Biological Investigations into Quaternary Ammonium Compounds	106
Chapter 4 – Synthetic and Biological Investigations into Simplified Analogs of SF2768	128
Chapter 5 – Supplementary Information	142
Appendix – Spectral Data	168

List of Figures

Chapter 1:

Figure 1.1 Graphs of Time Killing Assays – Persistence vs Resistance	4
Figure 1.2: Depiction of Bacterial Cultures Persistence vs Resistance	6
Figure 1.3: Structures of Antibiotics with Membrane Perturbing Mechanisms	10
Figure 1.4: Chemical Structures of Prenylated Compounds	12
Figure 1.5: Chemical Structure of SPI031	13
Figure 1.6: Chemical Structure of SPI0009	14
Figure 1.7: Chemical Structure of 1-geranylindole	16
Figure 1.8: Chemical Structure of NPIMA	17
Figure 1.9: Chemical Structure of SCH-79797	18
Figure 1.10: Chemical Structure of NCK-10	19
Figure 1.11: Chemical Structure of nTZDPa	22
Figure 1.12: Chemical Structure of CD437	23
Figure 1.13: Chemical Structure of Bithionol	24
Figure 1.14: Chemical Structure of Honokiol	26
Figure 1.15: Example Redox Reactions of Metal Ions in a Cell	30
Figure 1.16: Metalloregulatory Proteins	30
Figure 1.17: Chemical Structures of Example Siderophores	32
Figure 1.18: Depiction of the Fur Box and Control on Siderophore Production	33
Figure 1.19: Example Redox Reaction of Copper Ions to Produce Radical Species	37
Figure 1.20: Depiction of Copper Ion Uptake in Bacteria	39
Figure 1.21: Chemical Structures of Methanobactins	41
Figure 1.22: Chemical Structures of Coproporphyrin and Yersiniabactin	42
Figure 1.23: Chemical Structure of Salmycin A	44
Figure 1.24: Isonitrile Structure and Reactivity	45
Figure 1.25: Biosynthetic Pathways to Isonitrile Natural Products	47
Figure 1.26: Chemical Structure of Xanthocillin X	49

Figure 1.27: Chemical Structure of Kalihinol A	49
---	----

Chapter 2:

Figure 2.1: Image of <i>C. elegans</i> High-throughput Screen	72
Figure 2.2: Chemical Structures of Vitamin A, CD437, and Adapalene	73
Figure 2.3: CD437 Biological Activity	75
Figure 2.4: Chemical Structures of CD437 Analogs for Generation Two	81
Figure 2.5: Inspiration behind Ethanolamine Analogs for CD437	83
Figure 2.6: Resonance Structures of Azaborine Analogs	98

Chapter 3:

Figure 3.1: Chemical Structures of Common Antibiotics	106
Figure 3.2: Cartoon Representation of QACs Mechanism of Action	108
Figure 3.3: Cartoon Representation of QacA Expression	109
Figure 3.4: Chemical Structures of Common Alkaloids Skeletal Core Structures	111
Figure 3.5: Chemical Structures of 3-Alkyl Pyridine Natural Products	113
Figure 3.6: Example Synthesis of Halicyclins	114
Figure 3.7: Synthetic Methodology of Hydroarylation	115
Figure 3.8: Proposed Future Directions for Halicyclins Project	119

Chapter 4:

Figure 4.1: Chemical structure of xanthocillin X and its mechanism of action	128
Figure 4.2: Chemical structure of SF2768	129
Figure 4.3: Proposed biosynthetic pathway of SF2768	130
Figure 4.4: SF2768-Cu Complex	131
Figure 4.5: Simplified scheme of electron transport chain and possible target of SF2768	134
Figure 4.6: Comparison of previous and planned work on SF2768	135
Figure 4.5: Chemical structure of other isonitrile compounds analyzed	136

List of Schemes

Chapter 2:

Scheme 2.1: Retrosynthesis of CD437	77
Scheme 2.2: Forward Synthesis to obtain CD437 and Analogs 2.11 to 2.20	79
Scheme 2.3: Forward Synthesis to obtain Analogs 2.25 to 2.30	80
Scheme 2.4: Retrosynthesis towards Generation Three Analogs of CD437	84
Scheme 2.5: Forward Synthesis of Benzene Fragment	85
Scheme 2.6: Forward Synthesis of Ethanolamine Analogs	85
Scheme 2.7: Synthesis of Analogs 2.49 and 2.50	88
Scheme 2.8: Synthesis of Bithionol Analogs	89
Scheme 2.9: Retrosynthesis of Azaborine Analogs	93
Scheme 2.10: Synthesis of Azaborine Analogs	94

Chapter 3:

Scheme 3.1: Synthesis towards Halicloyclin and Analogs	115
---	-----

Chapter 4:

Scheme 4.1: Tan's Retrosynthesis and Forward Synthesis of SF2768	132
Scheme 4.2: Synthesis of Simplified SF2768 Analogs	136

List of Tables

Chapter 2:

Table 2.1: Reaction Conditions used to obtain Ethanolamine Cap on Primary Alcohol	87
Table 2.2: Minimum Inhibitory Concentrations of Ethanolamine Analogs	89
Table 2.3: Turbidimetric Assay Data	91
Table 2.4: Plasma Protein Binding Data	92
Table 2.5: Minimum Inhibitory Concentrations of Azaborine Analogs	97
Table 2.6: clogP Data for Azaborine Analogs	97

Chapter 3:

Table 3.1: Biological Data for Haliclocyclins and Analogs	117-118
--	---------

Chapter 4:

Table 4.1: Biological Data for SF2768 and Simplified Analogs	137
---	-----

Chapter 1: Introduction

*Reproduced from: **Schrank, C.L.**; Wilt, I. K.; Monteagudo Ortiz, C.; Haney, B.A.; and Wuest, W.M. Using membrane perturbing small molecules to target chronic persistent infections. *RSC Med. Chem.* 2021, 12, 1312. with permission from the Royal Society of Chemistry

The need for antibiotics with novel mechanisms of action has been a mounting problem for over a decade. In 2014, O'Neill released a mathematical analysis that predicted that antibiotic resistant infections may be the leading cause of death by 2050 if the situation remains unrectified.² In their 2019 review, the Centers for Disease Control and Prevention (CDC) found that over 2.8 million antibiotic resistant bacterial infections occur per year in the United States alone.³ Additionally, the CDC identified several urgent threat bacterial species, many of which are members of the ESKAPE pathogens (*Enterococcus faecium*, *Staphylococcus aureus*, *Klebsiella pneumoniae*, *Acinetobacter baumannii*, *Pseudomonas aeruginosa*, and *Enterobacter* species) that are known for their multi-drug resistance.⁴ This situation is more dire as there has been a dearth of new antibiotics brought to market over the last 20 years.⁵ The lack of novel commercialized antibiotics is a compounded issue involving strenuous approval processes from the Food and Drug Administration (FDA) as well as the lack of financial support from pharmaceutical companies.⁶⁻⁸ However, there is a larger antagonist: the constantly evolving bacteria.

Antibiotic compounds existed long before human interference and are utilized by bacteria to ward off competing microbes.⁹ Over time bacteria have been able to develop mechanisms to avoid the killing action by these natural products, which has translated to the development of resistant mechanisms against antibiotic drugs. Often, these mechanisms occur within a few years of when a therapeutic is approved; therefore, extensive research into the evolution of resistance is required prior to a drug's approval.¹⁰ Bacterial resistance is the summation of genetic adaptations that occur

either through alteration of the genome *via* random point mutations, or through targeted alterations to the drug's biological target, thereby disrupting its mechanism of action (MoA).¹¹⁻¹⁵ In addition to genetic mutations, bacteria can also obtain resistant genes through mobile genetic elements *via* horizontal gene transfer from a nearby resistant organism.^{16,17} These alterations to the bacterial genome can select for resistance through several mechanisms including structural modification of the drug target causing disruption of binding, upregulation of efflux pumps to remove the toxic compound, and drug-modifying enzymes rendering them ineffective, among others.

Though resistance is often the focus when discussing antibiotic development, bacterial persistence is a more elusive mechanism utilized by cells to avoid the killing power of antibiotics. Different from resistant bacterial populations, persister cells are genetically identical to wild type, but phenotypically dissimilar.^{18,19} These stochastically formed cells are present in most bacterial cultures at <1% population density.²⁰ They are often referred to as “dormant” and “metabolically inactive,” thereby evading common antibiotic mechanisms that rely on growth dependent processes (i.e., DNA gyrases, membrane phospholipid synthesis, etc.) as well as metabolically active targets (i.e., ATP-dependent enzymes, active efflux, etc.).²¹ These cells do not proliferate during antibiotic treatment, but rather once the pressure is removed they can switch back to a growth state, which can lead to chronic infections. Hence, the ability to target these cells has been a major area of research for antibiotic development.

To combat both resistance and persistence, novel mechanisms of action need to be explored. Discussed herein, I analyze three small molecule scaffolds that serve as tool compounds to explore novel mechanisms of action: membrane perturbation and disruption of metal homeostasis.

1.1 Membrane perturbation as a route to targeting persistent infections¹

*Reproduced from: **Schrank, C.L.**; Wilt, I. K.; Monteagudo Ortiz, C.; Haney, B.A.; and Wuest, W.M. Using membrane perturbing small molecules to target chronic persistent infections. *RSC Med. Chem.* 2021, 12, 1312. with permission from the Royal Society of Chemistry.

Although it is desirable to target proteins or enzymes to ensure increased selectivity of killing bacterial cells, most common targets are inactive in persister cells. Conversely, an underutilized MoA is targeting the structural integrity of the bacterial membrane as this is essential regardless of growth and metabolic activity.²² Within the past decade, several small molecules have been uncovered that perturb the membrane of both wild-type and persister cells of Gram-positive and Gram-negative bacteria. Through these studies a common chemotype has emerged, the inclusion of phenolic functional groups. In our analysis, we have also found that heteroaromatic structures further decorated with nitrogen based functional groups proved to increase activity in perturbing Gram-negative bacteria. Below is a focused group of small molecules that perturb bacterial membranes as a mechanism to target persister cells. Additionally, we explore common motifs, or chemotypes, of these small molecules to propose new avenues for antibiotic development. This review specifically highlights compounds that emulate the potential for future development as inhibitors or potentiators of bacterial/persister cells.

1.1.1. *Tolerance and Persistence*

Although resistance is often discussed as the major hurdle facing the development of antibiotics, another daunting issue overlooked is tolerance. The well-known, resistant bacteria are characterized by genetic mutations that give cells the ability to grow in the presence of high concentrations of antibiotics, thereby increasing the minimum inhibitory concentration (MIC) of the therapeutic.^{19,23} Conversely, tolerance is the ability of cells to temporarily evade or delay death

in the presence of high doses of bactericidal antibiotics without altering the MIC.^{24–27} Therefore, in comparison to resistant bacteria, tolerant bacteria require longer treatment times rather than higher concentrations of antibiotic. This archetype is achieved through slowed growth and reduced metabolism, which is induced through environmental stress. By slowing or halting these processes, the cells can avoid the bactericidal action of most antibiotics *via* reduced cellular uptake as well as decreased target activity as most biologic targets involve metabolism, growth, etc. Therefore, tolerant bacteria contribute to treatment failure.

The broad category of tolerance is a whole-population characteristic. Within this umbrella is a subcategory known as persistence, which is a subpopulation phenomenon and exists in most bacterial cultures at a 0.001 to 1% population density.²⁰ Though these numbers are small, these antibiotic evading cells can repopulate an infection leading to chronic illness. The term “persisters” was originally coined by Joseph Bigger in the 1940s when he discovered that a subpopulation of *Staphylococcus pyogenes* cells proved to be unaffected and actually viable after treatment with penicillin.²⁸ This novel concept has been reconfirmed through several studies.^{18,29–31} In addition, research over the past decade has focused on understanding how these cells form, their biological

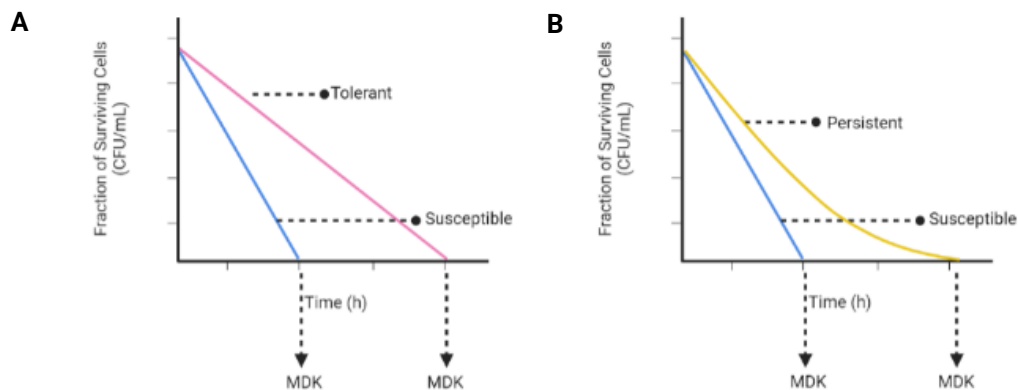


Figure 1.1 A) Comparison of time-kill curves of tolerant cells (pink) to a susceptible population (blue). Tolerant cells require longer treatment times. B) Comparison of time-kill curves of persistent cells (yellow) and susceptible populations (blue). Persistent cells have a biphasic time-kill curve. Figure was made using BioRender.

ramifications, and most importantly how to eradicate these elusive cells. These topics have been extensively reviewed previously.^{18,21,32-40}

Bacterial persisters are “slow-growing or growth arrested cells that have a decreased susceptibility to ... bactericidal antibiotics within an otherwise susceptible clonal population.”⁴¹ These cells can be distinguished from other tolerant bacteria by their time-kill curves.⁴² Bacterial populations containing persister cells have a “biphasic” killing curve (**Figure 1.1 B**). This two-part feature comes from an initial steep drop in concentration of the susceptible bacterial cells after the induction of the antibiotic stressor followed by decreased killing kinetics from the persister cells.^{42,43} In contrast, tolerant cells are characterized by slowed, but linear killing times in comparison to susceptible populations (**Figure 1.1 A**). To mark these differences, the minimum duration for killing (MDK) is used rather than the MIC because the MDK of a certain antibiotic against a strain of bacteria is different for persistent, tolerant, and resistant cultures. Additionally, persister killing concentration (PKC) is also used in place of MIC to distinguish between persister and wild-type assays. However, most studies rely primarily on MIC data to evaluate the efficacy of small molecules, which can limit identification of small molecule therapies for persistent populations.

Part of what makes persister cell research particularly challenging is the lack of universally accepted gene expression to account for phenotypic variation of the persister cell trait.^{30,44,45} High-throughput screening methods traditionally used to measure gene expression require high purity samples. Alas, obtaining high purity samples of persister cells, which are heterogenous and make up an extremely small portion of the bacterial population density, is a demanding task.⁴⁶ Visualization and quantification of the SOS response of persisters in a bacterial population has been accomplished by coupling microfluidics to a fluorescent SOS reporter. Although this

approach successfully differentiated persisters and monitored phenotypic changes of single cells during slow growth, in depth investigations of changes in gene expression remain underexplored.⁴⁷

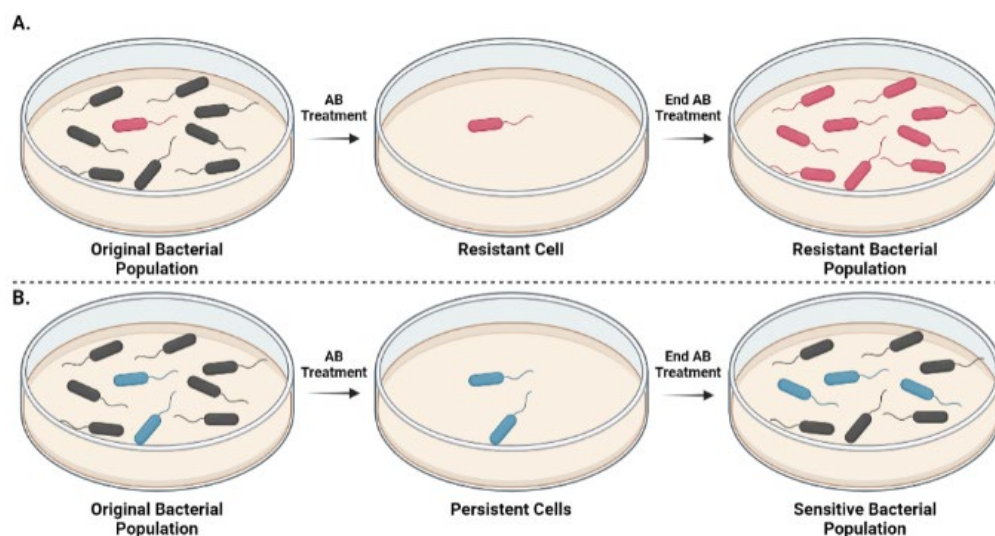


Figure 1.2. A) Resistant bacterial culture exposed to antibiotic. Red cells represent resistant cell. B) Persistent bacterial culture exposed to antibiotic. Blue cells represent persistent cells. Black cells represent wild-type cells. Figure was made using BioRender.

Fluorescence activated cell sorting (FACS) with flow cytometry has also been utilized to isolate persister cells, but high-purity samples are often unobtainable.^{48,49} Strategies to chemically induce dormant or slow growing states such as treatment with *m*-chlorophenylhydrazine (CCCP)⁵⁰ have been shown to increase persister cell numbers in *E. coli*⁵¹, *S. aureus*, and *P. aeruginosa* and may be used in conjunction with microfluidics in the future to eliminate the need for separation techniques and gain a better understanding of the role of protein expression in heterogeneous persister formation.⁵² Furthermore, advances in DNA and RNA sequencing, in particular the sensitivity of RNA-seq, will undoubtedly aid in real-time analysis of persister induction.

Current research capitalizes on environmental stressors that have been shown to increase the subpopulation to observable quantities.⁵³ These investigations are clinically relevant because stress-induced persister cells have demonstrated the ability to survive exposure to antibiotics in a dormant state that have been linked to chronic infections.^{26,43,54} After initial clearance of the susceptible population, persister cells lie dormant. Upon completion of antibiotic course, persister

cells may return to a growing, susceptible state, which can reconstitute infections (**Figure 1.2**). Although studies have commonly assumed persisters are metabolically dormant populations, there is growing evidence to suggest additional active mechanisms of persistence exist such as increased expression of efflux pumps or decreased intake of antibiotics.⁵⁵ Developing robust methods and best of practice procedures to study persistence will aid in elucidating and understanding these various mechanisms.

There are well-documented environmental stressors that increase persister cell concentrations including antibiotic exposure, nutrient deficiency, hypoxia, and oxidative stress, among others.^{51,56-58} These types of persister cell formation are termed “triggered persistence.”^{42,53} There is also “spontaneous persistence,” which occurs when a bacterial culture is at a steady-state exponential growth. In these conditions, persister cells form stochastically and remain constant if the growth conditions stay the same. However, triggered persistence is more common.

Perhaps the biggest detriment that arises from persister research is the replicability of studies.⁵⁹ It is critical that careful attention be paid to experimental design when assessing results. Regarding antibiotic-induced persistence, there are four focuses that should be acknowledged to differentiate persister cells from tolerant and resistant cells.^{42,60} First, studies should attempt to re-inoculate any surviving bacteria from the last portion of the kill assay to replicate the same biphasic curve. This is to ensure that the slow growth is not due to resistant cells because persister cells intrinsically show the same response to antibiotic exposure. Second, high concentrations of antibiotics should be utilized since resistant cell growth depends on antibiotic concentration. Conversely, the killing curve of persister cells is only weakly dependent on antibiotic MIC. Additionally, prophages expressed in response to stress have been shown to decrease persister cell numbers at lower concentrations of antibiotics and can interfere with results from subsequent bioactivity assays.⁶¹

Third, media conditions and antibiotic selection should be closely monitored to ensure that drug degradation or accidental starvation do not contribute to persister cell formation. Lastly, studies should note the conditions that occur after antibiotic exposure is removed and cells are allowed to recover. Because persister research should be dependent on time-kill assays, appropriate time should be given for the completion of the biphasic curve to emerge. Previous studies that have been conducted have ranged from 5 hours⁵⁹ to upwards of 24 hours.^{28,47,62}

1.1.2.: Targeting Persister Cells via Small Molecule Induced Membrane Perturbation

Not only do many challenges exist in the biological evaluation of the presence and study of persisters, but it is also difficult to evaluate the potential of small molecules in targeting persister cells. As our understanding of persister development has evolved over the past few decades, many have proposed targeting particular genes, proteins, etc. that appear to play a role in their development.^{34,38,40,63–66} This becomes difficult as persister cells often have decreased production of uptake machinery on their outer membrane, which can reduce the ability of antibiotics to access the cell. Additionally, the possibility of resistance development is much higher when targeting a particular protein or gene.⁶⁷ Because of this, Hurdle, *et al.* (2011) proposes that a more profitable mechanism of action to target persister cells would be membrane perturbation.²²

Membrane perturbation is a well-studied MoA in antibiotic research; however, it is often avoided by scientists due to potential off-target effects and toxicity. Though this is possible, there are several drugs currently on the market that utilize membrane perturbation as a mechanism of killing including nisin,^{68,69} daptomycin,⁷⁰ polymyxin B,^{71,72} and colistin (**Figure 1.3**).⁷³ When molecules target the membrane of bacterial cells, they generally do so in two ways.^{22,74–76} First, small molecules can act through permeabilization mechanisms in which the compound induces small pores or other destructive actions to the membrane structure. This can lead to increased

permeability of other small molecules to enter the cell as well as potential for leakage of cell machinery and nutrients—ultimately leading to cell death.^{77,78} The second mechanism is depolarization of the membrane. Through this mechanism, compounds can cause disruptions in the electronic gradient of the bacterial membrane *via* formation of ion-conducting pores, increasing ion-permeability or by acting as an ion carrier.⁷⁹ Each of these pathways ultimately affect the proton motive force of the bacterial cell, which drives ATP synthesis and other transporters across the membrane leading to either cell death or allowing for other molecules to execute killing action.⁸⁰

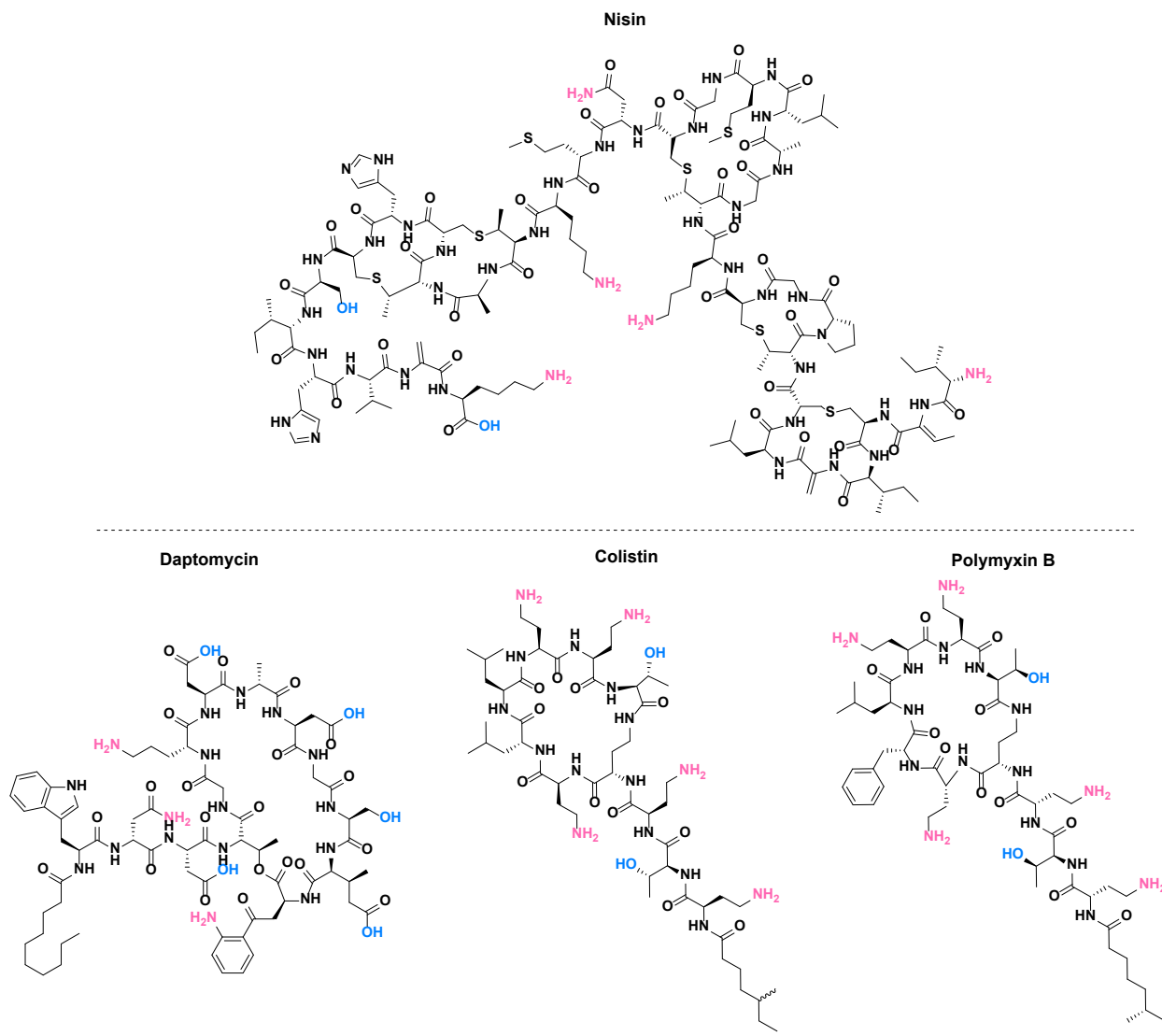


Figure 1.3. Chemical structures of daptomycin, colistin, nisin, and polymyxin B.

Assessing membrane permeability as a potential MoA can be directly studied with fluorogenic membrane dyes including Laurdan GP⁸¹ and DilC12⁸². Of note, both dyes are heteroaromatic compounds. SYTOX Green, a nucleic acid stain, is amenable to high-throughput screens to identify small molecule membrane permeabilizers.⁸³ Computational investigations using molecular dynamic simulations have also been insightful in the study of small molecule-membrane interactions, in particular small molecules that demonstrate selective activity for bacterial cells.⁸⁴⁻⁸⁶ Regardless of growth or metabolic activity of a bacterial cell, the membrane

is essential to the cell's survival. The membrane not only maintains the integrity of the cell's machinery, but it also regulates the influx/efflux of necessary nutrients. In addition, one third of the cell's proteins are located within the membrane.⁷⁶ These proteins are associated with essential cell processes such as active transport of nutrients, the expulsion of waste, and the aforementioned proton motive force that is associated with respiratory enzymes. These processes may be slowed within persister cells but are still active. Therefore, through either the permeabilization or depolarization mechanisms mentioned above, small molecules can cause lethal defects to persisters. Thus, membrane perturbation may be the “magic bullet” in targeting persister cells.

1.1.2.1.: Potential of Phenol and Aryl Compounds as Membrane Perturbers for Targeting Persister Cells

The natural sources of polyphenols and aryl compounds have been a place of inspiration for antibiotic development for decades with one of the largest classes being flavonoids. A recent review by Wąsik and co-workers in 2018 highlighted the different structural classes of phenolic compounds involved in antibacterial activity against *Staphylococcus aureus*.⁸⁷ These natural products often contain a phenyl or benzyl moiety further decorated with hydroxyl or other polar groups (halogens, amines, etc.). They can also be conjugated to other aryl structures or hydrophobic alkyl chains. Through years of research into the antibacterial properties of these compounds, many have found that they possess the ability to permeabilize the bacterial membrane leading to cell death as well as opening the door for synergistic therapies with other antibiotics as explored by Jeon and co-workers in 2015.⁸⁸ Though most of these compounds have only been analyzed against wild-type cells, we hypothesize that they would also have activity against persister cells due to other successes as discussed below, though further analysis is required.

1.1.2.1.A.: Prenylated Phenolic Compounds

A common tradition for centuries is the utilization of various plants as therapeutics. Through further analysis of the components of these plants, researchers uncovered therapeutic agents in these traditional medicines. Through this lens, Gruppen and co-workers turned to legumes, a

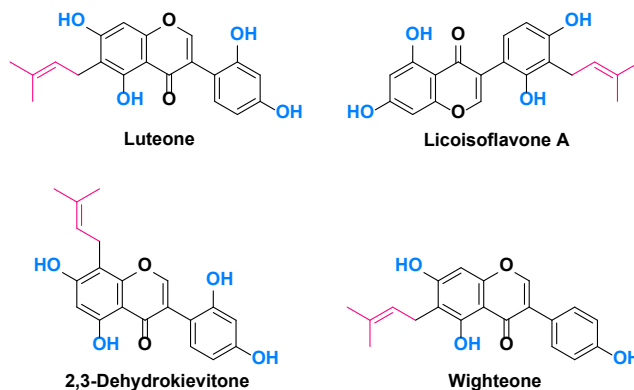


Figure 1.4. Examples of prenylated compounds attenuated in active fractions.

large plant family known to produce antimicrobial compounds—particularly prenylated phenolic compounds under stress induced conditions.⁸⁹ Through flash pool collection, the authors grouped 57 different phenolic compounds, 39 of which were prenylated and could be identified within the classes of isoflavonoid, flavonoid, stilbenoid, phenolic acid, and chromone.

Overall, the authors showed potent activity of the pooled compounds against *Listeria monocytogenes* with the most potent compound having an MIC of 10 $\mu\text{g}/\text{mL}$. Additionally, the compounds could elicit inhibitory activity against *Escherichia coli* when co-administered with an efflux inhibitor. They also confirmed through further analysis that the prenylated compounds in each fraction (ex: luteone, licoisoflavone A, 2,3-dehydrokievitone and wighteone) were responsible for the antibacterial activity (**Figure 1.4**). To elucidate the MoA, the authors performed a membrane permeabilization assay with propidium iodide, which showed that the prenylated compounds were able to rapidly permeabilize the membrane of *L. monocytogenes* at the MIC. The authors hypothesized that the prenylated compounds intercalated into the lipid bilayer thereby disrupting its packing density and increasing permeability. Additionally, the authors proposed that structural features such as a bent skeleton confirmation, prenylated chains, and increased

hydrophobicity contributed to potent antibacterial activity due to heightened perturbation of the membrane.

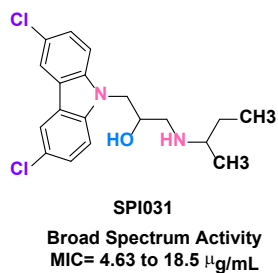


Figure 1.5. Chemical structure of *N*-alkylated 3, 6-dihalogenocarbazol 1-(*sec*-butylamino)-3-(3,6-dichloro-9*H*-carbazol-9-yl)propan-2-ol), SPI031.

1.1.2.1.B.: *N*-alkylated 3,6-dihalogenocarbazol 1-(*sec*-butylamino)-3-(3,6-dichloro,9*H*-carbazol-9-yl)propan-2-ol) (SPI031)

In 2016, Michiels and co-workers identified a novel compound they named SPI031, which had potent broad-spectrum activity, including clinically relevant pathogens *S. aureus* and *P. aeruginosa*, with MICs ranging from 4.63 to 18.5 µg/mL (**Figure 1.5**).⁹⁰ This complex carbazole had similar killing kinetics to that of polymyxin

B, a last line of defense antibiotic, as well as improved kinetics in comparison to vancomycin against *P. aeruginosa*. Through SYTOX Green assays, the researchers identified that SPI031 perturbed the membrane of methicillin-resistant *S. aureus* cells as well as the inner and outer membranes of *P. aeruginosa* exhibited by the cellular uptake of the fluorescent probes. This perturbation was further confirmed *via* phospholipid mimicking liposomes filled with carboxyfluorescein (CF) fluid. After treatment with SPI031, an increase of CF leakage was observed in comparison to negative controls.

In addition to these results, the authors also studied potential resistance mechanisms through whole-genome sequencing of spontaneous resistant mutants of *P. aeruginosa*. This analysis revealed mutations in multidrug efflux pumps as well as genes involved in outer membrane synthesis. They hypothesized that alteration of the outer membrane structure was able to confer resistance to SPI031. The authors suggest that this compound may be a very potent antimicrobial especially against persister cells, though these studies were not performed. However, they do point to potential toxicity issues due to targeting of human keratinocytes and human

hepatoma cells, which is often a point of contention for most membrane targeting small molecules. The authors suggest that further structural modifications to the scaffold may lead to improved specificity towards bacterial membranes over human.

1.1.2.1.C.: 1-((2,4-dichlorophenethyl)amino)-3-phenoxypropan-2-ol (SPI009)

Following the study published in 2016, Michiels and co-workers identified another compound they named SPI001 through a high-throughput screen of over 20,000 small molecules in 2017.^{91,92} The compound displayed potent activity in combination with 10 µg/mL of ofloxacin against persistent *P. aeruginosa* cells, with a >2,000-fold reduction in comparison to ofloxacin alone. With this initial hit, the researchers performed structure-activity-relationship (SAR) studies and found a more potent analog: 1-((2,4-dichlorophenethyl)amino)-3-phenoxypropan-2-ol, or SPI009 (Figure 1.6). At 68 µg/mL, SPI009

proved to have a 7,200-fold reduction in *P. aeruginosa* persister cell concentration in comparison to ofloxacin alone. To further analyze the killing capability, they treated isolated persister and non-persister cells at a range of concentrations from 17 to 68 µg/mL of SPI009 alone. This

study suggested that SPI009 could kill both persister and wild-type cells. Additionally, Michiels and co-workers displayed that SPI009's combination therapy was not only limited to ofloxacin, but also proved potent in combination with amikacin and ceftazidime.

After analyzing the compound's biological activity, the researchers turned to further understanding its MoA. They began with a *P. aeruginosa* knockout library to identify cells that had decreased sensitivity to the SPI009 and ofloxacin treatment. This showed an over-expression

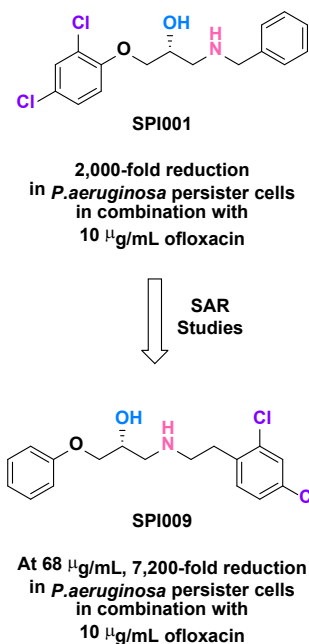


Figure 1.6. Chemical structure of the parent scaffold, SPI001, and the most potent analog (1-((2,4-dichlorophenethyl)amino)-3-phenoxypropan-2-ol (SPI009).

of genes generally involved in adaptation and protection as well as cell wall and lipopolysaccharides (LPS) synthesis and maintenance. Overall, these data suggested that membrane integrity was the target. To confirm these findings, they performed a macromolecular synthesis assay, which confirmed the ability of SPI009 to reduce the incorporation of precursors for DNA, RNA, proteins, fatty acids, and peptidoglycan. To analyze its ability to damage the membrane, they performed artificial bilayer and permeabilization studies in addition to analyzing treated cells under a microscope. The artificial membrane displayed increased CF leakage in comparison to an inactive analog. Additionally, the permeabilization assay with SYTOX Green showed that SPI009 targeted the inner and outer membrane, which was further confirmed through microscopic analysis. Altogether, these findings indicate that SPI009 can disrupt both the outer and inner membrane of *P. aeruginosa* persister cells as well as inhibit macromolecular synthesis. Through their findings, the authors propose that SPI009 would be a good therapeutic alone as well as in combination with outdated antibiotics that are deemed unusable due to decreased sensitivity.

1.1.2.2.: Substituted Indoles

Previous misconceptions that indole—an intra-species, inter-species, and interkingdom signal molecule—is responsible for an increase in persistence in various bacteria, have recently been widely disproven.⁹³ In fact, many recent studies have demonstrated the opposite, and it can now be said that substituted indoles may have significant potential against bacterial persister cells. Several studies have come to prove that substituted indoles are capable of killing dormant cells and decreasing persistence by disrupting the cell membrane.⁹⁴

1.1.2.2.A.: Amphiphilic Indole Derivatives

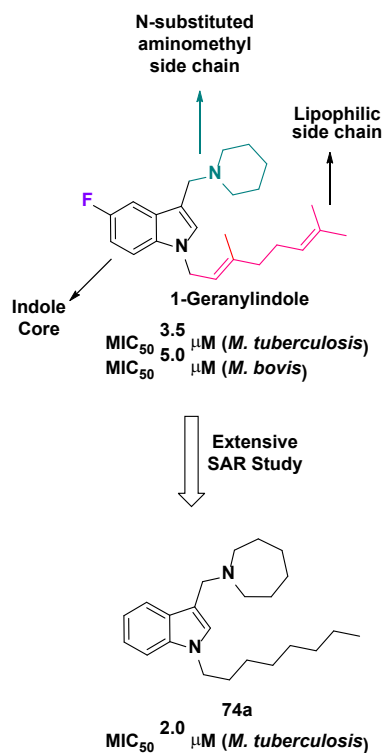


Figure 1.7. Chemical structure 1-geranylindole and potent analog, 74a.

In 2017, Yang and co-workers performed an extensive SAR study and biological evaluation of 1-geranylindole (**Figure 1.7**).⁹⁵ Previously, the authors had discovered this compound in a focused screen of indole-type small molecules. This amphiphile caught their interest as it had low micromolar activity with a minimum inhibitory concentration required to reduce bacterial growth by 50% (MIC₅₀) of 5 μM against *Mycobacterium bovis* and MIC₅₀ of 3.5 μM against *Mycobacterium tuberculosis*. Additionally, 1-geranylindole showed membrane perturbation, which was attributed to its amphiphilic nature. Though 1-geranylindole offered promise as a potent therapeutic, the authors found that it had toxicity against mammalian cells. To improve this issue, the authors sought to perform an extensive SAR study with five different series of analogs. These analogs explored the four different functionalities of 1-geranylindole: (1) role of the side chain at the indole nitrogen; (2) basic N-substituted aminomethyl side chain; (3) 5-fluoro substituent; and (4) replacing the indole with its isosteric equivalent, 7-azaindole. The fifth series of analogs was the compilation of the best structural changes from the previous series that offered improved selectivity towards the mycobacterium.

Through extensive analog development, the authors found that the lipophilic side chain at the indole nitrogen and the basic N-substituted aminomethyl side chain were required for activity. The other components of the molecule were otherwise amenable without significant change to its activity. Of the library of analogs synthesized and evaluated, analog 74a was ultimately selected due to its low micromolar activity (MIC₅₀ = 2 μM), selectivity for *M. tuberculosis*, therapeutically

relevant solubility, and *in vitro* metabolic stability. With this compound, the authors sought to further explore its MoA, namely its membrane perturbation capabilities. This was achieved by monitoring both the membrane potential and permeability. The membrane potential was measured with 3,3-diethylloxycarbocyanine iodide, which fluoresces red in polarized cellular membranes and green when membranes are depolarized due to lack of intracellular accumulation. 74a showed a time-dependent decrease of membrane polarization at $2 \times \text{MIC}$. Membrane permeabilization was measured with propidium iodide accumulation, which also showed a time-dependent increase in cell permeabilization. Additionally, 74a was able to not only inhibit growing cells of *M. tuberculosis* but also persister cells. To probe its broad-spectrum activity, the authors also explored the activity of 74a against *S. aureus* and *E. coli*. 74a retained activity against *S. aureus* with an MIC_{50} of $8 \mu\text{M}$ but was ineffective against *E. coli*. With these promising results, indole compounds offer a new avenue for novel therapeutic development.

1.1.2.2.B.: 5-nitro-3-phenyl-1H-indol-2-yl-methylamine hydrochloride (NPIMA)

In 2019, Song and co-workers discovered a substituted indole—5-nitro-3-phenyl-1H-indol-2-yl-methylamine hydrochloride (NPIMA)—in a high-throughput screen of a 10,000 small molecule library (**Figure 1.8**).⁹⁶

The screen was strategically designed to analyze the effectiveness of compounds against a persistent *E. coli* population through a pre-treatment of exponential phase cells with rifampicin. Ultimately, NPIMA stood out

from the remaining molecules of the screen because it had the greatest reduction in turbidity of the *E. coli* cells at an MIC of $100 \mu\text{M}$, which suggested a potential membrane MoA. Additionally, NPIMA was able to reduce exponentially growing cells at its MIC. To further explore the MoA, the authors performed a LIVE/DEAD kit on exponentially growing *E. coli* cells that were treated

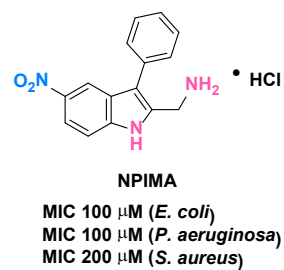


Figure 1.8.
Chemical structure
NPIMA.

with 100 μM of NPIMA. This showed that NPIMA was lysing the cells as extracellular DNA was stained by both SYTO9 and propidium iodide in the assay. This result was further confirmed by an observed increase of intracellular proteins and DNA concentrations within the supernatant as well as TEM imaging, which showed clear damage to the cell envelope.

After analysis of its efficacy against *E. coli* persister cells, the authors analyzed activity against other relevant pathogens, namely *P. aeruginosa* and *S. aureus* persister cells. NPIMA lysed both exponentially growing and persister cells of *P. aeruginosa* at 100 μM and *S. aureus* at 200 μM . Additionally, NPIMA showed the same membrane damage MoA for both *P. aeruginosa* and *S. aureus*. The efficacy of NPIMA was further evaluated in an *in vitro* Lubbock chronic wound pathogenic biofilm model containing both *P. aeruginosa* and *S. aureus*, which showed that NPIMA reduced total viable cells 10-fold after 6 hrs at 0.5 mM. The authors also noted that they were unable to produce resistant mutants after a 7-day resistance selection assay with *E. coli* cells. Though NPIMA does have promising biological activity, further analysis would be required as it showed toxicity above 50 μM against a human colon cancer cell line.

1.1.2.2.C.: SCH-79797

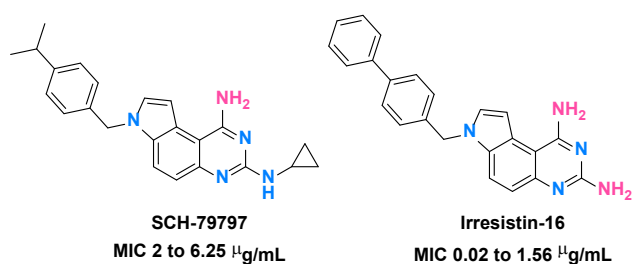


Figure 9. Chemical structure of SCH-79797 and Irresistin-16.

In summer of 2020, Gitai and co-workers disclosed the potent antibacterial activity of the pyrroloquinazolinodiamine complex, SCH-79797 (**Figure 1.9**).⁹⁷ They targeted this compound *via* a small molecule library screen of over 30,000 unique compounds that were

previously reported as human PAR-1 antagonists. SCH-79797 was previously identified as an antimicrobial by Gupta, *et al.* and had extensive studies on its *in vivo* efficacy in animal studies.⁹⁸⁻

¹⁰⁰ To further confirm its activity, the authors began with MIC assays, in which they discovered that the compound had potent broad-spectrum activity, including several ESKAPE pathogens with an MIC of 2 to 6.25 $\mu\text{g}/\text{mL}$.

After failed attempts to produce resistant mutants, the authors employed a multipronged approach to unveil SCH-79797's MoA. This began with bacterial cytological profiling, which analyzed SCH-79797 against a panel of known classes of antibiotics. Through this analysis, the authors identified that their compound had a unique MoA, which prompted the use of thermal proteome profiling, CRISPRi genetic sensitivity, and metabolomic profiling for further characterization. These analyses identified the possible targets as dihydrofolate reductase and the bacterial membrane. These were further confirmed *via* enzymatic assays as well as depolarization and permeabilization assays. Ultimately, the authors proved that SCH-79797 can simultaneously damage the integrity of bacterial membranes while also inhibiting folate synthesis through inhibition of dihydrofolate reductase. Additionally, they synthesized a simplified analog, Irresistin-16, which had increased activity as well as reduced toxicity. Although the authors did not specifically analyze this compound's efficacy against persister cells, we hypothesize that it has the capability and possible increased potency through its two-pronged MoA.

1.1.2.3.: Peptoid Mimics: Aryl-Alkyl-Lysines

In recent years, cationic antimicrobial peptides (AMPs) have become a large focus of antibiotic development, especially in targeting persister cells.^{101,102} These compounds often

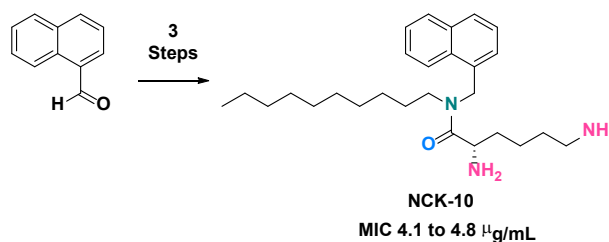


Figure 1.10. Synthetic scheme and structure of NCK-10.

mimic molecules that are a part of the innate immune system used as the body's first line of defense.^{103–105} They can inflict killing by perturbing and eventually lysing the bacterial

membrane.^{102,106} Additionally, as the compounds are quite complex, resistant mechanisms are rare. Though the use of AMPs seems a promising target for antibiotic development, they are limited by high levels of toxicity, ease of degradation in the presence of proteases, and high cost to produce at an industrial scale. To combat these issues, Halder and co-workers in 2014 sought to synthesize peptoid mimicking molecules in which they incorporated an L-lysine for cationic character, an aromatic core for hydrophobicity, and a varied alkyl chain (**Figure 1.10**).¹⁰⁷ They synthesized over 16 analogs through a three-step synthetic sequence with their best performing analog being NCK-10 (naphthalene core with decyl chain appendage) with an MIC of 4.1 to 4.8 $\mu\text{g/mL}$ against both wild-type and persister MRSA cells.¹⁰⁸

Additionally, in further analyzing the compound's activity, the authors found that NCK-10 was able to completely eradicate MRSA persister cells at $5 \times \text{MIC}$ in 30 min. In analyzing its MoA, they uncovered that NCK-10 rapidly depolarized the membrane of MRSA persister cells within 5 min of treatment, but the membrane permeabilization appeared weaker through observation of varying fluorescence intensity in their assays. In addition to the persister activity, NCK-10 reduced the number of viable cells within a biofilm as well as reduced the mass of pre-formed biofilm at $10 \times \text{MIC}$. Overall, Halder and co-workers showed the ability to simplify complex AMPs thereby producing several potent antibacterials that could be used to treat planktonic, persistent, and biofilm MRSA infections.

1.1.2.4.: Repurposed FDA Drugs prove Potent in Targeting Bacterial Persister Cells

In pursuit of antibiotics targeting persister cells, the Wuest lab at Emory University developed several projects focused on perturbing cell membranes. Rather than identifying new molecules, these projects explored repurposing drugs previously approved by FDA for novel antibiotic use. Through collaboration with Mylonakis's laboratory at Rhode Island Hospital, they

were able to uncover several potent small molecules *via* a high-throughput screen. This screen involved a *Caenorhabditis elegans*/ MRSA infection model, which enabled the investigation of compound potency as well as toxicity concurrently.^{109,110} From this screen and further analysis, they uncovered several compounds including three small molecules (nTZDpa, CD437, and bithionol) that proved efficacious against MRSA persister cells.

1.1.2.4.A.: nTZDPA

nTZDpa is a nonthiazolidinedione that consists of several key moieties including a 5-chloro-substituted indole core, a 1-chlorobenzyl substituent, a phenyl sulfide moiety, and a carboxylic acid (Figure 11). It has previously been investigated as a potential diabetes therapy.¹¹¹ After initial hits through the *C. elegans*-MRSA infection model, computational modeling was performed to further uncover the MoA of nTZDpa against MRSA cells.⁸⁶ This modeling showed that the MoA involved permeation of the membrane *via* high affinity of the carboxylic acid and two chlorine atoms for the phospholipid heads on the cell's surface. After association, perturbation from the aryl groups ultimately leads to cell lysis and death. Initial bioactive results showed relatively high but promising MIC of 4 $\mu\text{g/mL}$ against growing cells of *S. aureus*. Additionally, a PKC was measured at 64 $\mu\text{g/mL}$. Since compounds that are effective against bacterial membranes can also be toxic to mammalian cells,¹⁰⁹ hemolysis against human erythrocytes were measured to monitor toxicity with average hemolytic activity (HC_{50}) of nTZDpa measured at 47 $\mu\text{g/mL}$. These measurements served as the baseline by which future analogs were compared for their efficiency against persister cells while maintaining low toxicity to improve therapeutic viability.

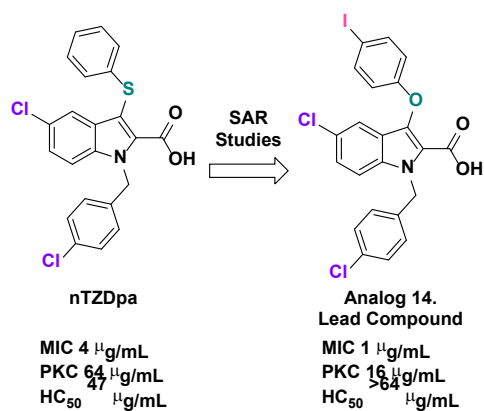


Figure 1.11. Chemical structure of nTZDpa and the lead compound, Analog 14.

The diverted synthesis of nTZDpa allowed for optimization of the parent scaffold. Among these key changes include a substitution of oxygen for sulfur to improve the toxicity profile as well as the addition of iodine to the aryl ether moiety for increased potency. The current lead analog contains a 4-iodo substitution to the aryl thioether moiety that resulted in an MIC of 1 $\mu\text{g/mL}$, PKC of 16 $\mu\text{g/mL}$, and HC₅₀ of >64 $\mu\text{g/mL}$ (**Figure 1.11**).

These changes to the scaffold have been consistent with rules of permeability for small molecules, such as a 600 Da cutoff, low number of rotatable bonds, and low three-dimensionality.¹¹²

In addition to the improved efficacy of nTZDpa analogs against growing and persistent MRSA cells, the original scaffold has been shown to work synergistically with other classes of antibiotics, specifically aminoglycosides such as gentamicin, tobramycin, neomycin, kanamycin, and streptomycin.⁸⁶ Since these aminoglycosides have reported resistance in clinical strains,¹¹³ the low probability of resistance to nTZDpa shows additional promise of implementing this drug into combination therapies. This is especially important as many antibiotics, such as aminoglycosides and β -lactams, require access to the cell's cytoplasm to disrupt their respective cellular target. Therefore, the ability of nTZDpa to perturb the membrane could serve as a bypass for these antibiotics in the challenges posed by persister cells.

1.1.2.4.B.: CD437

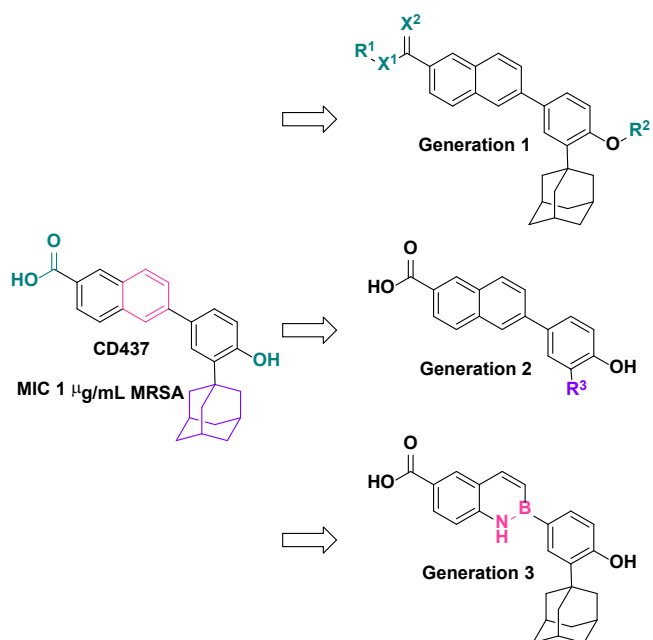


Figure 1.12. Chemical structure of CD437 as well as chemical representation of the analog substitutions for each generation. Generation 1: R¹ and R² = CH₃; X¹ = O, or NH; X² = O, or H,H. Generation 2: R³ = CH₃, Ph, *tert*-butyl, or varying chain lengths of saturated or unsaturated alkyl groups.

Another molecule uncovered in the *C. elegans*-MRSA infection model was the synthetic retinoid and analog of vitamin A, CD437 (**Figure 1.12**). After initial discovery, further analysis showed an MIC of 1 μg/mL against MRSA persister cells as well as a reasonable toxicity panel (HC₅₀ = 32 μg/mL; LC₅₀ = 20 μg/mL).⁸⁴ Additionally, the compound proved to have synergistic effects with gentamicin. To gain further insight into the molecule's MoA, a specific all-atom molecular dynamic simulation was performed utilizing a synthetic lipid bilayer

that imitates the bilayer of *S. aureus*. From this, researchers learned that the molecule's carboxylic acid and phenol moieties allowed it to interact with the hydrophilic heads of the bilayer followed by molecular rotation and insertion of the lipophilic adamantyl group thereby perturbing the membrane. This mechanism was further supported through molecular dynamics simulations in giant unilamellar vesicle experiments. These molecules also have the potential to aggregate to induce membrane damage. However, further testing is needed to support this hypothesis.

After CD437's initial discovery in 2018, three generations of analogs have been synthesized. The first explored changes to the carboxylic acid and phenol moieties, which led to a new lead compound: a primary alcohol derivative deemed "analog 2," which had an MIC of 2 μg/mL and improved cytotoxicity (HC₅₀ >32 μg/mL; LC₅₀ >31 μg/mL). Unfortunately, analog 2

possessed low solubility in serum due to its high affinity for retinol binding proteins (unpublished data), thus prompting the need for further analog exploration. The second generation of analogs explored the hydrophobic adamantyl group of the parent scaffold to mimic the fatty acid tails embedded in the lipid bilayer. These data were published in 2019, and the adamantyl moiety was found to have the greatest bactericidal capability.¹¹⁴

Following this generation, the authors sought to explore the broad-spectrum capability of the scaffold by attaching an alkylamine moiety to the molecule, as this addition has previously been shown to elicit activity against Gram-negative bacteria on similar substrates.¹¹⁵ Unfortunately, this alteration did not gain broad-spectrum activity and decreased the potency against Gram-positive bacteria. In the latest generation, an isosteric substitution of a carbon-carbon double bond for a nitrogen-boron bond within the naphthalene scaffold was synthesized in hopes of altering the electronics enough to reduce retinol protein binding.¹¹⁶ However, it was discovered that this substitution did not enhance the molecule's biological efficacy.

1.1.2.4.C.: Bithionol

Bithionol is a chlorinated bisphenol that is clinically approved for anti-parasitic treatment of trematode infections such as *Fasciola hepatica* in equine species (**Figure 1.13**).¹¹⁷ In 1965, Barr and co-workers disclosed that in addition to parasitic activity, bithionol also proved to have antibacterial activity with an MIC of ~8 to 15 $\mu\text{g/mL}$ against *S. aureus*. In an effort to reproduce the

results of the 1965 study, the Wuest and Mylonakis laboratories analyzed its antibacterial activity and performed SAR studies for this compound. They showed that bithionol had potent activity against several Gram-positive bacteria including the vancomycin-resistant *S. aureus* (VRSA).⁸⁵

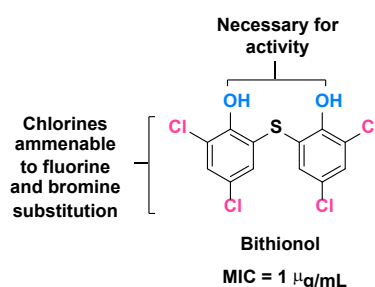


Figure 1.13. Chemical structure of bithionol.

Furthermore, they found that through their analysis it had an even lower MIC of 0.5 to 2 $\mu\text{g/mL}$ than demonstrated in the previous study in 1965.

In addition to preliminary bactericidal activity, bithionol also had a time-dependent reduction of *S. aureus* cell density like cetalkonium chloride, a common quaternary ammonium antiseptic, which indicated potential lytic activity. Further analysis *via* transmission electron micrographs (TEMs) confirmed this hypothesis with distorted cell membranes. This prompted further analysis of bithionol's activity against persister cells. Through analysis with MRSA MW2 strain planktonic and biofilm persisters, bithionol proved to kill these cells in a dose-dependent manner over a 2 h period, with complete eradication after 24 h exposure at $32 \times \text{MIC}$. Even more, it proved to have potent bactericidal activity against VRSA strain VRS1 persister cells with complete eradication at $32 \times \text{MIC}$.

With these results, the researchers sought to understand bithionol's MoA *via* all-atom molecular dynamic simulations. They showed that the phenol and chlorine moieties are initially attracted to the negatively charged heads of the bacterial membrane followed by penetration into the membrane, ultimately leading to membrane perturbation and cell death. This was further confirmed through biomembrane-mimicking giant unilamellar vesicle assays. Through SAR studies, the researchers showed that the phenol moieties were necessary for antibacterial activity. Additionally, substitution of the chlorine atoms with other halogens, such as fluorine and bromine, were somewhat tolerated with the latter being most active. It was hypothesized that the polar carbon-fluorine bond may increase its initial attachment to the membrane but disallows penetration further into the membrane.

1.1.2.4.D.: Honokiol

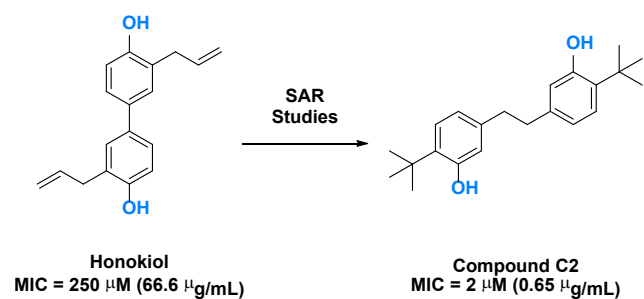


Figure 1.14. Chemical structures of Honokiol and Compound C2.

Honokiol is a natural product isolated from *Magnolia officinalis*. Initial analysis of this compound by Wang *et al.* showed potent activity against *Streptococcus mutans*, which naturally occurs in the oral cavity and is the causative agent of dental caries.¹¹⁸ Most

interesting was honokiol's apparent ability to disrupt *S. mutans* biofilm. However, upon further analysis by our groups, we discovered this activity only occurred in aerobic conditions, which is not a representative environment of the oral cavity.¹¹⁹ In our hands, honokiol had moderate activity with an MIC of 250 μ M under biologically relevant conditions (5% - CO₂ supplemented atmosphere).

Through SAR analysis, our groups discovered our lead analog, deemed C2, that showed potent activity against *S. mutans* planktonic cells with an MIC of 2 μ M (**Figure 1.14**). To further understand its MoA, resistance selection assays were first attempted against *S. mutans*.¹²⁰ However, these were unsuccessful. As it has been previously shown to be difficult to produce resistance for membrane perturbing compounds,²² we then decided to test its membrane depolarization and lysis capabilities. C2 did not show significant depolarization in comparison to the negative control, DMSO. However, C2 did show lytic activity as evidenced by the increased propidium iodide fluorescence. This lytic activity was further visualized in TEM images. To further confirm its permeabilization activity, SYTOX Green assays were performed, which showed increasing fluorescence in the presence of C2.

With its membrane perturbing action, its minimum bactericidal concentration (MBC) was determined to investigate if C2 was bactericidal or bacteriostatic. It was shown to have an MBC 4X its MIC indicating bactericidal affects. Though the original parent compound's, Honokiol, antibacterial activity was disproven, the lead analog, C2, displayed potent activity with membrane perturbing capabilities.

1.1.3.: Conclusions

Though bacterial resistance is frequently the focus in antibiotic development, the elusive tolerant and persister cells are often the overlooked culprit for chronic infections. Different from resistance, bacterial tolerance is a whole-population characteristic, in which the cells can evade the killing power of antibiotics without affecting the MIC of the therapeutic but rather require longer treatment times. These cells achieve this by reducing metabolism and slowing growth, which is induced through the environmental stress of the antibiotic. To make matters worse, within the umbrella of tolerant cells are persister cells. Existing in most bacterial populations at a 0.001-1.0% concentration, persisters are a subcategory of tolerance and are distinguished from tolerant cells through their time-kill kinetics, in which they produce a biphasic curve. This is due to an initial steep drop in the killing of the susceptible population followed by a slow decrease due to the presence of persister cells.

Looking forward, we propose a few areas to focus on for future investigations. Researchers have proposed developing small molecules that target certain genes or proteins that have been shown to lead to the formation of persister cells. Though this has potential as a therapeutic strategy, these small molecules are hindered due to their decrease ability to be actively transported into the cell. It was proposed in a review by Hurdle and co-workers that another method to target persister cells would be through membrane perturbation. As membranes are essential in all cells regardless

of level of growth or metabolism, utilizing this as a target for persister cells may be more fruitful. Clearly from the studies discussed above this is a viable strategy that garners more investigation.

In analyzing membrane perturbing molecules, we found that a common motif involved a polarized aryl moiety, often a phenol or indole, which was further decorated with additional hydroxyls, amines, or other halides. The group of molecules discussed in this review were discovered either in high-throughput screens of repurposed drugs or unique small molecule libraries or were simplified AMP mimics. Through analysis of the structure and activity, we propose that the membrane perturbation is generally achieved by initial attraction of the polarizable groups to the negatively charged heads of the lipid membrane. Once the compounds are associated with the membrane, the hydrophobic portions can intercalate into the membrane thereby disrupting the ordered fatty acid tails leading to cell leakage. This can either induce cell lysis causing cell death or can increase permeability of the membrane for synergistic treatment with other antibiotics. Additionally, the presence of heteroaromatic and amines groups showed broad spectrum activity, whereas phenol-based compounds were often limited to Gram-positive bacteria. Though not every study reported within this review explicitly analyzed activity against persister cells, with the success of membrane perturbation against persisters, we expect these compounds to also be successful.

Through this focused collection of membrane perturbing small molecules and identification of common chemical motifs, a proposed unifying foundation for membrane perturbation as a MoA against persister cells has been laid. This groundwork can serve as a starting point for rational design in developing novel antibiotics. As amphiphilic heteroaromatic compounds frequently displayed increased membrane perturbing effects, incorporation of these motifs to new or existing scaffolds may include this MoA. Beyond the development of novel

scaffolds for membrane perturbation, there is also a need for broadening analysis of existing phenolic and heteroaromatic structures against bacterial persister cells. As discussed, it is difficult to analyze the effects of small molecules on persister populations and even ensure the presence of persisters in appropriate assays. However, as these archetypal cells can cause recalcitrant infections, there is a great need to expand upon the research of persister inhibitors in the future.

1.2.: Inhibiting Bacteria via Disruption of Bacterial Metal Homeostasis

Metal ions are essential to all living organisms. Within biological systems, it is estimated that up to one-half of proteins require a metal ion in order to function correctly.^{121,122} Specifically, it has been shown that the d-block metal ions such as manganese, iron, cobalt, nickel, copper, and zinc among others are essential for protein function.¹²³ Although some proteins may only have temporary interactions with a metal ion, others utilize them as permanent cofactors: serving a catalytic role by acting as an electron carrier in chemical reactions.¹²⁴ Specifically, metal ions can serve as a catalysts for respiration, photosynthesis, nitrogen fixation, and other bioenergetic and biogeochemical processes.¹²⁵ Some metal ions, such as zinc, offer structural support to proteins via stabilizing interactions, which influences the protein folding as well as the active site orientation. Because they play essential roles in proper protein structure and function, the correct concentration of metal ions within the cell must be maintained in order to avoid off-target interactions. For example, if a metal ion concentration exceeds its normal range, it can bind and interact with other proteins in the cell. This process is known as mismetallation and can lead to a change in protein specificity, reactivity, or even deactivate the protein.¹²⁶ If metal ion concentrations exceed normal range, they can lead to development of reactive oxygen species (ROS) within the cell due to the ability of some metals to catalyze redox reactions that produce hydroxyl radicals ($\cdot\text{OH}$), superoxide ($\text{O}_2^{\cdot-}$), and hydrogen peroxide (H_2O_2) byproducts (**Figure**

1.15).^{122,127} These species are very reactive and can do severe damage to proteins, lipids, carbohydrates, and nucleic acids, which can ultimately lead to cell death.^{127,128} Due to these potential off

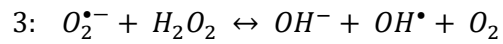
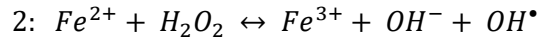
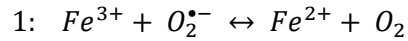


Figure 1.15 Example reactions with iron ions to generate reactive oxygen species within the cell. Reaction 1 = redox reaction with O_2 . Reaction 2 = Fenton reaction. Reaction 3 = Haber–Weiss reaction.

target effects, cellular organisms have developed specific regulatory pathways to maintain the appropriate levels of these essential minerals.

Specifically, within bacterial cells, various regulatory pathways are employed to maintain metal ion homeostasis. One of the most important pathways utilizes metalloregulatory proteins to sense both excess and limitation of metal ions intra- and extracellularly. Metalloregulatory proteins are multimeric DNA-binding proteins that undergo allosteric changes when bound to a metal ion.^{125,129} Through these metal-protein complexes, they can affect metal ion uptake, efflux, storage, and intracellular tracking to maintain homeostasis through control of gene expression responsible for these processes.¹²³ Some of these effects are briefly discussed below.

Proteins that are affected by metalloregulatory processes include metal transporters that shuttle metal ions or small molecule–metal chelates across the plasma membrane. These

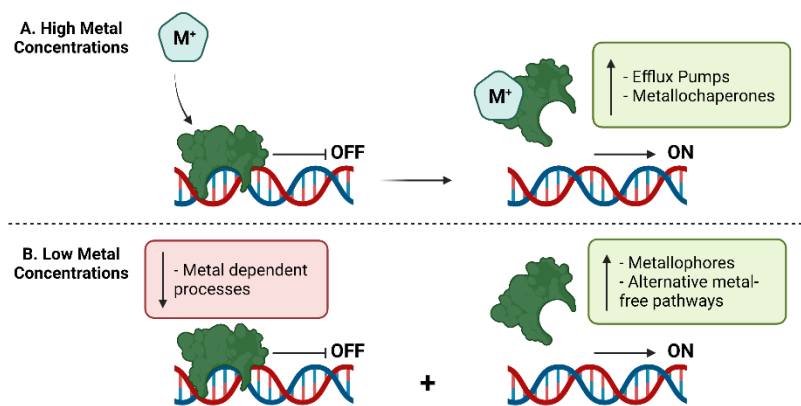


Figure 1.16. A) Metalloregulatory protein responses to high concentrations of specific metal ions in the cell. B) Metalloregulatory responses to low metal concentrations in the cell. This figure was made using BioRender.

transporters become upregulated during metal ion starvation to sequester the limited ion into the

cell (**Figure 1.16 B**). Metallochaperones are tightly regulated through these systems due to their ability to bind metal ions and transport them to the appropriate acceptor proteins or enzymes, which can inhibit production of ROS from excess metal ions in the cytoplasm, or mismetallate with off target proteins (**Figure 1.16 A**). Beyond trafficking proteins, efflux pumps' regulation and transcription are also affected via metalloregulatory proteins especially under metal excess. The upregulation of these can aid in the detoxification of metal ions if cellular concentrations exceed normal range.¹²⁵ Upregulation of the synthesis and excretion of small molecules that bind the limited metal ion may occur in order to sequester the metal from the surrounding environment.^{125,130,131} These small molecules, known as metallophores, exhibit high binding affinity to their metal of interest and are a great resource to bacteria in times of metal ion starvation.

1.2.1. Metallophores

The available metal ion concentrations in the bacterial environments are quite low. This is due in part to the limitation of soluble metal ions in aerobic environments as they often oxidize to their insoluble forms in the presence of oxygen. For example, the concentration of soluble iron (Fe^{2+}) is estimated as 10^{-18} M. However, bacteria require 10^{-7} – 10^{-5} M for ideal growth and function.^{131,132} More often within the environment, available iron exists in its insoluble, oxidized ferric form (Fe^{3+}), which is incapable of passive diffusion into the bacterial cell.¹³³ Because of this, bacteria have developed strategies to sequester these vital minerals by producing small, soluble molecules that selectively chelate metal ions. These molecules are called metallophores: small, organic molecules that have a high binding affinity for specific metal ions and function to supply this nutrient to the bacterial cell.¹³⁴

1.2.1.A. Siderophores

One of the most well-studied metallophores in bacteria are siderophores, Greek for “iron carrier.”¹³³ Soluble siderophore molecules (molecular mass < 1000 Da) are able to act as organic ligands and bind with high affinity to Fe³⁺ ($K_{\text{aff}} > 10^{30}$), which is the more abundant form of iron in bacterial environments.¹³⁰ As Fe(III) is most often solvated by water in a hexacoordinated octahedral geometry

(Fe(H₂O)₆³⁺) in aqueous environments, the

siderophore must

displace the water

molecules to form more stable complexes.¹³⁵

Generally, a 1:1 complex is formed if there are six

donor atoms available to

coordinate to the metal

ion. However, other

ligand to Fe(III) ratios have been observed depending upon the number of coordinating sites. This

stable siderophore-Fe(III) complex then enables the bacteria to intake it through siderophore-

specific uptake machinery.¹³³ Siderophores are classified by these iron binding structural motifs

that enable this coordination complex by four canonical categories: catecholates, hydroxamates,

phenolates, and carboxylates (**Figure 1.17**). It is also common for siderophores to have mixed

types of iron-binding motifs (i.e., carboxylate-phenolate compounds). Most commonly, the donor

atoms in these small molecules that form these binding interactions are oxygen atoms as they are

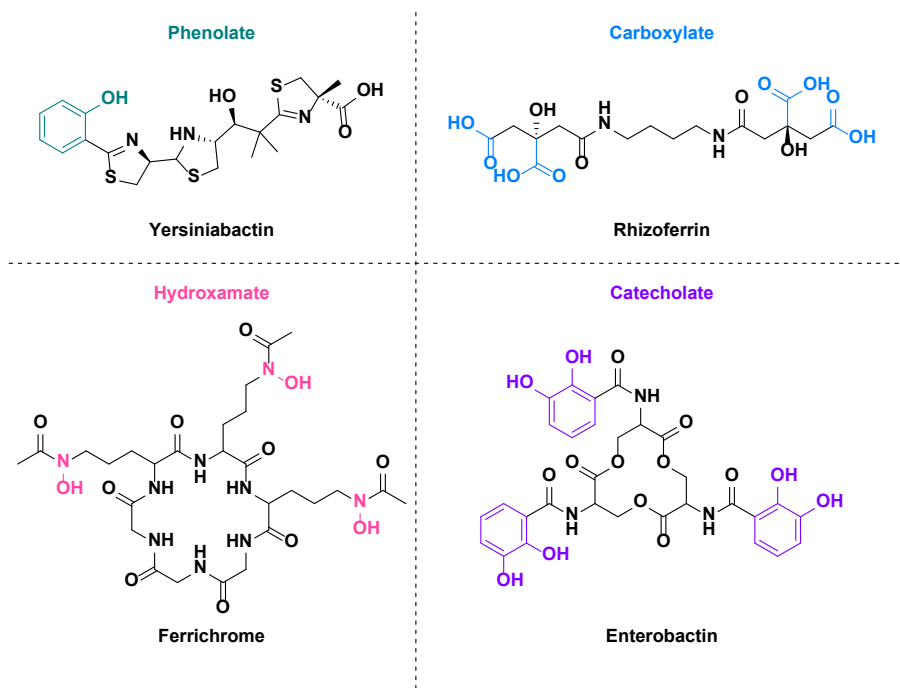


Figure 1.17 Examples of different known siderophore compounds. The canonical motifs are highlighted in each structure. Green = phenolate. Blue = carboxylate. Pink = hydroxamate. Purple = catecholate.

hard Lewis bases and are able to form strong ionic interactions with the Lewis acidity of Fe(III).¹³⁵ Conversely, the decreased Lewis acidity of Fe(II) prefers softer Lewis bases such as nitrogen and sulfur, though, these atoms can also participate in stabilizing interactions of the siderophore-Fe(III) complex as well.

The synthesis and excretion of these small molecules is controlled in part by the *fur* gene, which stands for ferric uptake regulation.^{133,136} The protein (Fur) produced by the *fur* gene is a 17-kDa polypeptide that acts as a transcriptional repressor for iron-regulated promoter genes due to

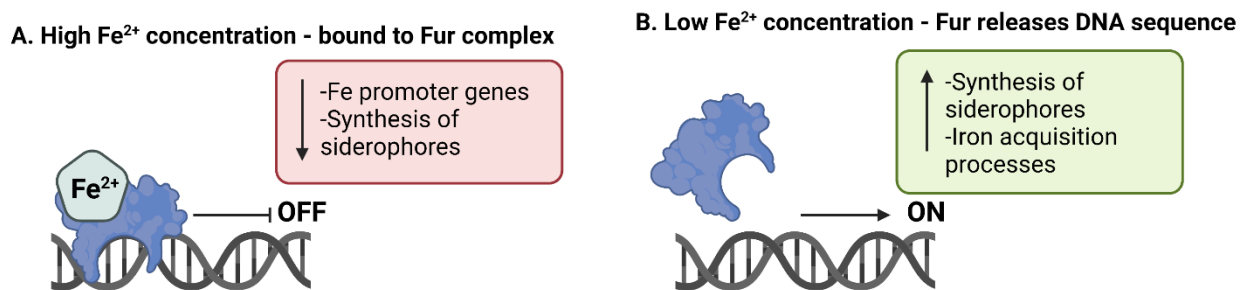


Figure 1.18 (A) Cartoon depiction of how Fur represses production of iron promoter genes in the presence of Fe²⁺ **(B)** Cartoon depiction of how Fur releases the DNA sequence during Fe²⁺ limited environments thereby promoting production of iron acquisition genes. This figure was made using BioRender.

its DNA-binding activity. When in the presence of excess Fe²⁺, Fur binds the divalent ion and forms a conformation that allows it to bind to its DNA sequence target thereby repressing the production of genes and operons that are related to iron acquisition (**Figure 1.18A**). This binding site complex is commonly referred to as the Fur box, or iron box. When Fe²⁺ concentrations are below normal range, the Fur-Fe(II) complex releases the ion which causes an allosteric conformation change thereby enabling the DNA sequence to be transcribed (**Figure 1.18B**). This then allows for the transcription of biosynthetic siderophore genes as well as other iron-related cellular processes to obtain the necessary mineral.

The release of Fur from the DNA sequence can promote the production of biosynthetic genes producing siderophores. Specifically, one way these small molecules are synthesized is through non-ribosomal peptide synthetases (NRPSs). Through this process, an assembly line of enzymes stitch together the small molecules through biological building blocks such as amino, carboxy, and hydroxy acids. Following the linkage of these, other enzymes in the NRPS pathway modify the linked product in order to produce the final siderophore. These substrate modifications are often carried out by modular domains such as adenylation, thiolation, and condensation.¹³⁵ Types of structural modifications can include cyclization of cysteine side chains into thiazoline heterocycles among others.¹³³ Additionally, siderophores can be synthesized independent of NRPSs. These most often are for hydroxamate and carboxylate type siderophores. The enzymes that synthesize these scaffolds are a diverse array of monooxygenases, amino acid ligases, aldolases, and others.

Once these molecules are fully synthesized, they are then prepared for secretion. The secretion of siderophores is an energy driven process mediated by efflux pumps.¹³³ These include the major facilitator superfamily (MFS); the resistance, nodulation, and cell division (RND) superfamily; and the ATP-binding cassette (ABC) superfamily.¹³⁵ The use of each efflux pump for excretion varies on the strain of bacteria and type of siderophore being excreted. Briefly, MFS transporters are a large superfamily that are able to act as uniports (excreting one molecule across a cell membrane), symports (excreting two molecules across a cell membrane), as well as antiports (excreting two molecules in opposite directions across the cell membrane). They exhibit a broad range of substrate specificity across the class including neurotransmitters, primary metabolites, organic and inorganic anions, and siderophores as well as iron-charged siderophores. These pumps generally have 12 α -helical transmembrane segments (TMSs) and are Fur-dependently controlled.

An example of an MFS-type transporter is LbtB: a 12TMS protein in *Legionella pneumophila* that is involved in secretion of legiobactin. Sequence conservancy across bacterial strains, though, are limited which hints at different specificities for siderophore types from strain to strain.

RND transporters, on the other hand, catalyze substrate efflux via an antiport mechanism. They can be used for several different types of substrates including various drug classes, heavy metals, lipids, pigments, and siderophores. They operate in concert with membrane fusion proteins (MFP) and outer membrane factors (OMF) in gram-negative strains to efflux substrates across the inner and outer membranes. An example of this is the efflux system MexA-MexB-OprM in *Pseudomonas aeruginosa*, which contains an RND efflux pump (MexB), an MFP (MexA), and an OMF (OprM).¹³⁵ This efflux system has been related to the excretion of pyoverdine, a siderophore and virulence factor of *P. aeruginosa*.

Lastly, the ABC transporters consist of both exporters and importers that enable transport via ATP hydrolysis without requiring protein phosphorylation.¹³⁵ Typically, they have four protein domains: two cytoplasmic domains that bind and hydrolyze ATP and two integral membrane domains. An example of this type of efflux pump is IdeR from *Mycobacterium smegmatis* that is responsible for exporting exochelin, a hydroxamate siderophore.

After secretion of the siderophore from the cell, the next step into finally acquiring iron is to uptake the siderophore-Fe(III) complex. The specific uptake of an iron loaded siderophore differs between gram-negative and gram-positive bacteria due to the added outer membrane of the former. For gram-negative strains, a β -barrel outer membrane receptor known as a TonB-dependent transporter (TBDT) is utilized to recognize the siderophore-Fe(III) complex, which undergoes a conformational change after engaging the complex.^{133,137} This conformational change, driven by a proton motive force, then translocates the complex into the periplasm. Within the

periplasm, the siderophore-Fe(III) complex is either further transported into the cytosol via an ABC importer, or the Fe(III) may be reduced to Fe(II) thereby releasing the ion from the complex and allowing it to diffuse into the cytosol. For gram-positive bacteria, because there is no outer membrane, the siderophore-Fe(III) complex is able to be transported directly into the cytosol via an ABC importer. Once in the cytosol, the Fe(III) can then be reduced to release it, or the siderophore may undergo hydrolysis to release the ion. Following release, siderophores may be recycled for further use in the cell.

1.2.1.B. Chalkophores

Iron ions are not the only essential metal that bacteria need to acquire from their environment, though its mechanism of acquisition is the most well understood. In recent years, interest has developed in exploring other metal acquisition mechanisms, one of which being copper ions. Copper (Cu) is an essential metal ion for both eukaryotic and prokaryotic cells. Most proteins within the bacterial cell interact with Cu only transiently as chaperone proteins, storage proteins, or transcriptional regulators.¹³⁸ However, Cu is an essential cofactor for many bacterial enzymes and catalyzes different cellular processes including superoxide dismutation and aerobic and anaerobic respiration.¹³⁸ Unlike Fe-dependent enzymes, most of the known cuproenzymes are located on the membrane, periplasmic space, or on the cell surface. This lack of cytosolic cuproenzymes may hint at the increased control of Cu by chaperones to avoid high levels of its reduced state, Cu(I), which has a high potential of producing ROS.

In comparison to iron, copper is a much more toxic metal when in excess. In fact, copper ions are employed by the innate immune system in fighting off bacterial infections within humans.¹³⁹ Specific copper utilization is still being investigated; however, it has been postulated

that phagocytes employ it to wield antibacterial properties. These antibacterial properties often involve overflowing the bacterial cell with copper

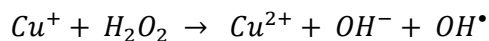


Figure 1.19 Example of a potential side reaction of Cu (I) leading to the production of reactive oxygen species. This reaction is analogous to Fenton reaction shown in section 1.2.1.A. with Fe.

ions to disrupt the cell's homeostasis. Cu exists almost exclusively as Cu(I) in the cytosol. However, Cu(I) is poised for electron transfer, and the redox reaction of the Cu(I)/ Cu(II) pair has a high redox potential (+ 160 mV) and is biologically accessible in the presence of oxygen (**Figure 1.19**). When coupled with the activity of the host's oxidase enzymes, which produce excess superoxide and nitrogen oxide species, Cu(I) can catalyze the redox cycle producing more reactive oxygen and nitrogen species. These ultimately lead to cell death through processes discussed in section 1.2.1.A.

Additionally, beyond a redox-dependent mechanism, Cu can also mismetalate when concentrations exceed normal range within the cell leading to disruption of protein function which can lead to cell death. The most well-known example of this is Cu(I) displacing Fe(II) from an iron-sulfur cluster.¹³⁹⁻¹⁴¹ The Fe-S cluster is an important redox active component in various bacterial enzymes that catalyze respiration, nitrogen fixation, and other vital processes.¹⁴² Therefore, disruption of this complex can have catastrophic effects on cellular survival.

Because of these potentially lethal repercussions of dysregulated Cu ion concentrations, bacterial cells have strict mechanisms to maintain homeostasis including detoxification systems if concentrations get too high. One of the most common proteins that aids in maintaining Cu(I) levels is a membrane bound ATPase named CopA.^{138,139,143} This protein can extrude excess Cu(I) from the cytoplasm and pumps it out into the extracellular matrix. It is controlled by the *copA* gene, which is regulated by Cu sensing transcription factors (e.g., CueR, CsoR, CopY).¹⁴⁴ These may

also promote transcription of Cu-chaperone proteins and Cu oxidases (CueO), which also aid in maintaining Cu ion homeostasis.

Although Cu detoxification is an important factor in homeostasis, it is also important to evaluate how bacteria acquire this essential mineral from their environment as well. These mechanisms are still quite limited in bacterial cells and more well understood in eukaryotic cells. However, most of the studies on import of Cu that have been done in bacteria focus on Gram-negative species. Therefore, description of these processes will focus on this class of bacteria. There are three main pathways that have been described as import systems of Cu. These include: porins, TonB-dependent importers, and chalkophores (“copper carriers”) (**Figure 1.20**). For porins, there have been a few studies that have shown aid in Cu uptake. For example, in *E. coli* it was shown that the outer membrane porins, OmpF and OmpC, played a role in Cu(II) uptake.^{138,145}

These types of porins have also been shown in mycobacterium, MspA and MspC, where knockout strains of these showed growth defects in Cu-limited media.^{138,146}

As for TonB-dependent importers, it's been shown that NosA, an outer membrane protein

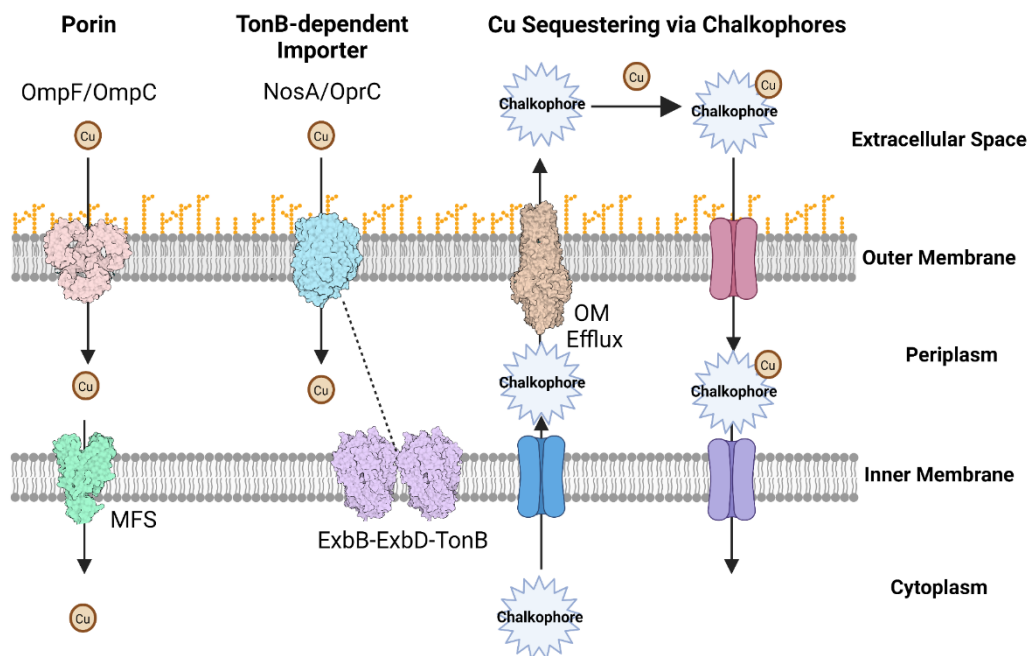


Figure 1.20 A visual representation of Cu transport across the outer and inner bacterial membranes. There are three main mechanisms utilized to import Cu into the cell: porins (OmpF/OmpC), TonB-dependent importers (NosA/OprC), and chalkophore sequestration. Dashed line indicates interaction of NosA/OprC interacting with the ExbB-ExbD-TonB complex. Structures shown were acquired from the protein database (PDB) and have the following IDs: 2OMF (OmpF porin from *E. coli*); 3WDO (MFS importer, YajR, from *E. coli*); 6Z9Y (OprC); 5ZFP (Hexameric complex of ExbB-ExbD-TonB complex); 1EK9 (TolC multidrug efflux and protein export). This figure was depicted using BioRender.

involved in the biogenesis of NosZ (a Cu-containing nitrous oxide reductase), also plays an important role in Cu uptake.^{138,147} This protein was identified in *Pseudomonas stutzeri*,¹⁴⁸ and shares homology with other known *E. coli* TonB-dependent importers. Although it shuttles Cu to NosZ, it has also been shown to generally import Cu to the periplasm as well. Another homologous TonB-dependent transporter is OprC found in *P. aeruginosa*.¹⁴⁹ This protein binds Cu(II) ($K_d = 2.6 \mu\text{M}$) and extrudes into the periplasm. Its synthesis and production is regulated by the Cu-dependent transcription factor CueR.^{138,150}

Both porins and TonB-dependent receptors are able to give access to Cu(II) directly into the periplasm. Once there, copper chaperones can then shuttle the ion to their necessary location. This may be to copper storage, or to inner membrane transporters to import the ion into the cytosol. Some of these importers are similar to previously discussed importers for iron in section 1.1.2.A. Additionally, there is a Cu specific importer, named CcoA, that is part of the major facilitator superfamily transporters that utilizes the proton gradient to extrude the ion across the membrane into the cytosol and was recently discovered from *Rhodobacter capsulatus*.^{138,151}

Beyond membrane-bound proteins that aid in the importation of Cu(II) across the inner and outer membrane, there are also small, organic molecules, similar to siderophores, that are excreted into the extracellular matrix to sequester this mineral. These small molecules are called chalkophores; derived from the Greek word “chalko” for copper.^{138,152} The most well-studied chalkophores are methanobactins (Mbns), which are peptidic, small molecules with nitrogen containing heterocycles and thioamide/ enethiol moieties that have specificity for Cu(I) and Cu(II) (**Figure 1.21**). Furthermore, Cu(II) is reduced to Cu(I) upon binding to Mbn through mechanisms that are yet to be understood. They are produced by methanotrophs, which utilize methane as its main carbon source and require Cu as a cofactor in their oxidase enzymes, specifically particulate methane monooxygenase (pMMO).^{152,153} The first structural characterization of these molecules began with the isolation from *Methylosinus trichosporium* OB3b in 2004, which led to the coining of the term chalkophore (**Figure 1.21**).^{152,154}

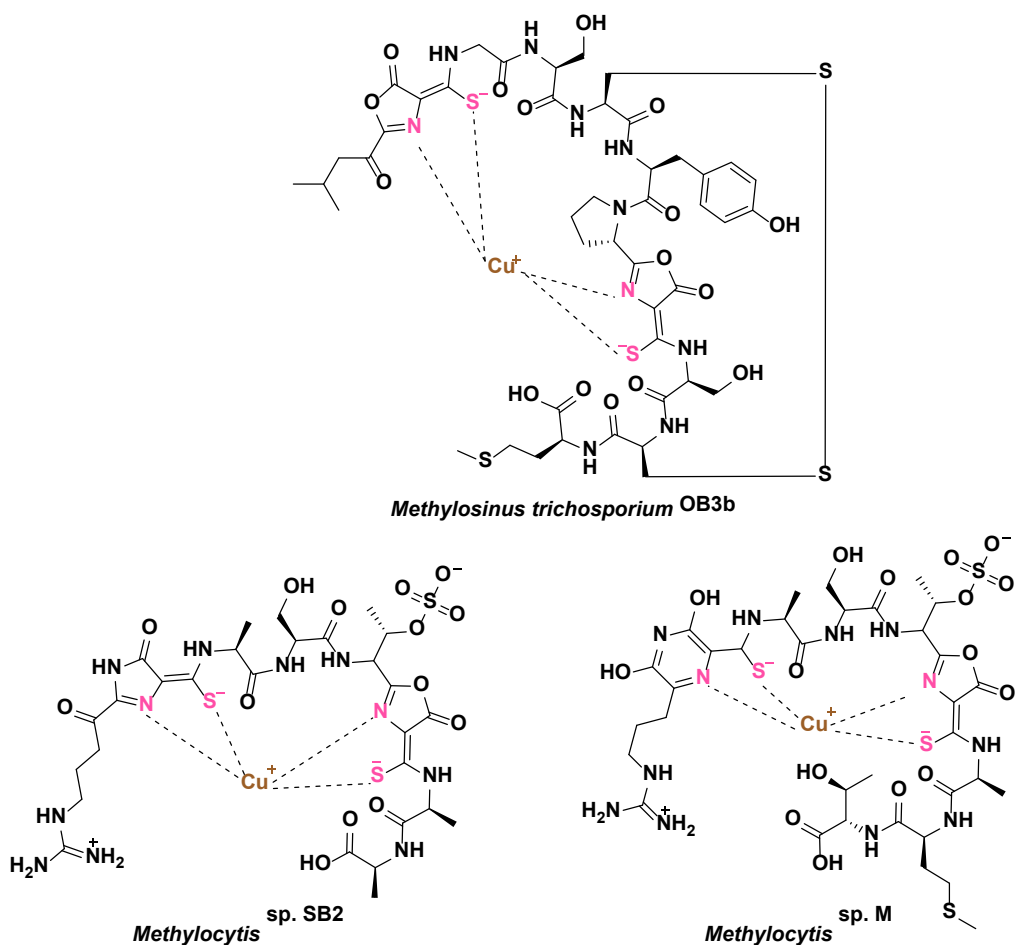


Figure 1.21 Example structures of methanobactins (Mbns). Top is a Mbn produced by *Methylosinus trichosporium* OB3b. It was the first Mbn isolated in 2004. Left is a Mbn produced by *Methylocytis* sp. SB2. Right is a Mbn produced by *Methylocytis* sp. M.

These molecules were initially hypothesized to be synthesized through NRPS like siderophores. However, after elucidation of a 30-amino acid, open reading frame in *Ms. trichosporium* OB3b in 2010 that encoded the peptidic backbone of Mbn, it was found that synthesis of these molecules followed ribosomally produced, posttranslationally modified natural products (RiPPs).^{155,156} The genes associated with this synthesis are *mbnABC* which are connected with all Mbn operons.

Following synthesis of these compounds, they are then secreted into the environment via the multidrug and toxic compound extrusion exporter, MbnM, which is a proton/ sodium antiporter.¹⁵⁶ Once in the extracellular matrix, Mbn can then exercise its high binding affinity to

Cu to extract it from other organic and biological environments. When the Cu is obtained, the Mbn-Cu complex is then ready for importation into the cell. This is driven by a TonB-dependent transporter, MbnT, that extrudes the complex into the periplasm. Further importation occurs through a similar importer on the inner membrane, MbnR, which imports the complex into the cytosol. Some complexes, though, can interact with the chaperone protein, MbnE, but its fate after binding is still unclear.¹⁵⁷ To finally release the Cu ion from the complex, similar mechanisms have been proposed related to siderophores in terms of oxidation from Cu(I) to Cu(II) to release the complex. However, because the Mbn can still bind Cu(II) and reduce it back to Cu(I), these hypotheses have been debated. However, there have been proteins (MbnH and MbnP) associated with the complex that may be capable of releasing the Cu in to the periplasmic space.

In addition to the class of Mbns, there are also a few other chalkophore molecules that have been disclosed, which includes coproporphyrin III and yersiniabactin (**Figure 1.22**). The former is excreted from *Paracoccus denitrificans* under copper-limited environments, indicated by the formation of a red pigment.¹⁵⁸ However, further analysis on how it is synthesized, excreted, and imported is still underway. The other known chalkophore, yersiniabactin (Ybt), is produced by *Yersinia pestis*, which is the causative agent of the bubonic plague.¹⁵² This species was noted as having siderophore capabilities in 1975¹⁵⁹ followed by structure elucidation of the metallophore, Ybt, in 1999.¹⁶⁰ It was originally classified as a siderophore, but it did not possess the canonical binding motifs

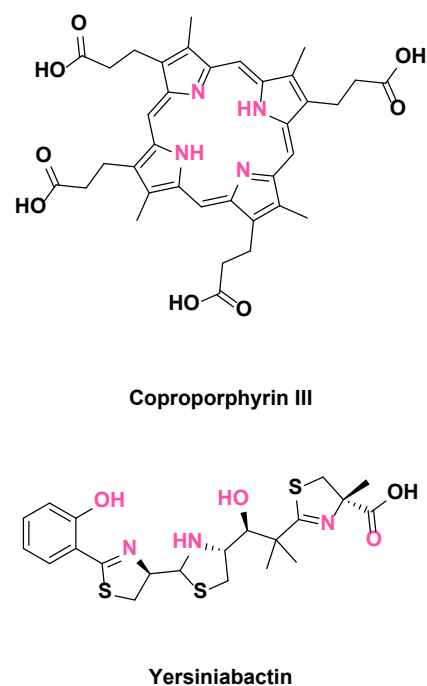


Figure 1.22 Structures of Coproporphyrin III (top) and Yersiniabactin (bottom). Atoms involved in binding Cu are highlight in pink.

seen in this class. However, it was shown that the thiazoline/thiazolidine binding groups played an important role in protecting the cell against Cu toxicity as it competitively binds Cu(II) and Fe(III), thereby preventing Cu(II) build up under host innate-immune response.¹⁶¹ Ybt is not the only metallophore with promiscuous activity towards other metals. There has been a collection of molecules classified as siderophores that have also shown ability to chelate Cu amongst other biologically relevant metal ions such as manganese, zinc, and others.¹³¹ In the case of binding Cu, though, the donor atoms in the molecule are often softer Lewis bases to account for the softer Lewis acidity of Cu in comparison to Fe.

1.2.2. Harnessing Metallophores as Antimicrobial Agents

As discussed above, bacteria and other species produce metallophores that are excreted to sequester necessary micronutrients such as iron and copper. This process is tightly regulated to ensure cell survival. However, if this regulatory system is disrupted it could lead to inhibition of growth, or cell death. To this end, there have been new strategies developed within the past decade to harness metallophore-like small molecules to disrupt bacterial growth and induce death. One of

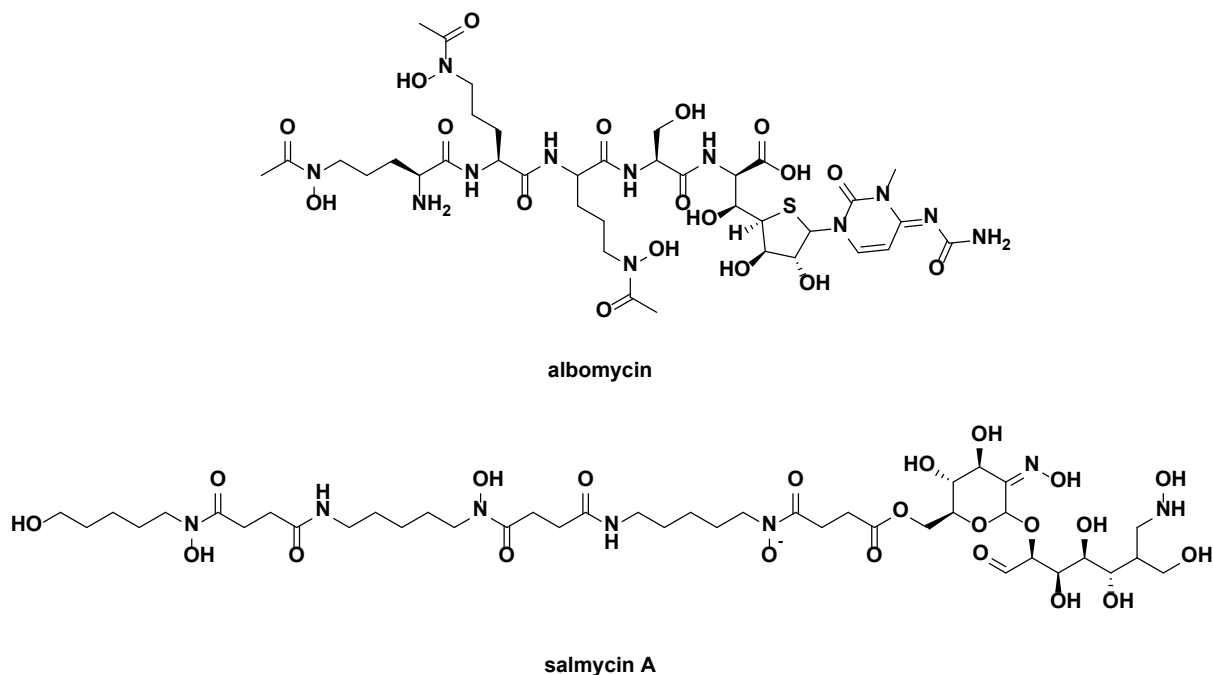


Figure 1.23 Structures of common sideromycins. Albomycin is active against Gram-negative bacteria, specifically *Enterobacteriaceae*. The hydroxamate moieties aid in its Fe^{3+} binding. Salmycin A contains the siderophore ferroxamine B (sidechain) to gain access to the cell and is active mainly against Gram-positive species.

the more well-understood processes is a Trojan Horse-type mechanism. This method utilizes an antibiotic small molecule that is covalently bonded to a metallophore. The most well-known Trojan-Horse example is sideromycins. These molecules contain a siderophore that is covalently linked to an antibiotic (**Figure 1.23**).¹⁶² These molecules are taken up by the cell through siderophore machinery where once inside the cell can induce its antibacterial properties.

Another approach to hijacking this process is through small molecules that can sequester these essential micronutrients away from the cell. To this end, there has been an immense interest in isonitrile small molecules that have shown the ability to not only bind copper and iron among other biologically relevant metal ions but also induce growth inhibition and even cell death in some cases.

1.2.2.A. Isonitriles – a New Class of Chalkophores to disrupt Metal Homeostasis

Isonitriles or isocyanides are organic functional groups that contain a nitrogen-carbon triple bond ($R - N^+ \equiv C^-$) with a stable divalent carbon and a quaternized, cationic nitrogen that connects to the organic framework.¹⁶³ It exists in two main resonance forms: one with the triple bond and formal split charges, and the other with a double bond exhibiting carbenoid character. The latter resonance form is responsible for the zwitterionic character of this functional

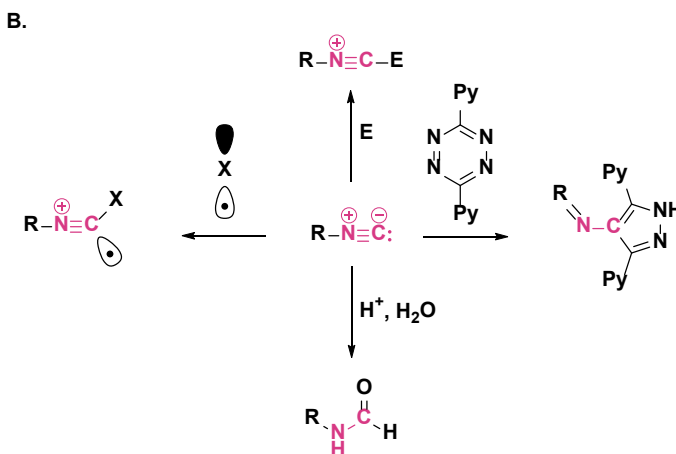
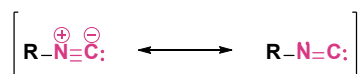


Figure 1.24 A) Main resonance forms of isonitriles. The carbenoid structure is responsible for the zwitterionic character of the functional group. B) General reaction schemes of isonitrile reactivity. Top: nucleophilic reactivity, E = generic electrophile; Right: [4+1] cycloaddition; Bottom: electrophilic reactivity; Left: radical acceptor.

group (**Figure 1.24 A**). They were first discovered by von W. Lieke in 1859¹⁶⁴ and since then, have garnered immense synthetic interest. This is due in part to the ability of the carbon atom to take on different roles within reaction systems. These include nucleophilic substitution to activated electrophiles and carbene-like reactivity in [4+1] cycloadditions, electrophiles, and radical acceptors (**Figure 1.24 B**).¹⁶⁵ In addition to its reactivity, the lone pair on carbon also aids in its ability to bind to metals leading to its use as ligands in metal catalysis.¹⁶⁶

Though it is isoelectronic to carbon monoxide, it displays vastly different coordination bonds. It has been shown that in metalated isonitriles both the nitrogen and carbon are able to act as π -hole acceptors to accept electron density from other atoms. In this interaction, the nitrogen acts through longer, electrostatic interactions whereas the carbon forms a shorter, charge-transfer complex with the metal center.¹⁶⁷ Interestingly, isonitriles can act as σ -donors as well as π -

acceptors, which allows them to bind various oxidation states of metals. The π -acceptor characteristics are further enhanced and form stronger bonds to the metal with aromatic isonitriles in comparison to aliphatics due to back donation from the aromatic system.¹⁶⁵ These reactivity characteristics of this functional group may aid in biological activity of the class of molecules that contain them. Additionally, isonitriles have lipophilic character that is matched with a large dipole moment like that of nitriles ($R - C \equiv N$). This allows for favorable interactions within the binding pocket of proteins and can help stabilize charged metalloproteins. They can also form hydrogen bonds through the terminal carbon, which may provide stabilizing interactions.¹⁶⁵

Naturally produced isonitriles were first discovered with the isolation of xanthocillin X from *Penicillium notatum* in the 1950s by Rothe and co-workers.^{165,168} Since then, hundreds of secondary metabolites have been identified from bacteria, cyanobacteria, fungi, and marine sponges. The ecological role of these natural products is still being investigated across the species that excrete them, but they have shown intriguing antifungal, antibacterial, and antiprotozoal activities. To gain further insight into the role these compounds play for the producing species, analysis into their biological synthesis has been investigated in several species.

One of the first biological pathways is late-stage functionalization via insertion of an isocyano group near the end of the natural product synthesis. This type of pathway is most often utilized for marine terpene-isocyanides and was first identified by Professor Mary Garson in her work uncovering the biosynthesis of 7,20-diisocyanoadocian.^{169,170} Through this mechanism, hydrogen cyanide produced via a dehydrogenase within the cell can intercept a tertiary carbocation of a sesquiterpene through an enzyme mediated mechanism thereby installing the isonitrile

(Figure 1.25 A). This pathway has also been identified for the synthesis of the isocyanopopokeananes.^{171,172}

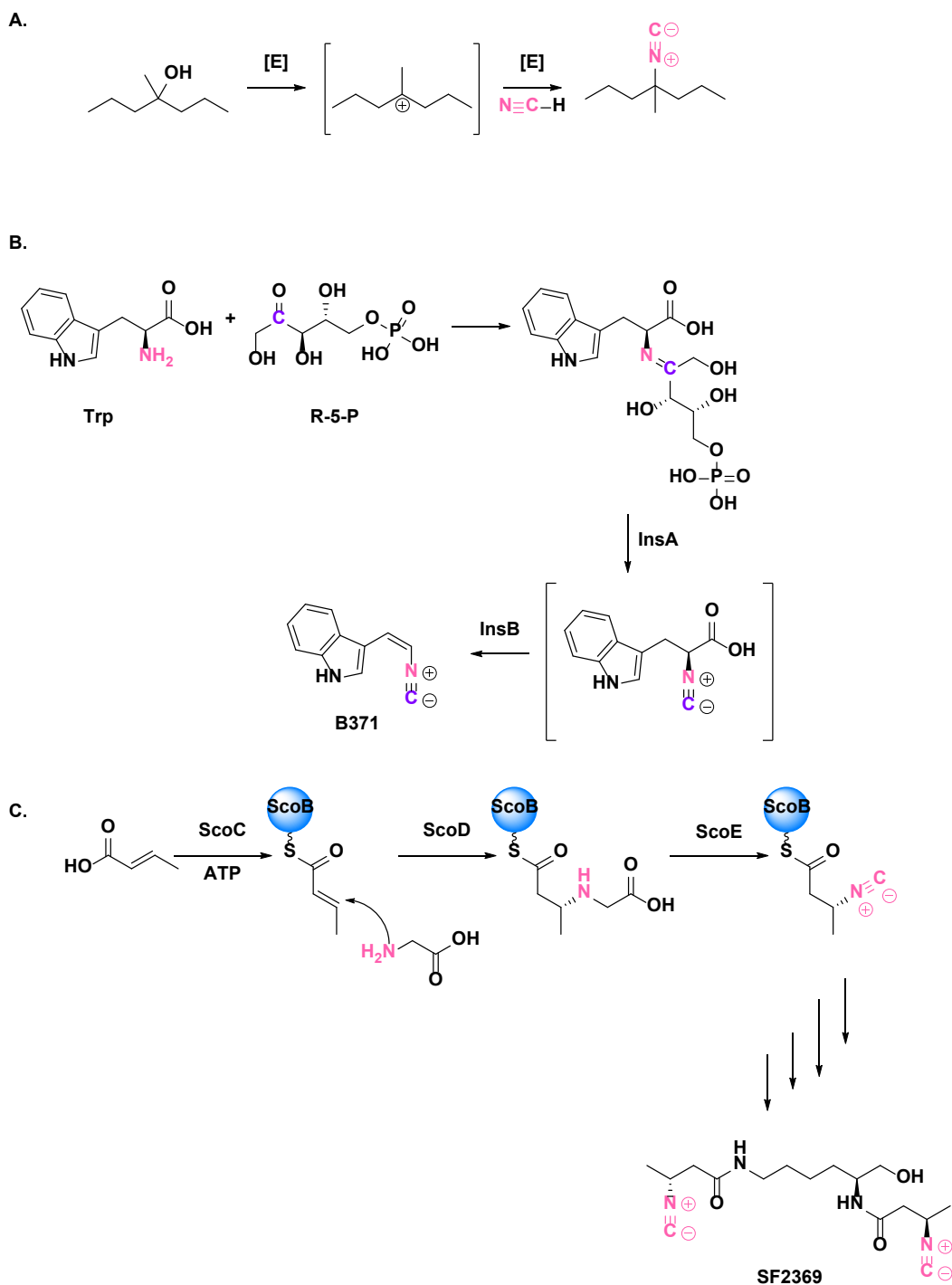


Figure 1.25 A) Representative mechanism for marine terpene-isocyanide installation. [E] = enzyme. B) Proposed biosynthetic mechanism to form B371. Trp = tryptophan; R-5-P = ribulose-5-phosphate. C) Proposed biosynthesis mechanism of SF2369.

The next pathway involved in isonitrile biosynthesis involves early-stage functionalization via manipulation of the nitrogen atom of amino acids, especially tyrosine and tryptophan. These pathways are most often found in fungi and bacteria. An example of this pathway is through the indole antibiotic B371 (**Figure 1.25 B**). The enzymes involved in this pathway are an isocyanide synthase (InsA) and a 2-oxoglutarate dependent oxygenase (InsB), which are produced by the genes *insA* and *insB* respectively.¹⁷³ Through this pathway, tryptophan reacts with ribulose-5-phosphate via a condensation reaction to form an imine.¹⁷⁴ This then undergoes a decarboxylation via an iron-mediated mechanism to obtain the final product. A similar mechanism occurs with tyrosine derived isonitrile natural products.

The last currently known biosynthetic pathway was discovered in the synthesis of SF2369, one of the linear analogs to SF2768, in which the isonitrile is derived from glycine.¹⁷⁵ Through this pathway, the nonheme iron(II) mediated α -ketoglutarate decarboxylase, ScoE, catalyzes the oxidative decarboxylation to form the isonitrile (**Figure 1.25 C**).

Beyond biosynthesis of isonitriles, their broad biological activities have also sparked interest. Briefly, a few notable isonitrile natural products and their biological activities are discussed herein. As noted, one of the first isonitrile natural products was xanthocillin X. This compound possesses potent broad-spectrum antibacterial activity as well as antifungal activity. After its discovery, it was used as a topical antibiotic under the drug name Brevicid for 15 years.¹⁷⁶ Recently, its mechanism of action was disclosed by Sieber and co-workers at the Technical University of Munich.¹⁷⁷ In generating resistant *A. baumannii* mutants, the authors identified a mutation in the enzyme porphobilinogen synthase (PbgS), which is essential for heme biosynthesis. Coupled with their genomic and proteomic data, the authors were able to identify that xanthocillin X inhibits *A. baumannii* via sequestering heme, which ultimately leads to

uncontrolled heme biosynthesis and elevated porphyrin levels. This culminates in dysregulation of several vital cellular pathways as well as production of reactive oxygen species which ultimately results in cell death.

Another well-known class of isonitriles are the kalihinols which contain more than 50

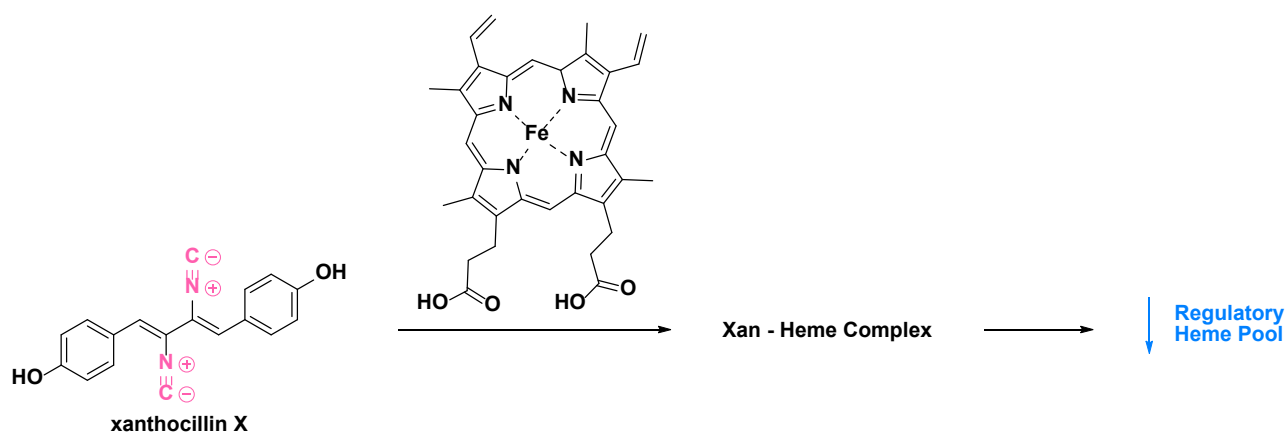


Figure 1.26 Xanthocillin X was shown to bind heme within *A. baumannii*, thereby reducing the regulatory heme pool in the cell. This leads to disruption of other cellular processes, which leads to production of reactive oxygen species and disruption of cellular growth.

compounds isolated from an *Acanthella* marine sponge (**Figure 1.27**). This class shows a broad

spectrum of biological activity. For example, one of the most potent analogs in the class is kalihinol A, which has shown a broad range of activity against numerous species. Briefly, it has potent antifouling activity ($EC_{50} = 0.087 \mu\text{g/mL}$) against *Balanus amphitrite*.¹⁷⁸

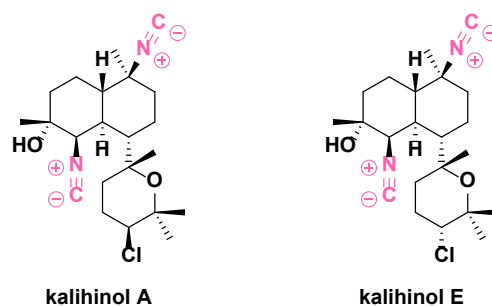


Figure 1.27 Structure of kalihinol A and E.

Additionally, it showed antimalarial activity against

*Plasmodium falciparum*¹⁷⁹ ($EC_{50} = 1.2\text{nM}$) as well as antibacterial activity against *Bacillus subtilis*, *Staphylococcus aureus* and antifungal activity against *Candida albicans*.^{180,181} In the case of its antibacterial activity, a proposed mechanism of action that has been described is the disruption of the bacterial folate biosynthesis.¹⁸² Though further analysis into its mechanism of

action against other biological systems is needed, it has been shown that the isonitrile is pivotal to its activity.

1.2.3.: Conclusions

Metal ions are essential to all living organisms. Specifically, bacteria utilize metal ions to catalyze various cellular reactions as well as stabilize protein and enzyme structure. Although metal ions are essential, they can also cause catastrophic results if not held within homeostatic concentrations. Because of this, bacteria utilize strict regulation systems to maintain metal homeostasis. One specific method utilized to increase metal ion uptake is through the excretion of metallophores. These are small molecules that can specifically chelate or bind metal ions within the environment and shuttle them to the cell. Two types of metallophores are siderophores (iron-binding small molecules) and chalkophores (copper-binding small molecules).

Although metallophores are helpful for cellular growth, their regulatory systems can also be hijacked to induce inhibition of cellular growth or induce death. There are two ways to do this. First, utilizing Trojan Horse-type mechanisms which utilize metallophore uptake machinery to gain access to the cell prior to inducing cell death. An example of this strategy is sideromycin molecules. Additionally, isonitrile molecules have gained interest in this area due to their ability to bind not only copper and iron but also heme. Through this process, they can sequester these necessary minerals in order to inhibit cell growth. Although there have been studies analyzing the impact of metal-binding molecules and their antibacterial activity. The question remains if the binding to the metal ion is required for the inhibitory activity, or how the molecules access the bacterial cell especially in the case for Gram-negative targeting compounds.

Chapter 1 References

1. Schrank, C. L., Wilt, I. K., Monteagudo Ortiz, C., Haney, B. A. & Wuest, W. M. Using membrane perturbing small molecules to target chronic persistent infections. *RSC Medicinal Chemistry* vol. 12 1312–1324 (2021).
2. O’Neill, J. *Antimicrobial Resistance : Tackling a crisis for the health and wealth of nations. Review on Antimicrobial Resistance* (2016).
3. CDC. Biggest Threats and Data | Antibiotic/Antimicrobial Resistance | CDC. 2019 1 (2019).
4. Pendleton, J. N., Gorman, S. P. & Gilmore, B. F. Clinical relevance of the ESKAPE pathogens. *Expert Rev. Anti. Infect. Ther.* **11**, 297–308 (2013).
5. Butler, M. S., Blaskovich, M. A. & Cooper, M. A. Antibiotics in the clinical pipeline at the end of 2015. *Journal of Antibiotics* vol. 70 3–24 (2017).
6. Rex, J. H. *et al.* A comprehensive regulatory framework to address the unmet need for new antibacterial treatments. *Lancet Infect. Dis.* **13**, 269–275 (2013).
7. Towse, A. *et al.* Time for a change in how new antibiotics are reimbursed: Development of an insurance framework for funding new antibiotics based on a policy of risk mitigation. *Health Policy (New. York)*. **121**, 1025–1030 (2017).
8. De Oliveira, D. M. P. *et al.* Antimicrobial resistance in ESKAPE pathogens. *Clin. Microbiol. Rev.* **33**, e00181-19 (2020).
9. Clardy, J., Fischbach, M. A. & Currie, C. R. The natural history of antibiotics. *Current Biology* vol. 19 R437 (2009).

10. Scheffler, R. J., Colmer, S., Tynan, H., Demain, A. L. & Gullo, V. P. Antimicrobials, drug discovery, and genome mining. *Applied Microbiology and Biotechnology* vol. 97 969–978 (2013).
11. Dever, L. A. & Dermody, T. S. Mechanisms of Bacterial Resistance to Antibiotics. *Arch. Intern. Med.* **151**, 886–895 (1991).
12. Lambert, P. A. Bacterial resistance to antibiotics: Modified target sites. *Advanced Drug Delivery Reviews* vol. 57 1471–1485 (2005).
13. Wright, G. D. Bacterial resistance to antibiotics: Enzymatic degradation and modification. *Advanced Drug Delivery Reviews* vol. 57 1451–1470 (2005).
14. Schroeder, J. W., Yeesin, P., Simmons, L. A. & Wang, J. D. Sources of spontaneous mutagenesis in bacteria. *Crit. Rev. Biochem. Mol. Biol.* **53**, 29–48 (2018).
15. Davies, J. Origins and evolution of antibiotic resistance. *Microbiologia* **12**, 9–16 (1996).
16. Andam, C. P., Fournier, G. P. & Gogarten, J. P. Multilevel populations and the evolution of antibiotic resistance through horizontal gene transfer. *FEMS Microbiol. Rev.* **35**, 756–767 (2011).
17. Von Wintersdorff, C. J. H. *et al.* Dissemination of antimicrobial resistance in microbial ecosystems through horizontal gene transfer. *Front. Microbiol.* **7**, 173 (2016).
18. Lewis, K. Persister cells. *Annual Review of Microbiology* vol. 64 357–372 (2010).
19. Brauner, A., Fridman, O., Gefen, O. & Balaban, N. Q. Distinguishing between resistance, tolerance and persistence to antibiotic treatment. *Nature Reviews Microbiology* vol. 14 320–330 (2016).

20. van den Bergh, B., Fauvart, M. & Michiels, J. Formation, physiology, ecology, evolution and clinical importance of bacterial persisters. *FEMS Microbiology Reviews* (2017) doi:10.1093/femsre/fux001.
21. Lewis, K. Persister Cells: Molecular Mechanisms Related to Antibiotic Tolerance. in 121–133 (Springer, Berlin, Heidelberg, 2012). doi:10.1007/978-3-642-28951-4_8.
22. Hurdle, J. G., O'Neill, A. J., Chopra, I. & Lee, R. E. Targeting bacterial membrane function: An underexploited mechanism for treating persistent infections. *Nature Reviews Microbiology* vol. 9 62–75 (2011).
23. McKeegan, K. S., Borges-Walmsley, M. I. & Walmsley, A. R. Microbial and viral drug resistance mechanisms. *Trends Microbiol.* **10**, S8–S14 (2002).
24. Wilmaerts, D., Windels, E. M., Verstraeten, N. & Michiels, J. General Mechanisms Leading to Persister Formation and Awakening. *Trends Genet.* **35**, 401–411 (2019).
25. Windels, E. M., Michiels, J. E., van den Bergh, B., Fauvart, M. & Michiels, J. Antibiotics: Combatting tolerance to stop resistance. *MBio* **10**, (2019).
26. Handwerger, S. & Tomasz, A. Antibiotic Tolerance Among Clinical Isolates of Bacteria. *Annu. Rev. Pharmacol. Toxicol.* **25**, 349–380 (1985).
27. Horne, D. & Tomasz, A. Tolerant response of *Streptococcus sanguis* to beta-lactams and other cell wall inhibitors. *Antimicrob. Agents Chemother.* (1977) doi:10.1128/AAC.11.5.888.
28. Bigger, J. W. Treatment of Staphylococcal Infections with Penicillin by Intermittent Sterilisation. *Lancet* 497–500 (1944).

29. Black, D. S., Irwin, B. & Moyed, H. S. Autoregulation of hip, an operon that affects lethality due to inhibition of peptidoglycan or DNA synthesis. *J. Bacteriol.* **176**, 4081–4091 (1994).
30. Moyed, H. S. & Bertrand, K. P. hipA, a newly recognized gene of Escherichia coli K-12 that affects frequency of persistence after inhibition of murein synthesis. *J. Bacteriol.* **155**, 768–775 (1983).
31. Maisonneuve, E. & Gerdes, K. Molecular mechanisms underlying bacterial persisters. *Cell* vol. 157 539–548 (2014).
32. Balaban, N. Q. & Liu, J. Evolution under antibiotic treatments: Interplay between antibiotic persistence, tolerance, and resistance. in *Persister Cells and Infectious Disease* 1–17 (Springer International Publishing, 2019). doi:10.1007/978-3-030-25241-0_1.
33. Harms, A., Brodersen, D. E., Mitarai, N. & Gerdes, K. Toxins, Targets, and Triggers: An Overview of Toxin-Antitoxin Biology. *Molecular Cell* vol. 70 768–784 (2018).
34. Defraigne, V., Fauvart, M. & Michiels, J. Fighting bacterial persistence: Current and emerging anti-persister strategies and therapeutics. *Drug Resistance Updates* vol. 38 12–26 (2018).
35. Kim, W., Escobar, I., Fuchs, B. B. & Mylonakis, E. Antimicrobial drug discovery against persisters. in *Persister Cells and Infectious Disease* vol. 1 273–295 (Springer International Publishing, 2019).
36. Dawson, C. C., Intapa, C. & Jabra-Rizk, M. A. “Persisters”: Survival at the Cellular Level. *PLoS Pathog.* **7**, e1002121 (2011).

37. Zhang, Y. Persisters, persistent infections and the Yin–Yang model. *Emerg. Microbes Infect.* **3**, 1–10 (2014).
38. Keren, I., Shah, D., Spoering, A., Kaldalu, N. & Lewis, K. Specialized persister cells and the mechanism of multidrug tolerance in *Escherichia coli*. *J. Bacteriol.* **186**, 8172–8180 (2004).
39. Kaldalu, N., Hauryliuk, V. & Tenson, T. Persisters—as elusive as ever. *Applied Microbiology and Biotechnology* vol. 100 6545–6553 (2016).
40. Równicki, M., Lasek, R., Trylska, J. & Bartosik, D. Targeting Type II Toxin–Antitoxin Systems as Antibacterial Strategies. *Toxins (Basel)*. **12**, 568 (2020).
41. Fisher, R. A., Gollan, B. & Helaine, S. Persistent bacterial infections and persister cells. *Nature Reviews Microbiology* vol. 15 453–464 (2017).
42. Balaban, N. Q. *et al.* Definitions and guidelines for research on antibiotic persistence. *Nat. Rev. Microbiol.* **17**, 441–448 (2019).
43. Tuomanen, E., Durack, D. T. & Tomasz, A. Antibiotic tolerance among clinical isolates of bacteria. *Antimicrobial Agents and Chemotherapy* (1986) doi:10.1128/AAC.30.4.521.
44. Wood, T. K. & Song, S. Forming and waking dormant cells: The ppGpp ribosome dimerization persister model. *Biofilm* **2**, 100036 (2020).
45. Goormaghtigh, F. *et al.* Reassessing the role of type II toxin-antitoxin systems in formation of *Escherichia coli* type II persister cells. *MBio* **9**, e00640-18 (2018).
46. Allison, K. R., Brynildsen, M. P. & Collins, J. J. Heterogeneous bacterial persisters and engineering approaches to eliminate them. *Current Opinion in Microbiology* vol. 14 593–

- 598 (2011).
47. Goormaghtigh, F. & Van Melderen, L. Single-cell imaging and characterization of *Escherichia coli* persister cells to ofloxacin in exponential cultures. *Sci. Adv.* **5**, 1–14 (2019).
 48. Roostalu, J., Jöers, A., Luidalepp, H., Kaldalu, N. & Tenson, T. Cell division in *Escherichia coli* cultures monitored at single cell resolution. (2008) doi:10.1186/1471-2180-8-68.
 49. Shah, D. *et al.* Persisters: a distinct physiological state of *E. coli*. (2006) doi:10.1186/1471-2180-6-53.
 50. Strahl, H. & Hamoen, L. W. Membrane potential is important for bacterial cell division. *Microbiol. Downloaded EMORY Univ. Libr. April* **107**, 2021 (2010).
 51. Kwan, B. W., Valenta, J. A., Benedik, M. J. & Wood, T. K. Arrested protein synthesis increases persister-like cell formation. *Antimicrob. Agents Chemother.* **57**, 1468–1473 (2013).
 52. Grassi, L. *et al.* Generation of persister cells of *Pseudomonas aeruginosa* and *Staphylococcus aureus* by chemical treatment and evaluation of their susceptibility to membrane-targeting agents. *Front. Microbiol.* **8**, 1917 (2017).
 53. Balaban, N. Q., Merrin, J., Chait, R., Kowalik, L. & Leibler, S. Bacterial persistence as a phenotypic switch. *Science (80-.)*. **305**, 1622–1625 (2004).
 54. Levin, B. R. Noninherited resistance to antibiotics. *Science (80-.)*. **305**, 1578–1579 (2004).

55. Pu, Y. *et al.* Enhanced Efflux Activity Facilitates Drug Tolerance in Dormant Bacterial Cells. *Mol. Cell* **62**, 284–294 (2016).
56. Gefen, O., Chekol, B., Strahilevitz, J. & Balaban, N. Q. TDtest: Easy detection of bacterial tolerance and persistence in clinical isolates by a modified disk-diffusion assay. *Sci. Rep.* **7**, 1–9 (2017).
57. Sohaskey, C. D. & Voskuil, M. I. In vitro models that utilize hypoxia to induce non-replicating persistence in mycobacteria. *Methods Mol. Biol.* **1285**, 201–213 (2015).
58. Vega, N. M., Allison, K. R., Khalil, A. S. & Collins, J. J. Signaling-mediated bacterial persister formation. *Nat. Chem. Biol.* **8**, 431–433 (2012).
59. Harms, A., Fino, C., Sørensen, M. A., Semsey, S. & Gerdes, K. Prophages and growth dynamics confound experimental results with antibiotic-tolerant persister cells. *MBio* **8**, e01964-17 (2017).
60. Song, S. & Wood, T. K. Are We Really Studying Persister Cells? doi:10.1111/1758-2229.12849.
61. Harms, A., Fino, C., Sørensen, M. A., Semsey, S. & Gerdes, K. Prophages and Growth Dynamics Confound Experimental Results with Antibiotic-Tolerant Persister Cells. (2017) doi:10.1128/mBio.01964-17.
62. Helaine, S. *et al.* Internalization of salmonella by macrophages induces formation of nonreplicating persisters. *Science (80-.)*. **343**, 204–208 (2014).
63. Mohiuddin, S. G., Hoang, T., Saba, A., Karki, P. & Orman, M. A. Identifying Metabolic Inhibitors to Reduce Bacterial Persistence. *Front. Microbiol.* **11**, 472 (2020).

64. Alumasa, J. N. *et al.* Ribosome Rescue Inhibitors Kill Actively Growing and Nonreplicating Persister Mycobacterium tuberculosis Cells. *ACS Infect. Dis.* **3**, 634–644 (2017).
65. Kim, J. S. *et al.* Selective killing of bacterial persisters by a single chemical compound without affecting normal antibiotic-sensitive cells. *Antimicrob. Agents Chemother.* **55**, 5380–5383 (2011).
66. Marques, C. N. H., Morozov, A., Planzos, P. & Zelaya, H. M. The fatty acid signaling molecule cis-2-decenoic acid increases metabolic activity and reverts persister cells to an antimicrobial-susceptible state. *Appl. Environ. Microbiol.* **80**, 6976–6991 (2014).
67. Silver, L. L. Challenges of antibacterial discovery. *Clin. Microbiol. Rev.* **24**, 71–109 (2011).
68. Ruhr, E. & Sahl, H. G. Mode of action of the peptide antibiotic nisin and influence on the membrane potential of whole cells and on cytoplasmic and artificial membrane vesicles. *Antimicrob. Agents Chemother.* **27**, 841–845 (1985).
69. Prince, A. *et al.* Lipid-II Independent Antimicrobial Mechanism of Nisin Depends on Its Crowding and Degree of Oligomerization. *Sci. Rep.* **6**, 37908 (2016).
70. Miller, W. R., Bayer, A. S. & Arias, C. A. Mechanism of action and resistance to daptomycin in Staphylococcus aureus and enterococci. *Cold Spring Harb. Perspect. Med.* **6**, a026997 (2016).
71. Salmelin, C., Hovinen, J. & Vilpo, J. Polymyxin permeabilization as a tool to investigate cytotoxicity of therapeutic aromatic alkylators in DNA repair-deficient Escherichia coli

- strains. *Mutat. Res. - Genet. Toxicol. Environ. Mutagen.* **467**, 129–138 (2000).
72. Zavascki, A. P., Goldani, L. Z., Li, J. & Nation, R. L. Polymyxin B for the treatment of multidrug-resistant pathogens: A critical review. *Journal of Antimicrobial Chemotherapy* 1206–1215 (2007) doi:10.1093/jac/dkm357.
73. Bialvaei, A. Z. & Samadi Kafil, H. Colistin, mechanisms and prevalence of resistance. *Curr. Med. Res. Opin.* **31**, 707–721 (2015).
74. McAuley, S., Huynh, A., Czarny, T. L., Brown, E. D. & Nodwell, J. R. Membrane activity profiling of small molecule: *B. subtilis* growth inhibitors utilizing novel dual-dye fluorescence assay. *Medchemcomm* **9**, 554–561 (2018).
75. Mingeot-Leclercq, M. P. & Décout, J. L. Bacterial lipid membranes as promising targets to fight antimicrobial resistance, molecular foundations and illustration through the renewal of aminoglycoside antibiotics and emergence of amphiphilic aminoglycosides. *MedChemComm* vol. 7 586–611 (2016).
76. Chen, H. *et al.* The Mycobacterial Membrane: A Novel Target Space for Anti-tubercular Drugs. *Front. Microbiol.* **9**, 1627 (2018).
77. Epanand, R. M., Walker, C., Epanand, R. F. & Magarvey, N. A. Molecular mechanisms of membrane targeting antibiotics. *Biochim. Biophys. Acta - Biomembr.* **1858**, 980–987 (2016).
78. Matsuzaki, K. Membrane permeabilization mechanisms. in *Advances in Experimental Medicine and Biology* vol. 1117 9–16 (Springer New York LLC, 2019).
79. te Winkel, J. D., Gray, D. A., Seistrup, K. H., Hamoen, L. W. & Strahl, H. Analysis of

- antimicrobial-triggered membrane depolarization using voltage sensitive dyes. *Front. Cell Dev. Biol.* **4**, 29 (2016).
80. Benarroch, J. M. & Asally, M. The Microbiologist's Guide to Membrane Potential Dynamics. *Trends in Microbiology* vol. 28 304–314 (2020).
 81. Strahl, H., Bürmann, F. & Hamoen, L. W. The actin homologue MreB organizes the bacterial cell membrane. *Nat. Commun.* **5**, (2014).
 82. Müller, A. *et al.* Daptomycin inhibits cell envelope synthesis by interfering with fluid membrane microdomains. doi:10.1073/pnas.1611173113.
 83. Kim, W. *et al.* Identification of an Antimicrobial Agent Effective against Methicillin-Resistant *Staphylococcus aureus* Persisters Using a Fluorescence-Based Screening Strategy. *PLoS One* **10**, e0127640 (2015).
 84. Kim, W. *et al.* A new class of synthetic retinoid antibiotics effective against bacterial persisters. *Nature* **556**, 103–107 (2018).
 85. Kim, W. *et al.* A selective membrane-targeting repurposed antibiotic with activity against persistent methicillin-resistant *Staphylococcus aureus*. *Proc. Natl. Acad. Sci. U. S. A.* **116**, 16529–16534 (2019).
 86. Kim, W. *et al.* Discovery and Optimization of nTZDpa as an Antibiotic Effective Against Bacterial Persisters. *ACS Infect. Dis.* **4**, 1540–1545 (2018).
 87. Mikłasińska-Majdanik, M., Kępa, M., Wojtyczka, R., Idzik, D. & Wąsik, T. Phenolic Compounds Diminish Antibiotic Resistance of *Staphylococcus Aureus* Clinical Strains. *Int. J. Environ. Res. Public Health* **15**, 2321 (2018).

88. Oh, E. & Jeon, B. Synergistic anti-Campylobacter jejuni activity of fluoroquinolone and macrolide antibiotics with phenolic compounds. *Front. Microbiol.* **6**, 1129 (2015).
89. Araya-Cloutier, C., Vincken, J. P., van Ederen, R., den Besten, H. M. W. & Gruppen, H. Rapid membrane permeabilization of *Listeria monocytogenes* and *Escherichia coli* induced by antibacterial prenylated phenolic compounds from legumes. *Food Chem.* **240**, 147–155 (2018).
90. Gerits, E. *et al.* Elucidation of the Mode of Action of a New Antibacterial Compound Active against *Staphylococcus aureus* and *Pseudomonas aeruginosa*. *PLoS One* **11**, e0155139 (2016).
91. Liebens, V. *et al.* Identification of 1-((2,4-dichlorophenethyl)amino)-3-phenoxypropan-2-ol, a novel antibacterial compound active against persisters of *pseudomonas aeruginosa*. *Antimicrob. Agents Chemother.* **61**, (2017).
92. Fauvart, M. & Michiels, J. 1-((2,4-Dichlorophenethyl)Amino)-3-Phenoxypropan-2-ol Kills *Pseudomonas aeruginosa* through Extensive Membrane Damage. *Front. Microbiol* **9**, 129 (2018).
93. Kim, J. S. & Wood, T. K. Persistent persister misperceptions. *Frontiers in Microbiology* vol. 7 2134 (2016).
94. Song, S. & Wood, T. K. Combatting Persister Cells With Substituted Indoles. *Frontiers in Microbiology* vol. 11 1565 (2020).
95. Yang, T. *et al.* Amphiphilic Indole Derivatives as Antimycobacterial Agents: Structure-Activity Relationships and Membrane Targeting Properties. *J. Med. Chem.* **60**, 2745–2763

- (2017).
96. Song, S., Gong, T., Yamasaki, R., Kim, J. & Wood, T. K. Identification of a potent indigoid persister antimicrobial by screening dormant cells. *Biotechnol. Bioeng.* **116**, 2263–2274 (2019).
 97. Martin, J. K. *et al.* A Dual-Mechanism Antibiotic Kills Gram-Negative Bacteria and Avoids Drug Resistance. *Cell* **181**, 1518-1532.e14 (2020).
 98. Gupta, N. *et al.* SCH79797 improves outcomes in experimental bacterial pneumonia by boosting neutrophil killing and direct antibiotic activity. *J. Antimicrob. Chemother.* **73**, 1586–1594 (2018).
 99. Gobbetti, T. *et al.* Serine protease inhibition reduces post-ischemic granulocyte recruitment in mouse intestine. *Am. J. Pathol.* **180**, 141–152 (2012).
 100. Strande, J. L. *et al.* SCH 79797, a selective PAR1 antagonist, limits myocardial ischemia/reperfusion injury in rat hearts. *Basic Res. Cardiol.* **102**, 350–358 (2007).
 101. Fjell, C. D., Hiss, J. A., Hancock, R. E. W. & Schneider, G. Designing antimicrobial peptides: Form follows function. *Nature Reviews Drug Discovery* vol. 11 37–51 (2012).
 102. Brogden, K. A. Antimicrobial peptides: Pore formers or metabolic inhibitors in bacteria? *Nature Reviews Microbiology* vol. 3 238–250 (2005).
 103. Hancock, R. E. W. & Sahl, H. G. Antimicrobial and host-defense peptides as new anti-infective therapeutic strategies. *Nature Biotechnology* vol. 24 1551–1557 (2006).
 104. Oppenheim, J. J. & Yang, D. Alarmins: Chemotactic activators of immune responses. *Current Opinion in Immunology* vol. 17 359–365 (2005).

105. Bowdish, D., Davidson, D. & Hancock, R. A Re-evaluation of the Role of Host Defence Peptides in Mammalian Immunity. *Curr. Protein Pept. Sci.* **6**, 35–51 (2005).
106. Yeaman, M. R. & Yount, N. Y. Mechanisms of antimicrobial peptide action and resistance. *Pharmacological Reviews* vol. 55 27–55 (2003).
107. Ghosh, C. *et al.* Small Molecular Antibacterial Peptoid Mimics: The Simpler the Better! (2014) doi:10.1021/jm401680a.
108. Ghosh, C. *et al.* Aryl-Alkyl-Lysines: Agents That Kill Planktonic Cells, Persister Cells, Biofilms of MRSA and Protect Mice from Skin-Infection. *PLoS One* **10**, e0144094 (2015).
109. Rajamuthiah, R. *et al.* Whole animal automated platform for drug discovery against multi-drug resistant staphylococcus aureus. *PLoS One* **9**, e89189 (2014).
110. Conery, A. L., Larkins-Ford, J., Ausubel, F. M. & Kirienko, N. V. High-throughput screening for novel anti-infectives using a *C. elegans* pathogenesis model. *Curr. Protoc. Chem. Biol.* **6**, 25–37 (2014).
111. Berger, J. P. *et al.* Distinct properties and advantages of a novel peroxisome proliferator-activated protein γ selective modulator. *Mol. Endocrinol.* **17**, 662–676 (2003).
112. Lewis, K. The Science of Antibiotic Discovery. *Cell* **181**, 29–45 (2020).
113. Schmitz, F. J. *et al.* The prevalence of aminoglycoside resistance and corresponding resistance genes in clinical isolates of staphylococci from 19 European hospitals. *J. Antimicrob. Chemother.* **43**, 253–259 (1999).
114. Cheng, A. V., Kim, W., Escobar, I. E., Mylonakis, E. & Wuest, W. M. Structure–Activity

- Relationship and Anticancer Profile of Second-Generation Anti-MRSA Synthetic Retinoids. *ACS Med. Chem. Lett.* 5–9 (2019) doi:10.1021/acsmchemlett.9b00159.
115. Cheng, A. V., Schrank, C. L., Escobar, I. E., Mylonakis, E. & Wuest, W. M. Addition of ethylamines to the phenols of bithionol and synthetic retinoids does not elicit activity in gram-negative bacteria. *Bioorganic Med. Chem. Lett.* **30**, 127099 (2020).
116. Haney, B. A., Schrank, C. L. & Wuest, W. M. Synthesis and biological evaluation of an antibacterial azaborine retinoid isostere. *Tetrahedron Lett.* 152667 (2020) doi:10.1016/j.tetlet.2020.152667.
117. Barr, F. S., Collins, G. F. & Wyatt, L. G. Potentiation of the antimicrobial activity of bithionol. *J. Pharm. Sci.* **54**, 801–802 (1965).
118. Wang, X., Wang, Y., Geng, Y., Li, F. & Zheng, C. Isolation and purification of honokiol and magnolol from cortex *Magnoliae officinalis* by high-speed counter-current chromatography. *J. Chromatogr. A* **1036**, 171–175 (2004).
119. Solinski, A. E. *et al.* Honokiol-Inspired Analogs as Inhibitors of Oral Bacteria. *ACS Infect. Dis.* **4**, 118–122 (2018).
120. Ochoa, C. *et al.* A Bisphenolic Honokiol Analog Outcompetes Oral Antimicrobial Agent Cetylpyridinium Chloride via a Membrane-Associated Mechanism. *ACS Infect. Dis.* **6**, 74–79 (2020).
121. Andreini, C., Bertini, I., Cavallaro, G., Holliday, G. L. & Thornton, J. M. Metal ions in biological catalysis: From enzyme databases to general principles. *J. Biol. Inorg. Chem.* **13**, 1205–1218 (2008).

122. Begg, S. L. The role of metal ions in the virulence and viability of bacterial pathogens. *Biochemical Society Transactions* vol. 47 77–87 (2019).
123. Ma, Z., Jacobsen, F. E. & Giedroc, D. P. Coordination chemistry of bacterial metal transport and sensing. *Chem. Rev.* **109**, 4644–4681 (2009).
124. Hänsch, R. & Mendel, R. R. Physiological functions of mineral micronutrients (Cu, Zn, Mn, Fe, Ni, Mo, B, Cl). *Current Opinion in Plant Biology* vol. 12 259–266 (2009).
125. Chandrangsu, P., Rensing, C. & Helmann, J. D. Metal homeostasis and resistance in bacteria. *Nature Reviews Microbiology* vol. 15 338–350 (2017).
126. Smith, A. M. CHAPTER 1: Interaction of metal ions with proteins as a source of inspiration for biomimetic materials. in *RSC Smart Materials* vols 2015-Janua 1–31 (2015).
127. Bradley, J. M. *et al.* Bacterial iron detoxification at the molecular level. *J. Biol. Chem.* **295**, 17602–17623 (2020).
128. Touati, D. Iron and oxidative stress in bacteria. *Arch. Biochem. Biophys.* **373**, 1–6 (2000).
129. Waldron, K. J., Rutherford, J. C., Ford, D. & Robinson, N. J. Metalloproteins and metal sensing. *Nature* **460**, 823–830 (2009).
130. Andrews, S. C., Robinson, A. K. & Rodríguez-Quñones, F. Bacterial iron homeostasis. *FEMS Microbiol. Rev.* **27**, 215–237 (2003).
131. Johnstone, T. C. & Nolan, E. M. Beyond iron: Non-classical biological functions of bacterial siderophores. *Dalton Transactions* vol. 44 6320–6339 (2015).
132. Pandey, A. & Boros, E. Coordination Complexes to Combat Bacterial Infections: Recent

- Developments, Current Directions and Future Opportunities. *Chem. - A Eur. J.* **27**, 7340–7350 (2021).
133. Kramer, J., Özkaya, Ö. & Kümmerli, R. Bacterial siderophores in community and host interactions. *Nat. Rev. Microbiol.* **18**, 152–163 (2020).
 134. Kraemer, S. M., Duckworth, O. W., Harrington, J. M. & Schenkeveld, W. D. C. Metallophores and Trace Metal Biogeochemistry. *Aquat. Geochemistry* **21**, 159–195 (2015).
 135. Miethke, M. & Marahiel, M. A. Siderophore-Based Iron Acquisition and Pathogen Control. *Microbiol. Mol. Biol. Rev.* **71**, 413–451 (2007).
 136. Escolar, L., Pérez-Martín, J. & De Lorenzo, V. Opening the iron box: Transcriptional metalloregulation by the fur protein. *J. Bacteriol.* **181**, 6223–6229 (1999).
 137. Noinaj, N., Guillier, M., Barnard, T. J. & Buchanan, S. K. TonB-dependent transporters: Regulation, structure, and function. *Annu. Rev. Microbiol.* **64**, 43–60 (2010).
 138. Andrei, A. *et al.* Cu homeostasis in bacteria: The ins and outs. *Membranes (Basel)*. **10**, 1–45 (2020).
 139. Djoko, K. Y., Ong, C. L., Walker, M. J. & McEwan, A. G. The role of copper and zinc toxicity in innate immune defense against bacterial pathogens. *J. Biol. Chem.* **290**, 1854–1861 (2015).
 140. Macomber, L. & Imlay, J. A. The iron-sulfur clusters of dehydratases are primary intracellular targets of copper toxicity. *Proc. Natl. Acad. Sci. U. S. A.* **106**, 8344–8349 (2009).

141. Chillappagari, S. *et al.* Copper stress affects iron homeostasis by destabilizing iron-sulfur cluster formation in *Bacillus subtilis*. *J. Bacteriol.* **192**, 2512–2524 (2010).
142. Ayala-Castro, C., Saini, A. & Outten, F. W. Fe-S Cluster Assembly Pathways in Bacteria. *Microbiol. Mol. Biol. Rev.* **72**, 110–125 (2008).
143. Solioz, M., Odermatt, A. & Krapf, R. Copper pumping ATPases: Common concepts in bacteria and man. *FEBS Lett.* **346**, 44–47 (1994).
144. Quintana, J., Novoa-Aponte, L. & Argüello, J. M. Copper homeostasis networks in the bacterium *Pseudomonas aeruginosa*. *J. Biol. Chem.* **292**, 15691–15704 (2017).
145. Lutkenhaus, J. F. Role of a major outer membrane protein in *Escherichia coli*. *J. Bacteriol.* **131**, 631–637 (1977).
146. Speer, A., Rowland, J. L., Haeili, M., Niederweis, M. & Wolschendorf, F. Porins increase copper susceptibility of *Mycobacterium tuberculosis*. *J. Bacteriol.* **195**, 5133–5140 (2013).
147. Stewart, L. J. *et al.* Handling of nutrient copper in the bacterial envelope. *Metallomics* **11**, 50–63 (2019).
148. Lee, H. S., Abdelal, A. H. T., Clark, M. A. & Ingraham, J. L. Molecular characterization of *nosA*, a *Pseudomonas stutzeri* gene encoding an outer membrane protein required to make copper-containing N₂O reductase. *J. Bacteriol.* **173**, 5406–5413 (1991).
149. Yoneyama, H. & Nakae, T. Protein C (OprC) of the outer membrane of *Pseudomonas aeruginosa* is a copper-regulated channel protein. *Microbiology* **142**, 2137–2144 (1996).
150. Han, Y. *et al.* A *Pseudomonas aeruginosa* type VI secretion system regulated by CueR

- facilitates copper acquisition. *PLoS Pathog.* **15**, (2019).
151. Khalfaoui-Hassani, B. *et al.* Widespread distribution and functional specificity of the copper importer CcoA: Distinct Cu uptake routes for bacterial cytochrome c oxidases. *MBio* **9**, (2018).
 152. Kenney, G. E. & Rosenzweig, A. C. Chalkophores. *Annu. Rev. Biochem.* **87**, 645–676 (2018).
 153. Lieberman, R. L. & Rosenzweig, A. C. Crystal structure of a membrane-bound metalloenzyme that catalyses the biological oxidation of methane. *Nature* **434**, 177–182 (2005).
 154. Kim, H. J. *et al.* Methanobactin, a copper-acquisition compound from methane-oxidizing bacteria. *Science (80-.)*. **305**, 1612–1615 (2004).
 155. Stein, L. Y. *et al.* Genome sequence of the obligate methanotroph Methylosinus trichosporium strain OB3b. *J. Bacteriol.* **192**, 6497–6498 (2010).
 156. Kenney, G. E. & Rosenzweig, A. C. Genome mining for methanobactins. *BMC Biol.* **11**, 1–17 (2013).
 157. Dassama, L. M. K., Kenney, G. E., Ro, S. Y., Zielazinski, E. L. & Rosenzweig, A. C. Methanobactin transport machinery. *Proc. Natl. Acad. Sci. U. S. A.* **113**, 13027–13032 (2016).
 158. Anttila, J. *et al.* Is coproporphyrin III a copper-acquisition compound in *Paracoccus denitrificans*? *Biochim. Biophys. Acta - Bioenerg.* **1807**, 311–318 (2011).
 159. Wake, A., Misawa, M. & Matsui, A. Siderochrome production by *Yersinia pestis* and its

- relation to virulence. *Infect. Immun.* **12**, 1211–1213 (1975).
160. Perry, R. D., Balbo, P. B., Jones, H. A., Fetherston, J. D. & Demoll, E. Yersiniabactin from *Yersinia pestis*: Biochemical characterization of the siderophore and its role in iron transport and regulation. *Microbiology* **145**, 1181–1190 (1999).
161. Chaturvedi, K. S., Hung, C. S., Crowley, J. R., Stapleton, A. E. & Henderson, J. P. The siderophore yersiniabactin binds copper to protect pathogens during infection. *Nat. Chem. Biol.* **8**, 731–736 (2012).
162. Braun, V., Pramanik, A., Gwinner, T., Köberle, M. & Bohn, E. Sideromycins: Tools and antibiotics. *BioMetals* **22**, 3–13 (2009).
163. Méndez, Y., Vasco, A. V, Humpierre, A. R. & Westermann, B. Isonitriles: Versatile Handles for the Bioorthogonal Functionalization of Proteins. *ACS Omega* **5**, 25505–25510 (2020).
164. Lieke, W. Ueber das Cyanallyl. *Justus Liebigs Ann. Chem.* **112**, 316–321 (1859).
165. Massarotti, A., Brunelli, F., Aprile, S., Giustiniano, M. & Tron, G. C. Medicinal Chemistry of Isocyanides. *Chem. Rev.* **121**, 10742–10788 (2021).
166. Knorn, M., Lutsker, E. & Reiser, O. Isonitriles as supporting and non-innocent ligands in metal catalysis. *Chem. Soc. Rev.* **49**, 7730–7752 (2020).
167. Mikherdov, A. S. *et al.* (Isocyano group)···lone pair interactions involving coordinated isocyanides: Experimental, theoretical and CSD studies. *CrystEngComm* **22**, 1154–1159 (2020).
168. Rothe, W. Vorläufige Mitteilung über ein neues Antibiotikum. *Pharmazie* **5**, 190 (1950).

169. Garson, M. J. Biosynthesis of the novel diterpene isonitrile diisocyanoadociane by a marine sponge of the amphimedon genus: Incorporation studies with sodium [¹⁴C]cyanide and sodium [2-¹⁴C]acetate. *J. Chem. Soc. Chem. Commun.* **1**, 35–36 (1986).
170. Fookes, C. J. R., Garson, M. J., MacLeod, J. K., Skelton, B. W. & White, A. H. Biosynthesis of diisocyanoadociane, a novel diterpene from the marine sponge *Amphimedon* sp. crystal structure of a monoamide derivative. *J. Chem. Soc. Perkin Trans. I* 1003–1011 (1988) doi:10.1039/p19880001003.
171. Hagadone, M. R., Scheuer, P. J. & Holm, A. On the Origin of the Isocyanate Function in Marine Sponges. *J. Am. Chem. Soc.* **106**, 2447–2448 (1984).
172. Karuso, P., Poiner, A. & Scheuer, P. J. Isocyanoneopupukeanane, a New Tricyclic Sesquiterpene from a Sponge. *J. Org. Chem.* **54**, 2095–2097 (1989).
173. Chen, T. Y. *et al.* Current Understanding toward Isonitrile Group Biosynthesis and Mechanism. *Chinese J. Chem.* **39**, 463–472 (2021).
174. Brady, S. F. & Clardy, J. Systematic Investigation of the *Escherichia coli* Metabolome for the Biosynthetic Origin of an Isocyanide Carbon Atom. *Angew. Chemie Int. Ed.* **44**, 7045–7048 (2005).
175. Harris, N. C. *et al.* Biosynthesis of isonitrile lipopeptides by conserved nonribosomal peptide synthetase gene clusters in Actinobacteria. *Proc. Natl. Acad. Sci. U. S. A.* **114**, 7025–7030 (2017).
176. Rossmann, B. Die Auftrennung des Antibioticums Brevicid in seine Komponenten. *Fresenius' Zeitschrift für Anal. Chemie* 1967 2305 **230**, 398–398 (1967).

177. Hübner, I. *et al.* Broad Spectrum Antibiotic Xanthocillin X Effectively Kills *Acinetobacter baumannii* via Dysregulation of Heme Biosynthesis. *ACS Cent. Sci.* **7**, 488–498 (2021).
178. Okino, T., Yoshimura, E., Hirota, H. & Fusetani, N. Antifouling kalihinenes from the marine sponge *Acanthella cavernosa*. *Tetrahedron Lett.* **36**, 8637–8640 (1995).
179. Miyaoka, H. *et al.* Antimalarial activity of kalihinol A and new relative diterpenoids from the Okinawan sponge, *Acanthella* sp. *Tetrahedron* **54**, 13467–13474 (1998).
180. Chang, C. W. J. *et al.* Kalihinol-A, a Highly Functionalized Diisocyano Diterpenoid Antibiotic from a Sponge. *J. Am. Chem. Soc.* **106**, 4644–4646 (1984).
181. Patra, A. *et al.* An Unprecedented Triisocyano Diterpenoid Antibiotic from a Sponge. *J. Am. Chem. Soc.* **106**, 7981–7983 (1984).
182. Bugni, T. S. *et al.* Kalihinols from two *Acanthella cavernosa* sponges: inhibitors of bacterial folate biosynthesis. *Tetrahedron* **60**, 6981–6988 (2004).

Chapter 2: Structure-Activity-Relationship Campaign of the synthetic retinoid, CD437

2.1 Background

2.1.1. Repurposing CD437 as an Antibiotic

As mentioned in chapter 1, bacterial persistence is a commonly overlooked, but problematic evasion tactic bacteria utilize to avoid antibiotic induced death. Briefly, bacterial persistence is a phenotypic trait in which a subpopulation of the bacterial culture (<1%) becomes “dormant,” or metabolically inactive.^{1,2} In doing so, they are able to evade the killing power of common antibiotic mechanisms that rely on growth dependent processes (i.e., ATP-dependent enzymes, active efflux, etc). In recent years, there has been an increased interest in developing novel compounds that can target these elusive persister cells.

One avenue to develop and access such molecules is through drug repurposing. This involves evaluating already approved Food & Drug Association (FDA) molecules and applying them for something different than their original intended purpose. To this end, Dr. Eleftherios Mylonakis at Brown University and his lab developed an automated, high-throughput screen utilizing *Caenorhabditis elegans* as the animal model to

identify molecules that could be repurposed for the use of targeting both wild-type methicillin-resistant *Staphylococcus aureus* as well as persistent MRSA cells.³ In this screen, 15 adult, nematodes are placed in each well of a 384-well plate containing a buffer-media solution. They are then inoculated with *S. aureus* MW2 cell culture (**Fig 2.1**). Following infection, they are then

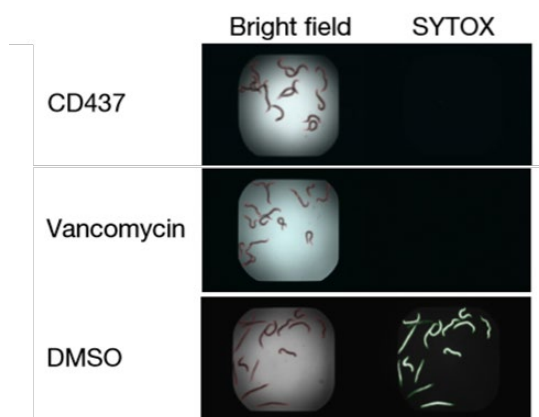
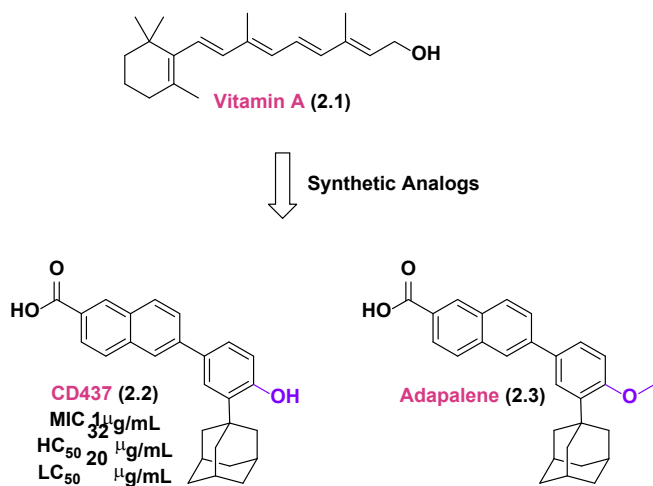


Figure 2.1. Images of MRSA-MW2-infected *C. elegans* in the presence of represented compounds.

treated with a panel of drug compounds to quickly assess the drug's potency and toxicity. After incubation, the wells were washed of any debris and then treated with SYTOX orange, a dye that stains nucleic acids in cells with compromised membranes which is indicative of cell death.⁴⁻⁶ Through this assay, dead *C. elegans* would fluoresce; indicating that either (1) the compound was ineffective at killing the MRSA cells leading to nematode death, or (2) the compound was toxic to the nematode resulting in death.

Through this HTS method, the Mylonakis lab was able to evaluate over 82,000 small, synthetic compounds and identified over 185 hits.⁷⁻¹¹ Of these hits, they further elucidated three lead compounds (CD437, bithionol, and nTZDpa) that showed potent activity against both MRSA and persistent-MRSA cells. Initial biological assays hinted at a potential, common mechanism in which the polar heads of the molecules engaged in hydrogen-bonding with the phosphate groups on the bacterial membrane surface followed by intercalation and membrane disruption. This discovery led to a collaboration with our laboratory that began in 2017 to undergo a structure-activity-relationship (SAR) campaign for each lead to identify their mechanism of action, essential molecule functionality, as well as a more potent compound. Specifically, I was tasked with



working on the CD437 project when I joined the Wuest laboratory in November 2018.

CD437 (2.2) is a synthetic retinoid that is part of a group of analogs of vitamin A (2.1, Figure 2.2). It is most closely related to adapalene (2.3), a common acne treatment, in which the methoxy group is replaced with a hydroxyl. This class of

Figure 2.2. Chemical structures of vitamin A (2.1), CD437 (2.2), and Adapalene (2.3). Structural difference between adapalene and CD437 are highlighted in purple.

retinoids have been shown to play an important role in eukaryotic cell growth regulation in both normal, malignant, and benign cells.^{12,13} Since its development in 1992, CD437 has been utilized as a test compound to analyze its effects on varying cancer cell lines to fully understand its mechanism of action (MoA). Briefly, in cancer cells, CD437 induces apoptosis through selective binding interactions with Retinoic Acid Receptor- γ (RAR γ), which ultimately leads to disruption in gene regulation and cell-induced death.¹³⁻¹⁶ Additionally, it has been shown that CD437's MoA can differ between cancer cell lines and can have both RAR γ -dependent and -independent apoptosis pathways. In the independent pathway, it aids in DNA adduct formation, which arrests the cell in the S-phase of the cell cycle.^{17,18} This arrest triggers a cell-damage response which is ultimately met with apoptosis. Although it has shown promising activity as a potential cancer treatment, it has not been formally approved by the Food and Drug Administration (FDA) and remains in the pipeline.

2.1.2 Analysis of CD437's Biological Activity

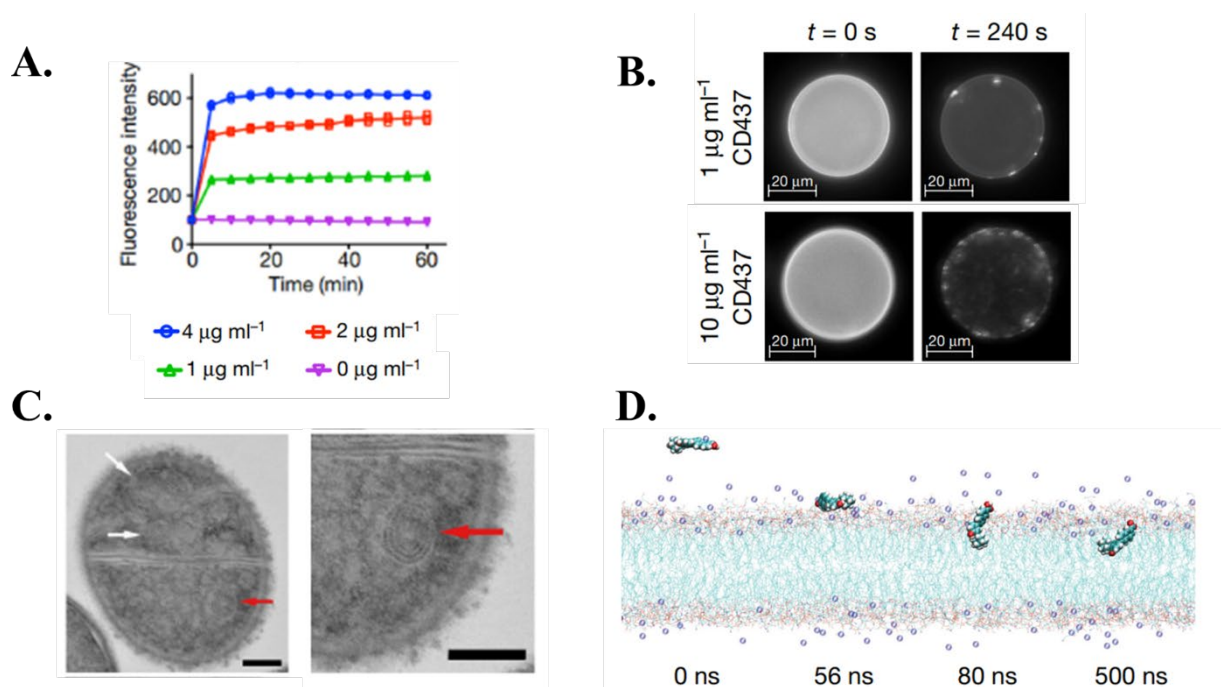


Figure 2.3. CD437 disrupts bacterial membranes. **A.** “Uptake of SYTOX Green (λ_{ex} =485nm, λ_{em} =525nm) by exponential phase *S. aureus* MW2 cells treated with CD437. **B.** Changes in giant unilamellar vesicles (DOPC:DOPG 7:3) labelled with 18:1 Liss Rhod PE (0.05%) treated with CD437 at 1µg/mL and 10µg/mL. **C.** Transmission electron micrographs showing mesosome-like structures. **D.** All-atom molecular dynamics simulation of CD437 interacting with a phospholipid membrane.” Adapted from 104 | N A T U R E | V O L 556 | 5 april 2018.

After the initial hit, the Mylonakis lab did further analysis of CD437 (2.2, Figure 2.2) and found it had a minimum inhibitory concentration (MIC) of 1 µg/mL against MRSA.⁹ In addition to its activity against wild-type MRSA cells, it also proved to be potent against persistent-MRSA cells. Furthermore, in a biological screen against a panel of bacteria, CD437 selectively targeted Gram-positive bacteria (*S. aureus* and *Enterococcus faecium*, two Gram-positive ESKAPE pathogens). To further analyze how this molecule may be inducing cell death, they performed a serial passage resistance assay over 100 days. Ultimately, CD437 yielded only putative resistant mutants in the MRSA MW2 strain. However, they were able to find mutations in the *graS*, *yibH*, and *manA* genes, all of which encode proteins related to membrane machinery hinting at a membrane mechanism. In concert, they performed a membrane permeabilization assay with SYTOX green, which is a dye impermeable to live cells but can penetrate membrane compromised

cells and fluoresces green when in contact with nucleic acids (**Figure 2.3**). Therefore, an increase in green fluorescence would indicate an increase in membrane permeabilization. When MRSA cells were treated with CD437, a concentration dependent green fluorescence increase was observed, indicating that CD437 was perturbing the membrane of the bacteria.

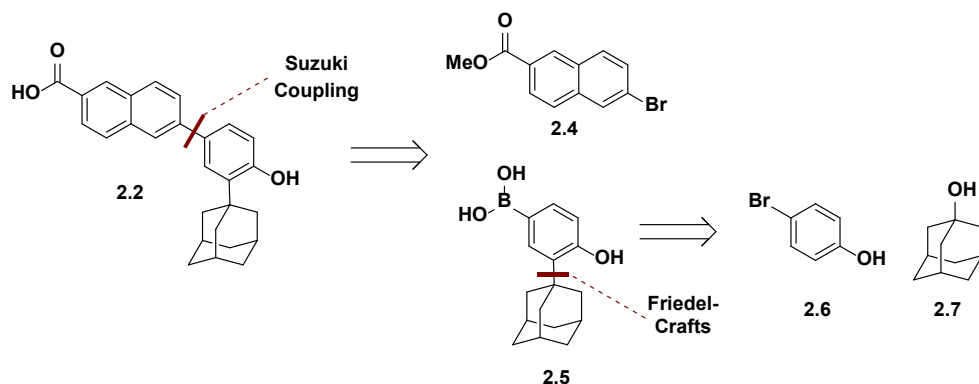
Furthering this hypothesis, the Mylonakis group also evaluated the cell morphology via transmission electron microscopy and noted mesosome-like structures formed in the presence of CD437. Additionally, they analyzed the membrane interaction of CD437 against biomembrane-mimicking giant, unilamellar vesicles. These synthetic vesicles fluoresce when their membrane is intact and will lose fluorescence as it becomes perturbed. In the presence of CD437, overtime the fluorescence of the vesicle decreased as well as became more mobile in structure indicating membrane perturbation. These results as well as the ones previously mentioned culminated into an all-atom molecular dynamics simulation. Through this simulation, the Mylonakis lab showed that CD437 was attracted to the bacterial membrane through hydrogen bonding interactions with the polar moieties of the molecule (alcohol and carboxylic acid) and the phosphate heads of the membrane. Upon anchoring to the membrane, CD437 then rotates, and the adamantyl group penetrates the lipid bilayer, disrupting the membrane. It should be noted that these simulations were performed using only one molecule of CD437 and a concert of molecules together may act differently *in cellulo*.

2.2 Results and Discussion

2.2.1 Generation One of CD437 Analogs¹⁹

Building on the biological elucidations from the Mylonakis lab, the Wuest lab worked to develop new analogs of CD437 to explore the activity scope of this class of molecules. These initial studies were performed by previous lab alumni, Dr. Andrew Steele and Dr. Colleen Keohane. The project goals from the synthetic standpoint were to develop a robust diverted

synthesis that could begin from cheap, commercially available starting materials.¹⁹ To this end, Keohane and Steele envisioned breaking the molecule into two parts via a Suzuki coupling



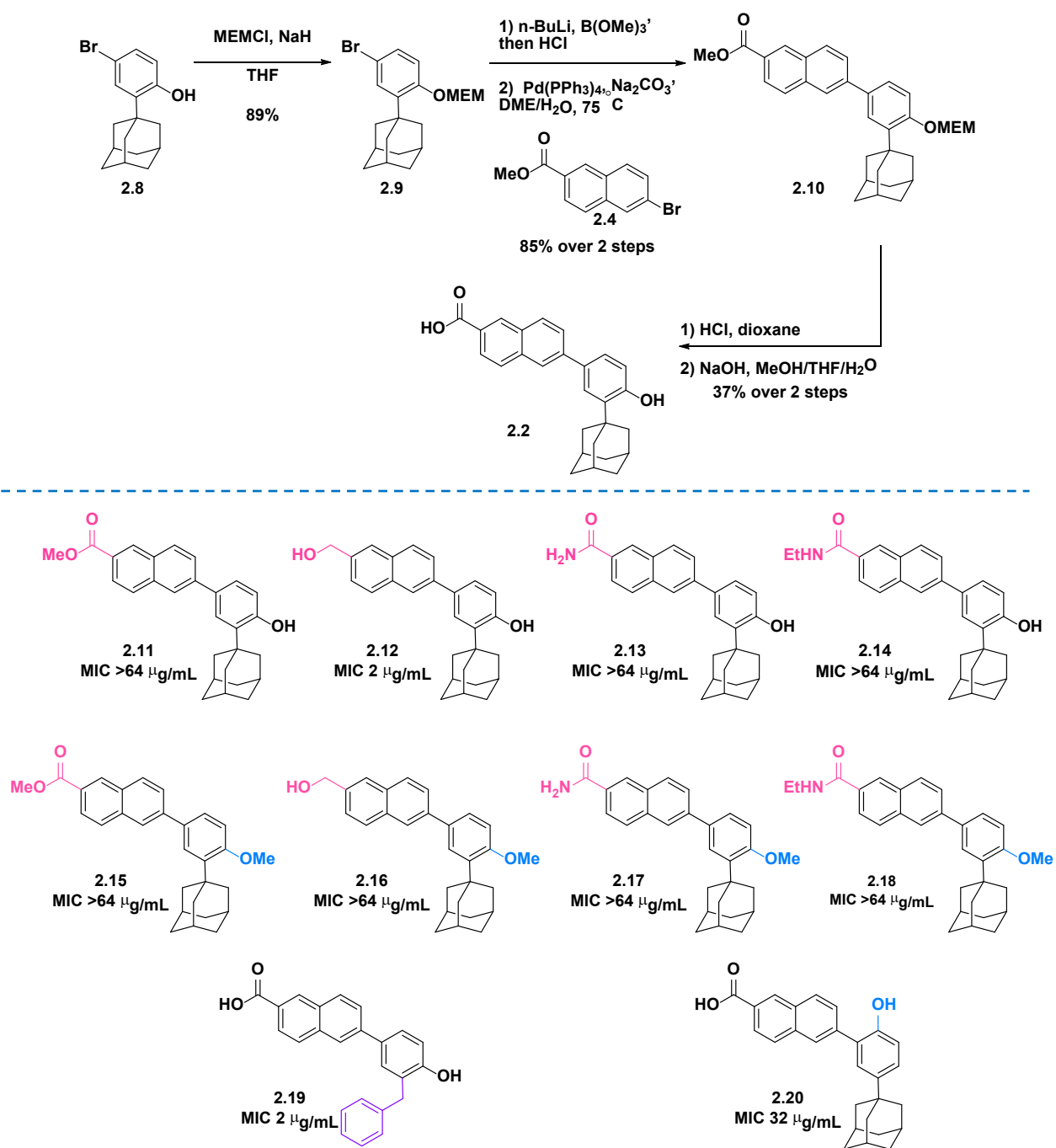
Scheme 2.1. Retrosynthetic Analysis of CD437 (**2.2**) for Generation 1 Analogs.

(**Scheme 2.1**). This would then yield a naphthalene fragment **2.4** and boronic acid **2.5**. The naphthalene was commercially available whereas the boronic acid fragment could be accessed via a Friedel-Crafts type reaction to yield 4-bromophenol **2.6** and 1-adamantanol **2.7**.

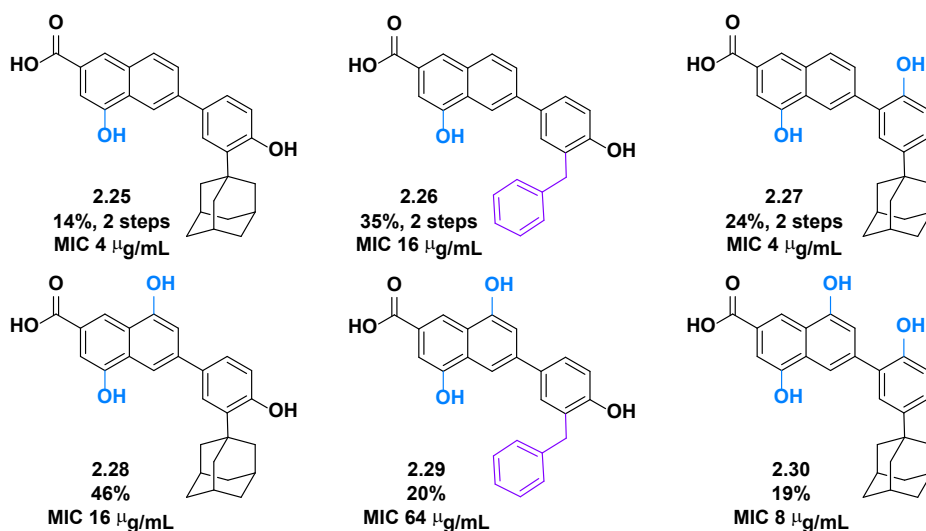
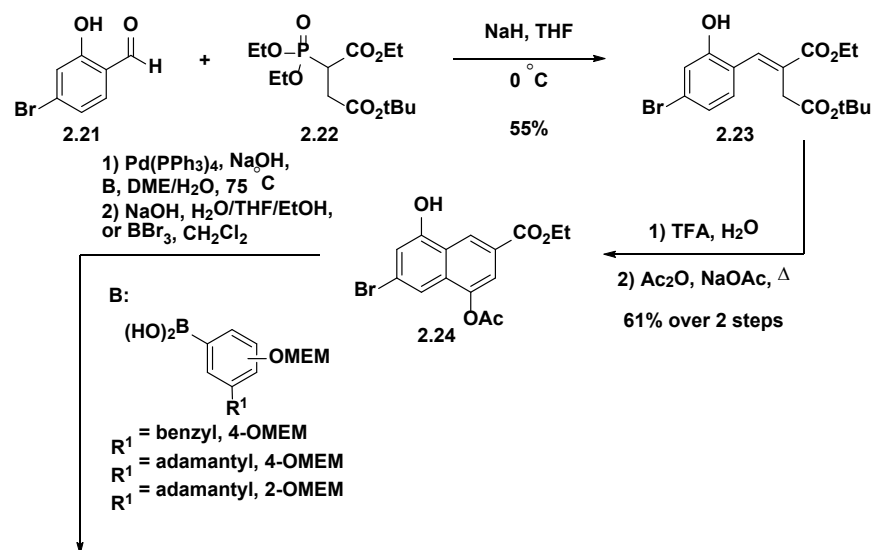
Utilizing the above retrosynthetic design, they aimed to analyze the position of the phenol, alter the carboxylic acid, mask the hydrogen-bonding capabilities, and make minor changes to the adamantyl group in their analog scope. In the forward direction, Keohane and Steele began with a Friedel-Crafts type reaction to append the adamantyl group onto 4-bromophenol to obtain **2.8** (**Scheme 2.2**). The hydroxyl was then protected via treatment with 2-methoxyethoxy methyl ether (MEM) in the presence of base to obtain **2.9**. The bromine was then borylated followed by subsection to a Suzuki coupling with **2.4** to obtain the fully protected CD437 scaffold **2.10**, which was then subjected to MEM-deprotection in the presence of acid followed by base mediated hydrolysis to obtain CD437 **2.2**. This general procedure was applied in the carboxylic acid, phenol, and benzyl analogs.

In addition, Keohane and Steele also employed an alternative route to access the remaining analogs in which additional hydroxyl groups were appended to both the phenol and naphthalene core. To achieve these, they employed a Horner-Wadsworth Emmons reaction between 4-bromo-

2-hydroxybenzaldehyde **2.21** and 4-(*tert*-butyl) 1-ethyl 2-(diethoxyphosphoryl)succinate **2.22** in the presence of sodium hydride to obtain **2.23** (**Scheme 2.3**). This was then subjected to acid catalyzed cyclization and acetate protection to obtain **2.24**. This naphthyl core was then coupled to the corresponding boronic acid in a Suzuki coupling to afford the fully protected scaffold, which was then deprotected under similar conditions as previously described. This procedure was utilized for analogs **2.25 – 2.30** (**Scheme 2.3**).



Scheme 2.2. General Forward Synthesis to obtain CD437 and structure of analogs **2.11-2.20**. MICs obtained for each analog are listed.



Scheme 2.3. Horner-Wadsworth Emmons Synthetic Approach to obtain analogs **2.25** – **2.30**. Alterations to original scaffold are highlighted in blue (polar alterations) and purple (hydrophobic alterations). MICs for analogs are listed.

Of the analogs developed in generation one, only Analog 2 (**2.12**, **Scheme 2.2**) maintained a reasonable MIC of 2 $\mu\text{g/mL}$, in comparison to the parent compound. Notably, this analog also had decreased toxicity regarding hemolytic activity (HC_{50}) of $>32\text{ }\mu\text{g/mL}$ and reduced cytotoxicity in a panel of human cell lines with a median lethal concentration (LC_{50}) of $\geq 31\text{ }\mu\text{g/mL}$ in comparison to the parent compound (**Figure 2.2**).

2.2.2. Second Generation of CD437 Analogs – Fatty Acid Tails²⁰

The second generation explored by Wuest lab alum, Dr. Ana Cheng, involved changing the adamantyl group to saturated and unsaturated fatty chains as well as varying the steric bulk of the hydrophobic moiety to explore if the globularity of adamantane was required for activity (**Figure 2.4**).²⁰ In addition, generation two analyzed the correlation between the primary alcohol analogs and its decreased toxicity in comparison to the carboxylic acid derivatives. To synthesize these analogs, Cheng employed a similar synthetic route as generation 1 apart from employing a Suzuki-Miyaura coupling to stitch the benzene and naphthalene fragments together, leading to a pinacolato boron intermediate rather than the boronic acid. Unfortunately, none of the new analogs proved more active or less toxic in comparison to CD437 **2.2**. Additionally, the adamantyl group proved to be the most optimal hydrophobic group for activity. Within this generation, our collaborators in the Mylonakis lab also analyzed these analogs anticancer activities against HeLa cells. However, there were no consistent trends that could be found.

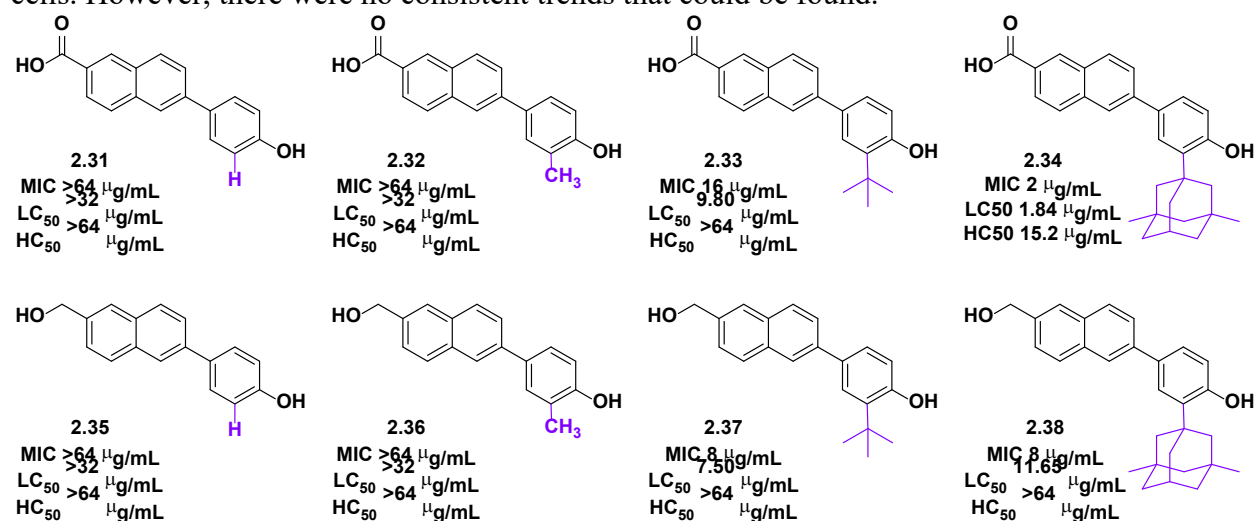


Figure 2.4. Chemical Structure of Generation Two analogs **2.31-2.38**. MICs as well as toxicity data are shown.

The main findings from the generations one and two were: 1) the adamantyl group was required for activity, 2) reduction of the carboxylic acid to the alcohol decreased toxicity (although this trend was not consistent across analog panels), and 3) maintaining hydrogen bonding capability allowed for highest activity.

2.2.3. Generation Three – Can we broaden activity?²¹

Adapted from: Cheng, A.V.[#]; **Schrank, C.L.[#]**; Escobar, I.E.; Mylonakis, E.; and Wuest, W.M. “Addition of ethylamines to the phenols of bithionol and synthetic retinoids does not elicit activity in gram-negative bacteria.” *Bioorg Med Chem Lett.*, **2020**, *30*,127099. DOI: 10.1016/j.bmcl.2020.127099

2.2.3.1. Introduction

It was at this time I joined the lab and began working towards the third generation of analogs of CD437. The plan for the third generation described herein was to explore the possibility of expanding the biological activity profile of CD437 to include Gram-negative pathogens, which are typically harder to treat. The difficulty of targeting Gram-negative bacteria is attributed to the inability of most small molecules to penetrate the outer membrane and accumulate within the cell.²² The inability to cross the outer membrane is associated with the compact, negatively charged lipopolysaccharide (LPS) structure, which is made up of lipid A molecules (4-7 carbons in length) directly attached to long, negatively charged oligosaccharides that protrude into the interstitial space. The negatively charged surface is stabilized with divalent cations. Small molecules that cross this layer commonly do so through two pathways: 1) porin uptake involving charged, amino-acid coated β -barrels, or 2) self-promoted uptake pathways involving disruption of the divalent cations to introduce membrane instability.^{22,23} If successful in crossing this barrier, most are ultimately removed via efflux pumps which decreases the ability of accumulation inside the cell.

Through retrospective analysis and computational modeling, it has been found that increased intracellular accumulation in Gram-negative species is associated with three main functionalities: 1) the presence of an amine, 2) amphiphilic and rigid structures, and 3) low-globularity.²³ With this knowledge, many studies have been performed to convert Gram-positive agents to -negative; with the most notable example being the conversion of penicillin G to ampicillin.²² In addition, a model experiment with the arylomycin antibiotic class demonstrated

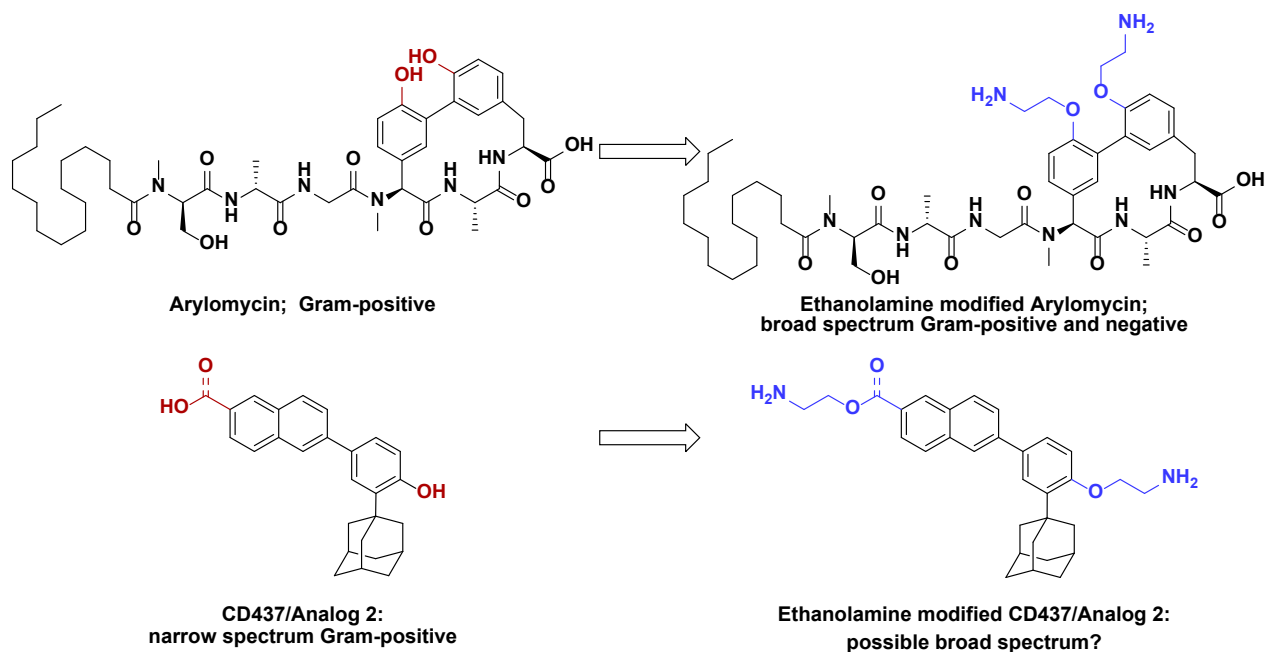
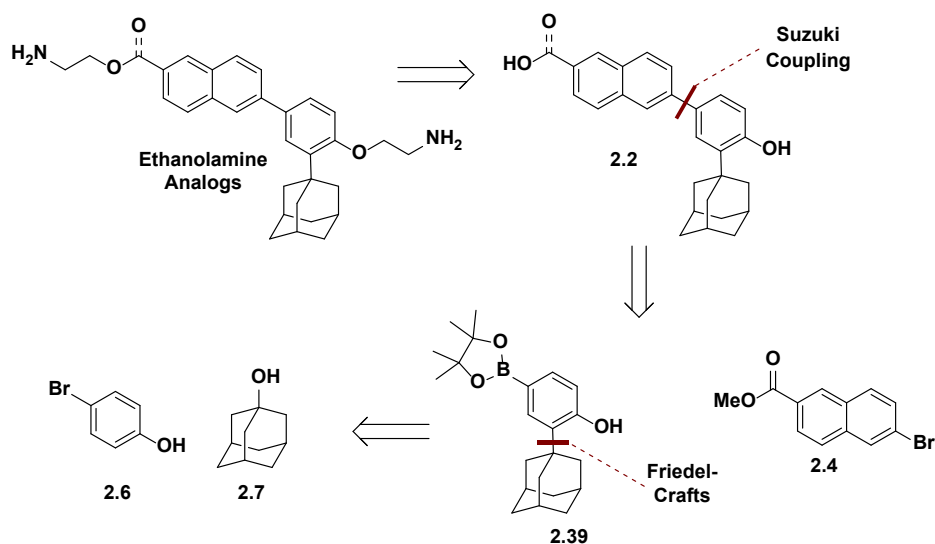


Figure 2.5. Arylomycin and modified ethanolamine structures with CD437/Analog 2 and modified ethanolamine/amine structures.

the ability to switch the activity to broad spectrum by appending an ethanolamine functional group to phenols (**Figure 2.5**).²⁴ This successful trial is attributed to the increased cationic character of the primary amine, which increases the ability of the compound to penetrate the LPS via the self-promoted uptake pathway.²² In this pathway, the positively charged amine temporarily disrupts the divalent cations on the LPS, therefore destabilizing the outer-membrane. Inspired by this phenomenon, we envisioned installing ethanolamine caps on the phenol and/or the primary alcohol of CD437 and its reduced analog to explore this as a possible Gram-negative strategy.

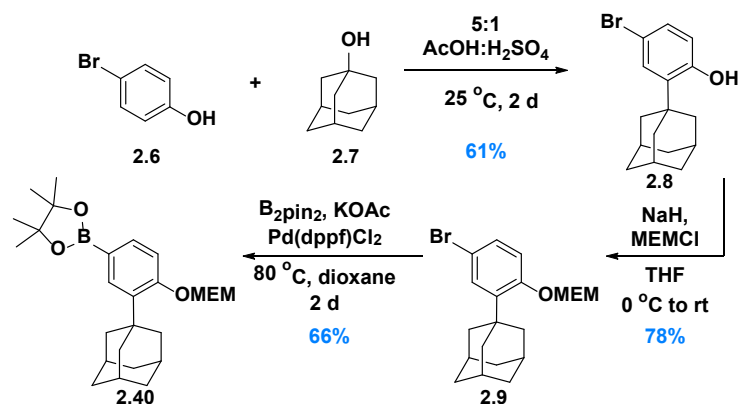
2.2.3.2. Results and Discussion



Scheme 2.4. Retrosynthetic analysis to achieve the ethanolamine analogs for generation three.

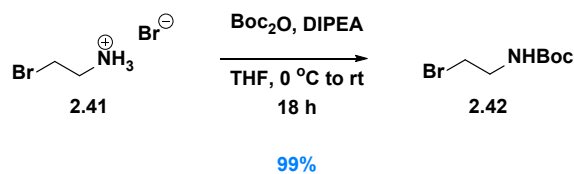
I synthesized each analog described utilizing the same synthetic procedure developed by Steele, Keohane, and Cheng.^{9,25} Analogues can be accessed via a key Suzuki coupling disconnection between the naphthalene and benzene ring (**Scheme 2.4**). The naphthalene portion is commercially available, and a Friedel-Crafts type reaction followed by a Miyaura borylation provided the benzene fragment **2.39**. Employing these synthons allows for quick access to the desired analogs.

In the forward direction, I synthesized the benzene fragment via a Friedel-Crafts type reaction with 4-bromophenol (**2.6**) and 1-adamantanol (**2.7**) to afford **2.8** in 61% yield (**Scheme 2.5**).²¹ I then protected the phenol in the presence of sodium hydride and 2-methoxyethoxymethyl (MEM) chloride to afford **2.9** in 78% yield. Compound **2.9** is then subjected to a Miyaura borylation to afford fragment **2.40** in 66% yield.

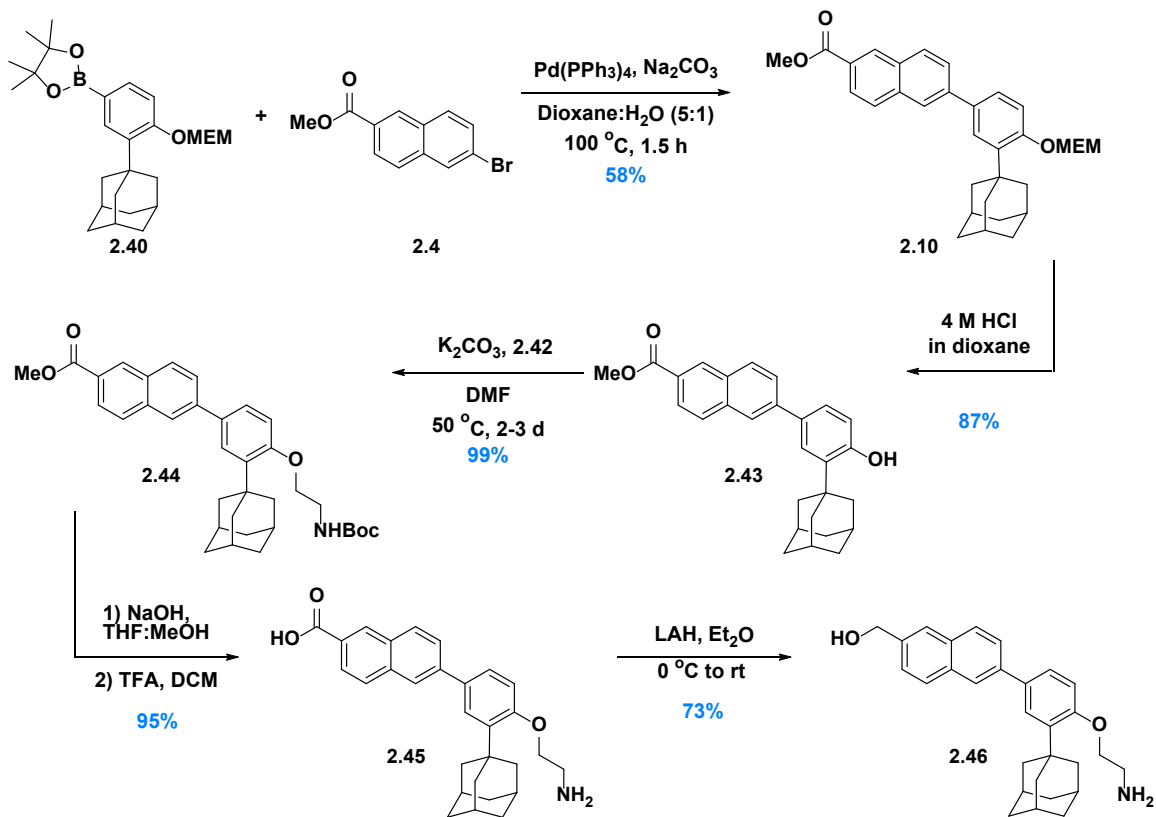


Scheme 2.5. Forward synthesis to obtain the benzene fragment **2.40**. Yields shown in blue are from C.L.Z.

A. Synthesis of Sidechain



B. Synthesis of Ethanolamine Analogs



Scheme 2.6. A. Synthesis of ethanolamine sidechain (**2.42**). B. End game synthesis to obtain ethanolamine analogs **2.45** and **2.46**. Yields shown in blue are from C.L.Z.

I then synthesized the Boc-protected ethanolamine sidechain (**2.42**) by subjecting 2-bromoethylamine hydrobromide (**2.41**) to di-*tert*-butyldicarbonate and DIPEA to afford **2.42** in 99% yield (**Scheme 2.6 A.**).²⁶ To obtain the scaffold, **2.40** and **2.4** were then subjected to a Suzuki coupling reaction followed by a MEM-deprotection to afford **2.43**. Subsequently, **2.43** is treated with potassium carbonate and **2.42** to obtain the protected analog **2.44** in 99% yield. I performed a hydrolysis followed by a Boc-deprotection to afford the first analog, **2.45**, in 95% yield (**Scheme 2.6.B.**). I accessed **2.46** in 73% yield through a reduction of the carboxylic acid using lithium aluminum hydride to afford **2.46** in 73% yield (**Scheme 2.6 B.**).

Next, we planned to also synthesize both analogs with mono and di-ethanolamine caps on the naphthalene ring. To achieve this, I attempted several different conditions utilizing the MEM-protected Analog 2 (R=MEM). Cheng also attempted capping both the primary alcohol and phenol (R=H) utilizing the following conditions (**Table 2.1**).

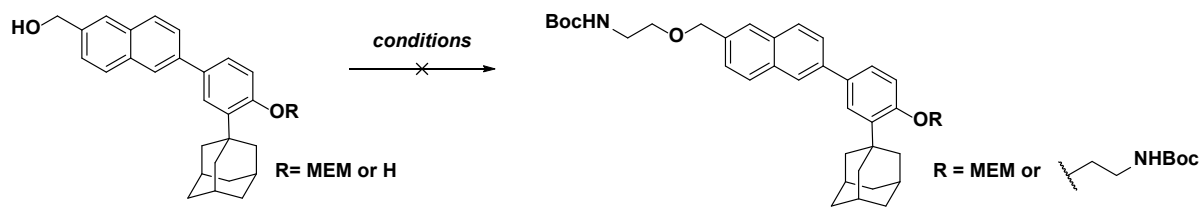
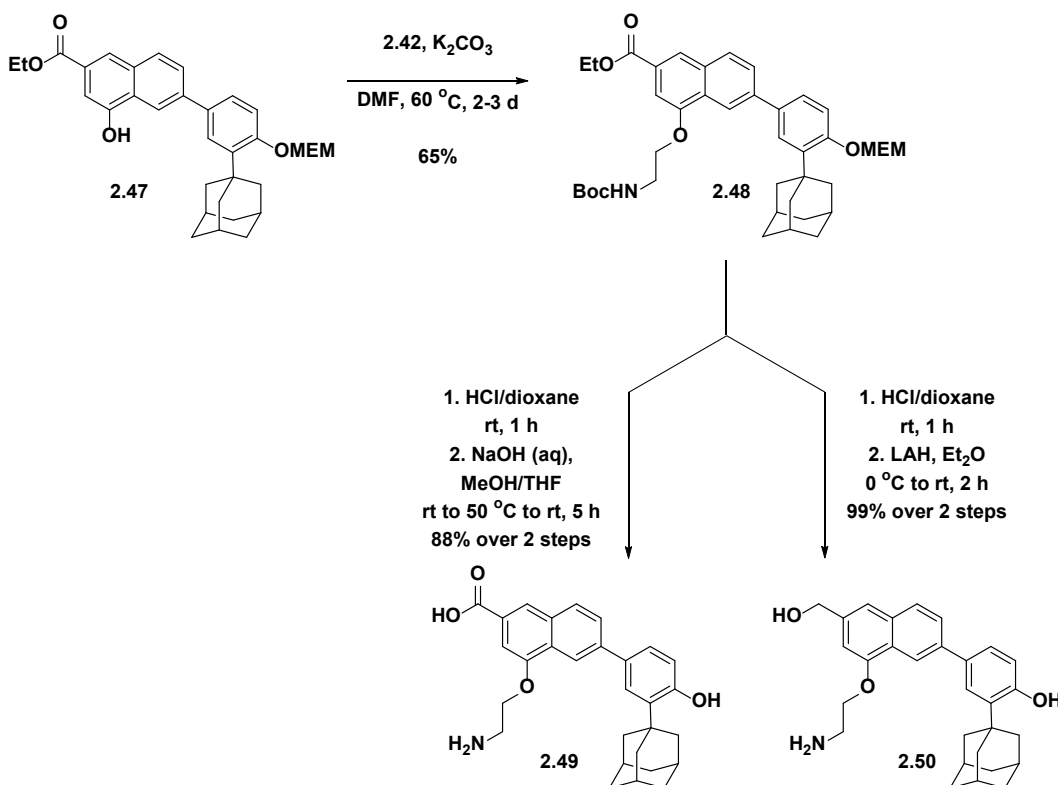


Table 2.1. Reaction conditions used in order to cap the primary alcohol and, or the phenol.

Identity of Alcohol SM	Equivs of SM	Equivs of Ethanolamine	Base Used	Equivs of Base	Solvent	Rxn Conc. (M)	Rxn Temp (°C)	TBAI Catalyst Used? (Y/N)
R = MEM	1	1.6	NaH	1.6	DMF	0.1	50	N
R = MEM	1.5	1	NaH	1.5	DMF	0.5	150	N
R = MEM	1	1.2	NaOH	3	THF	0.15	80	Y
R = MEM	1	1.15	<i>n</i> -BuLi	1.15	THF	0.5	67	Y
R = H	1	5	K ₂ CO ₃	8	DMF	0.1	50	N
R = H	1	2.3	NaH	2.2	DMF	0.1	50	N

Unfortunately, starting material or degradation products were recollected following each attempt. We hypothesized that this result may be due to the decreased acidity of the primary

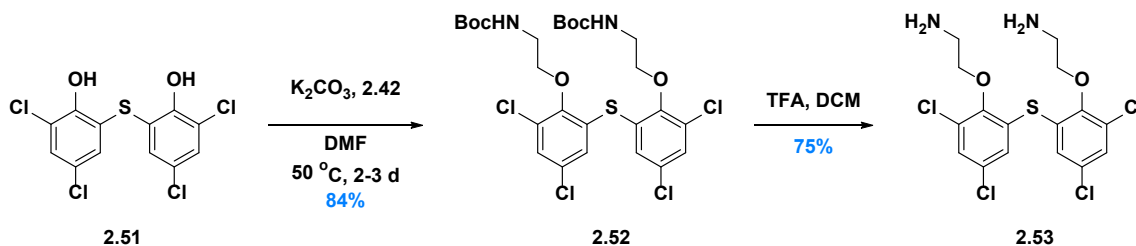
alcohol. Additionally, we hypothesize that the increased strength of base used caused a chain of side reactions to degrade the starting material.



Scheme 2.7. Synthesis of analogs **2.49** and **2.50**. Compounds were synthesized by A.V.C.

To complete the generation three, CD437 analogs, Cheng synthesized two other analogs (**2.49** and **2.50**, **Scheme 2.7**) that probed the ethanolamine functional group at the 3-position on the naphthalene core as informed by previous structure-activity relationship studies in generation one. To achieve these, Cheng began with **2.47** and subjected it to potassium carbonate and **2.42** to achieve the fully protected scaffold **2.48** in 65% yield. She then subjected it to hydrochloric acid followed by hydrolysis in the presence of sodium hydroxide to obtain the carboxylic acid analog (**2.49**) in 88% yield over two steps. For the other, she subjected **2.48** to hydrochloric acid followed by reduction in the presence of lithium aluminum hydride to obtain the primary alcohol analog (**2.50**) in 99% yield over two steps.

In addition to the CD437 analogs, we wanted to explore the alkylamine phenomenon with another MRSA membrane disruptor studied by our laboratory, bithionol (**2.51**, **Scheme 2.8**). To access this analog, I treated commercially available bithionol (**2.8**) with potassium carbonate and **2.42** to afford **2.52** in 84% yield (**Scheme 2.8**). I obtained the final analog (**2.53**) in 75 % yield via a Boc-deprotection in the presence of trifluoroacetic acid.



Scheme 2.8. Synthetic route to bithionol analog, **2.53**. Yields shown in blue are from C.L.Z.

Minimum Inhibitory Concentration ($\mu\text{g/mL}$) of Generation Three Analogs							
	2.45	2.46	2.49	2.50	2.53	2.2	2.51
MRSA MW2	>64	>64	8	4	64	2	1
MRSA BF1	>64	>64	8	4	64	2	1
MRSA BF2	>64	>64	16	4	64	2	1
MRSA BF3	>64	>64	4	4	32	1	0.5
<i>Pseudomonas aeruginosa</i> PA14	>64	>64	>64	>64	>64	>64	32
<i>Klebsiella pneumoniae</i> WGLW2	>64	>64	>64	>64	64	>64	64
<i>Acinetobacter baumannii</i> ATCC 178978	>64	>64	>64	>64	64	>64	16

Table 2.2. Minimum inhibitory concentrations (MICs) of generation 3 analogs (**2.45**, **2.46**, **2.49**, **2.50**, **2.53**) against several strains of MRSA, *P. aeruginosa*, *K. pneumoniae*, and *A. baumannii*. Positive controls used were CD437 (**2.2**) and bithionol (**2.51**). Three replicates were performed for each.

Antimicrobial activity of each analog was analyzed against four strains of MRSA, *Pseudomonas aeruginosa*, *Klebsiella pneumoniae*, and *Acinetobacter baumannii* by our collaborators in the Mylonakis lab (**Table 2.2**).

Contrary to previous reports on alkylamines, the ethanolamine analogs (**2.45**, **2.46**, **2.49**, **2.50**, **2.53**) did not exhibit broad-spectrum activity. However, **2.49** and **2.50** were able to maintain minimal activity (4-16µg/mL and 4µg/mL respectively) against the MRSA isolates in comparison to the controls **2.2** (CD437) and **2.51** (bithionol). This is in agreement with our previous findings for CD437 and bithionol that indicated that masking the polar heads (phenol and carboxylic acid) led to decreased activity in comparison to the parent compound.

2.2.3.3. Conclusions

In conclusion, we successfully synthesized four ethanolamine-capped analogs of CD437 as well as an ethanolamine-capped analog of bithionol. Biological evaluation revealed that the alterations to both the CD437 and bithionol scaffold were not tolerated in either MRSA strains and did not induce activity against Gram-negative bacteria. We hypothesize that the compounds work via specific binding interactions in bacteria that prevent toxicity against mammalian cells, thereby disallowing major changes to the scaffolding.

2.2.4: Azaborine-CD437 Analog Class²⁷

Adapted from: Haney, B.A.; **Schrank, C.L.**; Wuest, W.M. “Synthesis and biological evaluation of an antibacterial azaborine retinoid isostere.” *Tet. Lett.* **2020**, *62*, 152667.

DOI:10.1016/j.tetlet.2020.152667

2.2.4.1: Introduction:

After completion of the ethanolamine analog class, we tabulated all our results from the previous generations to determine a path forward. After three generations of analogs, our best-in-class analog remained the primary alcohol derivative, denoted as Analog 2 (**2.12**). This analog was promising in that it maintained potent activity against both persistent and wild-type MRSA cells

as well as improved the overall toxicity of the parent compound. In unpublished work, we sent these compounds to collaborators at Cyprotex to further probe **2.12**'s capabilities as a therapeutic. There were two assays performed to this end. The first assay was a turbidimetric solubility screen which investigates the kinetic solubility of a compound in order to determine its pharmacological dynamics. This assay analyzed Analog 2's solubility in PBS buffer with Verapamil as a high solubility control and Reserpine and Tamoxifen as low solubility controls. It was found that Analog 2's solubility limit after 2h was <3.91 μM , which was 10-fold less than the low solubility controls indicating overall low solubility (**Table 2.3**).

Table 2.3. Turbidimetric solubility screen. Solubility limit is highest concentration with no detectable precipitate (no evidence of turbidity).

Turbidimetric Solubility Screen			
Test Article	Buffer	Solubility Limit (μM) 2 Hour	Comment
Reserpine	PBS	15.6	Low Solubility Ctrl
Tamoxifen	PBS	15.6	Low Solubility Ctrl
Verapamil	PBS	>500	High Solubility Ctrl
2.12	PBS	<3.91	

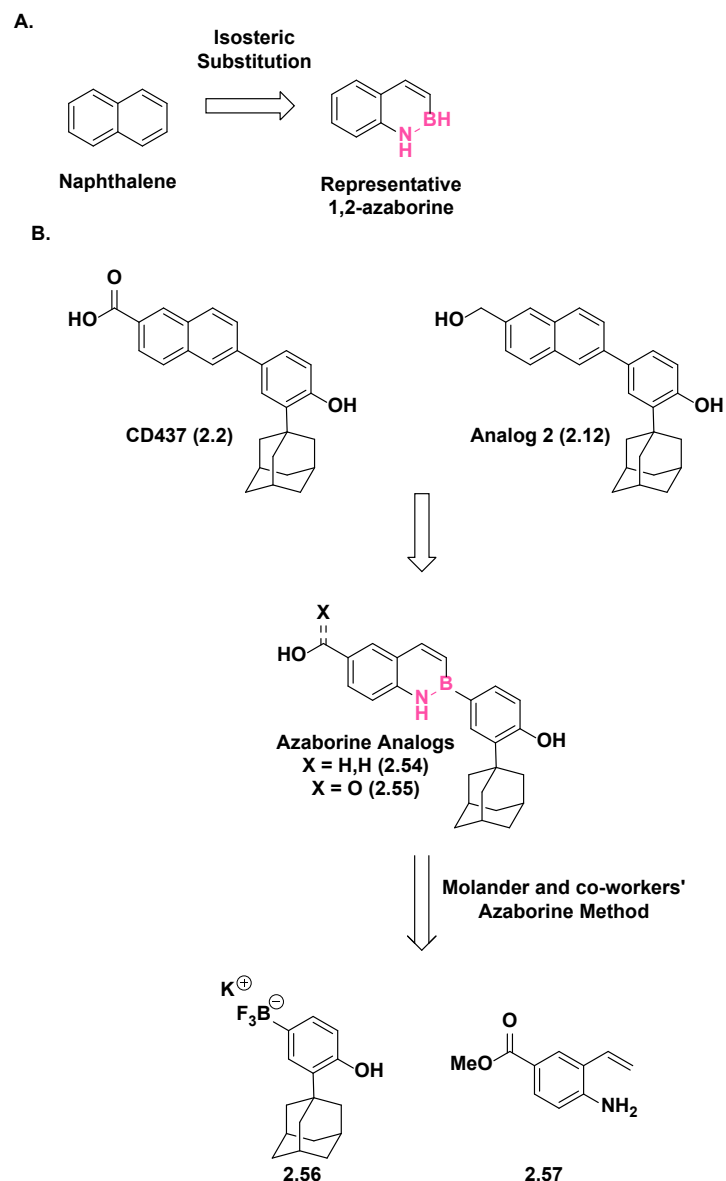
Following this assay, a plasma protein binding study was performed on Analog 2 (**2.12**) at a 5 μM test concentration. It was found that Analog 2 bound to the retinoid binding protein in >99.9% (**Table 2.4**). Overall, these results indicated that although Analog 2 showed the overall

best *in vitro* biological results, its limited bioavailability would remit it from becoming a viable therapeutic. To this end, we sought to develop a novel class of analogs that focused on substitute a nitrogen-boron single bond for a carbon-carbon double bond within the naphthalene scaffold in hopes of improving the solubility of the parent compound as well as reducing its binding affinity to retinoid binding proteins. This project has allowed me to not only explore new synthetic strategies, but also train and mentor an undergraduate student, Brittney Haney.

Plasma Protein Binding Assay					
Test Article	Test Species	Test Conc (μM)	Mean Plasma Fraction Unbound (%)	Mean Plasma Fraction Bound (%)	Post-Assay Recovery (%)
2.12	Mouse	5	<0.1	>99.9	89.3
2.12	Rat	5	<0.1	>99.9	88.1
Propranolol	Mouse	5	17.0	83	111
Propranolol	Rat	5	14.0	86	103
Warfarin	Mouse	5	20.7	79.3	101
Warfarin	Rat	5	1.07	98.9	109

Table 2.4. Data collected from plasma protein binding assay. Propranolol and Warfarin were used as controls. Assay performed in triplicates.

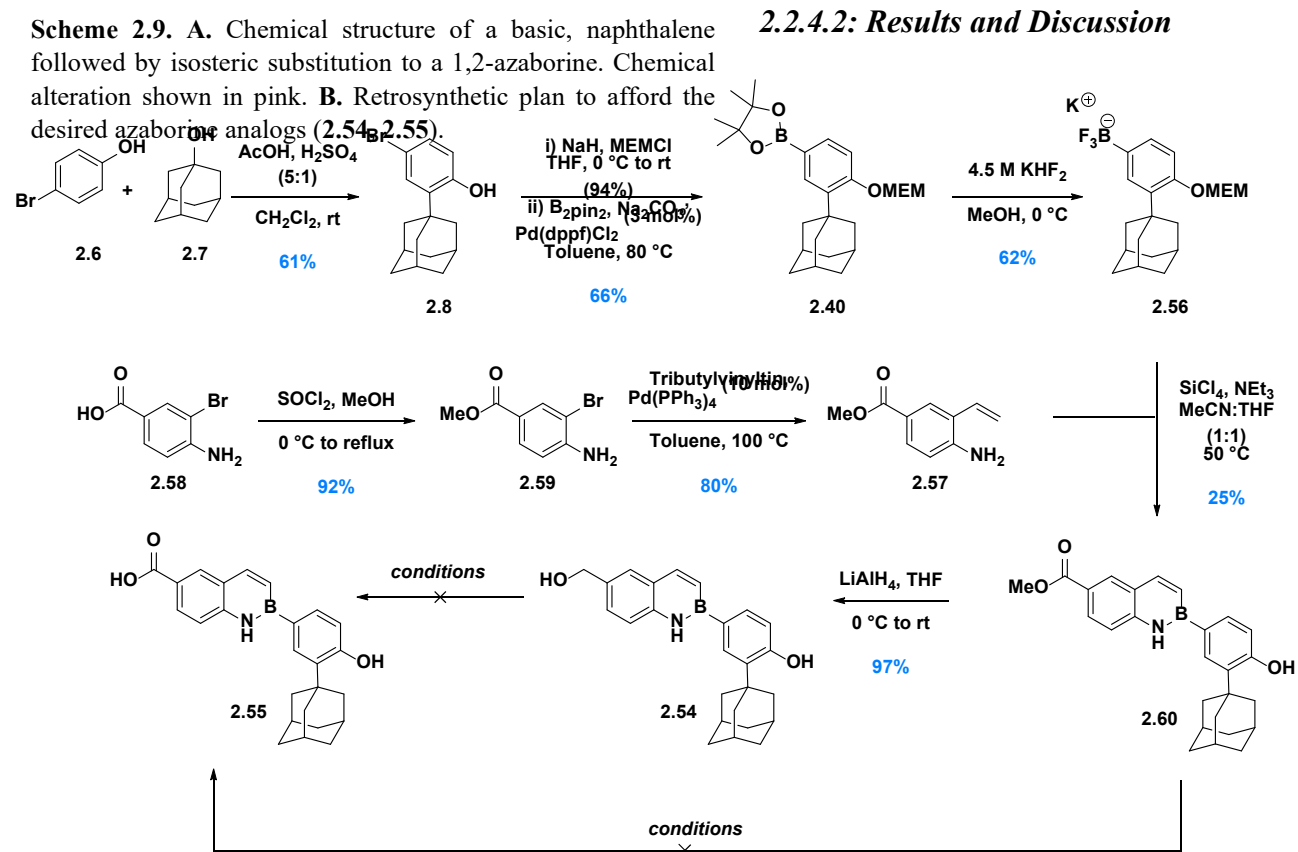
It is well-known that N-B bonds are isosteric to carbon-carbon bonds. The N-B bond, although isoelectronic, introduces a local dipole moment with the lone pair of the nitrogen donating into the empty p-orbital of boron.²⁸⁻³⁰ This polarity sharply alters the molecular and solid states of the compound, namely widening the HOMO-LUMO gap due to the lowered energy of the HOMO in comparison to parent C=C bonds.



With physical and molecular changes, N-B isosteres have garnered interest within the medicinal community in order to expand the structural diversity of therapeutic agents. Beginning in the early 1960s, this isostere was mainly explored in diazaborines (B-N-N), which exhibit antibacterial properties against Gram-negative strains.³¹⁻³³ Their specific mode of action has been extensively researched and hypothesized to target enoyl reductase; an enzyme involved in fatty-acid synthesis.³² Although diazaborines have been studied in bacterial systems, their sister structure, azaborine, has not. To date, azaborines

have been applied in various anti-cancer studies with the main focus on T-cell lysozyme targets.³⁴ With this background knowledge, we aimed to explore this isosteric model within the bacterial space in order to test if this isosteric substitution could lessen the binding affinity of our analogs to retinoid-binding protein. We predict this substitution may alter the binding affinity due to the numerous phenylalanine and tyrosine residues that are located within the 8-strand, β -barrel cavity

in which retinol is known to bind.^{35–37} By altering the electronics of the naphthalene ring, these π interactions may be disrupted enough to decrease the affinity.



We set out to synthesize the azaborine analog of CD437 utilizing methodology developed by Dr. Gary Molander at the University of Pennsylvania.^{38,39} This method proved to be amenable to our previously disclosed syntheses of the parent compound and allowed us to prepare the azaborine derivative quickly. The desired analogs (**2.54**, **2.55**) can be accessed via a silicon (IV) chloride coupling between an aminostyrene (**2.57**) and an organotrifluoroborate salt (**2.56**, **Scheme 2.9.B.**).

We began by synthesizing the trifluoroborate salt fragment (**2.56**) utilizing a previously described route for the synthesis of CD437 (**Scheme 2.10**).^{19–21} Upon achieving the borylated

compound, **2.40** was then subjected to aqueous potassium bifluoride in methanol to afford **2.56** in 62% yield.^{40,41} With the trifluoroborate fragment in hand, we then began synthesis of the aminostyrene fragment (**2.57**, **Scheme 2.10**). Beginning with commercially available 4-amino-3-bromobenzoic acid (**2.58**), a methyl protection in the presence of thionyl chloride and methyl iodide afforded **2.59**. This was then subjected to a Stille coupling to afford **2.57** in 80% yield.⁴²

With both fragments in hand, we then employed the method developed by Molander and co-workers utilizing silicon tetrachloride and triethylamine (**Scheme 2.10**).^{38,39} This method proved difficult with our scaffold as the MEM-protecting group was subsequently removed during the reaction progress due to the production of hydrochloric acid in situ. We hypothesized that the deprotected free phenol subsequently formed a stable bond with a neighboring boron, eliminating a fluoride anion and thereby limiting the availability of the trifluoroborate in solution. Although triethylamine was added to the reaction to neutralize the hydrochloric acid production, the removal of MEM still occurred regardless of the concentration of triethylamine used. In future use, the addition of a proton sponge would be a potential route to avoid these issues. However, the desired protected azaborine scaffold (**2.60**) could still be obtained in 25% yield. Although a change in protecting group strategy could potentially circumvent these issues, we sought to pursue a direct path to the desired analog for biological studies.

In achieving the formation of the desired scaffold, we proceeded with reduction and deprotection pathways to afford our planned primary alcohol and carboxylic acid analogs, respectively. Firstly, protected **2.60** was subjected to lithium aluminum hydride to afford the desired primary alcohol azaborine (**2.54**) in 97% yield. Upon obtaining **2.54**, we then turned to deprotection of the methyl ester **2.60**. Several hydrolysis methods were attempted to achieve the desired carboxylic acid analog (**2.55**) including base mediated hydrolysis (NaOH, KOH), acid-

mediated hydrolysis (HCl, H₂SO₄), as well as milder approaches with pig liver esterase (PLE). However, each method proved unsuccessful. The base mediated hydrolysis showed degradation in which the proposed degradative mechanism involved the hydroxide anion attacking the empty p-orbital of the boron, forming a stable O–B bond and eliminating the nitrogen, thereby breaking apart the scaffold. This degraded product was confirmed by NMR spectroscopy (data not shown). Additionally, the acid mediated hydrolysis and the PLE-mediated hydrolysis reactions yielded only recovered starting material. To avoid degradation of the scaffold, we attempted utilizing oxidation pathways from the primary alcohol **2.54**. First, we implemented a Swern-Pinnick oxidation sequence that yielded starting material as well as minor degradative products. Additionally, we attempted a TEMPO oxidation that yielded only recovered starting material. After these failed attempts to access **2.55**, we decided to focus on the primary alcohol analog (**2.54**) as it did mimic our best-in-class analog, analog 2 (**2.12**).

Antimicrobial activity of **2.54** was analyzed along with **2.12** against a panel of bacterial strains including three different strains of *Staphylococcus aureus* (SH1000, ATCC 33591, USA 300-0114), *Pseudomonas aeruginosa* (PA01), *Enterococcus faecalis* (OG1RF), and *Escherichia coli* (MC4100). We chose to use benzalkonium chloride (BAC) as a positive control as it is a common, commercially available quaternary ammonium compound that also induces bacterial killing via membrane perturbation. In addition to antimicrobial activity, the toxicity was analyzed using a red blood cell (RBC) lysis assay utilizing mechanically defibrillated sheep's blood. These values are indicated as Lysis₂₀ and are measured as the concentration that lyse 20% or less of RBC. Surprisingly, the azaborine analog (**2.54**) proved to have a higher MIC than its isosteric partner (**2.12**, **Table 2.5**). However, the toxicity was comparable to the parent compound (**Table 2.5**).

Minimum Inhibitory Concentration (μM)							Lysis ₂₀
Compound	MSSA	HA-MRSA	CA-MRSA	<i>E. faecalis</i>	<i>P. aeruginosa</i>	<i>E. coli</i>	(μM)
BAC	2	4	4	125	125	32	32
2.12	2	2	2	>250	>250	>250	125
2.54	125	64	250	>250	>250	>250	250

Table 2.5. Antimicrobial activity and toxicity data for analog 2 (**2.12**) and azaborine analog (**2.54**). All MIC and Lysis₂₀ data were acquired through an average of the highest value of three independent trials; all trials were within one dilution.

To further understand this decrease in biological activity, partition coefficients (P) for both analog 2 (**2.12**) and azaborine analog (**2.54**) were theoretically calculated via Schrodinger and experimentally determined through extraction protocols with *n*-octanol and deionized water.⁴³ This experiment was performed in triplicate, and the average P was determined. From this data, log(base 10) of P was calculated. We found that **2.12** had a logP of 0.93 and **2.54** had a logP of 0.12 (Table 2). These results indicate that the isosteric substitution in **2.54** switches the compound to become more hydrophilic in comparison to **2.12**.

	Analog 2 (2.12)	Azaborine Analog (2.54)
P	9.16	1.39
logP	0.93 \pm 0.20	0.12 \pm 0.19
cP ^a	7.687	6.792
clogP ^a	0.89	0.83
QM Dipole (D)	2.42	1.34

Table 2.6. Experimentally determined P and log P for analog 2 (**2.12**) and azaborine analog (**2.54**) as well as quantum mechanical calculated dipole expressed as debye D. Partition coefficients shown as an average over 3 independent trials. logP data shown with + / - standard deviation. ^a “c” indicates calculated data for the partition coefficient utilizing the ChemDraw3D program.

To further explore this, we performed a quantum mechanical analysis with Schrodinger to analyze the dipole moment of both compounds. Through these calculations, we found that analog 2 showed a higher dipole moment of 2.42 D vs 1.34 D for azaborine (**Table 2.6**). As was previously disclosed by our group, the proposed mechanism of action of this class of molecules is membrane perturbation. Although analog 2 has the greater dipole moment, we propose that the presence of the N-B bond may cancel out the dipole of the primary alcohol. However, as highlighted in **Figure**

2.6, azaborine analog has more points of possible hydrogen bond donor-acceptors, especially

considering the proposed resonance structure (**Figure 2.6**). Therefore, with a more hydrophilic structure and additional points for hydrogen bonding with water, **2.54** may be

unable to associate within the lipid bilayer to induce killing.

In addition to logP, we wanted to ensure that there was no degradation of the compound (as shown in hydrolysis experiments) throughout the MIC assays that may attribute to its decrease in activity. To probe this possibility, we suspended the compound in deionized water and heated to 37°C for 22-23h to mimic the *in vitro* conditions employed. The resulting mixture was then evacuated and analyzed by NMR. Based on the NMR results, the compound was proven to be stable in neutral water. Overall, we found that the azaborine isosteric substitution is not a viable option for improving biological activity of our retinoid class of antibacterial agents.

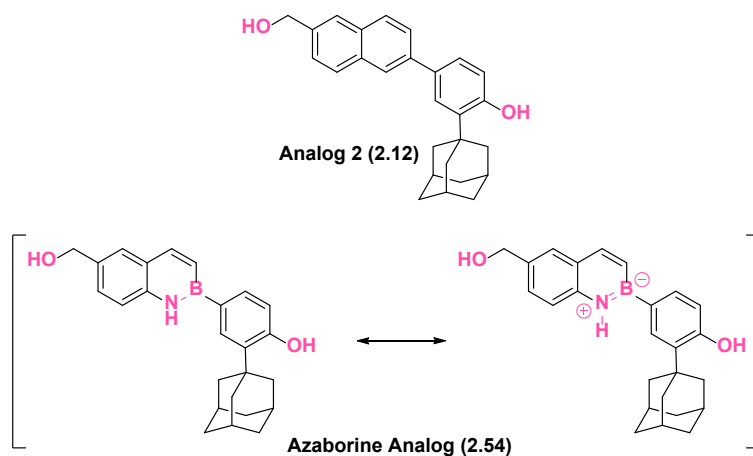


Figure 2.6. The structures of Analog 2 (**2.12**) and the azaborine analog (**2.54**), displaying contributing resonance structures. Highlighted in pink are hydrogen-bond donors and acceptors.

2.2.4.3: Conclusion

In summary, we were able to successfully synthesize the primary alcohol azaborine scaffold of CD437/Analog 2. Unfortunately, we observed a decrease in antimicrobial activity, which we attributed to the surprising increase in hydrophilicity of the scaffold as shown by the experimentally determined partition coefficient data. These results were surprising as the calculated partition coefficient was not significantly different from the parent scaffold. This isosteric substitution warrants further analysis in other antimicrobial natural products to fully understand its availability for drug discovery.

2.3: Future Directions

The synthetic retinoid, CD437 (**2.2**), proved to have potent activity against both wild-type and persistent MRSA cells *in vitro*. Through four SAR campaigns, our laboratory was able to demonstrate that the polar regions of the molecule (carboxylic acid and hydroxyl groups) were required for activity due to their hydrogen bond capabilities, allowing them to anchor to the negatively charged, phospholipid heads of the bacterial membrane. Additionally, we showed that reduction of the carboxylic acid group to the primary alcohol (Analog 2, **2.12**) reduced the overall toxicity of the compound while still maintaining antibacterial activity. This, however, was not demonstrated as a consistent trend across varying types of analogs as shown in generation two.²⁰ Beyond alterations to the three main functional groups of the molecule (carboxylic acid, hydroxyl, and adamantyl), we also showed that appending ethanolamine groups to the molecule as well as altering the naphthalene scaffold to an azaborine diminished activity and did not broaden the spectrum of activity.^{21,27}

With these results, we have found that our best-in-class analog of all four generations was Analog 2 (**2.12**) with an MIC of 2 $\mu\text{g/mL}$ against MRSA. Although this analog was able to maintain

potent activity, it maintained high plasma binding to retinoid binding proteins. This, therefore, may limit the capabilities for this compound to move forward as a viable therapeutic. We have proposed, instead, the possible use of these compounds to treat external infections, such as wound infections, to avoid limitations with internal availability.

Beyond our work on CD437 within the bacterial space, there has also been recent reports analyzing its activity against viral infections including the mumps virus. Research performed by Kato and co-workers showed that CD437 was able to inhibit the replication cycle of mumps virus with a half maximal effective concentration (EC_{50}) of $0.79 \pm 0.11 \mu\text{M}$ and a half maximal cytotoxic concentration (CC_{50}) of $34.9 \mu\text{M}$.⁴⁴ In addition, the authors also showed that CD437 had activity against other viruses in the Paramyxoviridae family as well as viruses in the Pneumoviridae family. This work bodes an exciting new space to explore in the arsenal of CD437's ability to inhibit cancer, bacterial, and viral cells.

Chapter 2 References

1. Lewis, K. Persister cells. *Annual Review of Microbiology* vol. 64 357–372 (2010).
2. Brauner, A., Fridman, O., Gefen, O. & Balaban, N. Q. Distinguishing between resistance, tolerance and persistence to antibiotic treatment. *Nature Reviews Microbiology* vol. 14 320–330 (2016).
3. Rajamuthiah, R. *et al.* Whole Animal Automated Platform for Drug Discovery against Multi-Drug Resistant *Staphylococcus aureus*. doi:10.1371/journal.pone.0089189.
4. Chiaraviglio, L. & Kirby, J. E. Evaluation of Impermeant, DNA-Binding Dye Fluorescence as a Real-Time Readout of Eukaryotic Cell Toxicity in a High Throughput Screening Format. doi:10.1089/adt.2014.577.
5. Yan, X. *et al.* Development of a Mechanism-Based, DNA Staining Protocol Using SYTOX Orange Nucleic Acid Stain and DNA Fragment Sizing Flow Cytometry. *Anal. Biochem.* **286**, 138–148 (2000).
6. Yan, X. *et al.* Probing the kinetics of SYTOX Orange stain binding to double-stranded DNA with implications for DNA analysis. *Anal. Chem.* **77**, 3554–3562 (2005).
7. Kim, W. *et al.* Identification of an Antimicrobial Agent Effective against Methicillin-Resistant *Staphylococcus aureus* Persisters Using a Fluorescence-Based Screening Strategy. *PLoS One* **10**, e0127640 (2015).
8. Kim, W. *et al.* NH125 kills methicillin-resistant *Staphylococcus aureus* persisters by lipid bilayer disruption. *Future Med. Chem.* **8**, 257–269 (2016).
9. Kim, W. *et al.* A new class of synthetic retinoid antibiotics effective against bacterial persisters. *Nature* **556**, 103–107 (2018).
10. Kim, W. *et al.* Discovery and Optimization of nTZDpa as an Antibiotic Effective Against Bacterial Persisters. *ACS Infect. Dis.* **4**, 1540–1545 (2018).

11. Kim, W. *et al.* A selective membrane-targeting repurposed antibiotic with activity against persistent methicillin-resistant *Staphylococcus aureus*. *Proc. Natl. Acad. Sci. U. S. A.* **116**, 16529–16534 (2019).
12. Sun, S. Y. *et al.* Mechanisms of apoptosis induced by the synthetic retinoid CD437 in human non-small cell lung carcinoma cells. *Oncogene* **18**, 2357–2365 (1999).
13. Bernard, B. A. *et al.* Identification of synthetic retinoids with selectivity for human nuclear retinoic acid receptor γ . *Biochem. Biophys. Res. Commun.* **186**, 977–983 (1992).
14. Mologni, L. *et al.* The Novel Synthetic Retinoid 6-[3-adamantyl-4-hydroxyphenyl]-2-naphthalene Carboxylic Acid (CD437) Causes Apoptosis in Acute Promyelocytic Leukemia Cells Through Rapid Activation of Caspases. *Blood* **93**, 1045–1061 (1999).
15. Sun, S. Y. *et al.* Dual mechanisms of action of the retinoid CD437: nuclear retinoic acid receptor-mediated suppression of squamous differentiation and receptor-independent induction of apoptosis in UMSCC22B human head and neck squamous cell carcinoma cells. *Mol. Pharmacol.* **58**, 508–514 (2000).
16. Zhao, X. *et al.* Retinoic acid receptor-independent mechanism of apoptosis of melanoma cells by the retinoid CD437 (AHPN). *Cell Death Differ.* **2001 89 8**, 878–886 (2001).
17. Liang, J. -Y. *et al.* Synthetic retinoid CD437 induces S-phase arrest and apoptosis in human prostate cancer cells LNCaP and PC-3. *Prostate* **38**, 228–236 (1999).
18. Han, T. *et al.* The antitumor toxin CD437 is a direct inhibitor of DNA polymerase α . *Nat. Chem. Biol.* **12**, 511–515 (2016).
19. Kim, W. *et al.* A new class of synthetic retinoid antibiotics effective against bacterial persisters. *Nature* **556**, 103–107 (2018).
20. Cheng, A. V., Kim, W., Escobar, I. E., Mylonakis, E. & Wuest, W. M. Structure–Activity

- Relationship and Anticancer Profile of Second-Generation Anti-MRSA Synthetic Retinoids. *ACS Med. Chem. Lett.* 5–9 (2019) doi:10.1021/acsmchemlett.9b00159.
21. Cheng, A. V., Schrank, C. L., Escobar, I. E., Mylonakis, E. & Wuest, W. M. Addition of ethylamines to the phenols of bithionol and synthetic retinoids does not elicit activity in gram-negative bacteria. *Bioorganic Med. Chem. Lett.* **30**, 127099 (2020).
 22. Richter, M. F. & Hergenrother, P. J. The challenge of converting gram-positive-only compounds into broad-spectrum antibiotics. *Ann. N. Y. Acad. Sci.* **1435**, 18–38 (2019).
 23. Richter, M. F. *et al.* Predictive compound accumulation rules yield a broad-spectrum antibiotic. *Nature* **545**, 299–304 (2017).
 24. Smith, P. A. *et al.* Optimized arylomycins are a new class of Gram-negative antibiotics. *Nat.* 2018 5617722 **561**, 189–194 (2018).
 25. Cheng, A. V., Kim, W., Escobar, I. E., Mylonakis, E. & Wuest, W. M. Structure-Activity Relationship and Anticancer Profile of Second-Generation Anti-MRSA Synthetic Retinoids. *ACS Med. Chem. Lett.* **11**, 393–397 (2020).
 26. Bartole, E. *et al.* UR-DEBa176: A 2,4-Diaminopyrimidine-Type Radioligand Enabling Binding Studies at the Human, Mouse, and Rat Histamine H4 Receptors. *J. Med. Chem.* **62**, 8338–8356 (2019).
 27. Haney, B. A., Schrank, C. L. & Wuest, W. M. Synthesis and biological evaluation of an antibacterial azaborine retinoid isostere. *Tetrahedron Lett.* 152667 (2020) doi:10.1016/j.tetlet.2020.152667.
 28. Liu, Z. & Marder, T. B. B-N versus C-C: How similar are they? *Angew. Chemie - Int. Ed.* **47**, 242–244 (2008).
 29. Bonifazi, D. *et al.* Boron-nitrogen doped carbon scaffolding: Organic chemistry, self-

- assembly and materials applications of borazine and its derivatives. *Chem. Commun.* **51**, 15222–15236 (2015).
30. Knack, D. H. *et al.* BN/CC Isosteric Compounds as Enzyme Inhibitors: N-and B-Ethyl-1,2-azaborine Inhibit Ethylbenzene Hydroxylation as Nonconvertible Substrate Analogues**. (2013) doi:10.1002/anie.201208351.
 31. Högenauer, G. & Woisetschläger, M. A diazaborine derivative inhibits lipopolysaccharide biosynthesis. *Nature* **293**, 662–664 (1981).
 32. Baldock, C. *et al.* A mechanism of drug action revealed by structural studies of Enoyl reductase. *Science (80-.)*. **274**, 2107–2110 (1996).
 33. Baldock, C., De Boer, G. J., Rafferty, J. B., Stuitje, A. R. & Rice, D. W. Mechanism of action of diazaborines. *Biochem. Pharmacol.* **55**, 1541–1549 (1998).
 34. Liu, L., Marwitz, A. J. V, Matthews, B. W. & Liu, S.-Y. Boron Mimetics: 1,2-Dihydro-1,2-azaborines Bind inside a Non-polar Cavity of T4 Lysozyme**. doi:10.1002/anie.200903390.
 35. Cowan, S. W., Newcomer, M. E. & Jones, T. A. Crystallographic refinement of human serum retinol binding protein at 2Å resolution. *Proteins Struct. Funct. Bioinforma.* **8**, 44–61 (1990).
 36. Folli, C., Favilla, R. & Berni, R. The interaction between retinol-binding protein and transthyretin analyzed by fluorescence anisotropy. *Methods Mol. Biol.* **652**, 189–207 (2010).
 37. Heller, J. & Horwitz, J. Involvement of tyrosine and lysine residues of retinol-binding protein in the interaction between retinol and retinol-binding protein and between retinol-binding protein and prealbumin. Acetylation with N-acetylimidazole and alkaline titration.

- J. Biol. Chem.* **250**, 3019–3023 (1975).
38. Molander, G. A., Wisniewski, S. R. & Amani, J. Accessing an azaborine building block: Synthesis and substitution reactions of 2-chloromethyl-2,1-borazaronaphthalene. *Organic Letters* vol. 16 5636–5639 (2014).
 39. Wisniewski, S. R., Guenther, C. L., Andreea Argintaru, O. & Molander, G. A. A convergent, modular approach to functionalized 2,1-borazaronaphthalenes from 2-aminostyrenes and potassium organotrifluoroborates. *J. Org. Chem.* **79**, 365–378 (2014).
 40. Santos-Filho, E. F., Sousa, J. C., Bezerra, N. M. M., Menezes, P. H. & Oliveira, R. A. Environmentally friendly homocoupling reaction of functionalized potassium aryl trifluoroborates salts in aqueous media. *Tetrahedron Lett.* **52**, 5288–5291 (2011).
 41. Vedejs, E. *et al.* Asymmetric memory at labile, stereogenic boron: Enolate alkylation of oxazaborolidinones. *J. Am. Chem. Soc.* **121**, 2460–2470 (1999).
 42. Aoyama, A. *et al.* Design, synthesis, and biological evaluation of novel transrepression-selective liver X receptor (LXR) ligands with 5,11-dihydro-5-methyl-11-methylene-6H-dibenz[*b, e*]azepin-6-one skeleton. *J. Med. Chem.* **55**, 7360–7377 (2012).
 43. Harris, M. F. & Logan, J. L. Determination of log K_{ow} Values for Four Drugs. (2014) doi:10.1021/ed400655b.
 44. Kato, F. *et al.* Antiviral Activity of CD437 Against Mumps Virus. *Front. Microbiol.* **12**, 3401 (2021).

Chapter 3: Synthetic and Biological Investigations into Quaternary Ammonium

Compounds

3.1: Introduction

3.1.1: Quaternary Ammonium Compounds

*Background on QAC resistance is adapted from Carden, R.G.; Sommers, K.J.; **Schrank, C.L.**; Letigeb, A.J.; Feliciano, J.A.; Wuest, W.M.; and Minbiole, K.P.C. Advancements in the Development of Non-Nitrogen-Based Amphiphilic Antiseptics to Overcome Pathogenic Bacterial Resistance. *ChemMedChem* **2020**, *15*, 1974-1984. This section of the paper was written solely by C.L.Z.¹

When society considers antimicrobials, they often reference prescribed medications used to treat microbial infections on living, human tissue. These may include orally prescribed

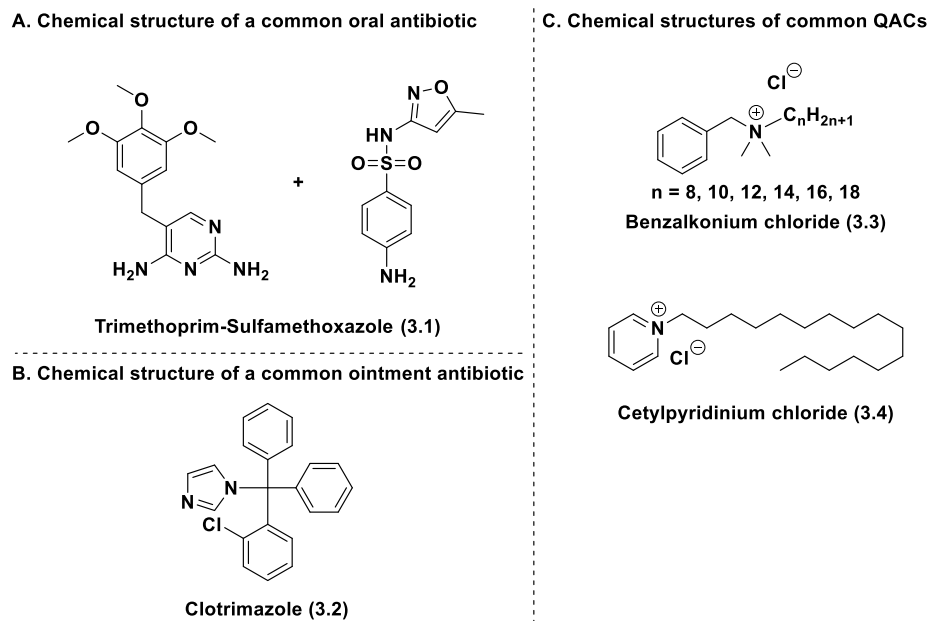


Figure 3.1 A. Chemical structure of a common oral antibiotic, trimethoprim-sulfamethoxazole (3.1). B. Chemical structure of a common antibiotic ointment, clotrimazole (3.2). C. Chemical structures of common QACs, benzalkonium chloride (3.3) and cetylpyridinium chloride (3.4).

antibiotics, such as trimethoprim-sulfamethoxazole (3.1), to treat illnesses such as urinary tract

infections (**Figure 3.1 A**),² or over-the-counter ointments, such as clotrimazole (**3.2**), used to treat external skin infections (**Figure 3.1 B**).³ Although these compounds are large contributors to antimicrobial use in the world, one of the largest, most used classes of antimicrobials are disinfectants and antiseptics. Disinfectants are compounds used to treat the surfaces of inanimate objects to either kill microbial species (biocide) or inhibit their growth (biostatic).⁴ Antiseptics, on the other hand, are compounds that can be applied either on the surfaces of inanimate objects or external human tissue such as on the skin or inside the mouth. These are more often adopted in order to prevent an infection from happening rather than inhibiting or killing populations of microbials. These materials exist as active ingredients in everyday products such as surface disinfectants (e.g., Clorox wipes), antimicrobial soaps, mouthwash, and hand sanitizing agents.

The most common active ingredient in disinfectant and antiseptic products are quaternary ammonium compounds (QACs). QACs are amphiphilic compounds that contain a positively charged quaternary amine as well as a lipophilic sidechain (**Figure 3.1**).⁵ These powerful compounds were discovered in the 1900s and have become one of the most widely used compounds in the antiseptic and disinfectant markets.⁶ One of the most prolific QACs is benzalkonium chloride (BAC, **3.3, Figure 3.1 C**). It was first marketed in 1935⁷ and is now in several household products including, but not limited to, personal hygiene products,⁸ contact lens solutions,⁹ and toilet cleaners.^{5,10} Additionally, cetylpyridinium chloride (CPC, **3.4, Figure 3.1 C**) is a heavily used QAC in the oral health industry, acting as the active ingredient in many mouthwashes.¹¹ This widespread use is due in part to QACs' chemical stability, allowing for formulation ease in various sanitizing products, including household products as well as food and hospital sanitation.¹²

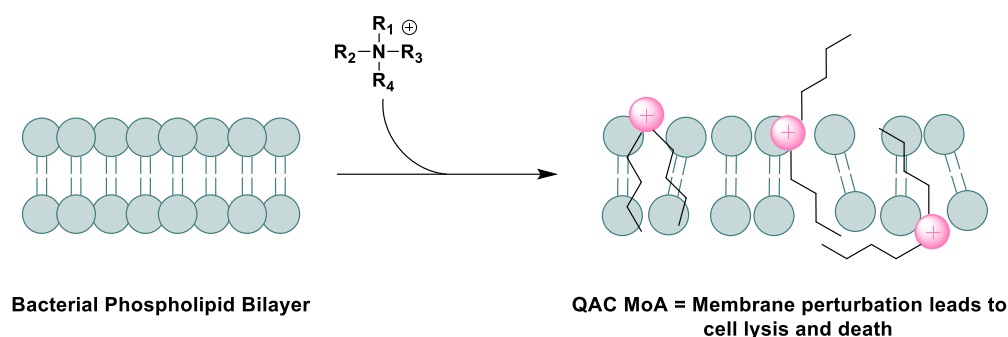


Figure 3.2. Cartoon representation of QACs mechanism of action against bacterial membranes.

The amphiphilic nature of QACs allows them to act as chemical detergents. In the case of disruption to bacterial cells, the positively charged amine is attracted to the negatively charged phospholipid heads of the membrane through electrostatic interactions (**Figure 3.2**).^{5,12–18} Once anchored, the lipophilic sidechains of the molecule can then intercalate into the membrane leading to perturbation.¹ This disruption can lead to leakage of cellular content culminating in cell death. Through this membrane targeting mechanism of action (MoA), they can act as broad-spectrum agents for different species of bacteria as well as common viruses. However, because they disrupt membrane integrity, they can also be toxic to human cells.⁵

These products have transformed daily life in terms of sanitation practices and public health. Recently, their importance starkly increased during the SARS-CoV-2 pandemic when their use rose exponentially.^{13,19,20} With this increase in employment, researchers have voiced concern about the rapid development and spread of QACs resistance. Because these compounds are stable and nonvolatile, they last in the environment for much longer.¹³ It has been estimated that over 75% of QACs are released into the environment through sewer and waste water treatment plants.^{19,21} Originally, QACs were thought to pose little threat of resistance due to their membrane perturbation MoA. Because the membrane is essential to the cell's survival, it was hypothesized that changes to the membrane were highly unlikely, or if they did occur it was an impermanent

change known as bacterial tolerance.²² Tolerance, or adaptation, is a non-genetic change that occurs due to outside pressure but is reversed once the stressor (QAC) is removed. Conversely, bacterial resistance is a genetic change that gives the cell the permanent ability to grow in the presence of a biocide. The first reported incidence of tolerance that occurred with QACs was in the 1950s and 1960s.²³ As tolerance is a reversible process, the ability of some bacteria to grow in the presence of QACs was not concerning at that time.

The first account of resistance to QACs was not reported until the late 1980s,^{24–27} and since then, there have been numerous reports detailing the emergence of QAC resistance, as well as research focused on clarifying the mechanism of resistance. One of the most prevalent resistance mechanisms to QACs is the acquisition of *qac* genes.¹⁶ This collection of genes is obtained through

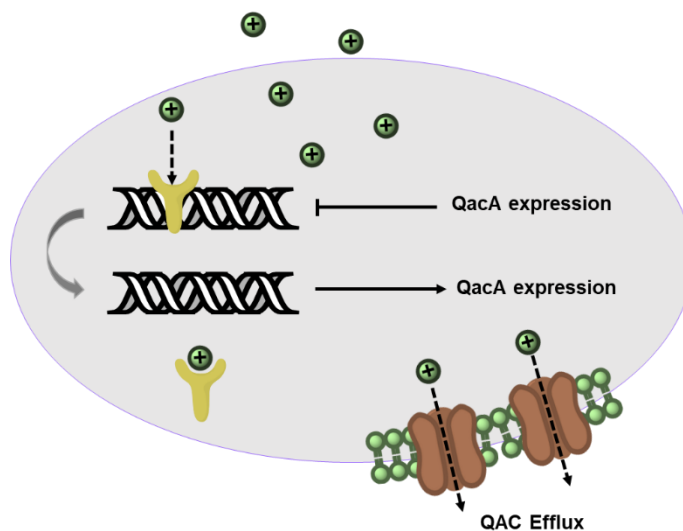


Figure 3.3. Cartoon representation of resistance mechanism against QACs conferred by *qacA/qacR* system. QACs (green) in the cytoplasm bind to QacR (yellow), which releases it from *qacA* and induces QacA (brown) expression. Utilizing a proton motive force, *qacA* removes QACs from the cell.*

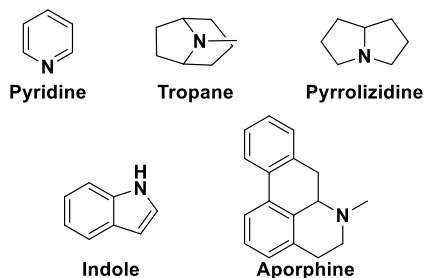
transferable plasmids, often containing other multi-drug resistant genes, and confers the ability to produce QAC-efflux pumps. The most well-studied among Gram-positive pathogens is the *qacAB* gene system. The gene *qacA* encodes for the transmembrane protein of the major facilitator superfamily, QacA.^{28–30} Composed of 14 transmembrane helical coils, this protein utilizes a key

aspartic acid residue to recognize both mono- and bisQACs and expel them from the cell through a proton motive force mechanism. Closely related is *qacB*, which only differs from *qacA* by 7 nucleotides. This gene codes for QacB, another transmembrane protein that in contrast to QacA, mostly recognizes monoQACs due to the presence of alanine rather than the charged aspartic acid residue. The system is regulated by *qacR*, which codes for the protein QacR and whose expression is induced by the presence of QACs. This protein is a negative transcriptional regulator that binds to the intergenic region IR1 of *qacA* (**Figure 3.3**).³¹ Once a QAC binds to QacR, a conformational change occurs causing the protein to release from *qacA*, inducing transcription and production of QacA efflux pumps.³² This mechanism allows for energy conservation and therefore metabolic regulation of this system.

Together with development of QAC resistance, overuse during the SARS-CoV-2 pandemic and extended exposure in the environment, there is a perfect storm for expedited spread of QAC resistance genes, which would alter our ability to utilize these necessary sanitation products. Because of this, there is a great need for further research into QAC development and the production of novel QAC compounds to delay resistance.

3.1.2. Natural Product Alkaloids

A. Common alkaloid skeletal structures



B. Chemical structure of first isolated alkaloid

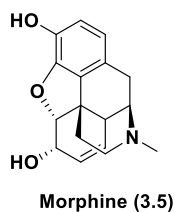


Figure 3.4. **A.** Common alkaloid skeletal structures. **B.** Chemical structure of the first isolated alkaloid, morphine (3.5).

An alkaloid is a naturally occurring compound with “alkali-like” properties containing at least one nitrogen atom, which is often contained within a ring structure (**Figure 3.4 A**).^{33,34}

The first known isolation of an alkaloid natural product occurred in 1805 from *Papaver somniferum L*, commonly called an opium poppy, by a German scientist, Friedrich Wilhelm Adam Sertürner.³⁵ After its isolation, it was given the name morphine (3.5, **Figure 3.4 B**). This powerful alkaloid has become the standard of care for anti-pain treatments with its earliest documentation of use in Europe in 1820.

Since this discovery, hundreds of other alkaloid natural products have been isolated from other plants, microorganisms, terrestrial species, and marine sponges to name a few.³⁶ These powerful molecules have allowed for tremendous advancements in modern medicine, with at least 60 approved, plant-derived alkaloid drugs on the market today.^{36,37} These compounds have also served as a great source of inspiration for the development of synthetic libraries to use in high-throughput screening for biological analysis as these compounds have proven to be very biologically potent and carry a specific mode of action against their biological target. Although there is an expansive library of known alkaloids, more compounds are discovered each year with, notably, 316 new alkaloids reported in the *Journal of Natural Products* in 2020.³⁶ Researchers predict that there are still more to uncover with 153 plant families not yet examined for alkaloids and less than 10⁻⁵% of the marine environment currently explored.^{36,38}

With the expansive biological activities of alkaloids, they have garnered great attention in recent years in application of antibacterial activities.³⁹ Briefly, the general mechanisms of action exhibited by alkaloids against bacteria are inhibition of cell wall synthesis, metabolism, nucleic acid and protein synthesis, as well as disruption of membrane permeation.³⁹ With diverse structures and these specific modes of action, the hope is that these compounds could make great strides in the fight against antibiotic resistance.

3.1.3: *Haliclona viscosa* and 3-Alkyl Pyridinium Alkaloids

Marine sponges have proven to be great source for the discovery of novel alkaloid natural products over the last three decades.⁴⁰ This great wealth of alkaloids is associated with the expansive biodiversity and the need of these organisms to produce compounds for both protection and survival.⁴¹ The most well researched areas for these sponges are usually in the tropics, whereas the arctic remains underexplored.⁴⁰ However, arctic sponges belonging to the genus *Haliclona* have been well-studied and prolific for the discovery of new natural products. These sponges are well-known to produce an array of secondary metabolites that have strong bioactivity.⁴² Specifically, this genus is one of the greatest producers of 3-alkyl pyridine alkaloids (3-APAs), which show a diverse range of bioactivity including antibacterial activity. 3-APAs typically consist of a pyridinium or a tetrahydropyridine (THPy).^{40,43} They are typically connected at the 1- and/or 3-position to an alkyl chain, varying in carbon length. Examples of these include methylaruguspongine C (**3.6**), halicyclamine A (**3.7**), sarain-1 (**3.8**), and manzamine (**3.9**, **Figure 3.5 A**). Within this genus, *Haliclona viscosa* produces five different classes of 3-APAs that vary in complexity: halilocyclins, cyclostelletamines, haliclamines, viscosamines, and viscosalines (**Figure 3.5 B**).⁴⁴⁻⁵² Throughout each class, compounds exist as monomers, dimers, trimers, or

polymers. They also vary in pyridine content, oxidation state, and alkyl chain length with reported lengths from 12 to 14 carbons between each class.

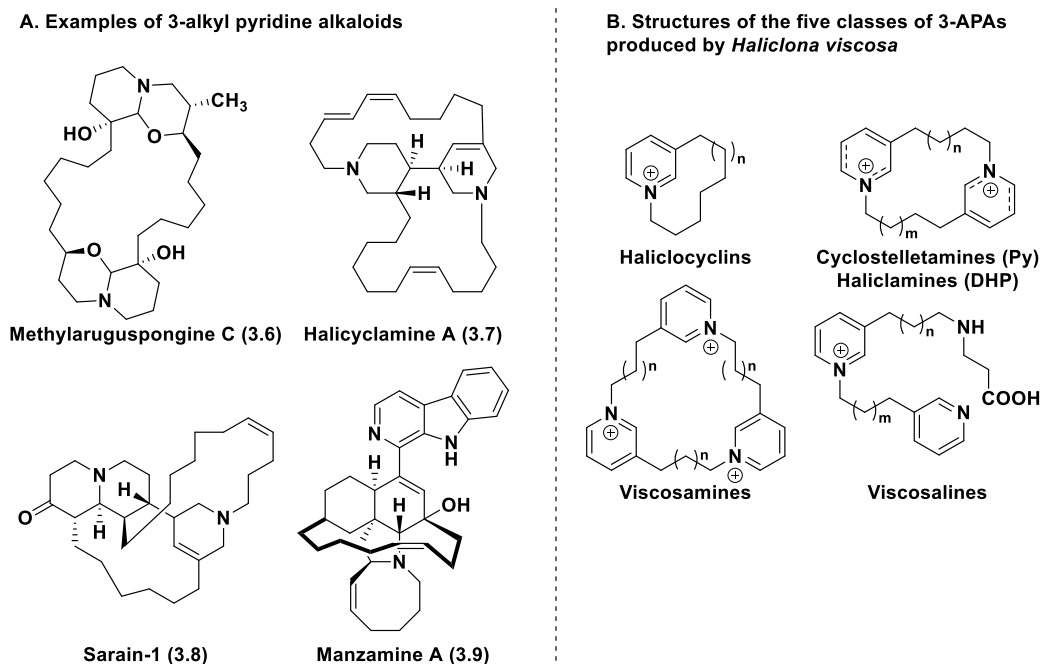


Figure 3.5. A. Chemical structures of 3-alkyl pyridine alkaloids natural products produced by *Haliclona*. B. Chemical structures of the five classes of 3-alkyl pyridine alkaloids produced by *Haliclona viscosa*. Py = pyridine. DHP = dihydropyridine.

Although the 3-APAs produced by *H. viscosa* are simple in comparison to the more complex structures produced by other *Haliclona* sponges, they still exhibit various biological activities. These include mouse embryonic fibroblast cytotoxicity,⁴⁹ epidermal growth factor antagonism,⁵³ muscarinic acetylcholine receptor antagonism,⁵⁴ and antibacterial activity.⁴⁹ Further biological analysis, though, is limited due to low availability of these natural products through isolation from the sponges due in part to low production of these molecules in less populated arctic ecosystems.⁴¹ Synthetic investigations of these molecules have been employed mostly for structural validation as these compounds are difficult to assess through nuclear magnetic resonance (NMR) spectroscopy due in part to the long alkyl chains and often dimeric complexes.⁴⁰

3.1.4: Previous Synthetic Efforts to 3-APAs and Haliclocyclins

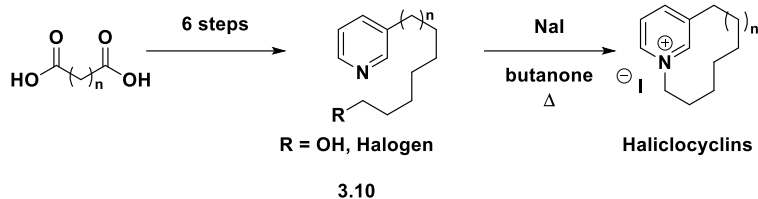


Figure 3.6 Example synthesis to access synthetic intermediate **3.10** followed by halicyclin scaffold employed by Köck and co-workers.

Synthetic efforts towards the five classes of 3-APAs produced by *H. viscosa* all share a common synthetic intermediate, (**3.10**, **Figure 3.6**).^{48,49,52–55} Although the

intermediate and structural classes of the 3-APAs appear to be simple, they require lengthy syntheses and harsh conditions to obtain the desired product. Typically, the synthetic intermediate **3.10** is achieved by a monohalogenation of a diacid (or diol), followed by hydroxyl protection, and finally coupling to 3-picoline via treatment with lithium diisopropylamide (LDA). From here, the syntheses diverge depending upon which class of 3-APA is desired. These conditions yield a foundation for improvement towards simplified synthesis without the need for protecting groups or harsh conditions.

In addition to improving upon the synthetic route to these molecules, their biological activity was of interest as 3-APAs also act as QACs. Most notably, the halicyclins structurally resemble CPC (see section 3.1.1., **Figure 3.1 B**, **3.4**), the active ingredient in most mouthwashes. Furthermore, previous research into the antibacterial activities of these molecules have been limited to disc-diffusion assays. While this assay is successful in assessing the susceptibility of bacteria to most antibiotics, the cationic nature of 3-APAs reduces the rate at which it diffuses on the agar, therefore limiting the accuracy of determining their antibacterial activity.⁵⁶ As such, there is also room for improvement in accurately analyzing the antibacterial activity of these compounds.

3.2: Results and Discussion

Adapted from the publication: Kaplan, A.R.*; Schrank, C.L.*; Wuest, W.M. An Efficient Synthesis of 3-Alkylpyridine Alkaloids Enables Their Biological Investigation. *ChemMedChem* **2021**, *16*, 2487 – 2490.⁴³ * indicates authors contributed equally to this work.

3.2.1.: Synthetic Strategy

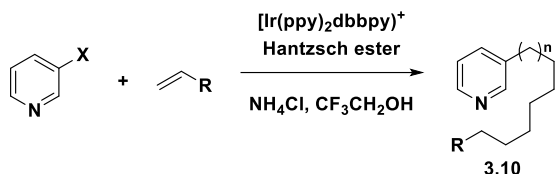
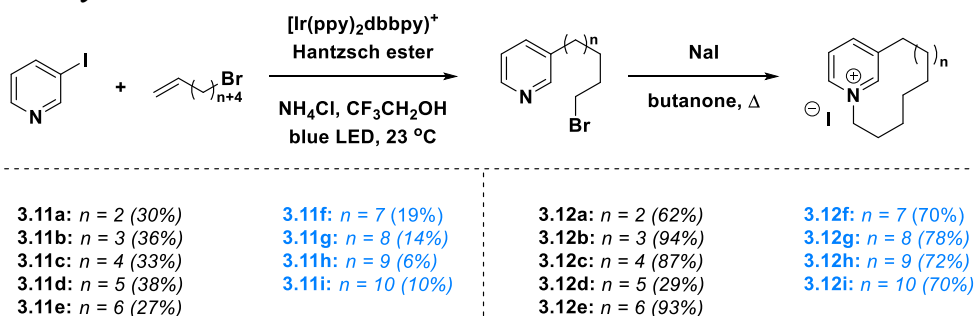


Figure 3.7 Hydroarylation reaction developed by Jui and co-workers that will allow for rapid access to intermediate **3.10**. X = halogen. R = halogen or OH.

University.^{57–59} This methodology would allow us to rapidly access the 3-alkyl pyridine intermediate (**3.10**, **Figure 3.7**) in a single step by utilizing mild, photocatalytic conditions, which removes the need for protecting group manipulations. This methodology has shown to be regioselective and tolerate a wide variety of functional groups as exemplified in Boyington and co-workers synthesis of the fungicide fluopyram produced by Bayer.⁵⁹ Through use of this methodology, we aimed to develop a concise synthetic route to afford the key intermediate (**3.10**) that would allow us to access a nine-compound library made up of two natural and seven unnatural halicyclins. This library could then be analyzed for its antibacterial and hemolytic activities.

3.2.2. Forward Synthesis



Scheme 3.1 Synthesis of halicyclins and analogs. Yields in blue were produced by CLZ. Yields in black were conducted by ARK.

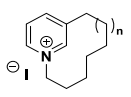
Synthesis of the desired analogs began with the hydroarylation of 3-iodopyridine with terminal-bromo alkenes containing 8-16 carbon atoms to yield the desired 3-alkylated adducts **3.11a-3.11i** (**Scheme 3.1**). There was a noticeable drop in yield as the carbon chain length of the alkene increased. We believe this is likely due to the decrease in solubility of the alkene in the highly polar reaction solvent. To circumvent this issue, we attempted adding up to 10% toluene to the reaction mixture. We did note a slight increase in yield; however, we did not continue to increase the concentration of toluene beyond 10% due to extensive evaluation of solvents previously done by Boyington and co-workers, in which they noted that the trifluoroethanol was necessary for catalytic reactivity.^{57,58} Additionally, alkenes with 13-16 carbon chain lengths were not accessible via commercial sources and had to be synthesized by both myself and ARK via Grignard reaction between 4-pentenylmagnesium bromide and the necessary dibromoalkane (see Supporting Information for more details). With these nine compounds in hand, we then cyclized them through treatment with sodium iodide refluxing in butanone to yield the desired 3-APA molecules **3.12a-I** (**Scheme 3.1**). Through the hydroarylation reaction, we were able to access all nine 3-APA compounds in two to three steps. This synthesis achieved our goal of reducing the step count in comparison to previously published work,⁴⁹ and employing milder conditions.

3.2.2.: Biological Analysis

Having accessed all nine compounds, we set out to evaluate their biological activity. To assess this, we tested the compounds against a panel of seven different strains of Gram-negative and Gram-positive bacteria (*Staphylococcus aureus*, community acquired-MRSA, hospital acquired-MRSA, *Enterococcus faecalis*, *Escherichia coli*, *Pseudomonas aeruginosa*, and *Streptococcus mutans*) utilizing a minimum inhibitory concentration (MIC) assay. In these assays, the MIC is determined as the minimum concentration of compound required to inhibit bacterial

growth by visual analysis.⁶⁰ This allows for a more accurate analysis of their activity in comparison to previously reported disc diffusion assays. Overall, we found that all nine compounds exhibited more potent activity against the Gram-positive strains of bacteria compared to the Gram-negative strains (**Table 3.1**). This hints at a shared mechanism between the halicyclins and QACs, namely membrane perturbation. Additionally, several compounds (**3.12c**, **3.12f-i**) displayed modest activity against *S. mutans*. Overall, the MIC values varied across the nine-compound library with increased potency trending with increased alkyl chain length. Previous work has shown that there is an optimal alkyl length for QACs with respect to their bioactivity, and this trend may also apply to the halicyclins.^{5,15,16,61–65} However, more work is needed to confirm this hypothesis.

In addition to antibacterial activity, we also assessed their toxicity profile through red blood cell (RBC) lysis assay using mechanically defibrillated sheep's blood. These values are shown as Lysis₂₀, which indicates the concentration of compound that lyse 20% or less of the RBCs. Overall, the library showed high toxicity indicated by low Lysis₂₀ values (**Table 3.1**). This, however, is not surprising as these class of molecules have shown cytotoxicity against mouse embryonic fibroblasts.⁴⁹

Compound 	Minimum Inhibitory Concentration (μM)							Lysis ₂₀
	<i>S. aureus</i>	CA-MRSA	HA-MRSA	<i>E. faecalis</i>	<i>E. coli</i>	<i>P. aeruginosa</i>	<i>S. mutans</i>	
3.12a (<i>n</i> =2)	32	32	32	64	32	64	64	2
3.12b (<i>n</i> =3)	32	32	16	64	32	64	125	0.25
3.12c (<i>n</i> =4)	32	32	16	64	32	64	32	0.5
3.12d (<i>n</i> =5)	32	32	32	64	64	64	125	0.125
3.12e (<i>n</i> =6)	32	32	16	125	125	125	64	8

3.12f (<i>n</i> =7)	16	16	8	125	32	125	16	4
3.12g (<i>n</i> =8)	32	32	16	250	64	250	32	16
3.12h (<i>n</i> =9)	32	16	16	250	64	250	32	16
3.12i (<i>n</i> =10)	8	8	8	125	64	125	16	8
CPC	0.5	1	1	250	32	250	1	16
BAC	2	4	4	125	64	125	1	8

Table 3.1 MIC and Lysis₂₀ values for compounds **3.12a** – **3.12i**. MIC values are reported as the highest concentration of compound required to inhibit growth completely across three replicate trials. Lysis₂₀ indicates the concentration of compound that lyse 20% or less of RBC. Both assays performed in triplicate. CA = community acquire; HA = hospital acquired. BAC = benzyalkonium chloride (positive control); CPC = cetylpyridinium chloride (positive control).

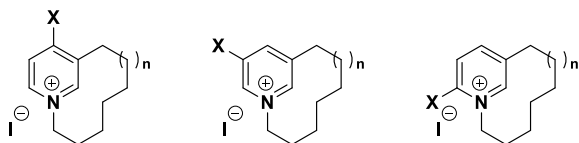
3.2.3.: Conclusion and Future Directions

Through this work, we were able to develop a concise, mild route to quickly access the monomeric, 3-APAs, haliclocyclins as well as structural analogs. In total, we synthesized a library of nine compounds in two to three steps and in moderate to good yields via photocatalytic conditions. Additionally, we were able to analyze their antibacterial activity and hemolytic activity through MIC and RBC lysis assays respectively. Although the activity was modest in comparison to the QAC positive controls, this work adds to the growing library of QAC bioactivity and structure-activity-relationship information for future studies into QAC development. Additionally, the new route we have developed would allow for quick access to not only the haliclocyclins, but also the other structural classes of 3-APAs produced by *H. viscosa* and enable further biological analysis and structural validation of these compounds.

Moving forward, we have proposed additional analogs that further explore functionalization of the pyridine ring such as halogen, hydroxyl, and carboxylic acid functional groups at the 4-, 5-, and 6-positions to assess if these modifications would improve the biological activity of these compounds (**Figure 3.8A**). We attempted accessing these compounds utilizing

the methodology described; however, we were unsuccessful in achieving the hydroarylation products. This reaction could be improved by either altering the synthetic sequence so that the hydroarylation would occur on the tethered product, or employing photocatalytic conditions that

A. Proposed future analog structures



where X = halogen, OH, or COOH

B. General synthetic scheme of carbon dioxide radical anion method from Hendy and co-workers⁶⁶

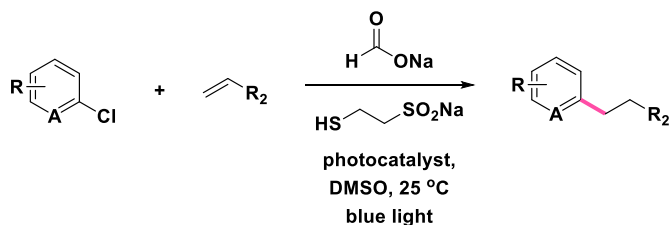


Figure 3.8 A. Structures of proposed future analogs where X = halogen, OH, or COOH. B. General synthetic scheme of the carbon dioxide radical anion method developed by Hendy and co-workers.⁶⁶

the 2-position of pyridine.

were recently

disclosed by Hendy

and co-workers

(**Figure 3.8B**).⁶⁶

These conditions

utilize a radical chain

reduction via a carbon

dioxide radical anion

to access radical

defluoroalkylation at

Chapter 3 References

1. Carden, R. G. *et al.* Advancements in the Development of Non-Nitrogen-Based Amphiphilic Antiseptics to Overcome Pathogenic Bacterial Resistance. *ChemMedChem* vol. 15 1974–1984 (2020).
2. Smilack, J. D. Trimethoprim-sulfamethoxazole. in *Mayo Clinic Proceedings* vol. 74 730–734 (Elsevier, 1999).
3. Sawyer, P. R., Brogden, R. N., Pinder, K. M., Speight, T. M. & Avery, G. S. Clotrimazole: A Review of its Antifungal Activity and Therapeutic Efficacy. *Drugs* 1975 96 9, 424–447 (2012).
4. McDonnell, G. & Russell, A. D. Antiseptics and disinfectants: Activity, action, and resistance. *Clinical Microbiology Reviews* vol. 12 147–179 (1999).
5. Morrison, K. R., Allen, R. A., Minbiole, K. P. C. & Wuest, W. M. More QACs, more questions: Recent advances in structure activity relationships and hurdles in understanding resistance mechanisms. *Tetrahedron Letters* vol. 60 150935 (2019).
6. Jacobs, W. A., Heidelberger, M. & Bull, C. G. The bactericidal properties of the quaternary salts of hexamethylenetetramine: III. the relation between constitution and bactericidal action in the quaternary salts obtained from halogenacetyl compounds. *J. Exp. Med.* **23**, 577–599 (1916).
7. PRICE, P. B. Benzalkonium chloride (zephiran chloride) as a skin disinfectant. *Arch. Surg.* **61**, 23–33 (1950).
8. Choi, S. M. *et al.* Risk assessment of benzalkonium chloride in cosmetic products. *J. Toxicol. Environ. Heal. - Part B Crit. Rev.* **21**, 8–23 (2018).
9. Cumming, J. L., Hawker, D. W., Nugent, K. W. & Chapman, H. F. Ecotoxicities of

- polyquaterniums and their associated polyelectrolyte- surfactant aggregates (PSA) to *Gambusia holbrooki*. *J. Environ. Sci. Heal. - Part A Toxic/Hazardous Subst. Environ. Eng.* **43**, 113–117 (2008).
10. Pereira, B. M. P. & Tagkopoulos, I. Benzalkonium chlorides: Uses, regulatory status, and microbial resistance. *Applied and Environmental Microbiology* vol. 85 (2019).
 11. Mao, X. *et al.* Cetylpyridinium chloride: Mechanism of action, antimicrobial efficacy in biofilms, and potential risks of resistance. *Antimicrob. Agents Chemother.* **64**, (2020).
 12. Gerba, C. P. Quaternary ammonium biocides: Efficacy in application. *Applied and Environmental Microbiology* vol. 81 464–469 (2015).
 13. Dewey, H. M., Jones, J. M., Keating, M. R. & Budhathoki-Uprety, J. Increased Use of Disinfectants During the COVID-19 Pandemic and Its Potential Impacts on Health and Safety. *ACS Chem. Heal. Saf.* **29**, 27–38 (2022).
 14. Schrank, C. L., Minbiole, K. P. C. & Wuest, W. M. Are Quaternary Ammonium Compounds, the Workhorse Disinfectants, Effective against Severe Acute Respiratory Syndrome-Coronavirus-2? *ACS Infectious Diseases* vol. 6 1553–1557 (2020).
 15. Jennings, M. C., Buttaro, B. A., Minbiole, K. P. C. & Wuest, W. M. Bioorganic Investigation of Multicationic Antimicrobials to Combat QAC-Resistant *Staphylococcus aureus*. *ACS Infect. Dis.* **1**, 304–309 (2016).
 16. Jennings, M. C., Minbiole, K. P. C. & Wuest, W. M. Quaternary Ammonium Compounds: An Antimicrobial Mainstay and Platform for Innovation to Address Bacterial Resistance. *ACS Infectious Diseases* vol. 1 288–303 (2015).
 17. Purohit, A. *et al.* Quaternary ammonium compounds and occupational asthma. *Int. Arch. Occup. Environ. Health* **73**, 423–427 (2000).

18. Wessels, S. & Ingmer, H. Modes of action of three disinfectant active substances: A review. *Regul. Toxicol. Pharmacol.* **67**, 456–467 (2013).
19. Hora, P. I., Pati, S. G., McNamara, P. J. & Arnold, W. A. Increased Use of Quaternary Ammonium Compounds during the SARS-CoV-2 Pandemic and Beyond: Consideration of Environmental Implications. *Environmental Science and Technology Letters* vol. 7 622–631 (2020).
20. Chen, Z., Guo, J., Jiang, Y. & Shao, Y. High concentration and high dose of disinfectants and antibiotics used during the COVID-19 pandemic threaten human health. *Environ. Sci. Eur.* **33**, (2021).
21. Boethling, R. S. Environmental fate and toxicity in wastewater treatment of quaternary ammonium surfactants. *Water Research* vol. 18 1061–1076 (1984).
22. Levin-Reisman, I., Brauner, A., Ronin, I. & Balaban, N. Q. Epistasis between antibiotic tolerance, persistence, and resistance mutations. *Proc. Natl. Acad. Sci. U. S. A.* **116**, 14734–14739 (2019).
23. Maxcy, R. B., Tiwari, N. P. & Sopley, P. R. Changes in *Escherichia coli* Associated with Acquired Tolerance for Quaternary Ammonium Compounds. *Appl. Microbiol.* **22**, 229–232 (1971).
24. Tennent, J. M., Lyon, B. R., Gillespie, M. T., May, J. W. & Skurray, R. A. Cloning and expression of *Staphylococcus aureus* plasmid-mediated quaternary ammonium resistance in *Escherichia coli*. *Antimicrob. Agents Chemother.* **27**, 79–83 (1985).
25. Gillespie, M. T., May, J. W. & Skurray, R. A. Plasmid-encoded resistance to acriflavine and quaternary ammonium compounds in methicillin-resistant *Staphylococcus aureus*. *FEMS Microbiol. Lett.* **34**, 47–51 (1986).

26. Skurray, R. A. *et al.* Multiresistant *Staphylococcus aureus*: genetics and evolution of epidemic Australian strains. *J. Antimicrob. Chemother.* **21 Suppl C**, 19–39 (1988).
27. Rouch, D. A., Cram, D. S., Di Berardino, D., Littlejohn, T. G. & Skurray, R. A. Efflux-mediated antiseptic resistance gene *qacA* from *Staphylococcus aureus*: common ancestry with tetracycline- and sugar-transport proteins. *Mol. Microbiol.* **4**, 2051–2062 (1990).
28. Mitchell, B. A., Brown, M. H. & Skurray, R. A. QacA multidrug efflux pump from *Staphylococcus aureus*: Comparative analysis of resistance to diamidines, biguanidines, and guanyldrazones. *Antimicrob. Agents Chemother.* **42**, 475–477 (1998).
29. Paulsen, I. T., Brown, M. H. & Skurray, R. A. Proton-dependent multidrug efflux systems. *Microbiol. Rev.* **60**, 575–608 (1996).
30. Brown, M. H. & Skurray, R. A. *QacA-Mediated Multidrug Resistance 163 Staphylococcal Multidrug Efflux Protein QacA JMMB Symposium. J. Mol. Microbiol. Biotechnol* vol. 3 www.caister.com/bacteria-plant (2001).
31. Schumacher, M. A., Miller, M. C. & Grkovic, S. Structural basis for cooperative DNA binding by two dimers of the multidrug-binding protein QacR. *EMBO J.* **21**, 1210–1218 (2002).
32. Godsey, M. H., Zheleznova Heldwein, E. E. & Brennan, R. G. Structural biology of bacterial multidrug resistance gene regulators. *Journal of Biological Chemistry* vol. 277 40169–40172 (2002).
33. Ain, Q. U., Khan, H., Mubarak, M. S. & Pervaiz, A. Plant alkaloids as antiplatelet agent: Drugs of the future in the light of recent developments. *Front. Pharmacol.* **7**, 292 (2016).
34. Kurek, J. Introductory Chapter: Alkaloids - Their Importance in Nature and for Human Life. in *Alkaloids - Their Importance in Nature and Human Life* (IntechOpen, 2019).

doi:10.5772/intechopen.85400.

35. Devereaux, A. L., Mercer, S. L. & Cunningham, C. W. DARK Classics in Chemical Neuroscience: Morphine. *ACS Chem. Neurosci.* **9**, 2395–2407 (2018).
36. Daley, S. K. & Cordell, G. A. Alkaloids in contemporary drug discovery to meet global disease needs. *Molecules* **26**, (2021).
37. Cordell, G. A., Quinn-Beattie, M. Lou & Farnsworth, N. R. The potential of alkaloids in drug discovery. *Phytotherapy Research* vol. 15 183–205 (2001).
38. Porras, G. *et al.* Ethnobotany and the Role of Plant Natural Products in Antibiotic Drug Discovery. *Chemical Reviews* vol. 121 3495–3560 (2021).
39. Yan, Y. *et al.* Research progress on antibacterial activities and mechanisms of natural alkaloids: A review. *Antibiotics* vol. 10 318 (2021).
40. Köck, M., Muñoz, J., Cychon, C., Timm, C. & Schmidt, G. The Arctic sponge *Haliclona viscosa* as a source of a wide array of 3-alkyl pyridine alkaloids. *Phytochemistry Reviews* vol. 12 391–406 (2013).
41. Ruzicka, R. & Gleason, D. F. Latitudinal variation in spongivorous fishes and the effectiveness of sponge chemical defenses. *Oecologia* **154**, 785–794 (2008).
42. Gupta, P. Chemical constituents of *Haliclona*: An overview. *J. Pharmacogn. Phytochem.* **8**, 823–827 (2019).
43. Kaplan, A. R., Schrank, C. L. & Wuest, W. M. An Efficient Synthesis of 3-Alkylpyridine Alkaloids Enables Their Biological Evaluation. *ChemMedChem* **16**, 2487–2490 (2021).
44. Fusetani, N., Asai, N., Matsunaga, S., Honda, K. & Yasumuro, K. Cyclostelletamines A–F, pyridine alkaloids which inhibit binding of methyl quinuclidinyl benzilate (QNB) to muscarinic acetylcholine receptors, from the marine sponge, *Stelletta maxima*.

- Tetrahedron Lett.* **35**, 3967–3970 (1994).
45. Volk, C. A. & Köck, M. Viscosamine: The first naturally occurring trimeric 3-alkyl pyridinium alkaloid. in *Organic Letters* vol. 5 3567–3569 (American Chemical Society, 2003).
 46. Volk, C. A. & Köck, M. Viscosaline: New 3-alkyl pyridinium alkaloid from the Arctic sponge *Haliclona viscosa*. *Org. Biomol. Chem.* **2**, 1827–1830 (2004).
 47. Volk, C. A., Lippert, H., Lichte, E. & Köck, M. Two new haliclamines from the Arctic sponge *haliclona viscosa*. *European J. Org. Chem.* **2004**, 3154–3158 (2004).
 48. Grube, A., Timm, C. & Köck, M. Synthesis and mass spectrometric analysis of cyclostelletamines H, I, K and L. *European J. Org. Chem.* **2006**, 1285–1295 (2006).
 49. Timm, C., Volk, C., Sasse, F. & Köck, M. The first cyclic monomeric 3-alkylpyridinium alkaloid from natural sources: Identification, synthesis, and biological activity. *Org. Biomol. Chem.* **6**, 4036–4040 (2008).
 50. Schmidt, G., Timm, C. & Köck, M. New haliclamines e and F from the Arctic sponge *Haliclona viscosa*. *Org. Biomol. Chem.* **7**, 3061–3064 (2009).
 51. Cychon, C., Schmidt, G., Mordhorst, T. & Köck, M. Structure elucidation of submilligram quantities of natural products - Application to haliclamines G and H from the Arctic marine sponge *Haliclona viscosa*. *Zeitschrift für Naturforsch. - Sect. B J. Chem. Sci.* **67**, 944–950 (2012).
 52. Schmidt, G., Timm, C., Grube, A., Volk, C. A. & Köck, M. Viscosalines B 1,2 and E 1,2: Challenging new 3-alkyl pyridinium alkaloids from the marine sponge *Haliclona viscosa*. *Chem. - A Eur. J.* **18**, 8180–8189 (2012).
 53. Davies-Coleman, M. T. *et al.* A New EGF-Active Polymeric Pyridinium Alkaloid from

- the Sponge *Callyspongia fibrosa*. *J. Org. Chem.* **58**, 5925–5930 (1993).
54. Anan, H. *et al.* Total synthesis of cyclostelletamine C, a bispyridinium macrocyclic alkaloid having muscarinic acetylcholine receptor antagonistic activity. *Tetrahedron* **52**, 10849–10860 (1996).
 55. Timm, C., Mordhorst, T. & Köck, M. Synthesis of 3-alkyl pyridinium alkaloids from the arctic sponge *Haliclona viscosa*. *Marine Drugs* vol. 8 483–497 (2010).
 56. Piddock, L. J. V. Techniques used for the determination of antimicrobial resistance and sensitivity in bacteria. *Journal of Applied Bacteriology* vol. 68 307–318 (1990).
 57. Boyington, A. J., Riu, M. L. Y. & Jui, N. T. Anti-Markovnikov Hydroarylation of Unactivated Olefins via Pyridyl Radical Intermediates. *J. Am. Chem. Soc.* **139**, 6582–6585 (2017).
 58. Seath, C. P., Vogt, D. B., Xu, Z., Boyington, A. J. & Jui, N. T. Radical Hydroarylation of Functionalized Olefins and Mechanistic Investigation of Photocatalytic Pyridyl Radical Reactions. *J. Am. Chem. Soc.* **140**, 15525–15534 (2018).
 59. Boyington, A. J., Seath, C. P., Zearfoss, A. M., Xu, Z. & Jui, N. T. Catalytic Strategy for Regioselective Arylethylamine Synthesis. *J. Am. Chem. Soc.* **141**, 4147–4153 (2019).
 60. Lambert, R. J. W. & Pearson, J. Susceptibility testing: Accurate and reproducible minimum inhibitory concentration (MIC) and non-inhibitory concentration (NIC) values. *J. Appl. Microbiol.* **88**, 784–790 (2000).
 61. Kontos, R. C. *et al.* An Investigation into Rigidity–Activity Relationships in BisQAC Amphiphilic Antiseptics. *ChemMedChem* **14**, 83–87 (2019).
 62. Allen, R. A. *et al.* Ester- and amide-containing multiQACs: Exploring multicationic soft antimicrobial agents. *Bioorganic Med. Chem. Lett.* **27**, 2107–2112 (2017).

63. Forman, M. E., Jennings, M. C., Wuest, W. M. & Minbiole, K. P. C. Building a Better Quaternary Ammonium Compound (QAC): Branched Tetracationic Antiseptic Amphiphiles. *ChemMedChem* **11**, 1401–1405 (2016).
64. Joyce, M. D. *et al.* Natural product-derived quaternary ammonium compounds with potent antimicrobial activity. *J. Antibiot. (Tokyo)*. **69**, 344–347 (2016).
65. Garrison, M. A., Mahoney, A. R. & Wuest, W. M. Tricepyridinium-inspired QACs yield potent antimicrobials and provide insight into QAC resistance. *ChemMedChem* **16**, 463–466 (2021).
66. Hendy, C. M., Smith, G. C., Xu, Z., Lian, T. & Jui, N. T. Radical Chain Reduction via Carbon Dioxide Radical Anion ($\text{CO}_2^{\bullet-}$). *J. Am. Chem. Soc.* **143**, 8987–8992 (2021).

Chapter 4: Synthetic and Biological Investigations into Simplified Analogs of SF2768

4.1: Background – SF2768

As discussed in chapter one, an emerging class of antibacterial small molecules are isonitrile natural products. In addition to their ability to inhibit bacterial growth, these compounds display preferential binding of Cu(I) ions, which classifies them as chalkophores. However, it is still unconfirmed if this binding event plays a role in their antibacterial activity. Of the isonitriles reported, there has been a broad range of activities with many having broad spectrum activity and others displaying selective activity, most notably for Gram-negative bacteria.¹⁻⁷ Of the few target identification analyses performed on isonitriles, heme synthesis has emerged as a common target both in bacteria² as well as *Plasmodium falciparum*, the causative agent for malaria.^{8,9}

One of the first isonitrile natural products was xanthocillin X. This compound possesses potent broad-spectrum antibacterial activity as well as antifungal activity. After its discovery, it was used as a topical antibiotic under the drug name Brevicid for 15 years.¹⁰ Recently, its mechanism of action was disclosed by Sieber and co-workers at the Technical University of Munich.² Though affinity and activity-based protein profiling were unsuccessful, they were able to generate resistant *Acinetobacter baumannii* mutants, which identified a mutation in the enzyme

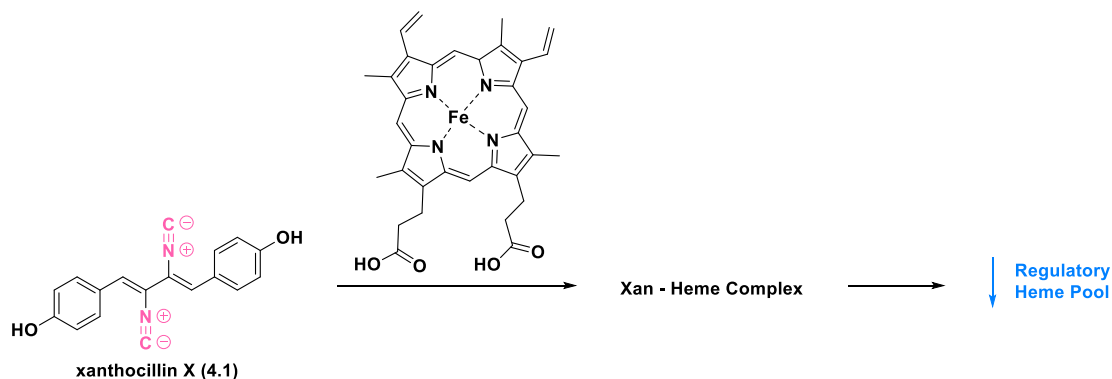


Figure 4.1 Chemical structure of xanthocillin X (4.1), and a generalized scheme of its proposed mechanism of action.

porphobilinogen synthase (PbgS), an essential enzyme in the biosynthesis of heme (**Figure 4.1**). Coupled with their genomic and proteomic data, the authors were able to identify that xanthocillin X inhibits *A. baumannii* via sequestering heme, which ultimately leads to uncontrolled heme biosynthesis and elevated porphyrin levels. This culminates in dysregulation of several vital cellular pathways as well as production of reactive oxygen species which ultimately results in cell death.² This mechanism of action coupled with its targeted Gram-negative activity poses as a promising foundation to further develop and analyze other isonitrile natural products.

One such molecule is the lipopeptide, SF2768 (**4.2, Figure 4.2**). This natural product was originally isolated by Tabata and coworkers in 1995 from *Streptomyces sp.* SF2768.¹¹ Within their isolation report, the authors utilized NMR decoupling experiments and COSY analysis in order to elucidate its structure. Through these analyses, they found that SF2768 exists as a mixture of anomers at the lactol position. However, further efforts to elucidate the stereochemical assignments of the amide side chains have proven difficult.

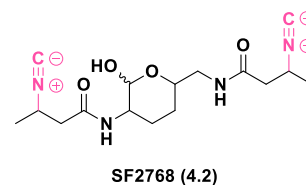


Figure 4.2 Chemical Structure of SF2768

In addition to the structure evaluation, the authors performed preliminary biological assays to evaluate SF2768's antimicrobial activity. Overall, they analyzed several bacterial and fungal strains including *Bacillus subtilis*, *Micrococcus luteus*, *Staphylococcus aureus*, *Escherichia coli*, *Saccharomyces cerevisiae*, *Candida albicans*, *Cryptococcus neoformans*, and *Trignopsis variabilis*. Each of the strains analyzed had an appreciable zone of inhibition, within 15 – > 35 nm. Additionally, they analyzed its minimum inhibitory concentration (MIC) against two different strains of *C. neoformans*. SF2768 had an MIC value of 0.39 $\mu\text{g/mL}$ against *C. neoformans* IMC F-10 and 3.13 $\mu\text{g/mL}$ against *C. neoformans* Cr-1.

Following its isolation, SF2768 was identified as a cryptic antibiotic in 2011 by Ueda and co-workers. They found that its production in *Streptomyces griseorubiginosus* was triggered by exposure to monensin, a polyether ionophore.¹² Although its biological activity proved promising, further exploration was relatively nonexistent until its revitalization in 2017 by He and coworkers.¹³ In their analysis, they identified an orphan nonribosomal peptide synthetase (NRPS) gene cluster, *sfa*, from *S. thioluteus* that directed the biosynthesis of SF2768.

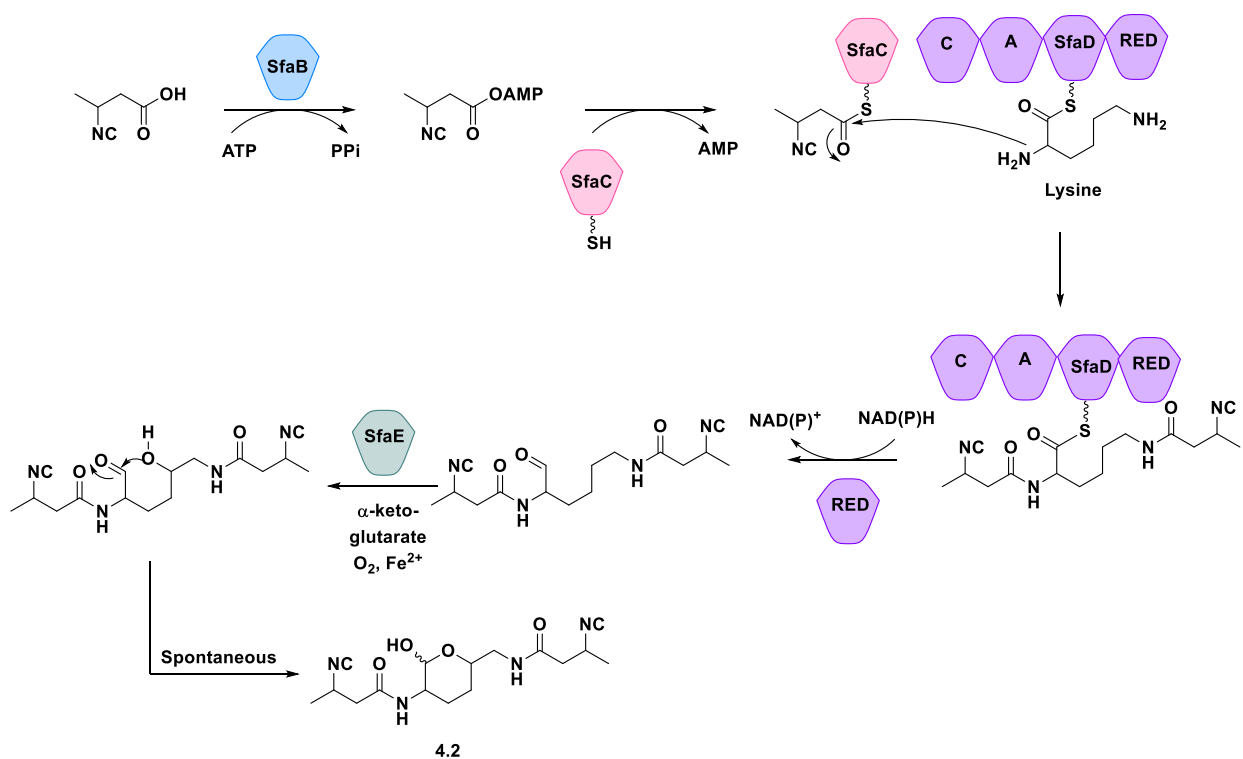


Figure 4.3 Proposed biosynthetic pathway towards SF2768 (**4.2**). C = condensation domain; A = adenylation domain; RED = reductase.

Through gene knockout studies as well as homology alignments via BLAST sequencing, they were able to propose a reasonable biosynthetic pathway (**Figure 4.3**). Briefly, the authors hypothesize that the biosynthetic pathway begins with 3-isocyanobutanoic acid, which is produced from an unknown pathway. The AMP-ligase, SfaB, then adenylates the carboxylic acid followed by, SfaC, a peptidyl carrier protein, transferring the compound to the building chain, which then

undergoes an amidation reaction with a SfaD bound lysine residue. The resulting compound is then cleaved from the chain via an NADPH dependent reductase. From this intermediate, a post-NRPS modification is made by the hydroxylase SfaE. This resulting hydroxyl group then spontaneously attacks the aldehyde to form the lactol core, thus producing SF2768 (**4.2**).

Additionally, they noted a putative ATP-binding cassette (ABC) transporter within the biosynthetic gene cluster which hinted that the product, SF2768, may be a siderophore, or iron binding molecule. This theory was further explored, and they noted that SF2768 actually reduced Cu (II) in the culture broth to Cu (I) upon binding. Further analysis showed that it formed stable Cu(I) complexes in a 2:1 stoichiometry rather than with iron (**Figure 4.4**).

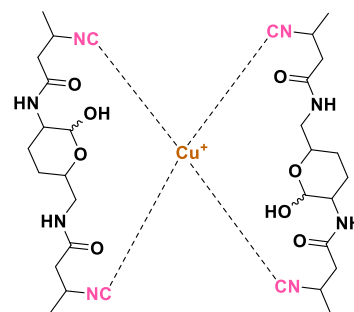
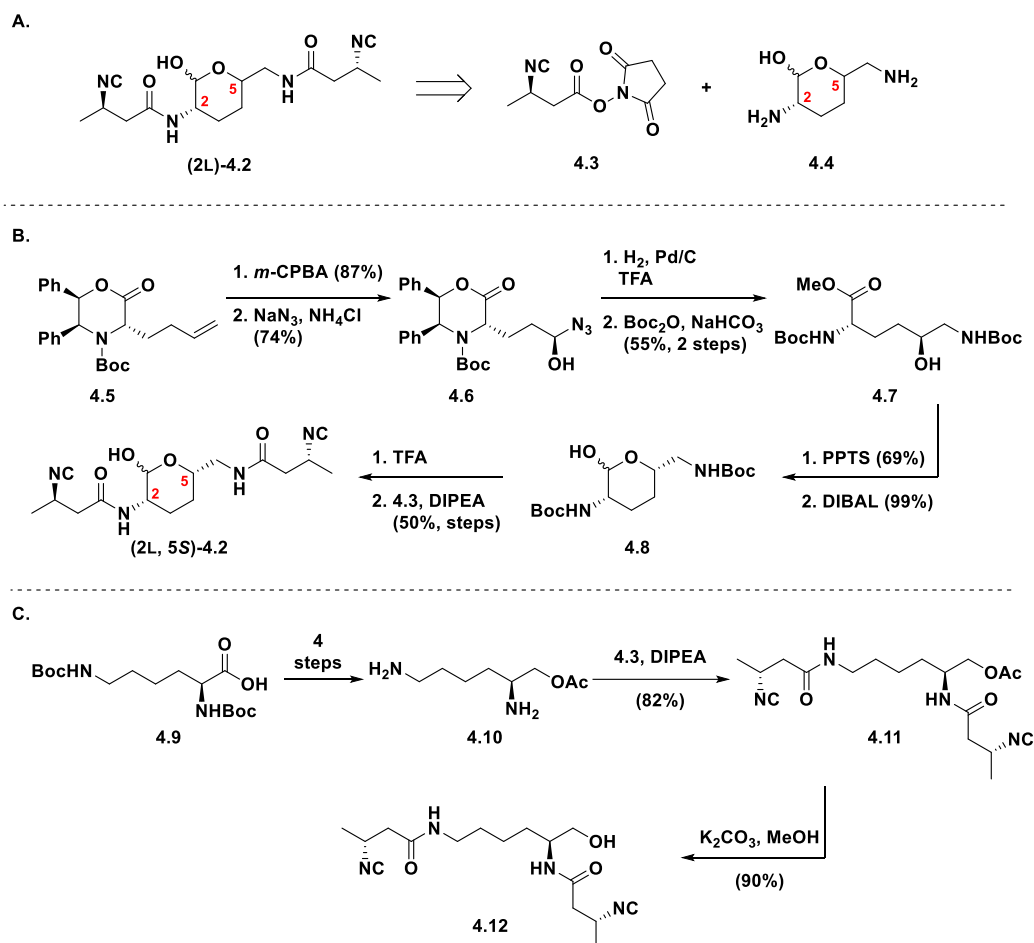


Figure 4.4 Proposed SF2768-Cu complex. Found to bind Cu(I) in a 2:1 stoichiometry.

In vivo analysis within a *Streptomyces lividans* model showed the SF2768-Cu complex was able to shuttle Cu(I) into the cell leading to an increase in Cu(I) concentrations, thereby confirming its activity as a chalkophore.

These data sparked interest in the natural product to further understand its metal binding capabilities as well as elucidate its stereochemical assignments. To this end in 2019, Derek Tan and co-workers performed the total synthesis of SF2768.¹⁴ Based upon earlier disclosures from Zhang and co-workers of the biosynthetic pathway of a related lipopeptide, SF2369, Tan's group presumed that the lactol motif of SF2768 arose from L-lysine.¹⁵ Additionally, the β -isocyanobutyrate sidechain was also determined to have an *R*-configuration within the same report by Zhang and co-workers. This left, then, the determination of the configuration at C5 (**Scheme 4.1A**). To begin, the sidechain was derived from an *N*-hydroxysuccinimide ester (**4.3**) in three synthetic steps. For the lactol core (**4.4**), they begin with epoxidation and ring opening of a



Scheme 4.1 (A) Retrosynthesis of SF2768 into two key intermediates, **4.3** and **4.4**. Remaining stereocenter to be determined is denoted as Carbon 5 in red. (B) Synthetic scheme towards achieving **(2L, 5S)-4.2**. Synthesis towards the other enantiomer was identical. (C) Synthetic scheme towards linear derivatives, SF2768 H (**4.11**) and SF2768 D (**4.12**).

butenylglycine precursor (**4.5**) to obtain the Boc-protected azido alcohol (**4.6**, **Scheme 4.1B**). This was then treated with trifluoroacetic acid, hydrogenated, and Boc-protected to produce 5-hydroxysilane intermediate (**4.7**). Lactonization via PPTS followed by a DIBAL reduction produced the protected lactol (**4.8**). This was then deprotected followed by amidation with **4.3** to obtain SF2768 **(2L,5S)-4.2** in a 7-step longest linear sequence. After obtaining both enantiomers, they were able to confirm the stereochemistry as 2L,5S.

In addition to the natural product, they also synthesized two acyclic derivatives, SF2768 H and SF2768 D, via bisacylation of L-lysine acetate (**4.10**) with **4.3** (**Scheme 4.1 C**). With the

compounds in hand, they then moved on to analyze their copper-binding properties. Complementary to previous studies, they performed NMR titrations of SF2768 H and SF2768. For the linear derivative, they were able to identify a 2:1 stoichiometry to Cu (I) through indicative NMR shifts of the proton adjacent to the isonitrile moiety. Unfortunately, NMR titration analysis of SF2768 was confounded due to overlapping and broadening of peaks. They also attempted to analyze zinc binding and found that it had weaker binding to Zn (II) in comparison to Cu (I).

These results were further built upon in 2020 by He and co-workers who sought to probe its mechanism of action.¹⁶ In their analysis, they found that SF2768 had an inhibition rate of ca. 60% at 100 μ M against *Bacillus subtilis*. They noted that in a disk assay the addition of CuCl₂ to the sample eliminated all inhibitory effects, which hints at the need for SF2768 to be uncomplexed for activity. Inductively coupled plasma mass spectrometry analysis of *B. subtilis* after a 1-hour incubation with SF2768 showed decreased cellular copper content by over 20%. This particular result led the authors to hypothesize that SF2768 executed its antibacterial activity by sequestering Cu from copper-dependent enzymes within the cell.

With this hypothesis, the authors proposed that the target of SF2768 could be cytochrome *c* oxidase (CcO), which is a copper-dependent transmembrane enzyme within the electron transport chain (**Figure 4.5**). If CcO was inhibited, an increased production of reactive oxygen species (ROS) and a decreased ATP synthesis would occur due to the loss of an electron acceptor. The author's found that ATP production decreased, and ROS levels increased after exposure of *B. subtilis* for 1 hour, which hinted at the possibility of targeting CcO. Additionally, they analyzed a panel of bacteria to further probe its antibacterial activity. They found significant inhibitory activity against *Acinetobacter baumannii* (ca. 57%) and *B. subtilis* (ca. 50%) at 10 μ M and noted an increase in intracellular ROS after incubation with SF2768.

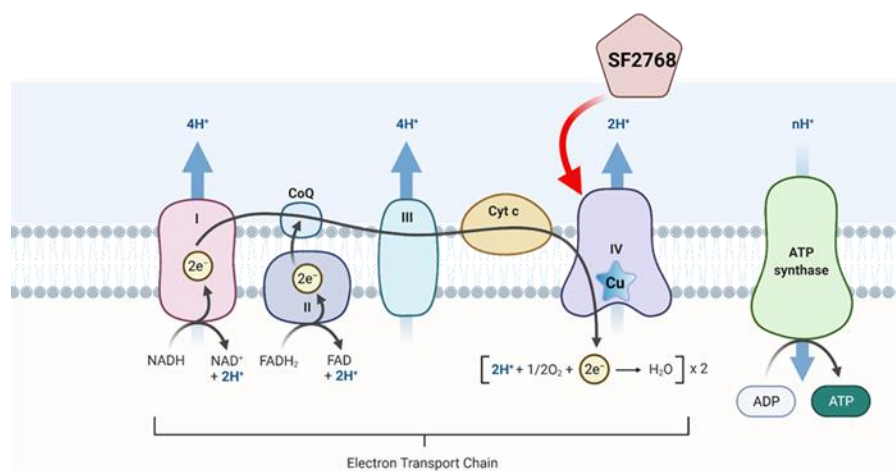


Figure 4.5 Simplified scheme of the bacterial electron transport chain. He and co-workers proposed that SF2768 targets CcO, marked as IV, due to the increased production of ROS and decrease in ATP production. Figure made with BioRender.

To further analyze SF2768's ability to inhibit other copper-dependent enzymes, *in vitro* analysis was performed on tyrosinase. They found that SF2768 had ca. 80% inhibition at 1.0 mM. This data somewhat supports

SF2768's possible targets as copper-dependent enzymes, however, additional analysis is required to confirm *in vivo* activity within these bacterial species as the inhibitory concentration is likely not physiologically relevant.

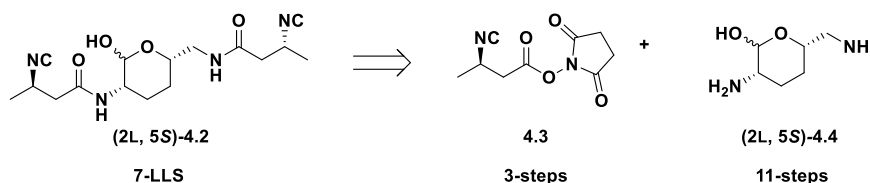
2.2: Results and Discussion

Together with the synthetic and biological investigations, an initial foundation has revealed the possible role of SF2768 in bacterial metal homeostasis as well as its potential as an antibiotic agent, however, further biological investigations are needed. To this end, I sought to synthesize simplified analogs to evaluate the role of the difficult-to-synthesize lactol core and further investigate SF2768's bioactivity (**Figure 4.6**). Described herein is the synthesis of simplified cyclic analogs of SF2768 as well as their biological activities.

2.2.1. Synthesis of Simplified Analogs of SF2768

The synthesis of the simplified analogs was taken on by myself and my undergraduate mentee, Brittney Haney. Our goal for the derivatives was to use a benzene core to limit the synthetic steps required to produce each compound. In comparison to the route to the natural

A. Previous Work: Xu, Y. and Tan, D.S. *Org. Lett.* 2019, 21, 8731-8735.



B. This Work: How important is the lactol moiety to SF2768's biological activity?

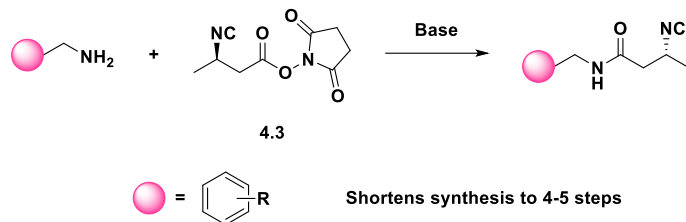
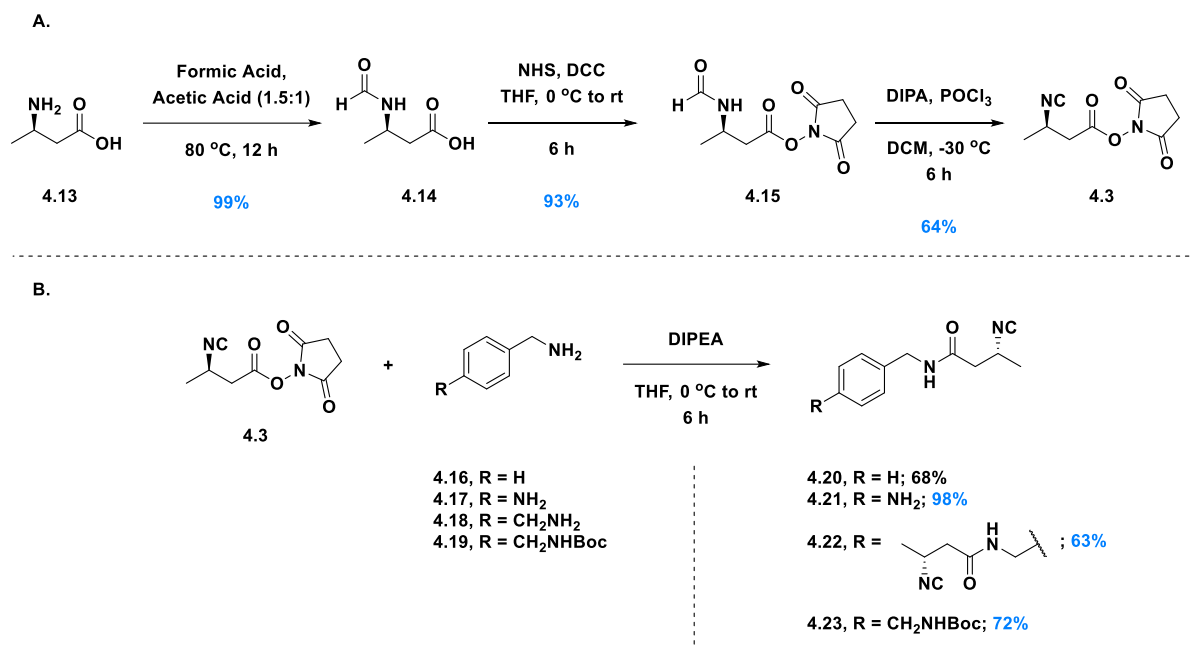


Figure 4.6 (A) Previous work towards SF2768 by Tan and co-workers (B) This work in which we will simplify the lactol core to benzene derivatives.

product, our simplified analogs reduced the total longest linear step count by three and removed the complex synthesis to achieve the lactol core. In our approach towards our desired analogs, we utilized the previously published route towards the sidechain disclosed by Tan and co-workers.¹⁴

Beginning with (*R*)-3-aminobutanoic acid, a formylation followed by *N*-hydroxysuccinimide produced **4.15** (**Scheme 4.2A**). This was then treated with POCl₃ and base to produce the isonitrile NHS ester **4.3**. With the sidechain in hand, we then performed an amide coupling with each benzene core to produce four new simplified benzene analogs (**Scheme 4.2B**). In addition to the simplified analogs and natural product, we also wanted to analyze the biological activity of the two linear analogs discussed in Tan and co-workers' publication. To produce both, we utilized Tan's published route (**Scheme 4.2 C**). I was able to produce SF2768 H **4.11** in 59 %



Scheme 4.2 (A) Synthesis of the *N*-hydroxysuccinimide ester sidechain **4.3**. (B) Synthesis of simplified benzene analogs. All yields shown in blue are produced by C.L.Z.

yield, and Haney was able to synthesize SF2768 D **4.12** in 77% yield. In addition to our synthesized library of compounds, we also obtained SF2768 from Tan's group as well as a stilbene isonitrile derivative (**4.24**) produced by Dai and co-workers^{17–19} to complete our library of compounds to test against a panel of bacteria (**Figure 4.7**).

2.2.2. Biological Analysis

With these compounds in hand, I then set out to analyze their activity in bacterial inhibitory assays. In this experiment, I analyzed a panel of medically relevant bacteria including *A. baumannii*, two strains of *Pseudomonas aeruginosa* (PAO1 and PA14), *Enterococcus faecalis*, hospital acquired-methicillin-resistant

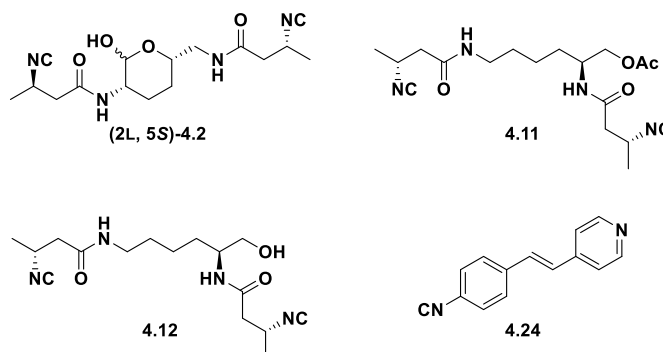


Figure 4.7 Chemical structures of other compounds analyzed in biological assays. SF2768 (2L-, 5S)-**4.2**; SF2768 H **4.11**; SF2768 D **4.12**; and a stilbene derivative produced by Dai and co-workers **4.24**

Staphylococcus aureus, community-acquired MRSA, methicillin-susceptible *S. aureus*, and *Escherichia coli*. The positive control was a well-known quaternary ammonium compound, benzalkonium chloride (BAC). The negative control was the vehicle, DMSO. The results are summarized in **Table 4.1**. Briefly, we found that all compounds had the greatest inhibitory effect against *A. baumannii*, with the best in class being **4.24** and SF2768 with half maximal inhibitory concentrations (IC₅₀) of 3 μM and 8 μM respectively. Of the simplified analogs synthesized, the diisonitrile derivative (**4.22**) showed the best inhibitory activity compared to the others and performed similarly to the linear derivatives of SF2768 against *A. baumannii* (**Table 4.1**). This result is consistent with previously

Compound	<i>P. aeruginosa</i> (PAO1)	<i>P. aeruginosa</i> (PA14)	<i>A. baumannii</i>	<i>E. coli</i>	MSSA	CA-MRSA	<i>E. faecalis</i>
4.11	204	-	20	-	-	-	145.7
4.12	-	-	23	-	-	-	-
4.20	-	-	146	-	-	-	-
4.21	-	-	149	-	-	-	-
4.22	-	102	23	-	-	-	183
4.24	-	-	3	-	-	-	-
SF2768	282	100	8	-	-	6	121
BAC	71	78	34	29	4	4	90

Table 4.1 IC₅₀ values for library of compounds (**4.11-4.12, 4.20-4.24, SF2768**). IC₅₀ values reported are in μM. They were determined by measuring the optical density of each well at 600 nm followed by further analysis on Prism using nonlinear regression. Assays performed in biological triplicate. CA = community acquired; BAC = benzalkonium chloride (positive control).

published data that found that removing isonitrile moieties ablated activity. Overall, SF2768 showed activity against Gram-negative bacteria with the greatest activity against *A. baumannii*. Additionally, it showed potent activity against CA-MRSA with an IC₅₀ of 6 μM.

2.3: Conclusions and Future Directions

In conclusion, we were able to successfully synthesize four simplified benzene analogs of SF2768. In our synthesis, we shortened the longest linear sequence by three steps and were able to avoid the complex synthesis toward the lactol core of the natural product. In addition to the synthesized library of analogs, we also synthesized two linear analogs (SF2768 H and SF2768 D) of SF2768 that were disclosed by Tan and co-workers. To complete the library of compounds for biological testing, we also analyzed a stilbene derivative produced by Dai and co-workers (**4.24**).

In total, we analyzed all 7 compounds' biological activity against a panel of medically relevant bacteria via inhibitory concentration assays. Overall, we found that all compounds showed the greatest activity against *A. baumannii*, with the most active being SF2768 and **4.24**. Of the simplified analogs, the diisonitrile (**4.22**) was the most active and showed comparable activity to the linear analogs of SF2768. Additionally, SF2768 showed to be most active against Gram-negative bacteria, but did show potent activity against CA-MRSA. These results described herein give further information towards the biological activity of isonitrile compounds and shows that the lactol moiety does aid in its activity albeit within a dilution of the simplified benzene analogs.

Chapter 4 References

1. Umezawa, H., Takeuchi, T., Tasuta, K., Isshika, K. & Imoto, M. US4925877A - Physiologically active erbstatin analogue compounds and compositions. (1990).
2. Hübner, I. *et al.* Broad Spectrum Antibiotic Xanthocillin X Effectively Kills *Acinetobacter baumannii* via Dysregulation of Heme Biosynthesis. *ACS Cent. Sci.* **7**, 488–498 (2021).
3. Bills, G. F. *et al.* EP2821394A1 - Compounds with antibacterial activity. (2015).
4. Koodkaew, I., Sunohara, Y., Matsuyama, S. & Matsumoto, H. Isolation of ambiguine D isonitrile from *Hapalosiphon* sp. and characterization of its phytotoxic activity. *Plant Growth Regul.* **68**, 141–150 (2012).
5. Smitka, T. A. *et al.* Ambiguine Isonitriles, Fungicidal Hapalindole-Type Alkaloids from Three Genera of Blue-Green Algae Belonging to the Stigonemataceae. *J. Org. Chem.* **57**, 857–861 (1992).
6. Mo, S., Kronic, A., Chlipala, G. & Orjala, J. Antimicrobial ambiguine isonitriles from the cyanobacterium *Fischerella ambigua*. *J. Nat. Prod.* **72**, 894–899 (2009).
7. Mo, S., Kronic, A., Santarsiero, B. D., Franzblau, S. G. & Orjala, J. Hapalindole-related alkaloids from the cultured cyanobacterium *Fischerella ambigua*. *Phytochemistry* **71**, 2116–2123 (2010).
8. Wright, A. D. *et al.* Inhibition of heme detoxification processes underlies the antimalarial activity of terpene isonitrile compounds from marine sponges. *J. Med. Chem.* **44**, 873–885 (2001).

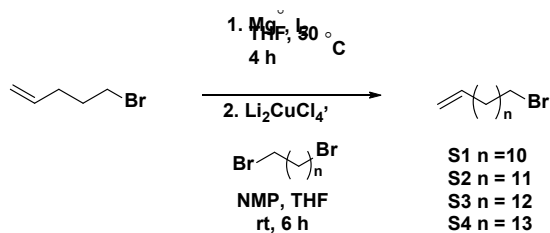
9. Brown, D. G., Lister, T. & May-Dracka, T. L. New natural products as new leads for antibacterial drug discovery. *Bioorg. Med. Chem. Lett.* **24**, 413–418 (2014).
10. Rossmann, B. Die Auftrennung des Antibioticums Brevicid in seine Komponenten. *Fresenius' Zeitschrift für Anal. Chemie 1967 2305* **230**, 398–398 (1967).
11. Tabata, Y., Hatsu, M., Amano, S., Shimizu, A. & Imai, S. SF2768, a new isonitrile antibiotic obtained from *Streptomyces*. *Sci. Rep. Meiji Seika Kaisha* **34**, 1–9 (1995).
12. Amano, S. I. *et al.* A cryptic antibiotic triggered by monensin. *Journal of Antibiotics* vol. 64 703 (2011).
13. Wang, L. *et al.* Diisonitrile Natural Product SF2768 Functions As a Chalkophore That Mediates Copper Acquisition in *Streptomyces thioluteus*. *ACS Chem. Biol.* **12**, 3067–3075 (2017).
14. Xu, Y. & Tan, D. S. Total Synthesis of the Bacterial Diisonitrile Chalkophore SF2768. *Org. Lett.* **21**, 8731–8735 (2019).
15. Harris, N. C. *et al.* Biosynthesis of isonitrile lipopeptides by conserved nonribosomal peptide synthetase gene clusters in Actinobacteria. *Proc. Natl. Acad. Sci. U. S. A.* **114**, 7025–7030 (2017).
16. Zhu, M. *et al.* Diisonitrile-Mediated Reactive Oxygen Species Accumulation Leads to Bacterial Growth Inhibition. *J. Nat. Prod.* **83**, 1634–1640 (2020).
17. Kyei-Baffour, K., Mohammad, H., Seleem, M. N. & Dai, M. Second-generation aryl isonitrile compounds targeting multidrug-resistant *Staphylococcus aureus*. *Bioorg. Med. Chem.* **27**, 1845–1854 (2019).

18. Mohammad, H., Kyei-Baffour, K., Abutaleb, N. S., Dai, M. & Seleem, M. N. An aryl isonitrile compound with an improved physicochemical profile that is effective in two mouse models of multidrug-resistant *Staphylococcus aureus* infection. *J. Glob. Antimicrob. Resist.* **19**, 1–7 (2019).
19. Davis, D. C. *et al.* Discovery and characterization of aryl isonitriles as a new class of compounds versus methicillin- and vancomycin-resistant *Staphylococcus aureus*. *Eur. J. Med. Chem.* **101**, 384–390 (2015).

Chapter 5: Supplementary Information

5.1: Supplementary Figures

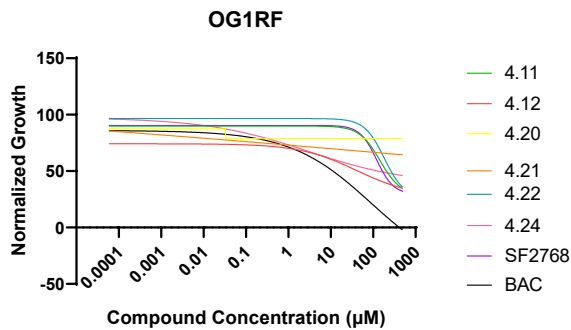
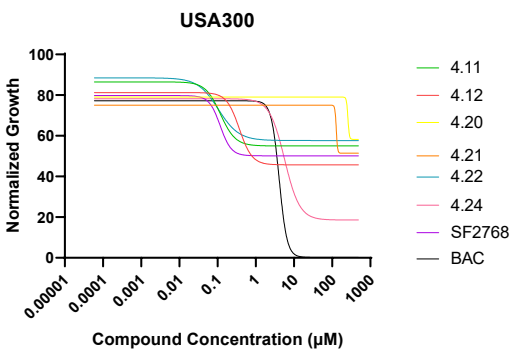
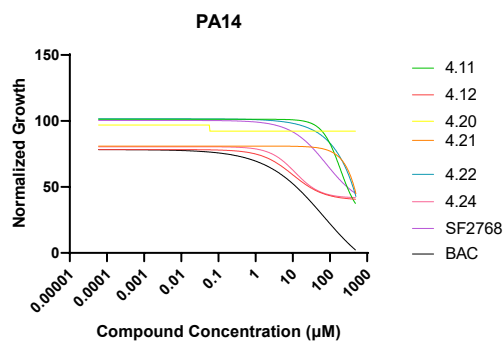
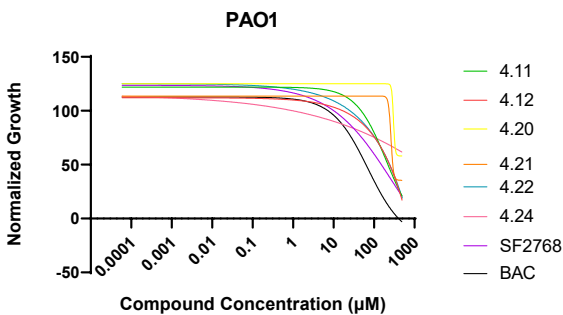
5.1.1: Chapter 3

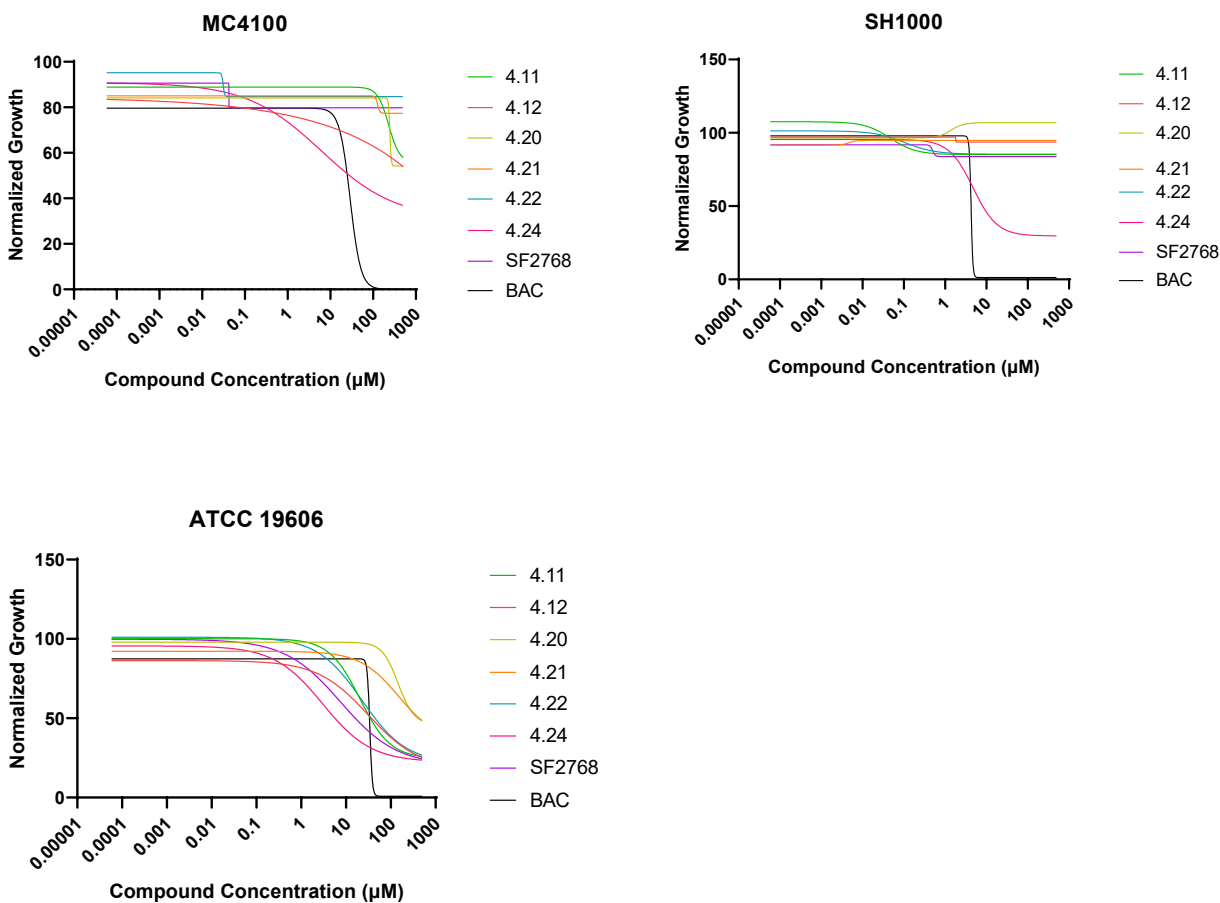


Scheme S5.1: General synthetic scheme towards longer chain bromoalkenes (n = 10, 11, 12, 13).

5.1.2: Chapter 4

IC₅₀ Graphs





5.2: Biology: General Notes

Bacterial strains were acquired as generous gifts from Prof. Bettina Buttaro (Lewis Katz School of Medicine, Temple University). Bacterial cultures of methicillin-susceptible *Staphylococcus aureus* MSSA (SH1000), community-acquired methicillin-resistant *Staphylococcus aureus* CA-MRSA (USA300-0114), hospital-acquired methicillin-resistant *Staphylococcus aureus* HA-MRSA (ATCC 33591), *Enterococcus faecalis* (OG1RF), *Escherichia coli* (MC4100), *Pseudomonas aeruginosa* (PAO1), *Pseudomonas aeruginosa* (PA14), and *Acinetobacter baumannii* (ATCC 19606) were grown from freezer stocks for 16 hours at 37 °C, 200 rpm in 10 mL of media (Mueller-Hinton for SH1000, OG1RF, MC4100, PAO1, PA14, and ATCC 19606; Todd Hewitt Broth for USA300-0114 and ATCC 33591). Bacterial cultures of *Streptococcus*

mutans (UA159) were grown from a freshly streaked Petri dish containing Todd Hewitt Broth agar for 16 hours at 37 °C statically with 5% CO₂ in 10 mL of media (Todd Hewitt Broth with 5% sucrose).

5.3: Biology: Procedures and Supplemental Information

Minimum Inhibitory Concentration (MIC). Each compound was serially diluted from 10% DMSO in sterile DI water (v/v) stock solutions with sterile DI water to yield 12 concentrations ranging from 500 μM to 0.250 μM. The overnight cultures for each bacterium were then inoculated into 5 mL of their respective fresh media and grown until exponential phase. Once in exponential phase, each bacteria was diluted to ca. 10⁶ CFU/mL in Mueller-Hinton broth and 100 μL was added to each well of 96 well U-bottom plates (VWR 15705-064) containing 100 μL of each concentration to yield test concentrations ranging from 250μM to 0.125 μM. The bacteria were grown for 22-23 hours at 37°C before visual inspection for the MIC, which was determined as the lowest concentration at which no growth could be seen to the naked eye over three independent trials. 10% DMSO in sterile DI water served as the positive control to confirm the concentration of DMSO was not responsible for cell death. Mueller-Hinton Broth served as the negative control, showing that the media was not contaminated.

IC₅₀ Assay Procedure. Overnight cultures of the indicated bacteria were diluted 1:100 in fresh LB media and regrown at 37 °C with 200 rpm shaking. When the cultures reached mid-log phase, bacteria were diluted to a concentration of 0.004 using the following equation: (x μL O/N)(OD reading) = (0.004)(volume needed) and 100 μL was inoculated into each well of a 96-well plate (Corning ® 96-well clear bottom plates), which contained 100 μL of serially diluted compound. Compound serial dilutions were done starting from a 10 mM stocksolution in DMSO, which was diluted with LB media to arrive at the desired final concentration. 96-well plates were grown

statically at 37 °C for 16 hours, upon which time the OD at 600 nm was measured using a plate reader. IC₅₀ values were calculated by fitting the OD readings in triplicate from separate O/N cultures vs. concentration with a 5-parameter-logistic model.

Hemolysis Assay. Compounds were dissolved in 10% DMSO/90% H₂O to give 1 mM stock solutions, which were serially diluted with phosphate-buffered saline (PBS) yielding twelve starting test concentrations ranging from 500 mM to 2.5 mM. 1.5 mL of defibrinated sheep blood (Hemostat Labs: DSB030) was centrifuged at 10,000 rpm for 10 minutes. The supernatant was removed, and the blood resuspended in 1 mL of (PBS) and centrifuged again as described above. This process was repeated until the supernatant appeared clear to the naked eye. The clear supernatant was then removed, and the cells resuspended once more in 1 mL of PBS, then diluted 1:20 with PBS. 100 μ L was then aliquoted into each well of a U-bottom 96-well plate (BD Biosciences, BD351177) containing the serially diluted compounds giving final test concentrations of 250 mM to 1.25 mM. The plate was then incubated at 37 °C with shaking at 200 rpm for 1 hour after which it was centrifuged at 10,000 rpm for 10 minutes. 100 μ L of supernatant from each sample was then transferred to a flat-bottom 96-well plate (Corning 3370) and absorbance measurements taken at 540 nm using a plate reader. The positive control was TritonX (1% by volume, 100% lysis marker) and the negative control was sterile PBS (0% lysis marker). The assay was performed in triplicate.

5.4: Chemistry: General Notes

NMR spectra were recorded using the following spectrometers: Varian INOVA400, Varian INOVA500, VNMR400, and Bruker Ascend 600. Chemical shifts are quoted in ppm relative to the indicated solvents. The following abbreviations are used to describe splitting: s (singlet), d (doublet), t (triplet), q (quartet), m (multiplet), and dd (doublet of doublets). Accurate mass spectra

were recorded using a Thermo LTQ-FTMS. Infrared spectra were obtained using a Thermo Nicolet Nexus 670 FTIR spectrophotometer. Specific rotation measurements were made with a 1 dm path length using a Perkin Elmer 341 Polarimeter with a sodium lamp set to 589 nm. Non-aqueous reactions were performed using flame-dried glassware under an atmosphere of Argon with HPLC-grade solvents purified on a Pure Process Technology solvent purification system. Brine refers to a saturated solution of sodium chloride, sat. Na_2CO_3 to a saturated aqueous solution of sodium carbonate, sat. NaHCO_3 to a saturated solution of sodium bicarbonate, and MgSO_4 to magnesium sulfate. Column chromatography was performed using a Biotage® flash chromatography purification system. Chemicals were used as received from Oakwood, Sigma-Aldrich, Alfa Aesar, or AK Scientific. All final compounds were assessed for >95% purity using an Agilent Technologies 1100 Series HPLC with the following parameters: $5\mu\text{m}$ 9.4 x 250mm FLOW column, a mobile phase gradient of water-acetonitrile dosed with 0.1% formic acid, and a MWD UV/Vis Detector.

Partition Coefficient Experiments. Compound of interest was weighed for three triplicate trials into tared screwcap vials. Each was suspended into 0.5mL of 1-octanol followed by addition of 0.5mL of deionized water. The mixture was vortexed for 2 mins followed by sonication at room temperature for 5 mins. The mixture was then allowed to rest for 1 min, or until visible layers were formed. The organic layer was then extracted from the aqueous layer and placed into a separate tared vial. Both were concentrated *in vacuo*. Once dry, residual compound was measured by mass in both vials. To calculate the partition coefficient (P) the concentration of compound in both the aqueous and organic layer was first determined by calculating the amount of mmoles of compound in both followed by dividing this by 0.5mL to obtain molarity. Then the concentration of organic

layer divided by the concentration of the aqueous to obtain P. This value was then subject to \log_{10} to obtain $\log P$. See sample calculations below.

$$P = \frac{[C_{octanol}]}{[C_{water}]}$$

$$\log_{10} P = \log_{10} \left(\frac{[C_{octanol}]}{[C_{water}]} \right)$$

Where C is the concentration of compound in molarity.

Data collected for this experiment are listed below. For all experiments, 0.5 mL of octanol and 0.5 mL of deionized water were used.

Analog and Trial	Initial Sample Mass (mg)	Mass in Octanol Layer (mg)	Mass in Water Layer (mg)	logP
Azaborine Trial 1	0.86	0.54	0.32	0.23
Azaborine Trial 2	0.73	0.46	0.27	0.23
Azaborine Trial 3	0.75	0.33	0.42	0.11
Analog 2 Trial 1	2.80	2.33	0.47	0.70
Analog 2 Trial 2	4.01	3.65	0.36	1.0
Analog 3 Trial 3	3.27	3.02	0.25	1.1

Table S5.1 Data collected for partition coefficient experiments for azaborine analog and analog 2.

$\log P$ was calculated using sample calculations shown above.

Schrodinger Modeling for Dipole Moment Calculations. Analogue 2 and Azaborine analog were subjected to the Ligprep protocol (default settings) as launched from within the Schrodinger 2020-3 suite of modelling software. The two compounds were then subjected to a flexible alignment to ensure that they held near identical conformations. A structure optimization was then performed using the Jaguar Optimization panel as launched from within the Schrodinger 2020-3 suite of software. Density Functional Theory was utilized for this process with an accuracy level set to fully analytic. The maximum number of steps was set to 1000 and the PBF Water solvent

model was employed. All other settings were default. As the end of the optimization, the two structures retained near identical conformations.

5.5: Chemistry: Experimental Procedures and Characterization

5.5.1: Chapter 2

[2.52] Di-*tert*-butyl (((thiobis(4,6-dichloro-2,1-phenylene))bis(oxy))bis(ethane-2,1-diyl)) dicarbamate. Bithionol **[2.51]** (1.0 eq, 250 mg, 0.70 mmol) and potassium carbonate (10.0 eq, 97 mg, 7.0 mmol) were dissolved in 7 mL DMF at 60 °C and stirred for 15 mins. *N*-Boc-2-bromoethylamine **[S2]** (8.0 eq, 1.26g, 5.6 mmol) was then added and stirred for 2 d. The reaction was quenched with sat. Na₂CO₃ and extracted with EtOAc (3x). The combined organic layers were dried over MgSO₄, concentrated, and purified by flash column chromatography in a gradient of hexanes and ethyl acetate to afford the product as a yellow oil (451 mg, 84% yield). **¹H NMR** (500 MHz, acetone-d₆) δ 7.49 (s, 2H), 7.15 (s, 2H), 6.15 (s, 2H), 4.16 (t, *J* = 5.8 Hz, 4H), 3.50 (q, *J* = 5.9 Hz, 4H), 1.40 (s, 18H). **¹³C NMR** (126 MHz, acetone-d₆) δ 382.49, 333.07, 329.88, 308.78, 307.51, 307.07, 306.93, 306.56, 255.35, 249.80, 217.68, 205.07.

[2.53] 2,2'-((Thiobis(4,6-dichloro-2,1-phenylene))bis(oxy))bis(ethan-1-amine). **[2.52]** (1.0 eq, 279 mg, 0.43 mmol) was dissolved in 0.50 mL DCM at room temperature. Trifluoroacetic acid (10 eq, 0.5 mL, 4.3 mmol) was then added and stirred at room temperature for 18 h. The reaction was concentrated and purified by flash column chromatography in a gradient of hexanes and ethyl acetate to afford a yellow oil (145 mg, 75% yield). **¹H NMR** (600 MHz, DMSO-d₆) δ 7.76 (d, *J* = 2.5 Hz, 2H), 7.19 (d, *J* = 2.5 Hz, 2H), 5.76 (s, 4H), 4.23 (t, *J* = 5.5 Hz, 4H), 3.18 (t, *J* = 5.6 Hz, 4H). **¹³C NMR** (151 MHz, DMSO-d₆) δ 151.68, 131.07, 130.16, 129.91, 129.79, 128.87, 70.58, 55.02. **HRMS (ES⁺):** Found 440.9762 (0.52 ppm) C₁₆H₁₇O₂N₂³⁵Cl₄³²S (M+H⁺) requires 440.9759.

[2.45] 6-(3-((3r,5r,7r)-Adamantan-1-yl)-4-(2-((tert-butoxycarbonyl)amino)ethoxy)phenyl)-2-naphthoic acid. CD-437 [2.2] (1.0 eq, 32 mg, 0.080 mmol) and potassium carbonate (10.0 eq, 111 mg, 0.80 mmol) were dissolved in 1 mL DMF at 60 °C and stirred for 15 mins. *tert*-butyl (2-bromoethyl)carbamate (8.0 eq, 143 mg, 0.6424 mmol) then added at temperature and stirred for 2-3 d. The reaction was quenched with sat. Na₂CO₃ and extracted with EtOAc (3x). The combined organic layers were dried over MgSO₄, concentrated, and purified by flash column chromatography in a gradient of hexanes and ethyl acetate to afford the product as a white solid (28 mg, 65% yield). ¹H NMR (500 MHz, CDCl₃) δ 8.61 (s, 1H), 8.06 (dd, *J* = 8.6, 1.7 Hz, 1H), 8.02 – 7.96 (m, 2H), 7.91 (d, *J* = 8.6 Hz, 1H), 7.78 (dd, *J* = 8.5, 1.8 Hz, 1H), 7.59 (d, *J* = 2.3 Hz, 1H), 7.43 (dd, *J* = 8.1, 2.2 Hz, 1H), 6.79 (d, *J* = 8.1 Hz, 1H), 4.91 (s, 1H), 4.45 (t, *J* = 5.2 Hz, 2H), 3.64 – 3.56 (m, 2H), 2.21 (s, 7H), 2.13 (s, 4H), 1.82 (s, 7H), 1.46 (s, 9H). ¹³C NMR (126 MHz, CDCl₃) δ 154.81, 141.59, 137.09, 136.19, 133.10, 131.37, 131.15, 129.88, 128.42, 126.65, 125.89, 125.74, 124.86, 117.53, 110.17, 40.74, 37.21, 37.09, 29.20, 28.54.

[2.45] 6-(3-((3r,5r,7r)-Adamantan-1-yl)-4-(2-aminoethoxy)phenyl)-2-naphthoic acid. [2.44] (1.0 eq, 97 mg, 0.17 mmol) was dissolved in 0.5 mL DCM with 0.5 mL trifluoroacetic acid (10 eq, 1.7 mmol). This reaction stirred at room temperature for 18 h. It was then quenched with sat. NaHCO₃, extracted with DCM (3x), and dried over MgSO₄, concentrated, and purified by flash column chromatography in a gradient of hexanes and ethyl acetate to yield a white solid (74 mg, 95% yield). ¹H NMR (500 MHz, DMSO-d₆) δ 13.03 (s, 1H), 8.60 (d, *J* = 1.7 Hz, 1H), 8.22 (s, 1H), 8.11 (dd, *J* = 38.9, 8.6 Hz, 2H), 7.93 (ddd, *J* = 42.1, 8.5, 1.8 Hz, 2H), 7.63 (dd, *J* = 8.4, 2.3 Hz, 1H), 7.58 (d, *J* = 2.4 Hz, 1H), 7.09 (d, *J* = 8.6 Hz, 1H), 6.98 (t, *J* = 5.5 Hz, 1H), 4.07 (t, *J* = 5.7 Hz, 2H), 3.44 (q, *J* = 5.7 Hz, 2H), 2.15 (s, 7H), 2.06 (s, 4H), 1.84 – 1.68 (m, 7H). ¹³C NMR (126 MHz, DMSO-d₆) δ 167.45, 157.60, 155.57, 140.17, 138.09, 135.46, 131.51, 130.90, 130.22,

129.82, 128.34, 127.63, 125.91, 125.67, 125.47, 125.16, 124.06, 113.07, 77.67, 66.19, 36.68, 36.53, 28.49, 28.21. **HRMS (ES⁺):** Found 442.2378 (0.82 ppm) C₂₉H₃₂O₃N (M+H⁺) requires 442.2377.

[2.46] (6-(3-((3r,5r,7r)-Adamantan-1-yl)-4-(2-aminoethoxy)phenyl)naphthalen-2-yl)methanol. Lithium aluminum hydride (1.1 eq, 2.0 mg, 0.05 mmol) was dissolved in 0.4 mL Et₂O. To this, **[2.45]** (1.0 eq, 20 mg, 0.045mmol) was added at 0 °C. The reaction mixture stirred, warming to room temperature, for 2 h. It was then cooled to 0 °C and quenched with 0.4 mL of water and 0.4 mL of 1M aqueous NaOH. The slurry was filtered over celite and washed with EtOAc. The collected filtrate was then extracted with EtOAc (3x). The combined organic layers were washed with brine, dried over MgSO₄, filtered, concentrated, and purified by flash column chromatography in a gradient of hexanes and ethyl acetate to yield a yellow oil (14 mg, 73% yield). **¹H NMR** (600 MHz, Acetone-d) δ 8.10 (dd, *J* = 1.9, 0.8 Hz, 1H), 7.93 (d, *J* = 8.4 Hz, 2H), 7.87 – 7.85 (m, 1H), 7.79 (dd, *J* = 8.5, 1.8 Hz, 1H), 7.64 (d, *J* = 2.4 Hz, 1H), 7.59 (dd, *J* = 8.4, 2.4 Hz, 1H), 7.52 (dd, *J* = 8.4, 1.7 Hz, 1H), 7.11 (d, *J* = 8.4 Hz, 1H), 6.16 (s, 1H), 4.80 (s, 2H), 4.18 (t, *J* = 5.8 Hz, 2H), 3.62 (q, *J* = 5.8 Hz, 3H), 2.24 (s, 6H), 2.10 (s, 3H), 1.90 – 1.77 (m, 7H). **¹³C NMR** (151 MHz, Acetone-d) δ 317.23, 315.77, 315.62, 310.51, 310.29, 305.51, 302.74, 302.71, 301.74, 290.23, 255.22, 243.84, 241.17, 217.82, 217.43, 214.19, 209.04, 205.01, 199.74, 193.37, 190.77. **HRMS (ES⁺):** Found 428.2581 (-0.68 ppm) C₂₉H₃₄O₂N (M+H⁺) requires 428.2584.

[2.48] Ethyl 6-(3-((3r,5r,7r)-adamantan-1-yl)-4-((2-methoxyethoxy)methoxy)phenyl)-4- (2-((tert-butoxycarbonyl)amino)ethoxy)-2-naphthoate. **[2.47]** (1.0 eq, 263 mg, 0.495 mmol) and K₂CO₃ (8.0 eq, 547 mg, 3.96 mmol) were dissolved in DMF (5 mL) and stirred at 50 °C. After 1 h, **[S2]** (5.0 eq, 554 mg, 2.48 mmol) was added and the reaction was stirred for 3 d. Once complete, water was added and the reaction solution was extracted with ethyl acetate 4x. The organic layers

were combined, washed with brine, dried with sodium sulfate, concentrated, and purified via flash column chromatography in a gradient of hexanes and ethyl acetate to yield the product as a yellow solid (216 mg, 65% yield). $^1\text{H NMR}$ (400 MHz, Acetone- d_6) δ 8.56 (s, 1H), 8.23 (s, 1H), 8.08 (d, $J = 8.4$ Hz, 1H), 7.90 (dd, $J = 8.6, 1.9$ Hz, 1H), 7.66 (d, $J = 2.4$ Hz, 1H), 7.60 (dd, $J = 8.4, 2.3$ Hz, 1H), 7.43 (d, $J = 1.4$ Hz, 1H), 7.28 (d, $J = 8.5$ Hz, 1H), 6.42 (t, $J = 6.2$ Hz, 1H), 5.42 (s, 2H), 4.40 (q, $J = 7.1$ Hz, 2H), 4.32 (t, $J = 5.3$ Hz, 2H), 3.92 – 3.85 (m, 2H), 3.70 (q, $J = 5.5$ Hz, 2H), 3.62 – 3.55 (m, 2H), 3.32 (s, 3H), 2.25 (d, $J = 2.9$ Hz, 6H), 2.10 (s, 3H), 1.83 (s, 6H), 1.41 (t, $J = 7.1$ Hz, 3H), 1.35 (s, 9H). $^{13}\text{C NMR}$ (126 MHz, Acetone- d_6) δ 166.92, 157.50, 156.83, 155.79, 141.47, 139.57, 134.44, 133.20, 130.41, 128.97, 128.65, 127.59, 126.77, 126.70, 123.80, 120.07, 116.07, 104.59, 94.25, 78.74, 72.40, 68.96, 68.74, 61.59, 58.84, 41.39, 40.73, 37.97, 37.75, 30.02, 28.61, 14.69.

[2.49] 6-(3-((3r,5r,7r)-Adamantan-1-yl)-4-hydroxyphenyl)-4-(2-aminoethoxy)-2-naphthoic acid. [2.48] (1.0 eq, 84 mg, 0.13 mmol) was dissolved in 4.0 M HCl in dioxane (3 mL) and stirred at room temperature for 1 h. The solution was quenched with saturated aqueous Na_2CO_3 solution and extracted with ethyl acetate 3x. The organic layers were combined, washed with brine, dried with sodium sulfate, and concentrated. The resultant intermediate was dissolved in 5 mL 2:1 methanol:THF and 1 mL 1 M aqueous NaOH and stirred for 3 h. The solution was heated to 50 °C for a further 2 h to drive the reaction to completion, then quenched with 1 M aqueous HCl and extracted with ethyl acetate 3x. The organic layers were combined, washed with brine, dried with sodium sulfate, concentrated, and purified via preparative TLC utilizing a mobile phase of 5% methanol in dichloromethane and 1% acetic acid to yield the product as a light tan solid (50 mg, 88% yield). $^1\text{H NMR}$ (400 MHz, Methanol- d_4) δ 8.42 (d, $J = 1.8$ Hz, 1H), 7.85 (d, $J = 8.5$ Hz, 1H), 7.72 (dd, $J = 8.5, 1.9$ Hz, 1H), 7.50 – 7.44 (m, 2H), 7.42 (dd, $J = 8.2, 2.3$ Hz, 1H), 7.00 (d, $J = 1.3$

Hz, 1H), 6.84 (d, J = 8.2 Hz, 1H), 4.76 (s, 2H), 4.47 (t, J = 5.0 Hz, 2H), 3.55 (t, J = 5.0 Hz, 2H), 2.25 (d, J = 2.9 Hz, 6H), 2.09 (s, 3H), 1.84 (s, 6H). ¹³C NMR (151 MHz, d₆-DMSO) δ 156.08, 153.85, 140.28, 137.44, 135.78, 132.46, 130.81, 127.84, 125.69, 125.24, 124.95, 124.49, 118.05, 117.03, 116.48, 104.66, 63.22, 40.43, 40.06, 36.66, 36.31, 28.43, 22.24. **HRMS** Accurate mass (ES⁺): found 458.23153, C₂₉H₃₂O₄N (M+H⁺) requires 458.56868.

[2.50] 2-((3r,5r,7r)-Adamantan-1-yl)-4-(8-(2-aminoethoxy)-6-(hydroxymethyl)naphthalen-2-yl) phenol. [2.49] (1.0 eq, 102 mg, 0.15 mmol) was dissolved in 4.0 M HCl in dioxane (3 mL) and stirred at room temperature for 1 h. The solution was quenched with saturated aqueous Na₂CO₃ solution and extracted with ethyl acetate 3x. The organic layers were combined, washed with brine, dried with sodium sulfate, and concentrated. The resultant intermediate was suspended in 2 mL diethyl ether and THF was added until fully dissolved. Lithium aluminum hydride (1.2 eq, 7 mg, 0.18 mmol) dissolved in ether was added and the solution was stirred at room temperature for 3 h. The solution was quenched with 1 M aqueous HCl and extracted with ethyl acetate 3x. The organic layers were combined, washed with brine, dried with sodium sulfate, concentrated, and purified via flash column chromatography in a gradient of dichloromethane with 1% acetic acid and methanol to yield the product as a tan solid (67 mg, 99% yield). ¹H NMR (600 MHz, DMSO-d₆) δ 9.73 (s, 1H), 8.44 (s, 1H), 8.11 (s, 1H), 7.95 (d, J = 8.4 Hz, 1H), 7.75 (d, J = 8.0 Hz, 1H), 7.49 (d, J = 8.2 Hz, 1H), 7.45 – 7.33 (m, 2H), 6.97 (d, J = 8.2 Hz, 1H), 4.40 (s, 2H), 3.33 (s, 2H), 2.13 (s, 6H), 2.02 (s, 3H), 1.71 (s, 6H). ¹³C NMR (151 MHz, DMSO) δ 169.31, 156.44, 153.31, 139.48, 135.82, 132.10, 131.86, 130.52, 129.24, 126.61, 126.03, 125.68, 125.25, 122.41, 118.38, 117.10, 105.24, 64.96, 40.43, 38.46, 36.69, 36.35, 28.45. **HRMS** Accurate mass (ES⁺): found 444.25257, C₂₉H₃₄O₃N (M+H⁺) requires 444.58516.

[2.56] (3-((3r,5r,7r)-adamantan-1-yl)-4-((2-methoxyethoxy)methoxy)phenyl)trifluoroborate.

Borylated compound [2.40] (1.0 eq, 174 mg, 0.394 mmol) was dissolved in 2.0 mL of methanol. Once dissolved, the solution was cooled to 0°C. Then an aqueous solution of potassium bifluoride (~4.5M aq, 4.0 eq, 0.40 mL) was added dropwise. The reaction was warmed slowly to room temperature. After stirring for 30 minutes, the white solid formed was filtered and washed with diethyl ether and water. After drying, a white solid was obtained (102 mg, 62% yield). **¹H NMR** (400 MHz, Acetone) δ 7.41 (d, *J* = 1.6 Hz, 1H), 7.23 (dd, *J* = 7.9, 1.6 Hz, 1H), 6.88 (dd, *J* = 8.0, 0.8 Hz, 1H), 5.24 (s, 2H), 3.83 – 3.80 (m, 2H), 3.56 – 3.53 (m, 2H), 3.30 (s, 3H), 2.80 – 2.78 (m, 2H), 2.14 (d, *J* = 3.0 Hz, 6H), 1.79 (s, 7H). **¹³C NMR** (151 MHz, Acetone) δ 155.74, 136.22, 131.09, 130.57, 114.09, 94.60, 72.59, 68.67, 58.92, 42.08, 41.70, 38.15, 37.96, 37.62. **HRMS:** Accurate Mass (ES⁻): found 382.20549, C₂₀H₂₇O₃BF₃ (M-K⁺), requires 382.20471.

[2.57] Methyl 4-amino-3-vinylbenzoate. Methyl 4- amino- 3- bromobenzoate [2.59] (1.0 eq, 1.05g, 4.58 mmol) and tetrakis(triphenylphosphine)palladium(0) (10 mol%, 0.53g) were dissolved in 23 mL of toluene. To this mixture, tributylvinyl tin (1.13 eq, 1.51 mL, 5.17 mmol) was added in one portion. The reaction was then stirred at 100°C for ~6 h. Once complete by TLC, the reaction mixture was filtered through celite and rinsed with ethyl acetate (40 mL). The filtrate was then quenched with water (40 mL). The organic layer was extracted (3x, 20 mL) and washed with brine (20 mL). The combined organic layers were then dried with magnesium sulfate, concentrated, and purified by flash chromatography in a gradient of hexanes to ethyl acetate to afford the product as an orange solid (811 mg, 80% yield). **¹H NMR** (600 MHz, CDCl₃) δ 7.96 (d, *J* = 2.0 Hz, 1H), 7.74 (dd, *J* = 8.4, 2.1 Hz, 1H), 6.67 (dd, *J* = 17.4, 11.0 Hz, 1H), 6.62 (d, *J* = 8.4 Hz, 1H), 5.66 (dd, *J* = 17.3, 1.3 Hz, 1H), 5.33 (dd, *J* = 11.1, 1.3 Hz, 1H), 4.27 (s, 2H), 3.84 (s, 3H). **¹³C NMR** (151 MHz,

CDCl₃) δ 167.27, 148.23, 131.79, 130.48, 129.49, 122.81, 119.72, 116.87, 114.87, 51.65. **HRMS:** Accurate Mass (+pAPCI): found 178.08633, C₁₀H₁₂O₂N (M+H⁺), requires 178.08626.

[2.60] Methyl 2-(3-((3r,5r,7r)-adamantan-1-yl)-4-hydroxyphenyl)-1,2-dihydrobenzo[e][1,2]azaborinine-6-carboxylate. In an oven dried microwave vial equipped with a stir bar, **[2.56]** (1.0 eq, 177 mg, 0.420 mmol) was charged. This vial was then evacuated and backfilled with argon 3x. In a separate vial **[6]** (1.2 eq, 89.3 mg, 0.504 mmol) was dissolved in a 1:1 mixture of acetonitrile and toluene (0.25 M, 1.67 mL). This solution was then added to the trifluoroborate salt under argon. Stirring vigorously, triethylamine (1.5 eq, 0.10 mL, 0.629 mmol) was added dropwise followed by a dropwise addition of silicon tetrachloride (2.0 eq, 0.10 mL, 0.839 mmol). The reaction was then heated to 50°C for 18 h. Upon completion, the reaction was diluted with hexanes and flushed through a silica plug which was rinsed and collected into three different fractions with dichloromethane (250 mL), a 4:1 hexanes to ethyl acetate mixture (250 mL), and finally ethyl acetate (250 mL). Each collected fraction was then concentrated and subjected to flash chromatography in a gradient of hexanes and ethyl acetate to afford a white solid (43.8 mg, 25% yield). **¹H NMR** (600 MHz, CDCl₃) δ 8.37 (s, 1H), 8.11 (d, *J* = 11.7 Hz, 2H), 8.08 (dd, *J* = 8.5, 1.9 Hz, 1H), 7.79 (d, *J* = 1.7 Hz, 1H), 7.65 (dd, *J* = 7.8, 1.6 Hz, 1H), 7.35 (d, *J* = 8.5 Hz, 1H), 7.30 (dd, *J* = 11.7, 1.9 Hz, 1H), 6.78 (d, *J* = 7.8 Hz, 1H), 5.01 (s, 1H), 3.95 (s, 3H), 2.22 (s, 6H), 2.13 (s, 3H), 1.82 (s, 6H). **¹³C NMR** (151 MHz, CDCl₃) δ 167.22, 156.73, 145.44, 143.75, 136.27, 132.08, 131.96, 129.26, 125.10, 122.82, 118.30, 117.15, 52.18, 40.78, 37.24, 37.00, 29.21. **HRMS:** Accurate Mass (+pAPCI): found 413.22663, C₂₆H₂₉O₃NB (M+H⁺), requires 413.22713.

[2.54] 2-((3r,5r,7r)-adamantan-1-yl)-4-(6-(hydroxymethyl)benzo[e][1,2]azaborinin-2(1H)-yl)phenol. To a flame dried round bottom flask equipped with a stir bar, lithium aluminum hydride

(1.1 eq, 0.7 mg, 0.0186 mmol) was dissolved in 0.14 mL of diethyl ether (0.12 M). This mixture was then cooled to 0°C. A solution of [2.60] (1.0 eq, 7 mg, 0.0169 mmol) dissolved in 0.14 mL of diethyl ether (0.12 M) was added dropwise. The reaction mixture was then warmed to room temperature and stirred at room temperature for 2 h. Upon completion, the reaction was cooled to 0°C. Once cool, 0.14 mL of water followed by 0.14 mL of 1.0M aqueous NaOH were added. This slurry was then filtered over celite and washed with ethyl acetate (5 mL). The filtrate was then extracted with ethyl acetate (3x). Combined organic layers were washed with brine (5 mL) and water (5 mL), dried with magnesium sulfate, concentrated, and subjected to flash chromatography with a gradient of hexanes and ethyl acetate to afford a tan solid (6.3 mg, 97% yield). ¹H NMR (600 MHz, CDCl₃) δ 8.07 (d, *J* = 11.5 Hz, 1H), 8.02 (s, 1H), 7.79 (s, 1H), 7.67 – 7.60 (m, 2H), 7.45 (dd, *J* = 8.3, 1.9 Hz, 1H), 7.33 (d, *J* = 8.3 Hz, 1H), 6.77 (d, *J* = 7.7 Hz, 1H), 5.12 (s, 1H), 4.77 (s, 2H), 3.35 (s, 2H), 2.62 (s, 5H), 2.22 (s, 5H), 2.12 (s, 3H). ¹³C NMR (151 MHz, CDCl₃) δ 156.47, 145.09, 140.12, 136.15, 133.41, 131.78, 128.20, 127.78, 125.62, 118.56, 117.07, 77.37, 77.16, 76.95, 65.49, 56.14, 41.13, 37.26, 36.98, 29.51, 29.23. HRMS Accurate mass (–pAPCI): found 383.21739, C₂₅H₂₇O₂NB (M–H⁺) requires 383.21766.

5.5.2. Chapter 3

General Procedure A: Grignard Addition. Procedure based on previously described.¹ To a 1.3 M solution of Mg⁰ (1.0 equiv) in THF was added a catalytic amount of I₂, giving an orange solution. 5-bromopentene (0.5 equiv) was then added dropwise. The resulting clear solution was then heated to 50 °C, stirred 4 hours. This Grignard solution was then cooled to room temperature before use. To a separate flask cooled to 0 °C was added dibromoalkane (1.0 equiv), followed by a 0.1 M solution of Li₂CuCl₄ in THF (0.0125 equiv), then THF, and lastly N-methylpyrrolidinone (2.0 equiv). The Grignard solution was then added dropwise, and the resulting solution was

warmed to room temperature and stirred for 16 hours. The reaction was then quenched with NH_4Cl , extracted with Et_2O (3x), washed with brine (1x), dried over MgSO_4 , concentrated under reduced pressure, and purified by flash column chromatography (100% hexanes).

General Procedure B: Hydroarylation. Procedure based on previously described.² An oven-dried 30 mL screw-top test tube was charged with corresponding 3-iodopyridine (1.0 equiv), Hantzsch ester (1.3 equiv), solid NH_4Cl (2.0 equiv), photoredox catalyst $\text{Ir}[\text{ppy}]_2\text{dtbbpy}\cdot\text{PF}_6$ (1.0 mol %) and alkenes (if solid, 5.0 equiv). The atmosphere was exchanged three times by applying vacuum then backfilling with argon. Alkene (if liquid, 5.0 equiv) was added in a solution of degassed 2,2,2-trifluoroethanol if prepared or directly followed by degassed 2,2,2-trifluoroethanol if purchased commercially to give a 0.1 M reaction solution relative to the corresponding 3-iodopyridine. The resulting solution was stirred for 16 hours under irradiation with a blue LED (Hydrofarm PowerPAR 15-watt LED Bulb-Blue). The reaction was then quenched with NaHCO_3 , extracted with EtOAc (3x), washed with brine (1x), dried over Na_2SO_4 , concentrated under reduced pressure, and purified by flash column chromatography (0 \rightarrow 20% EtOAc /hexanes).

General Procedure C: Cyclization. Procedure based on previously described.³ A solution of alkylpyridine (1.0 equiv) and NaI (1.2 equiv) in a 1:1 mixture of butanone/methanol (0.5 M) and stirred at 80 °C for 16 hours. The resulting solution was then concentrated under reduced pressure and purified using reverse phase flash column chromatography (40% $\text{MeCN}/\text{H}_2\text{O}$).

[S1] 13-Bromo-1-tridecene. Following general procedure B, 1,8-dibromooctane (1.84 mL, 10.0 mmol) yielded the title compound as a clear oil (2.25 g, 87%). $^1\text{H NMR}$ (600 MHz, CDCl_3) δ 5.81 (ddt, $J = 16.9, 10.2, 6.6$ Hz, 1H), 4.99 (dq, $J = 17.1, 1.7$ Hz, 1H), 4.93 (ddt, $J = 10.2, 2.4, 1.3$ Hz, 1H), 3.41 (t, $J = 6.9$ Hz, 2H), 2.04 (q, $J = 7.2$ Hz, 2H), 1.85 (dt, $J = 14.4, 7.2$ Hz, 2H), 1.40 (m, 4H), 1.33 – 1.24 (m, 14H). $^{13}\text{C NMR}$ (151 MHz, CDCl_3) δ 139.40, 114.25, 34.20, 33.96, 33.00,

29.69, 29.66, 29.62, 29.58, 29.28, 29.09, 29.91, 28.33. **HRMS** Accurate mass (APCI⁺): Found 257.08921, C₁₃H₂₂Br (M+H-2H₂⁺) requires 257.08994.

[S2] 14-Bromo-1-tetradecene. Following general procedure B, 1,9-dibromononane (2.03 mL, 10.0 mmol) yielded the title compound as a clear oil (2.61 g, 95%). **¹H NMR** (600 MHz, CDCl₃) δ 5.81 (ddt, *J* = 17.0, 10.3, 6.7 Hz, 1H), 4.99 (dq, *J* = 17.1, 1.7 Hz), 4.93 (ddt, *J* = 10.2, 2.5, 1.5 Hz), 3.41 (t, *J* = 6.9 Hz, 2H), 2.04 (q, *J* = 6.7 Hz, 2H), 1.85 (dt, *J* = 14.6, 7.0 Hz, 2H), 1.40 (m, 4H), 1.33 – 1.24 (m, 14H). **¹³C NMR** (151 MHz, CDCl₃) δ 139.42, 114.24, 34.20, 33.97, 33.00, 29.74, 29.73, 29.68, 29.64, 29.58, 29.30, 29.10, 28.92, 28.33. **HRMS** Accurate mass (APCI⁺): Found 271.10488, C₁₄H₂₄Br (M+H-2H₂⁺) requires 271.1056.

[S3] 15-Bromo-1-pentadecene. Following general procedure B, 1,10-dibromodecane (2.25 mL, 10.0 mmol) yielded the title compound as a clear oil (1.84 g, 64%). **¹H NMR** (600 MHz, CDCl₃) δ 5.81 (ddt, *J* = 16.9, 10.2, 6.6 Hz, 1H), 4.99 (dq, *J* = 17.1, 1.7 Hz, 1H), 4.93 (ddt, *J* = 10.2, 2.6, 1.5 Hz, 1H), 3.41 (t, *J* = 6.9 Hz, 2H), 2.04 (q, *J* = 6.7 Hz, 2H), 1.85 (dt, *J* = 14.6, 7.0 Hz, 2H), 1.85 (dt, *J* = 14.5, 7.0 Hz, 2H), 1.40 (m, 4H), 1.32 – 1.24 (m, 16H). **¹³C NMR** (151 MHz, CDCl₃) δ 139.42, 114.23, 34.20, 33.97, 33.00, 29.77, 29.75, 29.68, 29.65, 29.59, 29.30, 29.10, 28.92, 28.33. **HRMS** Accurate mass (APCI⁺): Found 285.12054, C₁₅H₂₆Br (M+H-2H₂⁺) requires 285.12124.

[S4] 16-Bromo-1-hexadecene. Following general procedure B, 1,11-dibromoundecane (1.70 mL, 7.23 mmol) yielded the title compound as a clear oil (1.74 g, 57%). **¹H NMR** (400 MHz, CDCl₃) δ 5.81 (ddt, *J* = 16.9, 10.1, 6.7 Hz, 1H), 4.99 (dq, *J* = 17.2, 1.8 Hz, 1H), 4.93 (ddt, *J* = 10.2, 2.6, 1.4 Hz, 1H), 3.41 (t, *J* = 6.9 Hz, 2H), 2.04 (q, *J* = 6.7 Hz, 2H), 1.85 (dt, *J* = 14.6, 7.0 Hz, 2H), 1.40 (m, 4H), 1.33 – 1.23 (m, 18H). **¹³C NMR** (151 MHz, CDCl₃) δ 139.42, 114.22, 34.19, 33.97, 33.00, 29.79, 29.76, 29.69, 29.66, 29.59, 29.31, 29.10, 28.33. **HRMS** Accurate mass (APCI⁺): Found 303.1686, C₁₆H₃₂Br (M+H⁺) requires 303.16819.

[3.11a] 3-(8-bromooctyl)pyridine. Following general procedure C, 3-iodopyridine (205 mg, 1.00 mmol) and 8-bromooctene (950 mg, 5.00 mmol) yielded the title compound as a yellow oil (80.1 mg, 30%). ¹H NMR (600 MHz, CDCl₃) δ 8.43 (m, 2H), 7.49 (dt, *J* = 7.6, 2.0 Hz, 1H), 7.20 (dd, *J* = 7.8, 4.8 Hz, 1H), 3.40 (t, *J* = 6.9 Hz, 2H), 2.60 (t, *J* = 7.8 Hz, 2H), 1.84 (p, *J* = 7.0 Hz, 2H), 1.62 (m, 2H), 1.41 (m, 2H), 1.36 – 1.27 (m, 10H). ¹³C NMR (151 MHz, CDCl₃) δ 150.04, 147.29, 138.04, 135.97, 123.41, 34.12, 33.13, 32.91, 31.21, 29.34, 29.15, 28.79, 28.25. HRMS Accurate mass (APCI⁺): Found 270.08447, C₁₃H₂₁N⁷⁹Br (M+H) requires 270.08519.

[3.11b] 3-(9-bromononyl)pyridine. Following general procedure C, 3-iodopyridine (205 mg, 1.00 mmol) and 9-bromononene (1.02 g, 5.00 mmol) yielded the title compound as a yellow oil (102 mg, 36%). ¹H NMR (600 MHz, CDCl₃) δ 8.42 (m, 2H), 7.48 (dt, *J* = 7.8, 2.0 Hz, 1H), 7.20 (dd, *J* = 7.7, 4.8 Hz, 1H), 3.40 (t, *J* = 6.9 Hz, 2H), 2.60 (t, *J* = 7.7 Hz, 2H), 1.84 (p, *J* = 7.2 Hz, 2H), 1.61 (p, *J* = 7.5 Hz, 2H), 1.42 (m, 2H), 1.37 – 1.17 (m, 14H). ¹³C NMR (151 MHz, CDCl₃) δ 150.05, 147.28, 138.07, 135.95, 123.39, 34.16, 33.14, 32.93, 31.23, 29.44, 29.41, 28.84, 28.26. HRMS Accurate mass (APCI⁺): Found 284.10005, C₁₄H₂₃N⁷⁹Br (M+H) requires 284.10084.

[3.11c] 3-(10-bromodecyl)pyridine. Following general procedure C, 3-iodopyridine (205 mg, 1.00 mmol) and 10-bromodecene (1.09 g, 5.00 mmol) yielded the title compound as a yellow oil (98.9 mg, 33%). ¹H NMR (600 MHz, CDCl₃) δ 8.42 (m, 2H), 7.48 (dt, *J* = 7.8, 2.0 Hz, 1H), 7.19 (ddd, *J* = 7.7, 4.8, 1.0 Hz, 1H), 3.40 (t, *J* = 6.9 Hz, 2H), 2.59 (t, *J* = 7.7 Hz, 2H), 1.84 (p, *J* = 7.2 Hz, 2H), 1.61 (p, *J* = 7.5 Hz, 2H), 1.41 (m, 2H), 1.36 – 1.19 (m, 14H). ¹³C NMR (151 MHz, CDCl₃) δ 150.08, 147.29, 138.08, 135.92, 123.37, 34.17, 33.14, 32.95, 31.24, 29.53, 29.51, 29.47, 29.24, 28.86, 28.28. HRMS Accurate mass (APCI⁺): Found 298.11575, C₁₅H₂₅N⁷⁹Br (M+H) requires 298.11649.

[3.11d] 3-(11-bromoundecyl)pyridine. Following general procedure C, 3-iodopyridine (205 mg, 1.00 mmol) and 11-bromoundecene (1.10 mL, 5.00 mmol) yielded the title compound as a yellow oil (114 mg, 38%). ¹H NMR (600 MHz, CDCl₃) δ 8.42 (m, 2H), 7.48 (dt, *J* = 7.8, 2.1 Hz, 1H), 7.19 (ddd, *J* = 7.8, 4.8, 1.0 Hz, 1H), 3.40 (t, *J* = 6.9 Hz, 2H), 2.59 (t, *J* = 7.8 Hz, 2H), 1.85 (p, *J* = 7.4 Hz, 2H), 1.62 (p, *J* = 7.5 Hz, 2H), 1.42 (m, 2H), 1.35 – 1.20 (m, 16H). ¹³C NMR (151 MHz, CDCl₃) δ 150.08, 147.28, 138.09, 135.91, 132.35, 34.18, 33.14, 32.95, 31.25, 29.60, 29.52, 29.50, 29.47, 29.25, 28.86, 28.28. HRMS Accurate mass (APCI⁺): Found 312.13132, C₁₆H₂₇N⁷⁹Br (M+H) requires 312.13214.

[3.11e] 3-(12-bromododecyl)pyridine. Following general procedure C, 3-iodopyridine (205 mg, 1.00 mmol) and 12-bromododecene (1.23 g, 5.00 mmol) yielded the title compound as a yellow oil (86.9 mg, 27%). ¹H NMR (600 MHz, CDCl₃) δ 8.43 (m, 2H), 7.48 (dt, *J* = 7.8, 2.0 Hz, 1H), 7.20 (ddd, *J* = 7.8, 4.8, 0.9 Hz, 1H), 3.40 (t, *J* = 6.9 Hz, 2H), 2.60 (t, *J* = 7.7 Hz, 2H), 1.85 (p, *J* = 7.0 Hz, 2H), 1.62 (p, *J* = 7.4 Hz, 2H), 1.42 (p, *J* = 7.3 Hz, 2H), 1.35 – 1.23 (m, 17H). ¹³C NMR (151 MHz, CDCl₃) δ 150.10, 147.30, 138.13, 135.93, 123.37, 33.17, 32.98, 31.28, 29.69, 29.65, 29.64, 29.56, 29.54, 29.29, 28.90, 28.32, 24.52. HRMS Accurate mass (APCI⁺): Found 326.14688, C₁₇H₂₉N⁷⁹Br (M+H) requires 326.14779.

[3.11f] 3-(13-bromotridecyl)pyridine. Following general procedure C, 3-iodopyridine (205 mg, 1.00 mmol) and 13-bromotridecene (1.31 g, 5.00 mmol) yielded the title compound as a yellow oil (64.7 mg, 19%). ¹H NMR (600 MHz, CDCl₃) δ 8.43 (m, 2H), 7.49 (d, *J* = 7.8 Hz, 1H), 7.20 (dd, *J* = 7.8, 4.7 Hz, 1H), 3.41 (t, *J* = 6.9 Hz, 2H), 2.60 (t, *J* = 7.7 Hz, 2H), 1.85 (p, *J* = 6.9 Hz, 2H), 1.61 (p, *J* = 7.4 Hz, 2H), 1.42 (p, *J* = 7.4 Hz, 2H), 1.35 – 1.23 (m, 16H). ¹³C NMR (151 MHz, CDCl₃) δ 150.06, 147.25, 138.16, 135.99, 123.39, 34.21, 33.17, 32.99, 31.29, 29.74, 29.72, 29.67,

29.66, 29.57, 29.55, 29.30, 28.91, 28.32. **HRMS** Accurate mass (APCI⁺): Found 340.16338, C₁₈H₃₁NBr (M+H) requires 340.16344.

[3.11g] 3-(14-bromotetradecyl)pyridine. Following general procedure C, 3-iodopyridine (205 mg, 1.00 mmol) and 14-bromotetradecene (1.38 g, 5.00 mmol) yielded the title compound as a yellow oil (48.3 mg, 14%). **¹H NMR** (600 MHz, CDCl₃) δ 8.43 (m, 2H), 7.49 (d, *J* = 7.8 Hz, 1H), 7.20 (dd, *J* = 7.7, 4.8 Hz, 1H), 3.40 (t, *J* = 6.9 Hz, 2H), 2.60 (t, *J* = 7.7 Hz, 2H), 1.85 (p, *J* = 7.0 Hz, 2H), 1.61 (m, 10H), 1.42 (p, *J* = 7.3 Hz, 2H), 1.34 – 1.21 (m, 18H). **¹³C NMR** (151 MHz, CDCl₃) δ 149.98, 147.18, 138.21, 136.05, 123.41, 34.22, 33.17, 32.99, 31.28, 29.76, 29.73, 29.67, 29.58, 29.55, 29.30, 28.91, 28.32. **HRMS** Accurate mass (APCI⁺): Found 354.17871, C₁₉H₃₃NBr (M+H) requires 354.17909.

[3.11h] 3-(15-bromopentadecyl)pyridine. Following general procedure C, 3-iodopyridine (205 mg, 1.00 mmol) and 13-bromopentadecene (1.45 g, 5.00 mmol) yielded the title compound as a yellow oil (2.19 mg, 6%). **¹H NMR** (600 MHz, CDCl₃) δ 8.44 (m, 2H), 7.50 (d, *J* = 7.8 Hz, 1H), 7.21 (dd, *J* = 7.8, 4.8 Hz, 1H), 3.41 (t, *J* = 6.9 Hz, 2H), 2.60 (t, *J* = 7.7 Hz, 2H), 1.85 (p, *J* = 7.0 Hz, 2H), 1.61 (p, *J* = 7.5 Hz, 2H), 1.42 (p, *J* = 7.2 Hz, 2H), 1.35 – 1.22 (m, 20H). **¹³C NMR** (151 MHz, CDCl₃) δ 149.97, 147.16, 138.23, 136.08, 123.42, 34.22, 33.18, 32.99, 31.28, 29.78, 29.76, 29.69, 29.59, 29.56, 29.30, 28.92, 28.33. **HRMS** Accurate mass (APCI⁺): Found 368.1947, C₂₀H₃₅NBr (M+H) requires 368.19474.

[3.11i] 3-(16-bromohexadecyl)pyridine. Following general procedure C, 3-iodopyridine (205 mg, 1.00 mmol) and 13-bromohexadecene (1.52 g, 5.00 mmol) yielded the title compound as a yellow oil (3.76 mg, 10%). **¹H NMR** (600 MHz, CDCl₃) δ 8.44 (m, 2H), 7.51 (d, *J* = 7.9 Hz, 1H), 7.22 (dd, *J* = 7.8, 4.7 Hz, 1H), 3.41 (t, *J* = 6.9 Hz, 2H), 2.61 (t, *J* = 7.7 Hz, 2H), 1.85 (p, *J* = 6.9 Hz, 2H), 1.62 (p, *J* = 7.4 Hz, 2H), 1.42 (p, *J* = 7.3 Hz, 2H), 1.36 – 1.21 (m, 22H). **¹³C NMR** (151 MHz,

CDCl₃) δ 149.77, 146.97, 138.34, 136.27, 123.48, 34.22, 33.17, 33.00, 31.27, 29.79, 29.78, 29.76, 29.69, 29.59, 29.56, 29.30, 28.33. **HRMS** Accurate mass (APCI⁺): Found 382.21034, C₂₁H₃₇NBr (M+H) requires 382.21039.

[3.12a] Cyclic pyridinium. Following general procedure D, **3-(8-bromooctyl)pyridine (3.11a)** (68.0 mg, 0.253 mmol) yielded the title compound as a yellow solid (49.8 mg, 62%). **¹H NMR** (600 MHz, CD₃OD) δ 9.10 (m, 1H), 8.92 (m, 1H), 8.50 (m, 1H), 8.03 (m, 1H), 4.68 (t, *J* = 7.6 Hz, 2H), 2.91 (t, *J* = 7.8 Hz, 2H), 2.06 (m 2H), 1.76 (t, *J* = 7.7 Hz, 2H), 1.45-1.21 (m, 12H). **¹³C NMR** (151 MHz, CD₃OD) δ 146.73, 145.65, 145.33, 143.36, 128.97, 125.15, 62.81, 33.46, 32.54, 31.44, 29.97, 29.86, 29.79, 27.03. **HRMS** Accurate mass (APCI⁺): Found 318.0704, C₁₃H₂₁N¹²⁷I (M+H) requires 318.07132.

[3.12b] Cyclic pyridinium. Following general procedure D, **3-(9-bromononyl)pyridine (3.11b)** (84.4 mg, 0.298 mmol) yielded the title compound as a yellow solid (93.2 mg, 94%). **¹H NMR** (600 MHz, CD₃OD) δ 9.12 (m, 1H), 8.94 (m, 1H), 8.51 (m, 1H), 8.04 (m, 1H), 4.69 (m, 2H), 2.91 (t, *J* = 8.0 Hz, 2H), 2.06 (m 2H), 1.75 (t, *J* = 7.1 Hz, 2H), 1.47-1.22 (m, 14H). **¹³C NMR** (151 MHz, CD₃OD) δ 146.76, 145.65, 145.34, 143.34, 128.97, 62.81, 33.47, 32.55, 31.49, 30.19, 30.09, 29.94, 29.91, 27.04. **HRMS** Accurate mass (APCI⁺): Found 332.08594, C₁₄H₂₃N¹²⁷I (M+H) requires 332.08697.

[3.12c] Cyclic pyridinium. Following general procedure D, **3-(10-bromodecyl)pyridine (3.11c)** (82.6 mg, 0.278 mmol) yielded the title compound as a yellow solid (83.5 mg, 87%). **¹H NMR** (600 MHz, CD₃OD) δ 9.11 (m, 1H), 8.93 (m, 1H), 8.51 (m, 1H), 8.04 (m, 1H), 4.68 (m, 2H), 2.91 (t, *J* = 7.2 Hz, 2H), 2.06 (m 2H), 1.75 (t, *J* = 7.2 Hz, 2H), 1.46-1.22 (m, 16H). **¹³C NMR** (151 MHz, CD₃OD) δ 146.73, 145.64, 145.31, 143.33, 128.97, 62.80, 33.47, 32.56, 31.53, 30.41, 30.33,

30.23, 30.01, 29.97, 27.07. **HRMS** Accurate mass (APCI⁺): Found 346.10164, C₁₅H₂₅N¹²⁷I (M+H) requires 346.10262.

[3.12d] Cyclic pyridinium. Following general procedure D, **3-(11-bromoundecyl)pyridine (3.11d)** (102 mg, 0.327 mmol) yielded the title compound as a yellow solid (34.3 mg, 29%). **¹H NMR** (600 MHz, CD₃OD) δ 9.10 (m, 1H), 8.93 (m, 1H), 8.50 (m, 1H), 8.04 (m, 1H), 4.69 (m, 2H), 2.91 (t, *J* = 7.7 Hz, 2H), 2.05 (m 2H), 1.75 (t, *J* = 6.6 Hz, 2H), 1.48-1.20 (m, 18H). **¹³C NMR** (151 MHz, CD₃OD) δ 146.71, 145.63, 145.31, 143.33, 128.97, 62.82, 33.47, 32.56, 31.54, 30.52, 30.46, 30.39, 30.31, 30.04, 30.01, 27.09. **HRMS** Accurate mass (APCI⁺): Found 360.11716, C₁₆H₂₇N¹²⁷I (M+H) requires 360.11827.

[3.12e] Cyclic pyridinium (2e). Following general procedure D, **3-(12-bromododecyl)pyridine (3.11e)** (31.8 mg, 0.097 mmol) yielded the title compound as a yellow solid (34.0 mg, 93%). **¹H NMR** (600 MHz, CD₃OD) δ 9.08 (m, 1H), 8.91 (m, 1H), 8.49 (m, 1H), 8.04 (m, 1H), 4.67 (m, 2H), 2.91 (t, *J* = 8.0 Hz, 2H), 2.06 (m 2H), 1.75 (t, *J* = 7.1 Hz, 2H), 1.47-1.22 (m, 20H). **¹³C NMR** (151 MHz, CD₃OD) □ 146.73, 145.32, 143.33, 141.98, 129.93, 62.67, 33.49, 32.55, 31.56, 30.59, 30.56, 30.51, 30.45, 30.35, 30.06, 27.11, 24.52. **HRMS** Accurate mass (APCI⁺): Found 374.13289, C₁₇H₂₉N¹²⁷I (M+H) requires 374.13392.

[3.12f] Cyclic pyridinium. Following general procedure D, **3-(13-bromotridecyl)pyridine (3.11f)** (56.8 mg, 0.1669 mmol) yielded the title compound as a yellow solid (45.4 mg, 70%). **¹H NMR** (600 MHz, CD₃OD) δ 9.10 (m, 1H), 8.93 (m, 1H), 8.50 (m, 1H), 8.04 (m, 1H), 4.68 (m, 2H), 2.91 (t, *J* = 7.2 Hz, 2H), 2.04 (m, 2H), 1.75 (t, *J* = 7.2 Hz, 2H), 1.42 – 1.21 (m, 18H). **¹³C NMR** (151 MHz, CD₃OD) δ 146.71, 145.61, 145.28, 143.32, 128.98, 62.80, 34.81, 33.46, 32.53, 31.53, 30.61, 30.56, 30.51, 30.43, 30.35, 30.09, 27.07. **HRMS** Accurate mass (APCI⁺): Found 388.14961, C₁₈H₃₁NI (M+H) requires 388.14957.

[3.12g] Cyclic pyridinium. Following general procedure D, **3-(14-bromotetradecyl)pyridine (3.11g)** (43.5 mg, 0.1227 mmol) yielded the title compound as a yellow solid (38.3 mg, 78%). **¹H NMR** (600 MHz, CD₃OD) δ 9.05 (m, 1H), 8.91 (m, 1H), 8.49 (m, 1H), 8.04 (m, 1H), 4.68 (m, 2H), 2.91 (t, *J* = 8.0 Hz, 2H), 2.04 (m, 2H), 1.75 (t, *J* = 7.4 Hz, 2H), 1.45 – 1.20 (m, 20H). **¹³C NMR** (151 MHz, CD₃OD) δ 146.71, 145.65, 145.29, 143.33, 129.00, 62.85, 34.84, 33.48, 32.53, 31.55, 30.67, 30.59, 30.56, 30.46, 30.38, 30.32, 30.12, 30.05, 27.10. **HRMS** Accurate mass (APCI⁺): Found 402.16553, C₁₉H₃₃Ni (M+H) requires 402.16522.

[3.12h] Cyclic pyridinium. Following general procedure D, **3-(15-bromopentadecyl)pyridine (3.11h)** (18.8 mg, 0.05103 mmol) yielded the title compound as a yellow solid (15.2 mg, 72%). **¹H NMR** (600 MHz, CD₃OD) δ 9.05 (m, 1H), 8.89 (m, 1H), 8.48 (m, 1H), 8.03 (m, 1H), 4.66 (m, 2H), 2.91 (t, *J* = 8.0 Hz, 2H), 2.04 (m, 2H), 1.75 (t, *J* = 6.6 Hz, 2H), 1.41 – 1.25 (m, 22H). **¹³C NMR** (151 MHz, CD₃OD) δ 146.70, 145.68, 145.30, 143.33, 128.99, 62.88, 34.85, 33.50, 32.52, 31.55, 30.72, 30.69, 30.61, 30.58, 30.48, 30.39, 30.33, 30.13, 30.06, 27.11. **HRMS** Accurate mass (APCI⁺): Found 416.18112, C₂₀H₃₅Ni (M+H) requires 416.18087.

[3.12i] Cyclic pyridinium. Following general procedure D, **3-(16-bromohexadecyl)pyridine (3.11i)** (26.2 mg, 0.0685mmol) yielded the title compound as a yellow solid (20.7 mg, 70%). **¹H NMR** (600 MHz, CD₃OD) δ 9.01 (m, 1H), 8.88 (m, 1H), 8.47 (m, 1H), 8.03 (m, 1H), 4.65 (m, 2H), 2.90 (t, *J* = 8.2 Hz, 2H), 2.04 (m, 2H), 1.75 (t, *J* = 7.4 Hz, 2H), 1.40 – 1.25 (m, 24H). **¹³C NMR** (151 MHz, CD₃OD) δ 146.71, 145.71, 145.29, 143.34, 129.00, 62.91, 34.86, 33.51, 32.53, 31.57, 30.77, 30.73, 30.64, 30.61, 30.51, 30.47, 30.43, 30.35, 30.14, 30.08, 27.14. **HRMS** Accurate mass (APCI⁺): Found 430.197, C₂₁H₃₇Ni (M+H) requires 430.1965.

References

1. W. Qu, K. Ploessl, H. Truong, M-P. Kung, H. F. Kung, *Bioorg. Med. Chem. Lett.* **2009**, *19*, 3382-3385.
2. A. J. Boyington, M-L. Y. Riu, N. T. Jui, *J. Am. Chem. Soc.* **2017**, *139*, 6582-6585.
3. C. Timm, T. Mordhorst, M. Köck, *Mar. Drugs.* **2010**, *8*, 483-497.

5.5.3. Chapter 4

[4.3] 2,5-dioxopyrrolidin-1-yl (R)-3-isocyanobutanoate. Procedure adapted from: Xu, Y; Tan, D.S., Total Synthesis of the Bacterial Diisonitrile Chalkophore SF2768, *Org. Lett.*, 2019, **21**, 8731-8735

1.1 g, 64% yield; ¹H NMR (400 MHz, CDCl₃) δ 4.16 (h, J = 6.8 Hz, 1H), 3.10 (dd, J = 16.4, 6.5 Hz, 1H), 2.95 – 2.78 (m, 5H), 1.55 (dt, J = 6.7, 1.9 Hz, 3H).

[4.11] (S)-2,6-bis((R)-3-isocyanobutanamido)hexyl acetate. Procedure adapted from: Xu, Y; Tan, D.S., Total Synthesis of the Bacterial Diisonitrile Chalkophore SF2768, *Org. Lett.*, 2019, **21**, 8731-8735

114mg, 59% yield; ¹H NMR (600 MHz, DMSO) δ 7.97 (t, J = 5.6 Hz, 1H), 7.94 (d, J = 8.4 Hz, 1H), 4.11 – 4.04 (m, 2H), 3.99 (dd, J = 10.7, 4.7 Hz, 1H), 3.94 (dq, J = 13.6, 4.8, 4.1 Hz, 1H), 3.84 (dd, J = 10.7, 6.4 Hz, 1H), 3.10 – 2.99 (m, J = 6.5 Hz, 3H), 2.49 – 2.42 (m, 2H), 2.42 – 2.35 (m, 2H), 1.99 (s, 3H), 1.50 – 1.22 (m, 15H).

[4.12] (3R,3'R)-N,N'-((S)-6-hydroxyhexane-1,5-diyl)bis(3-isocyanobutanamide). Procedure adapted from: Xu, Y; Tan, D.S., Total Synthesis of the Bacterial Diisonitrile Chalkophore SF2768, *Org. Lett.*, 2019, **21**, 8731-8735

34mg, 77% yield; ¹H NMR (600 MHz, DMSO) δ 7.97 (t, *J* = 5.6 Hz, 1H), 7.74 (d, *J* = 8.5 Hz, 1H), 4.63 (t, *J* = 5.6 Hz, 1H), 4.07 (d, *J* = 7.2 Hz, 2H), 3.70 (d, *J* = 5.0 Hz, 1H), 3.29 – 3.21 (m, 2H), 3.02 (dh, *J* = 13.2, 6.6 Hz, 2H), 2.48 – 2.33 (m, 6H), 1.57 – 1.49 (m, 1H), 1.44 – 1.21 (m, 15H).

[4.20] (*R*)-*N*-benzyl-3-isocyanobutanamide. To a flame dried round bottom flask equipped with a stir bar, phenylmethanamine (1.0 eq, 23mg, 0.22 mmol) was dissolved in tetrahydrofuran (0.2M, 1.1mL) and *N,N*-diisopropylethylamine (1.5 eq, 0.06mL). This mixture was then cooled to 0°C. **[4.3]** (1.0 eq, 50 mg, 0.24 mmol) was then added in portions. The mixture was then warmed to room temperature and stirred for six hours. Once complete by TLC, the reaction mixture was quenched with water (4 mL). The organic layer was extracted (3x, 10 mL) and washed with brine (10 mL). The combined organic layers were then dried with magnesium sulfate, concentrated, and purified by flash chromatography in 100% ethyl acetate to afford the product as a white solid (25 mg, 57% yield). ¹H NMR (600 MHz, DMSO) δ 8.55 (t, *J* = 6.0 Hz, 1H), 7.34 – 7.20 (m, 5H), 4.35 – 4.26 (m, 2H), 4.16 – 4.09 (m, 1H), 2.56 (ddt, *J* = 14.7, 8.4, 1.5 Hz, 1H), 2.49 – 2.44 (m, 1H), 1.33 (dt, *J* = 6.7, 2.2 Hz, 3H). ¹³C NMR (151 MHz, DMSO) δ 168.16, 155.05, 139.16, 128.26, 127.21, 126.81, 47.05, 47.01, 46.98, 42.22, 42.08, 21.02. **HRMS** Accurate mass (APCI⁺): Found 203.1183 C₁₂H₁₅N₂O (m+1H), requires 203.11789. [α]_D = + 3.655 (c = 1.0 in DMSO). **IR** 3211.87, 2361.75, 2322.79, 1667.99, 1010.80 cm⁻¹.

[4.21] (*R*)-*N*-(4-aminobenzyl)-3-isocyanobutanamide. To a flame dried round bottom flask equipped with a stir bar, 4-aminobenzylamine (1.0 eq, 0.040 mL, 0.35 mmol) was dissolved in tetrahydrofuran (0.2 M, 1.75 mL). To this solution, diisopropylethylamine (2.5 eq, 0.15 mL, 0.87 mmol) was added. The reaction mixture was then cooled to 0 °C followed by addition of 2,5-dioxopyrrolidin-1-yl (*R*)-3-isocyanobutanoate (2.1 eq, 154 mg, 0.73 mmol) in portions. Reaction

mixture was allowed to stir for 6 h while slowly warming to room temperature. Upon completion, deionized water was added (2 mL). The organic layer was extracted with dichloromethane (3x, 5 mL) and washed with water (2x, 3mL). The combined organic layers were then dried with magnesium sulfate, filtered, concentrated, and purified by flash chromatography (100% ethyl acetate) to afford the desired product as a white solid (75 mg, 99% yield). **¹H NMR** (600 MHz, DMSO) δ 8.31 (t, J = 5.9 Hz, 1H), 6.95 – 6.88 (m, 2H), 6.55 – 6.47 (m, 2H), 4.94 (s, 2H), 4.11 (q, J = 7.3, 6.3 Hz, 4H), 2.43 (ddt, J = 14.6, 5.6, 2.9 Hz, 1H), 1.31 (dt, J = 6.6, 2.2 Hz, 3H). **¹³C NMR** (151 MHz, DMSO) δ 167.77, 154.96, 147.58, 128.26, 125.86, 113.66, 47.05, 47.01, 46.98, 42.23, 41.89, 21.01. **HRMS** Accurate mass (APCI+): Found 218.12917 C₁₂H₁₆ON₃ (mass + 1H), required 218.12879 [α] = +10.788 (c = 1.0 in DMSO). **IR** 3405.26, 3176.17, 1839.33, 2007.18, 1985.68, 1665.23, 1009.13 cm⁻¹.

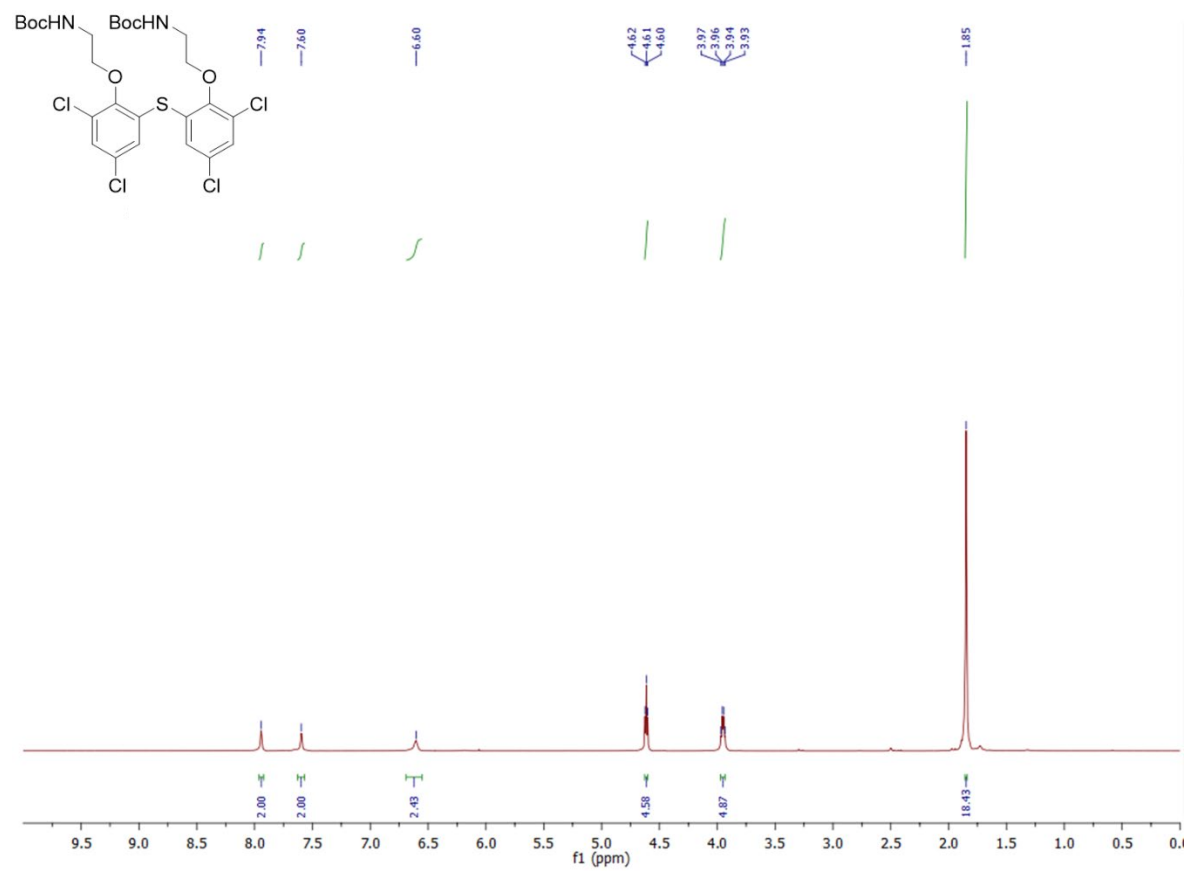
[4.22] (3*R*,3'*R*)-*N,N'*-(1,4-phenylenebis(methylene))bis(3-isocyanobutanamide). To a flame dried round bottom flask equipped with a stir bar, 1,4-phenylenedimethanamine (1.0 eq, 7.8 mg, 0.058 mmol) was dissolved in tetrahydrofuran (0.2 M, 0.30 mL). To this solution, diisopropylethylamine (2.5 eq, 0.025 mL, 0.144 mmol) was added. The reaction mixture was then cooled to 0 °C followed by addition of 2,5-dioxopyrrolidin-1-yl (R)-3-isocyanobutanoate (2.1 eq, 25.4 mg, 0.121 mmol) in portions. Reaction mixture was allowed to stir for 6 h while slowly warming to room temperature. Upon completion, deionized water was added (1 mL). The organic layer was extracted with dichloromethane (3x, 5 mL) and washed with water (2x, 3mL). The combined organic layers were then dried with magnesium sulfate, filtered, concentrated, and purified by flash chromatography (gradient of 100% dichloromethane to 10% methanol) to afford the desired product as a white solid (10.1 mg, 57% yield). **¹H NMR** (500 MHz, DMSO) δ 8.53 (t, J = 5.9 Hz, 2H), 7.19 (s, 4H), 4.35 – 4.17 (m, 5H), 4.16 – 4.01 (m, 2H), 2.56 – 2.50 (m, 2H), 1.31

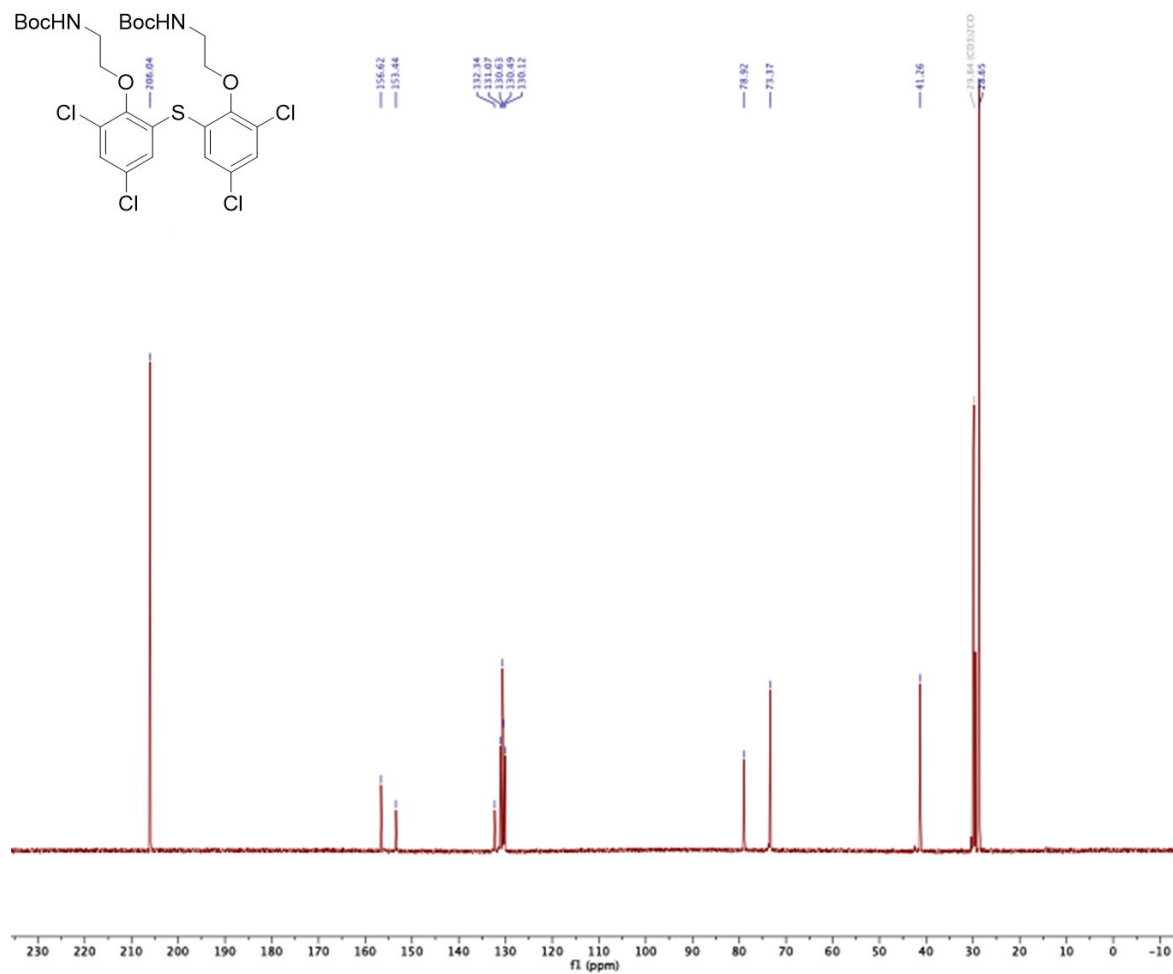
(dt, $J = 6.7, 2.2$ Hz, 6H). **^{13}C NMR** (126 MHz, DMSO) δ 168.57, 138.23, 127.64, 47.71, 42.67, 42.25, 21.47. **HRMS** Accurate mass (APCI+): Found 327.18187 $\text{C}_{18}\text{H}_{23}\text{O}_2\text{N}_4$ (mass + 1H), required 327.18155. $[\alpha] = +4.439$ ($c = 1.0$ in DMSO). **IR** 3315.88, 2933.83, 2827.70, 1443.07, 1023.08, 994.07 cm^{-1} .

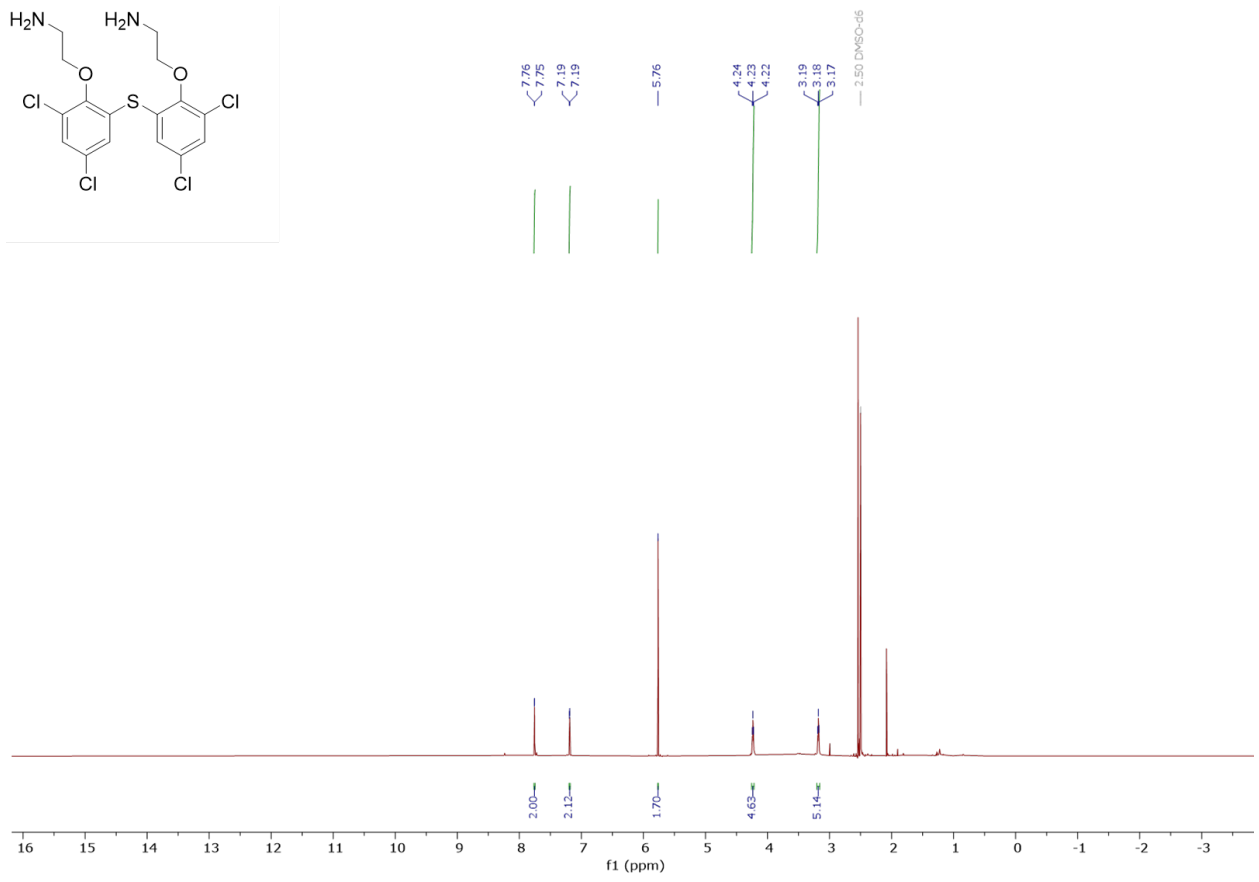
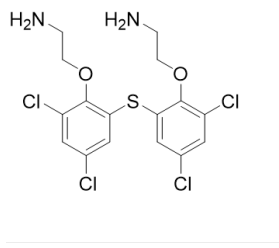
[4.23] *tert*-butyl (*R*)-(4-((3-isocyanobutanamido)methyl)benzyl)carbamate To a flame dried round bottom flask equipped with a stir bar, *tert*-butyl (4-(aminomethyl)benzyl)carbamate (1.0 eq, 12 mg, 0.051 mmol) was dissolved in tetrahydrofuran (0.2 M, 0.26 mL). To this solution, diisopropylethylamine (0.5 eq, 4.4 μL , 0.025 mmol) was added. The reaction mixture was then cooled to 0 $^{\circ}\text{C}$ followed by addition of 2,5-dioxopyrrolidin-1-yl (*R*)-3-isocyanobutanoate (0.75 eq, 8 mg, 0.038 mmol) in portions. Reaction mixture was allowed to stir for 6 h while slowly warming to room temperature. Upon completion, deionized water was added (2 mL). The organic layer was extracted with dichloromethane (3x, 5 mL) and washed with water (2x, 3mL). The combined organic layers were then dried with magnesium sulfate, filtered, concentrated, and purified by flash chromatography (100% ethyl acetate) to afford the desired product as a white solid (12.1 mg, 72% yield). **^1H NMR** (500 MHz, DMSO) δ 8.53 (t, $J = 5.8$ Hz, 1H), 7.37 (t, $J = 6.2$ Hz, 1H), 7.23 – 7.13 (m, 4H), 4.32 – 4.21 (m, 2H), 4.16 – 4.09 (m, 1H), 4.08 (d, $J = 6.2$ Hz, 2H), 1.38 (s, 7H), 1.32 (dt, $J = 6.7, 2.2$ Hz, 3H). **^{13}C NMR** (126 MHz, DMSO) δ 207.76, 168.12, 155.76, 138.80, 137.49, 127.14, 126.87, 77.74, 47.08, 46.98, 43.08, 42.22, 41.84, 28.24, 21.03. **HRMS** Accurate mass (APCI+): Found 354.17803 $\text{C}_{18}\text{H}_{25}\text{O}_3\text{N}_3$ (mass + ^{23}Na), required 354.17881.

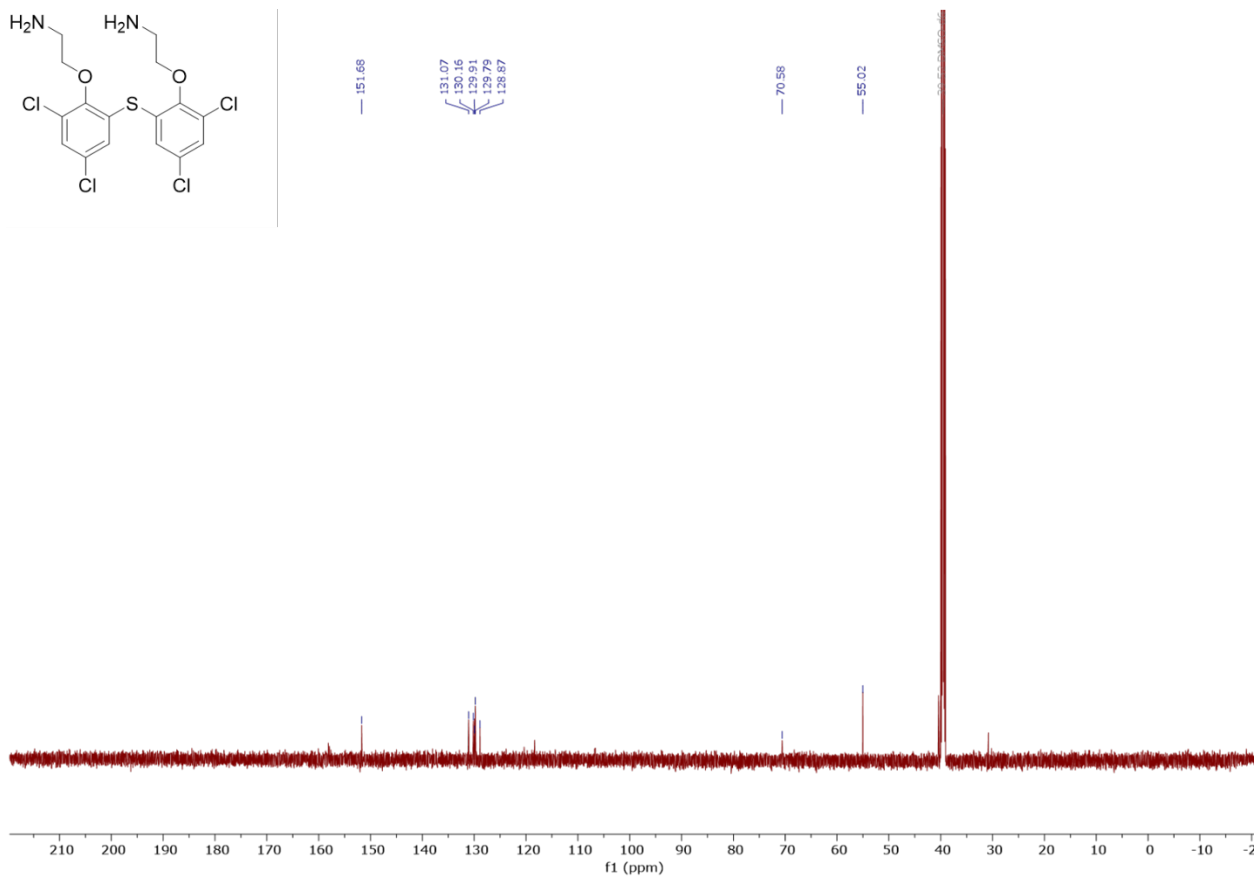
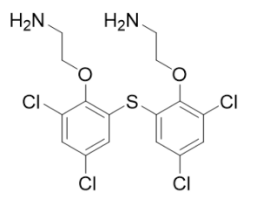
Appendix: Spectra

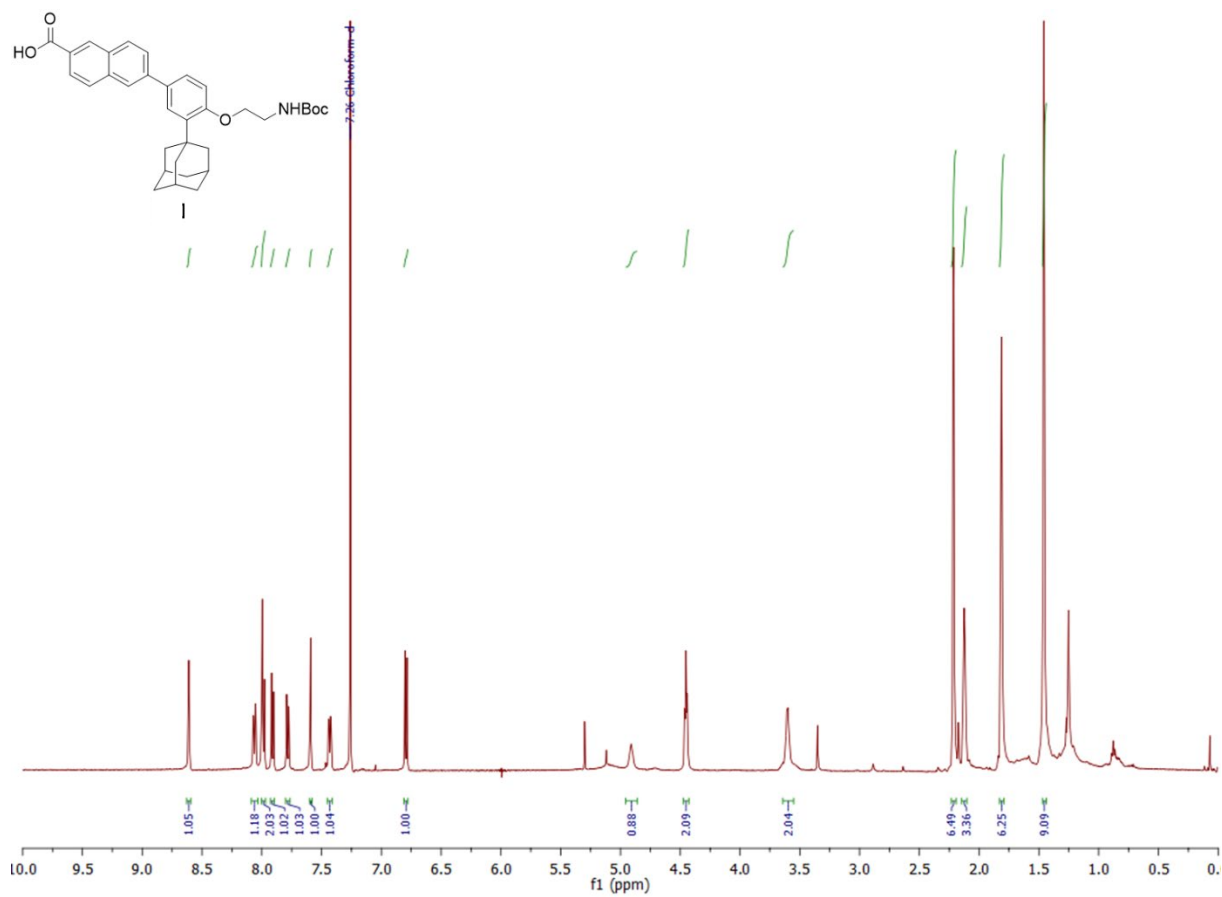
Appendix. Chapter 2

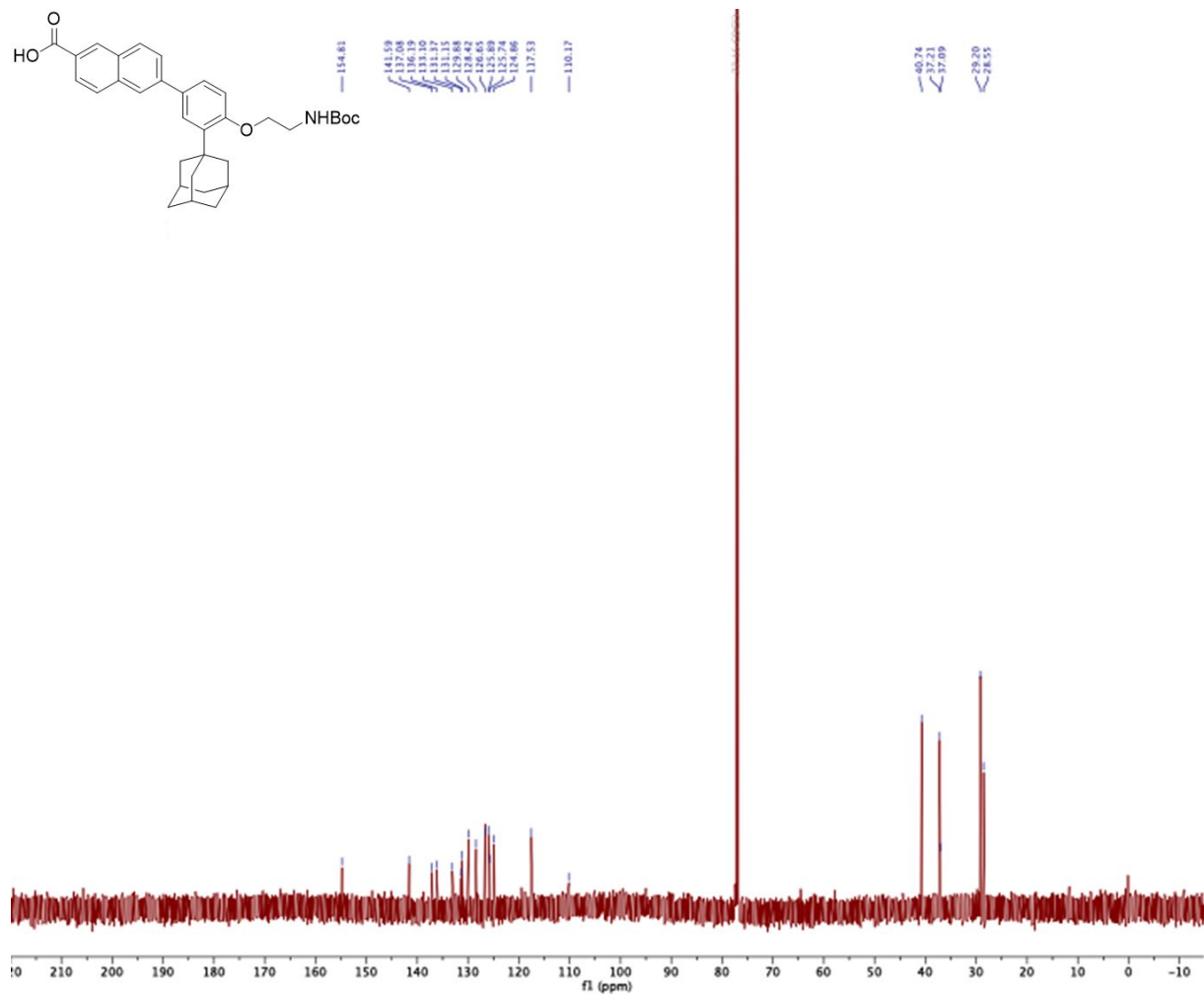


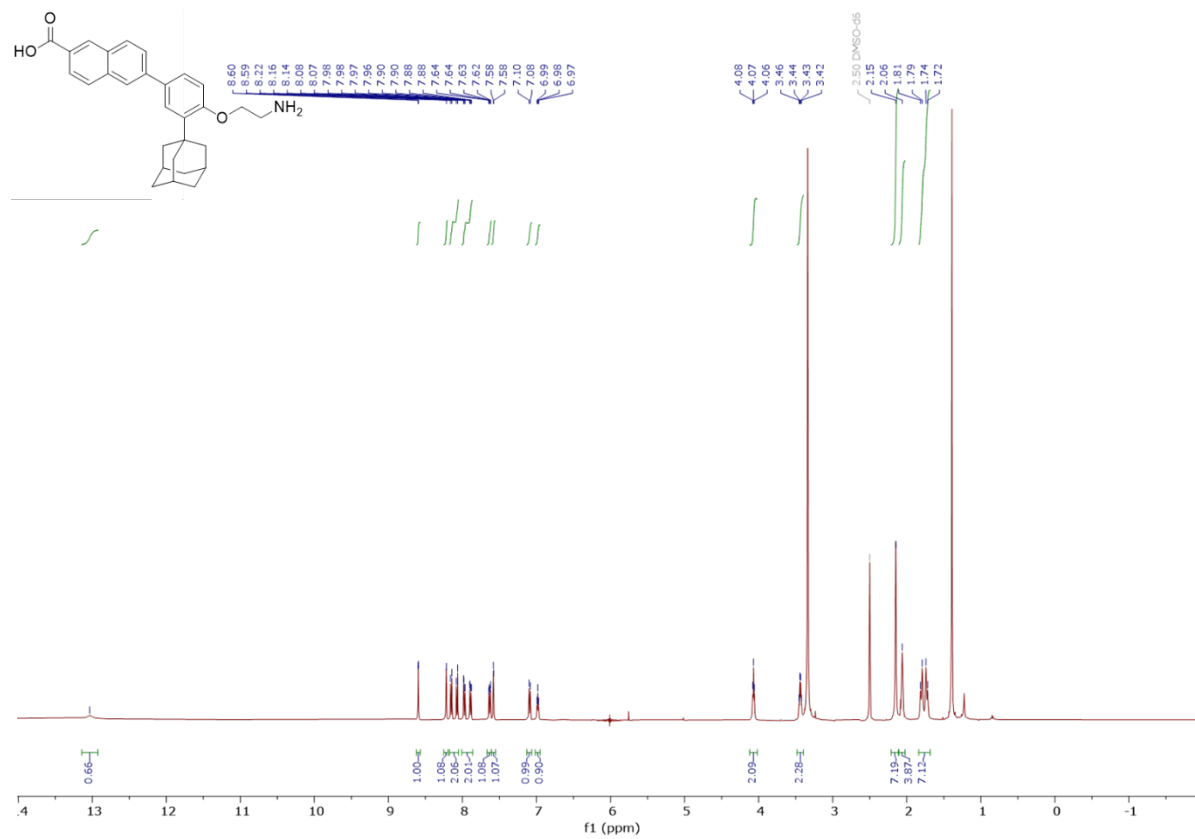


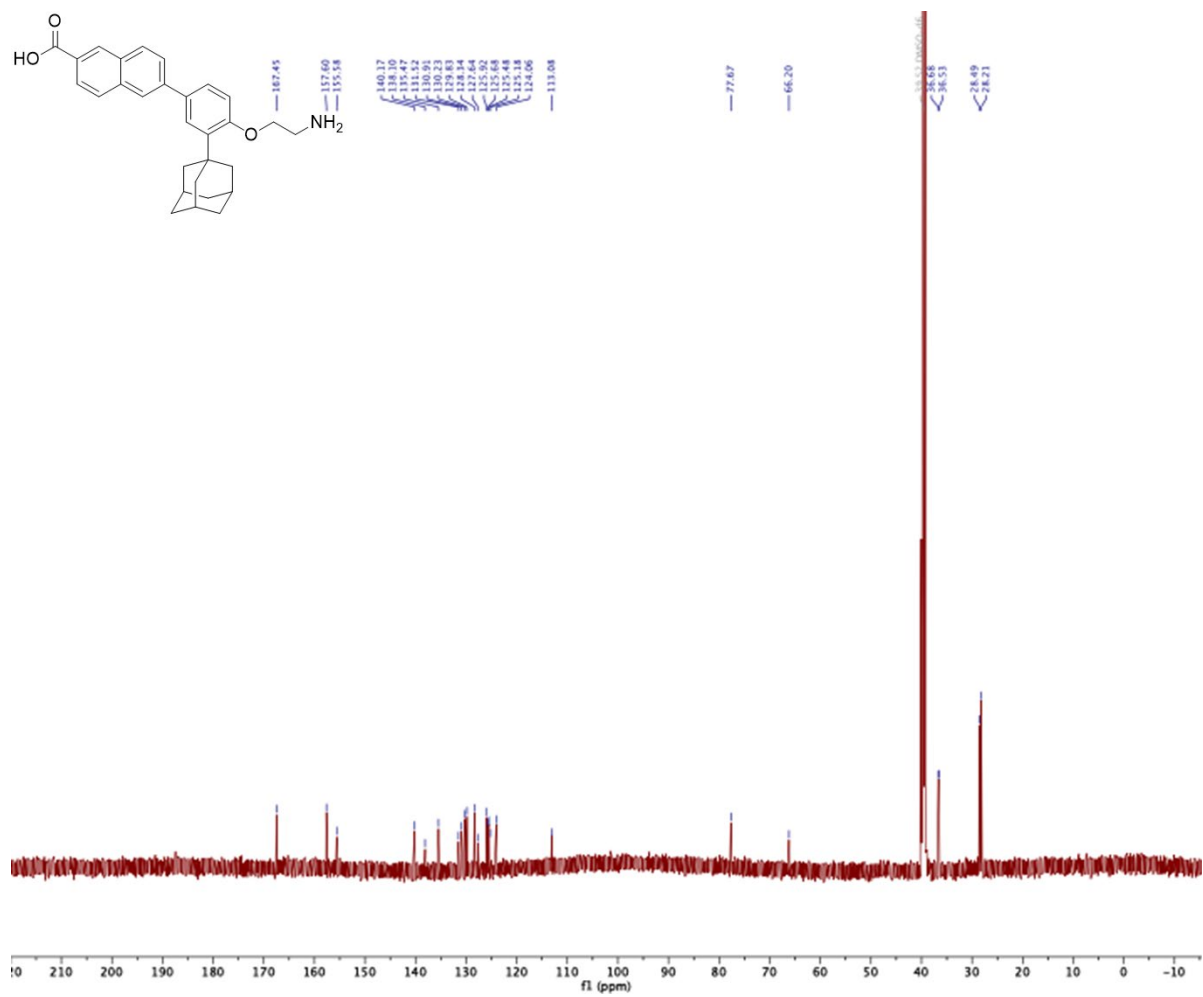


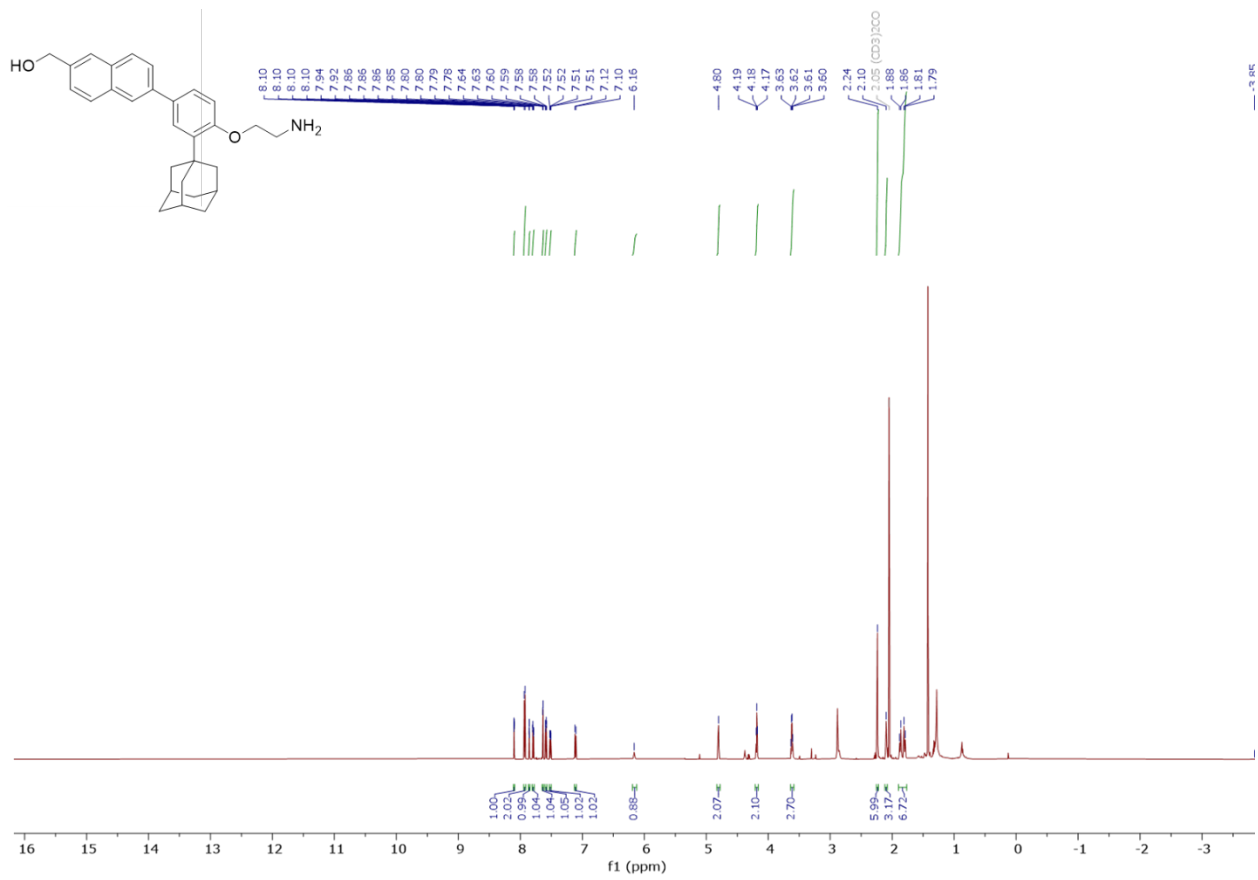


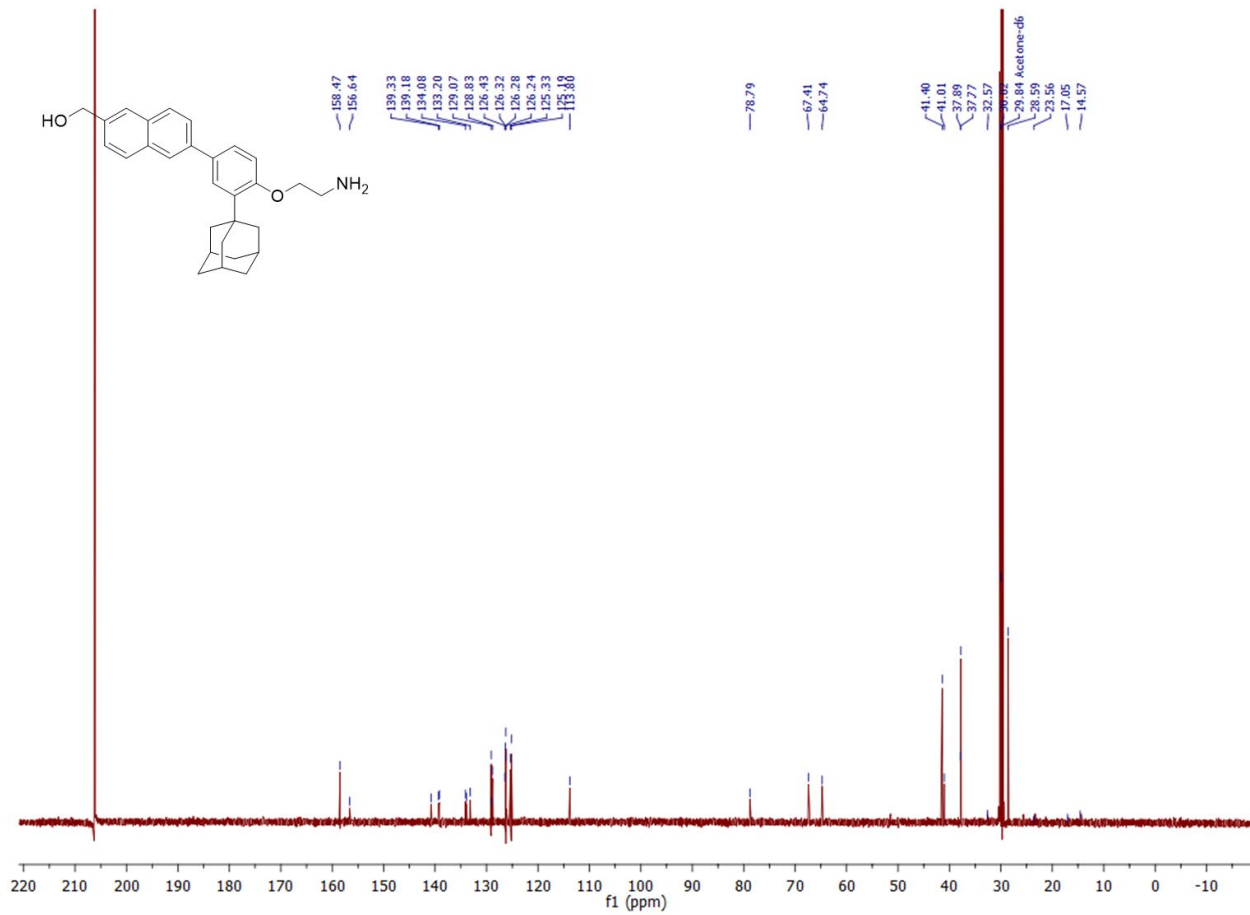


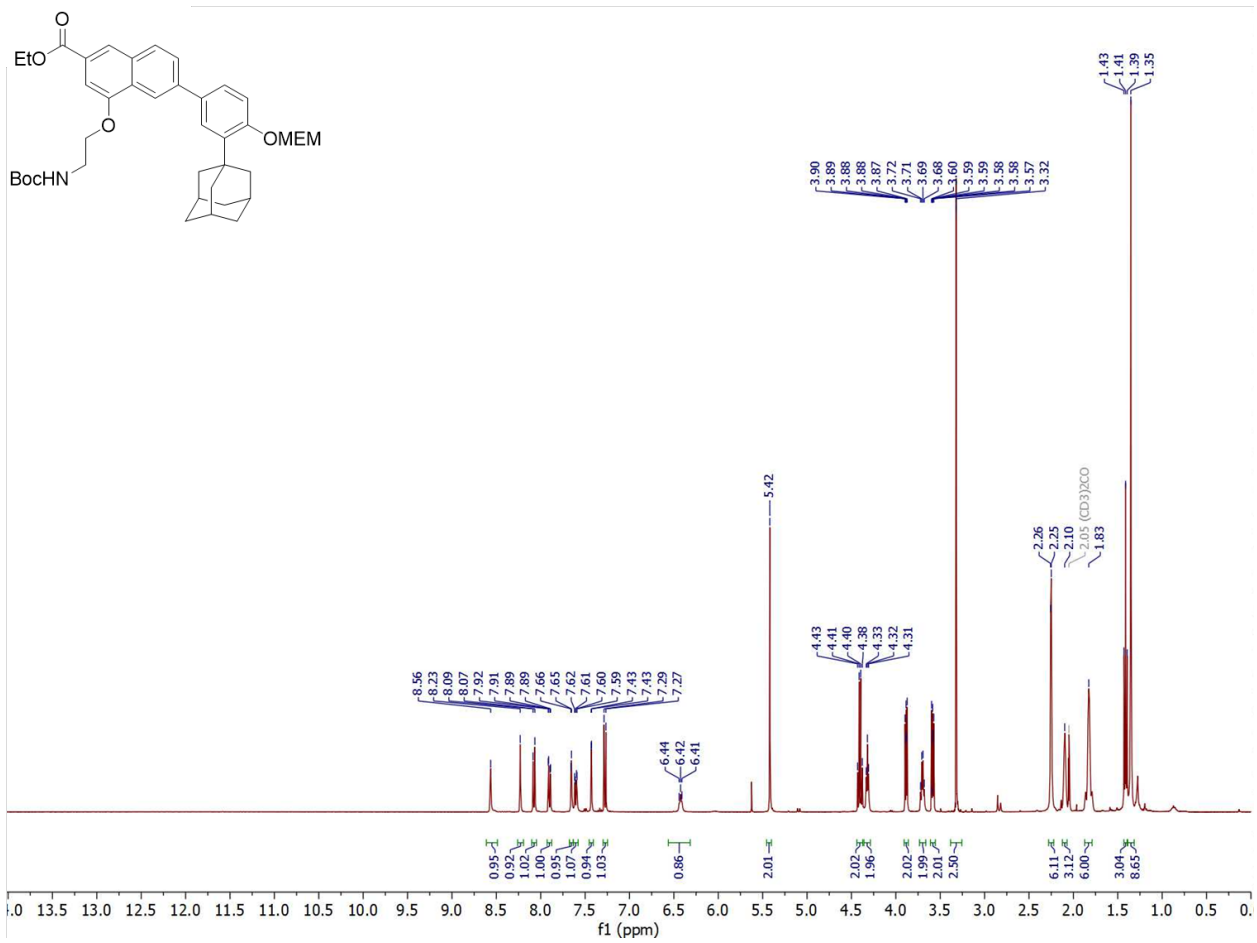


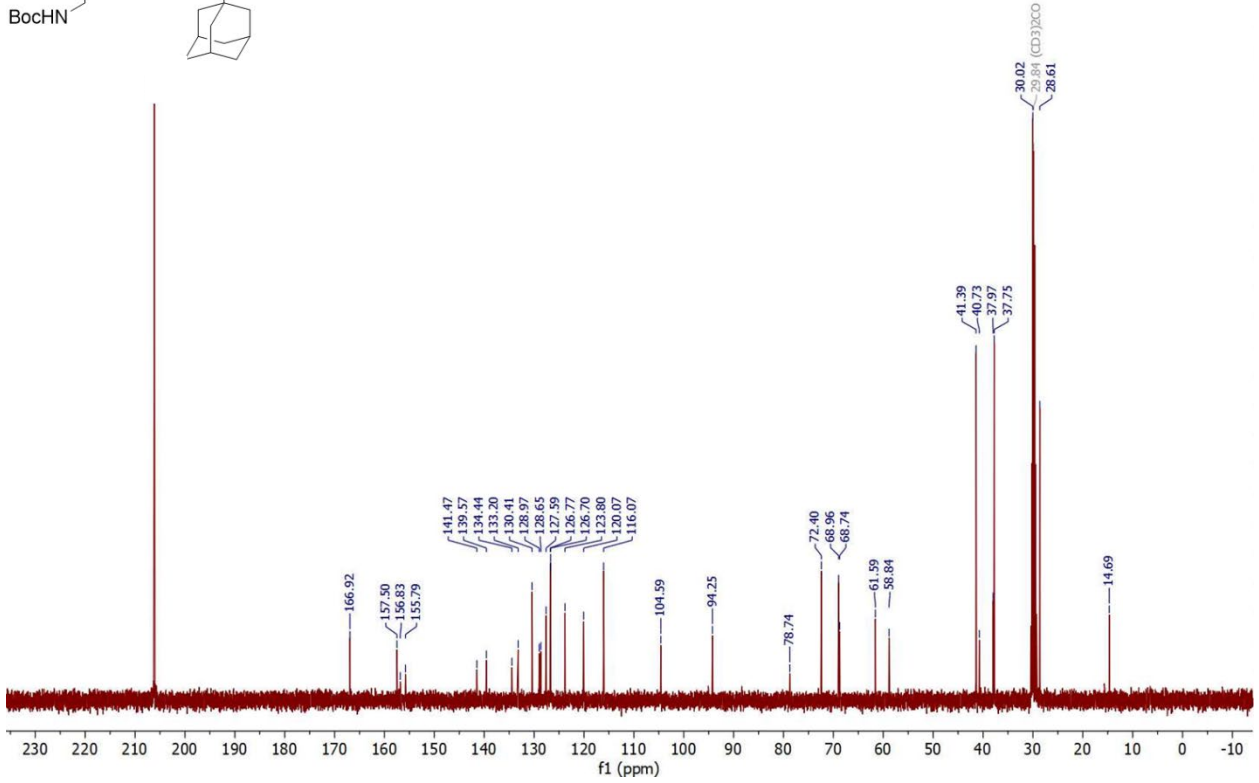
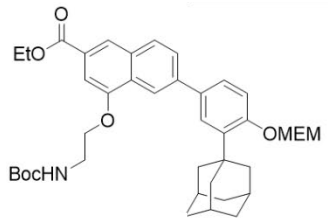


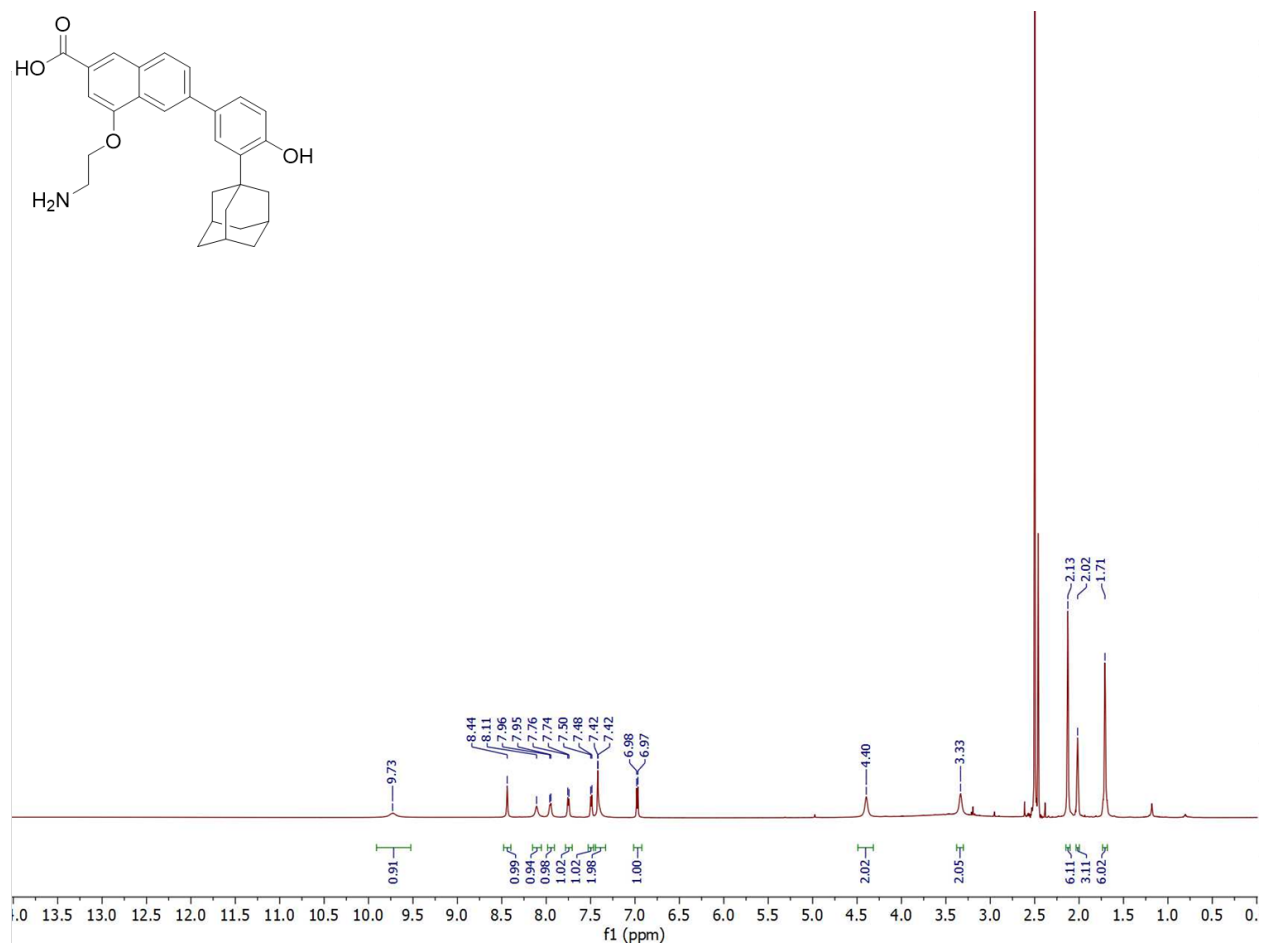
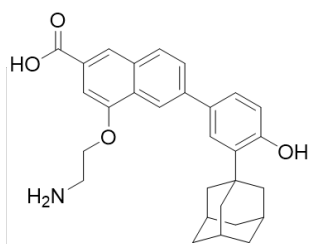


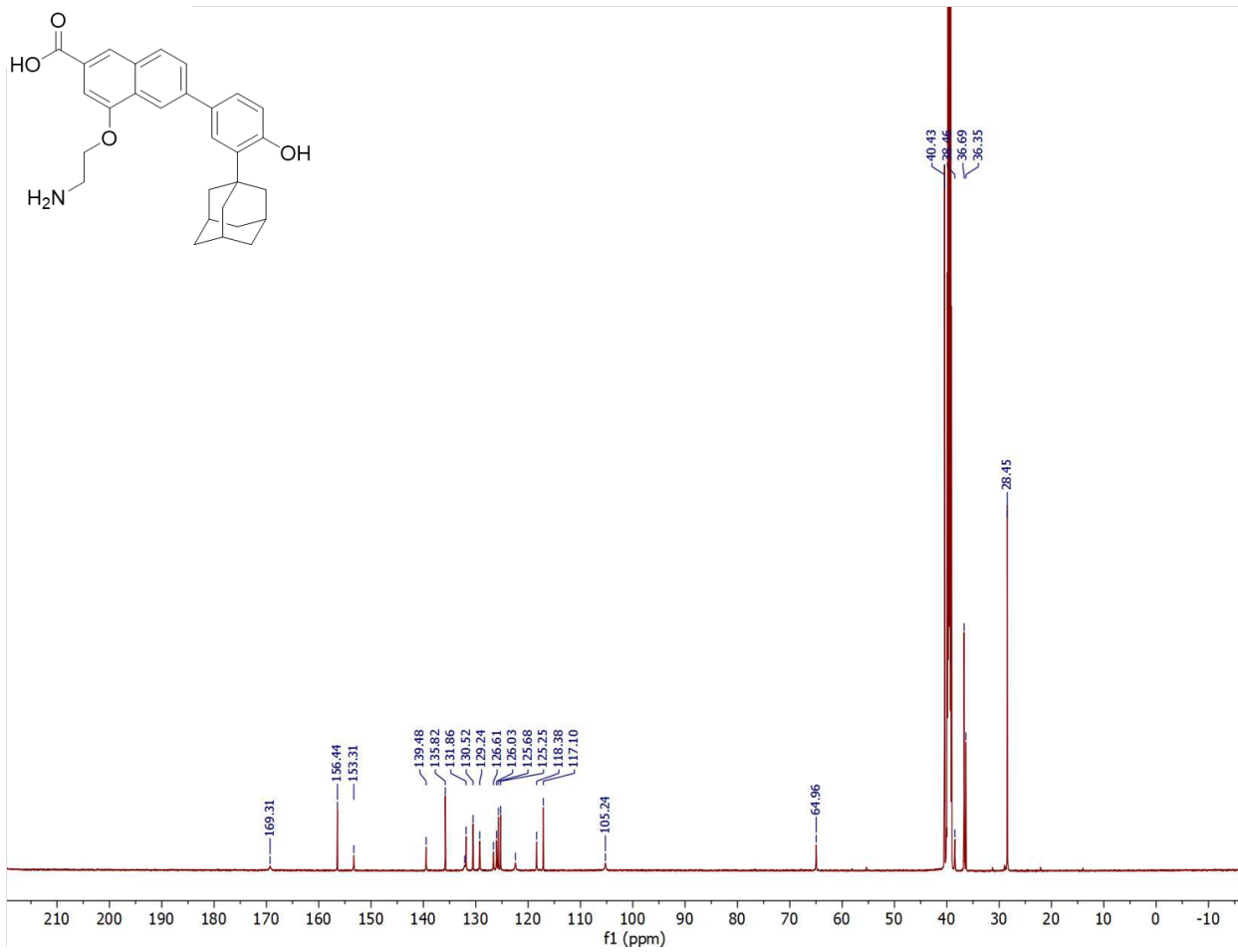


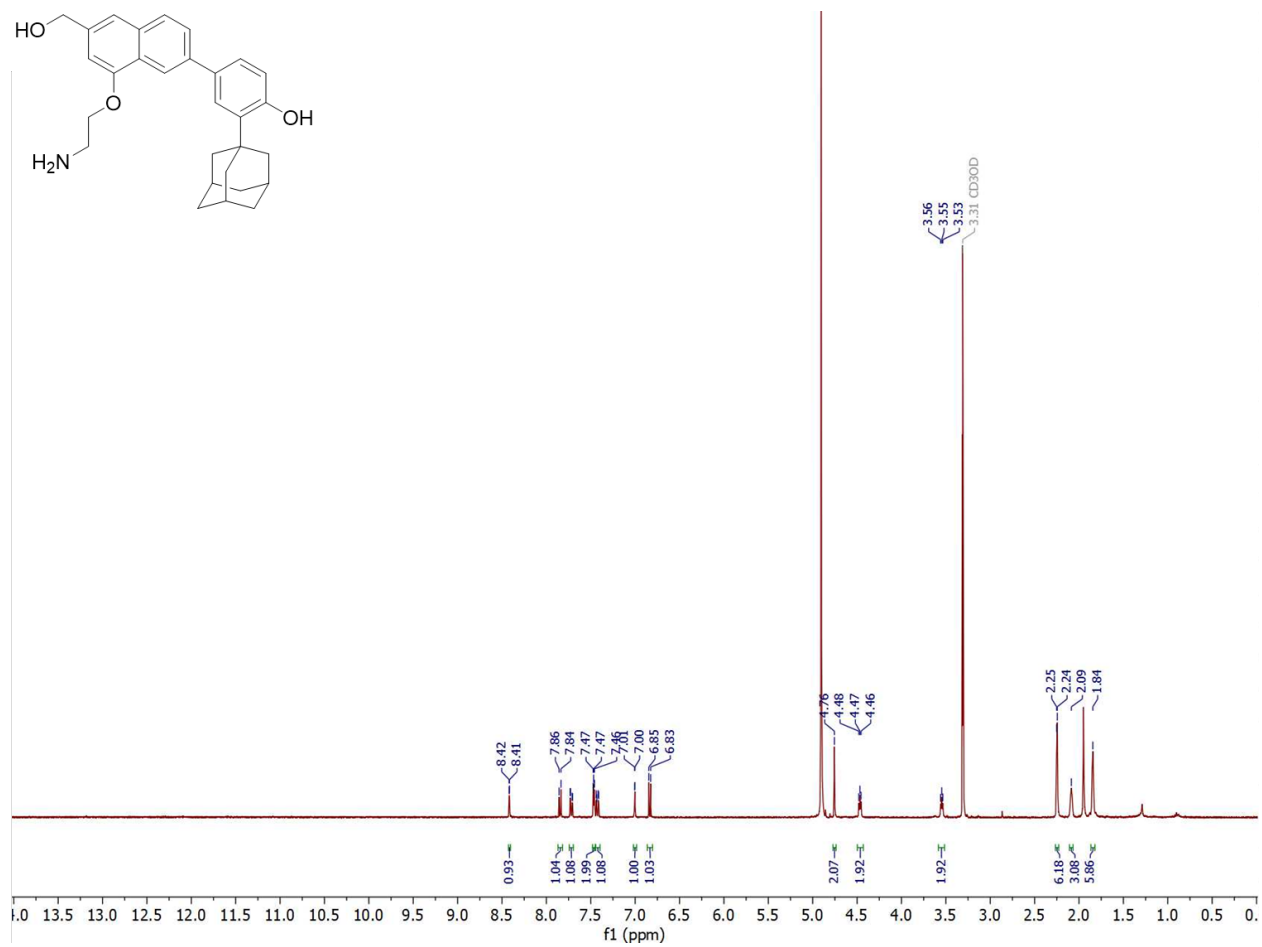
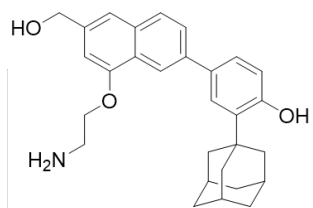


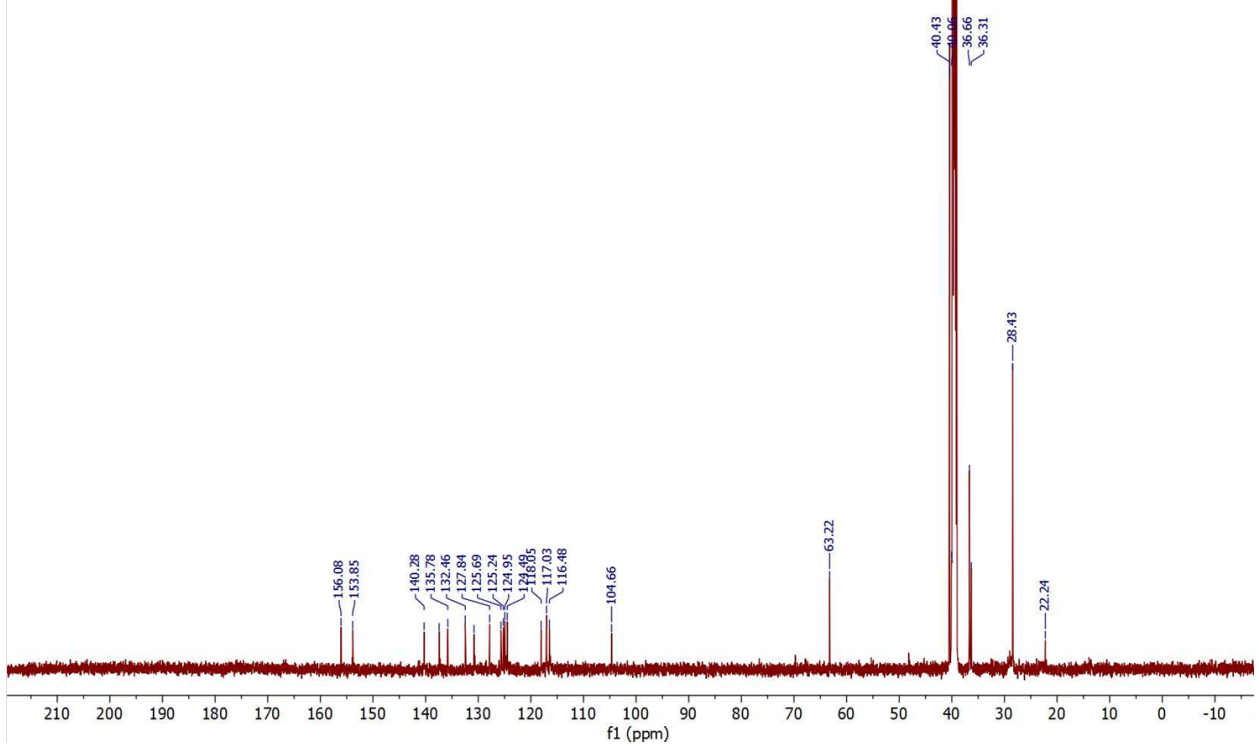
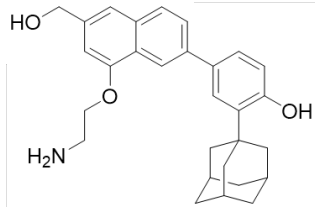


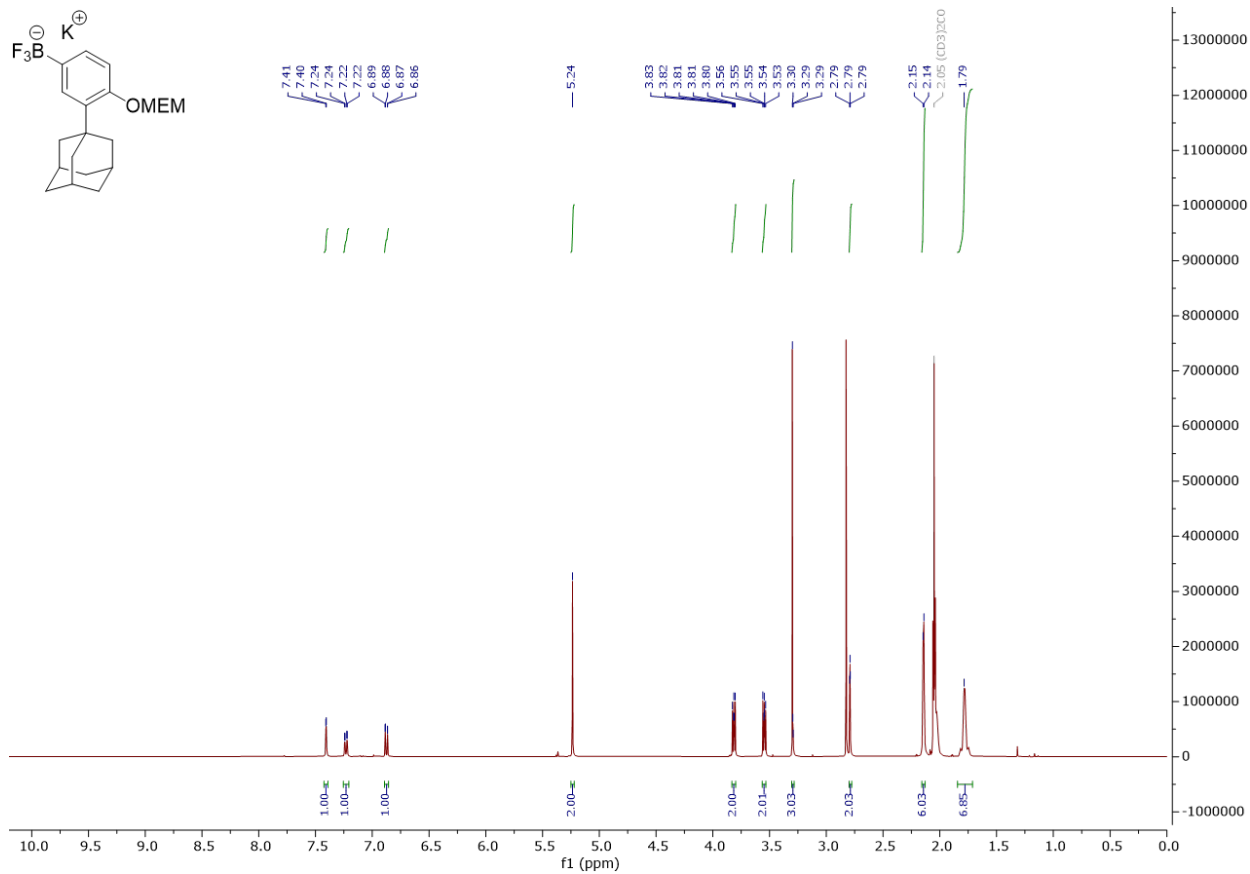
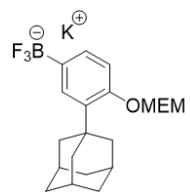


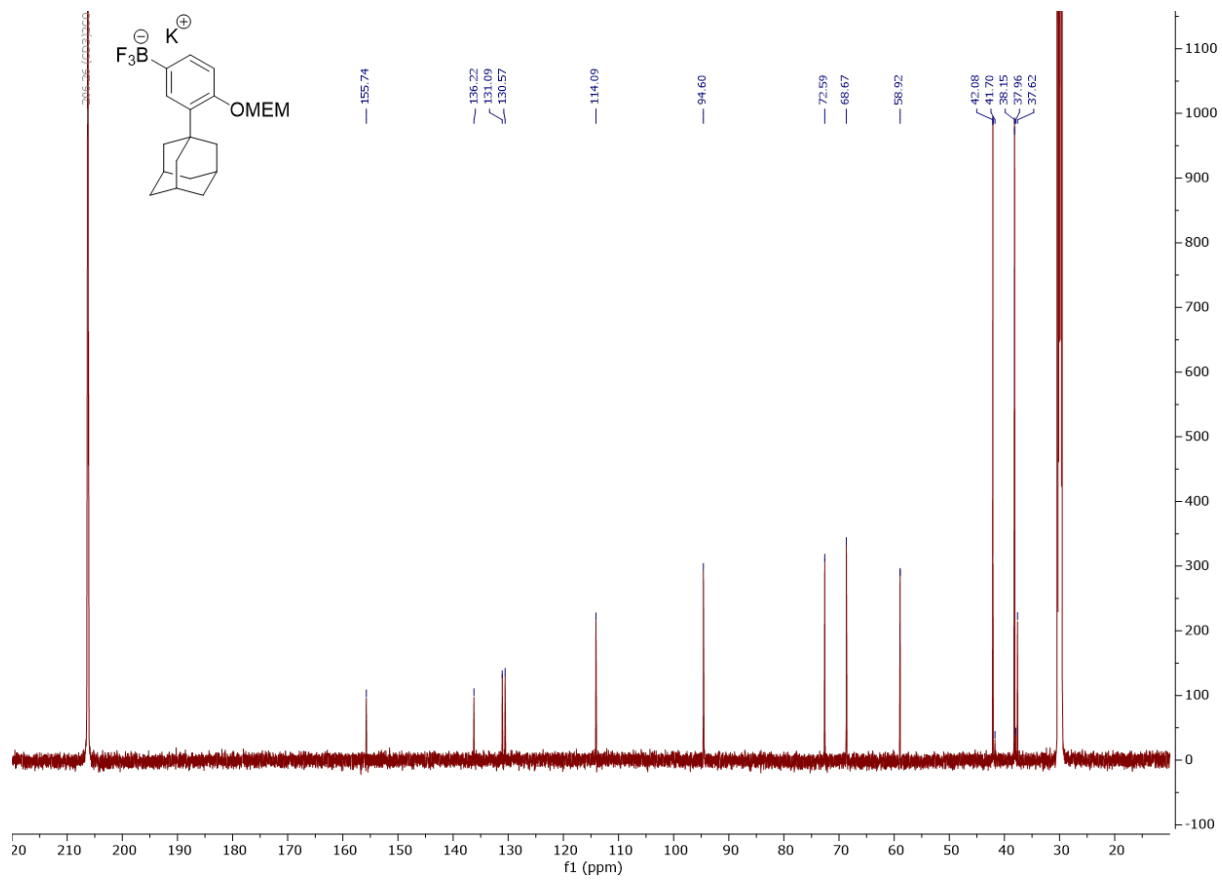


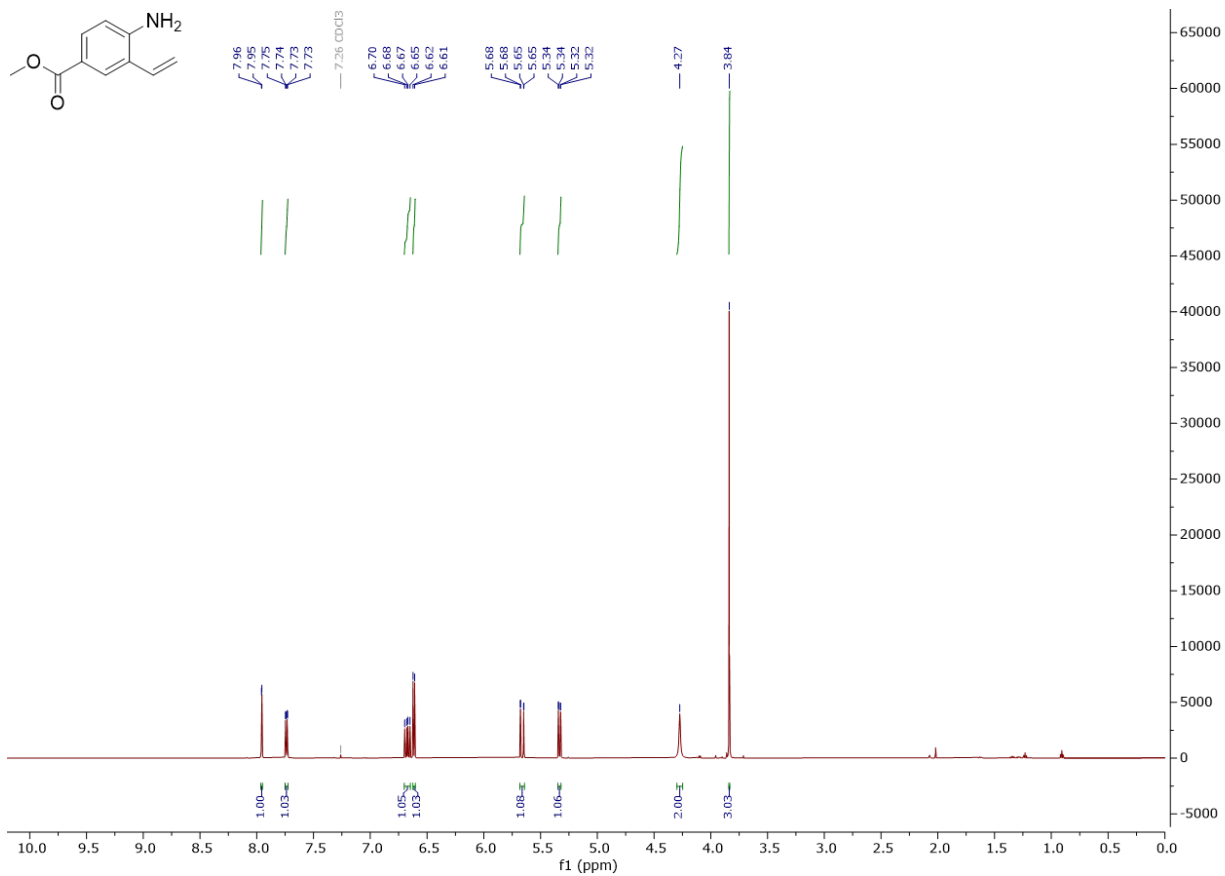


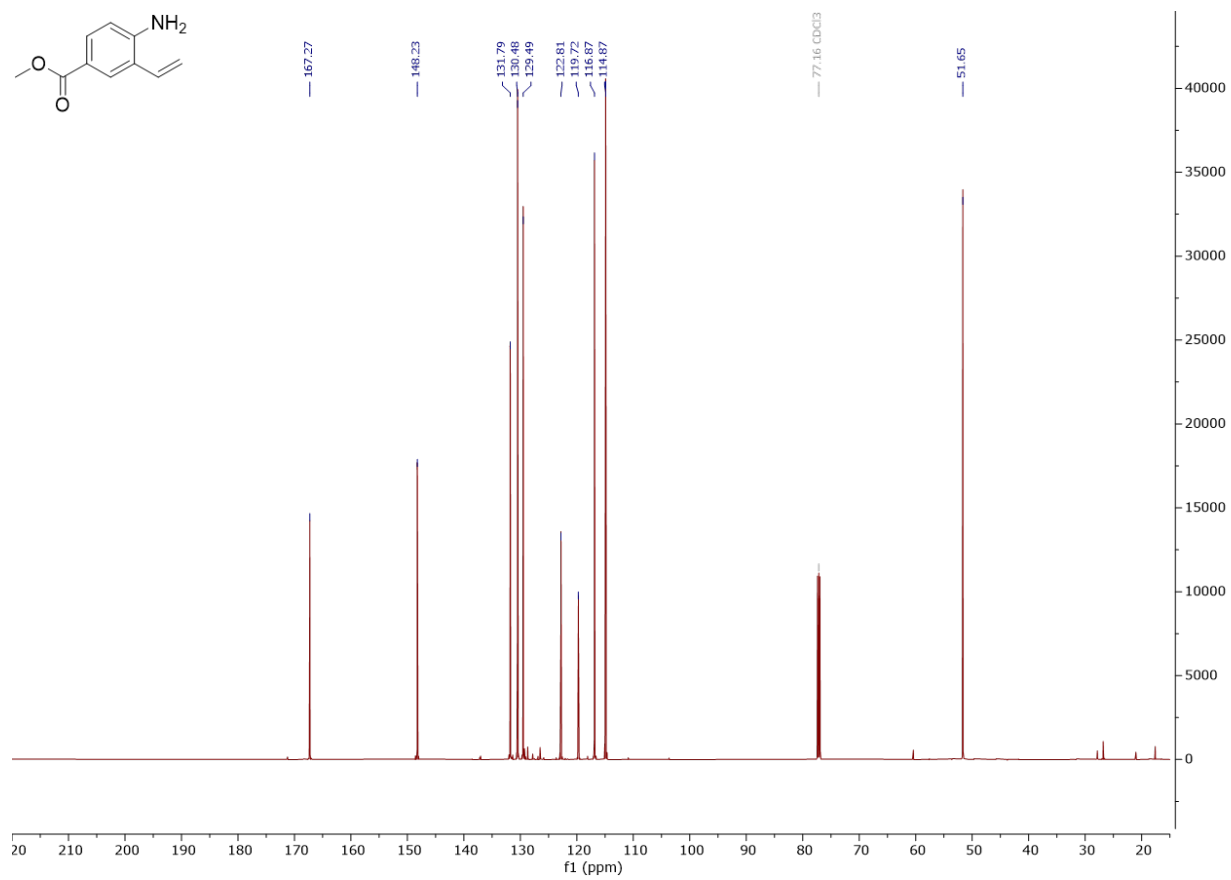
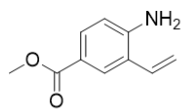


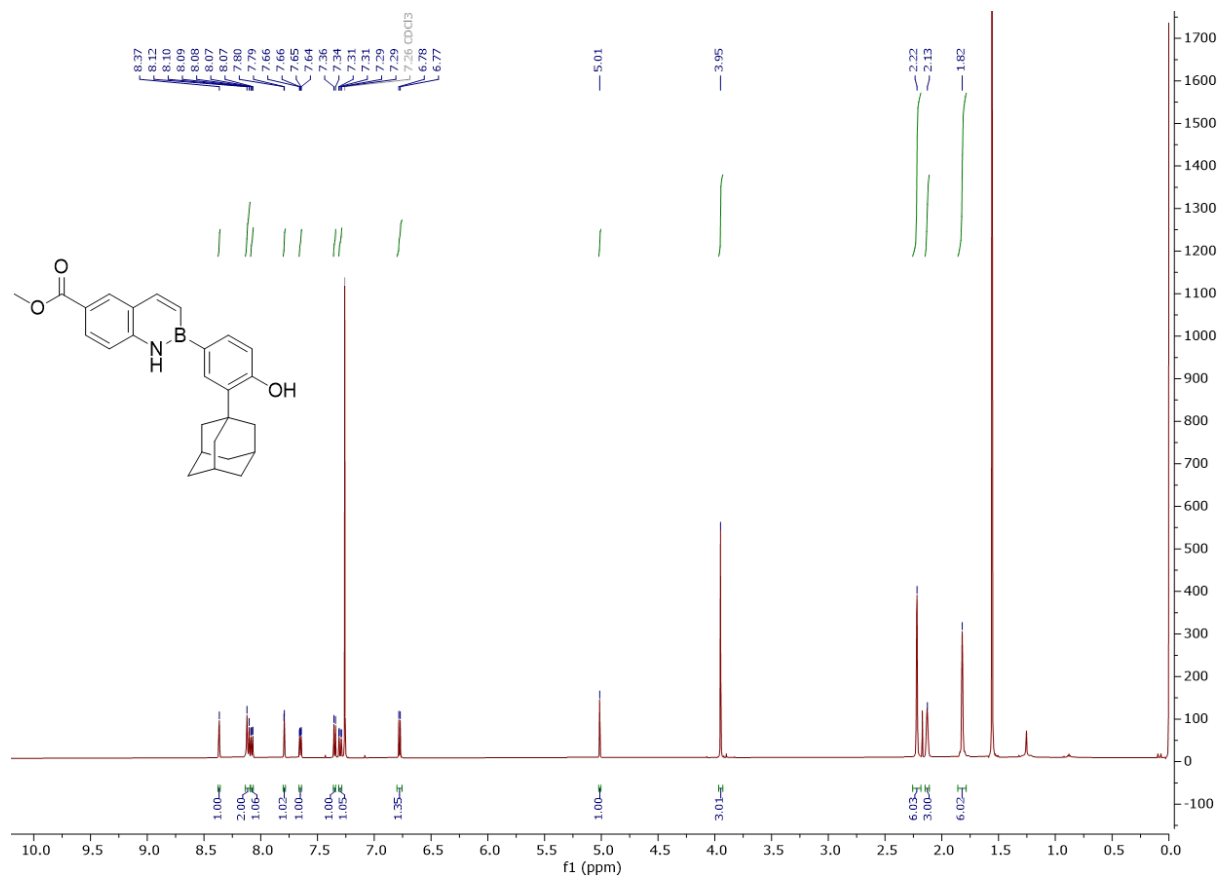


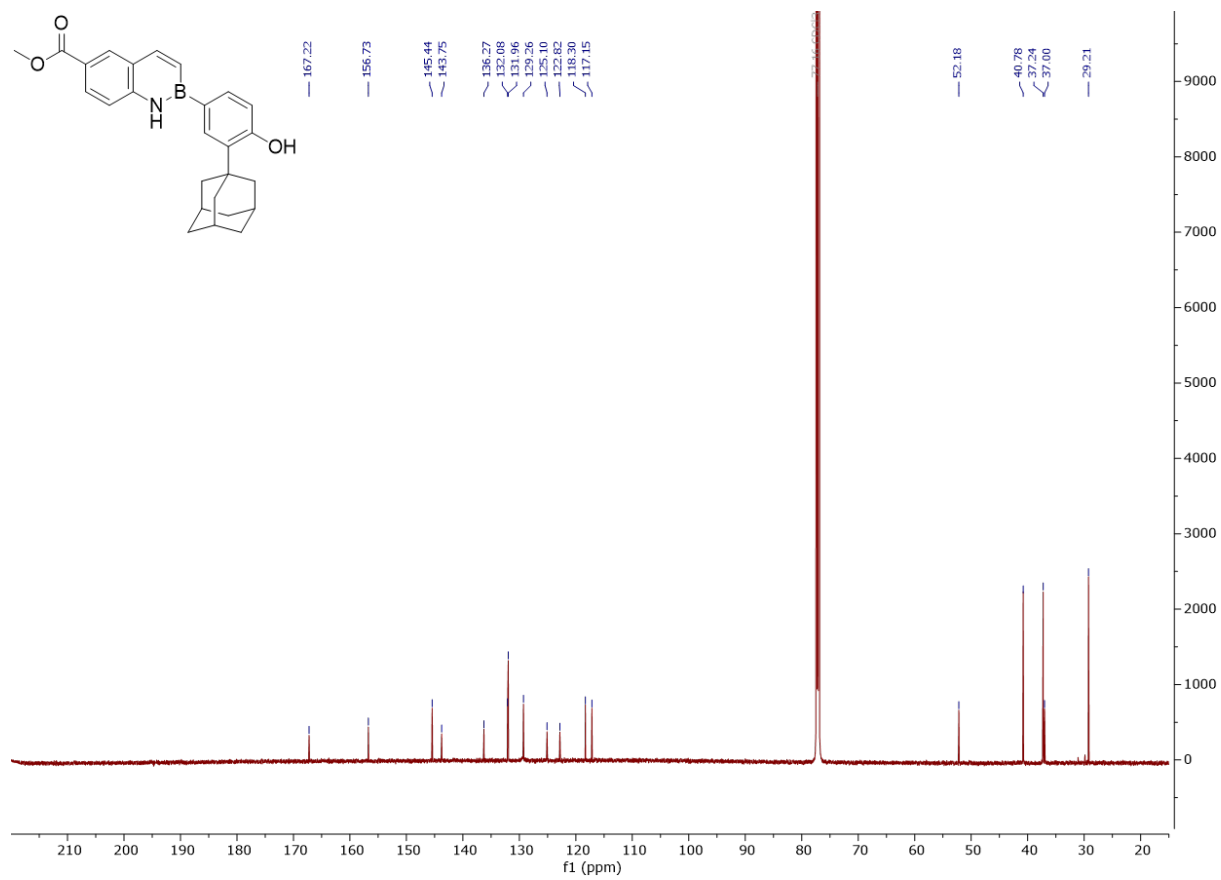


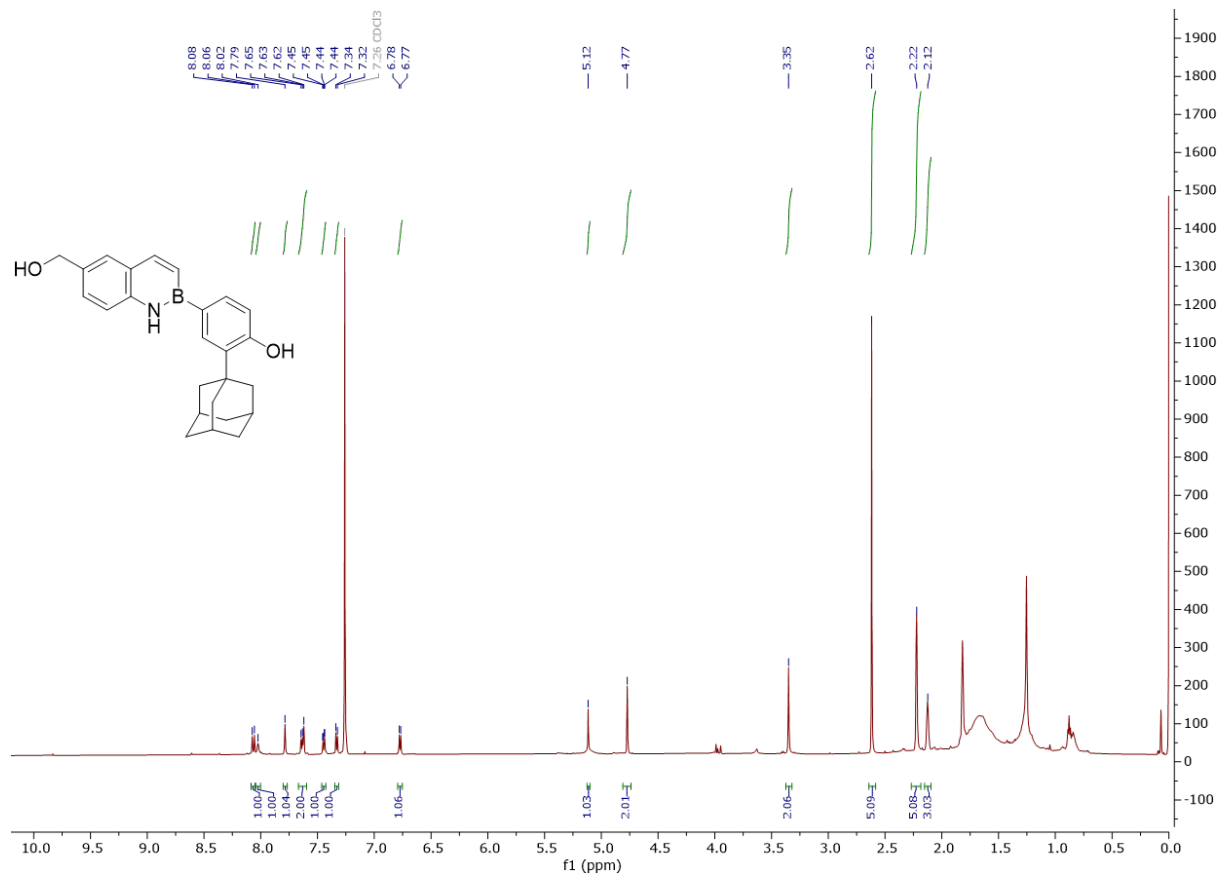


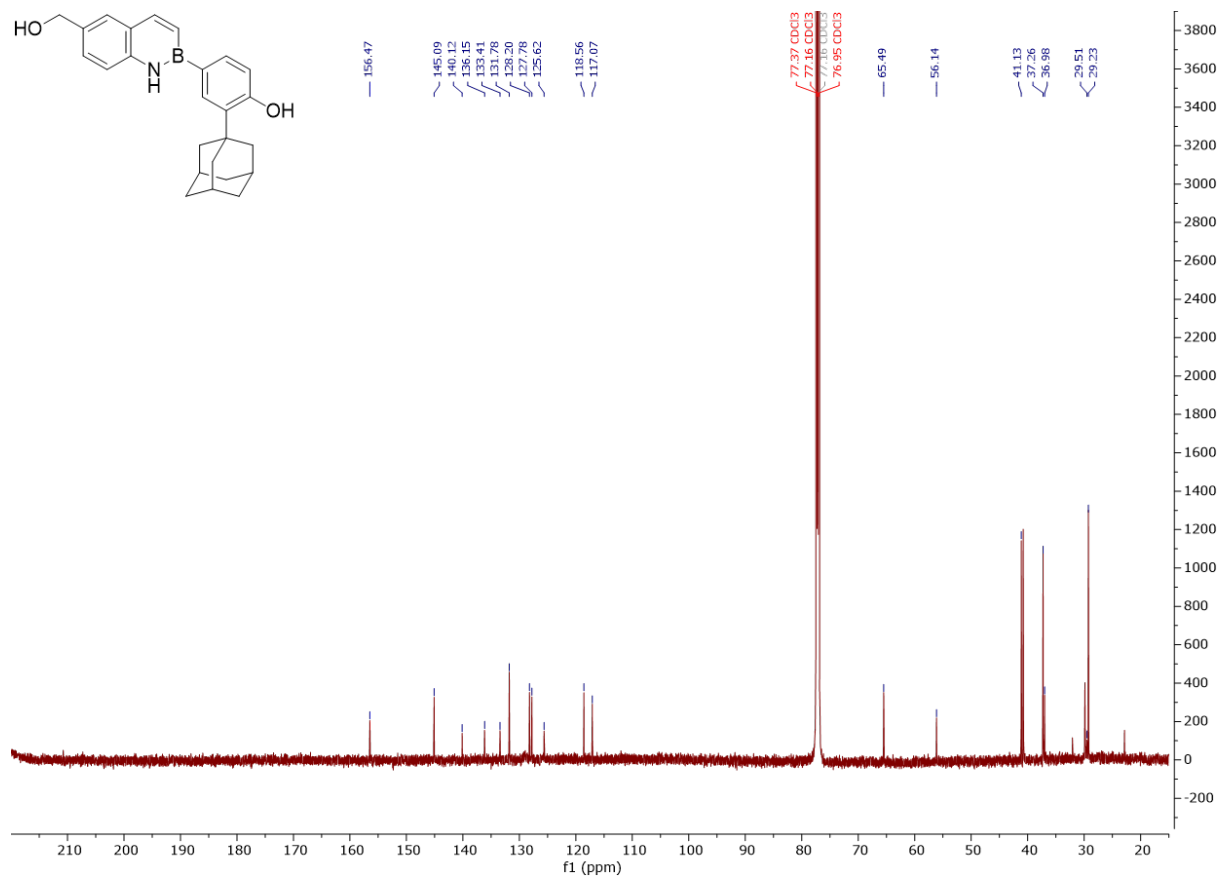
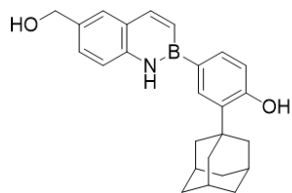




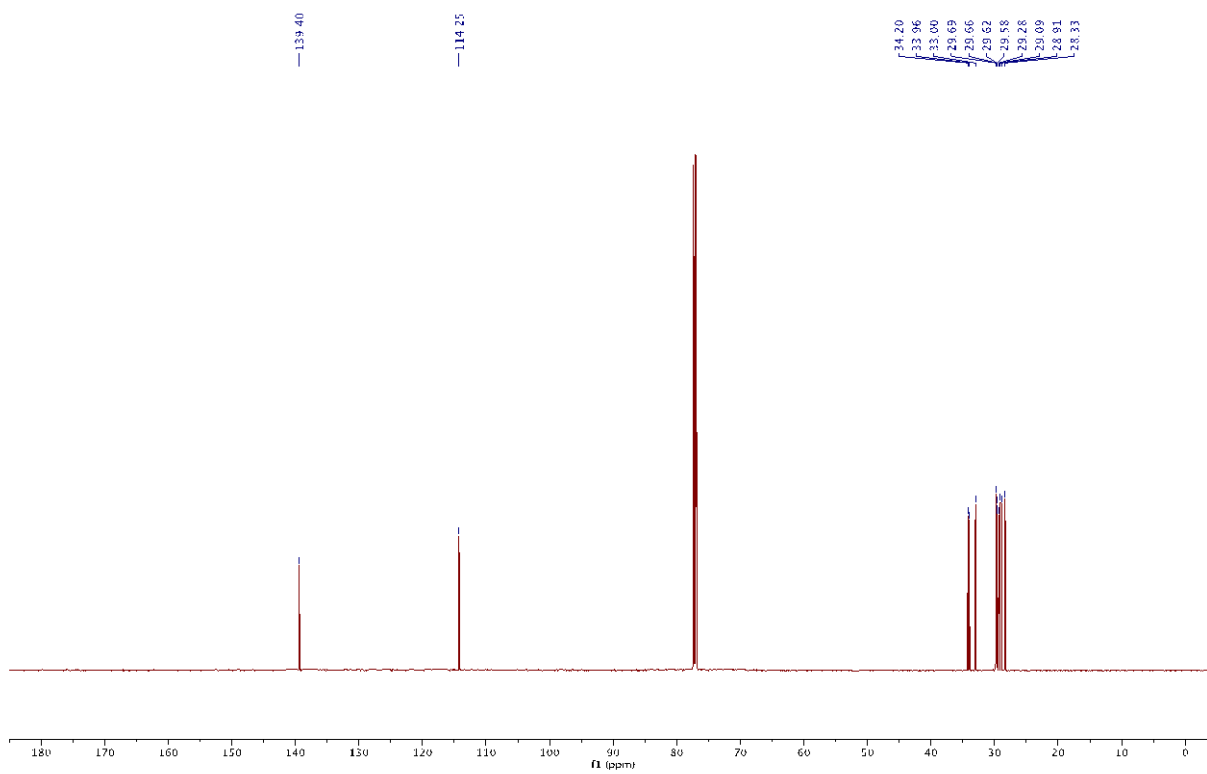
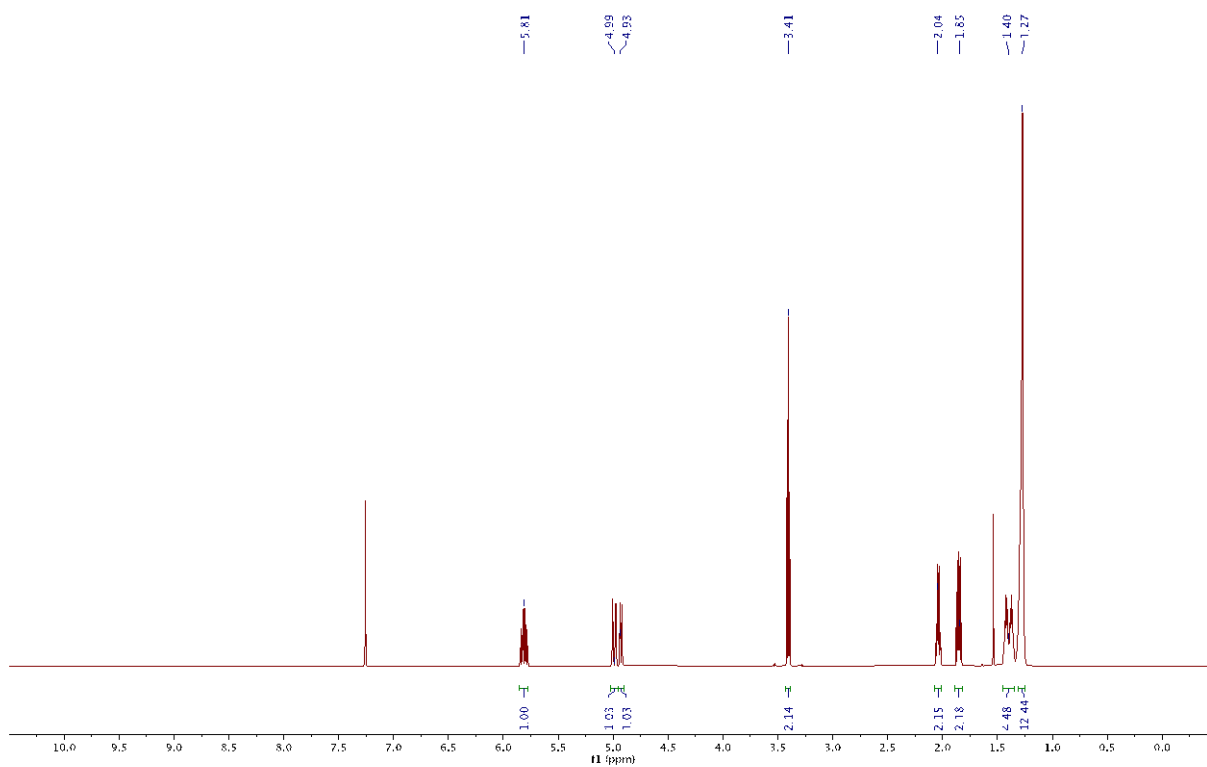
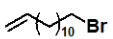


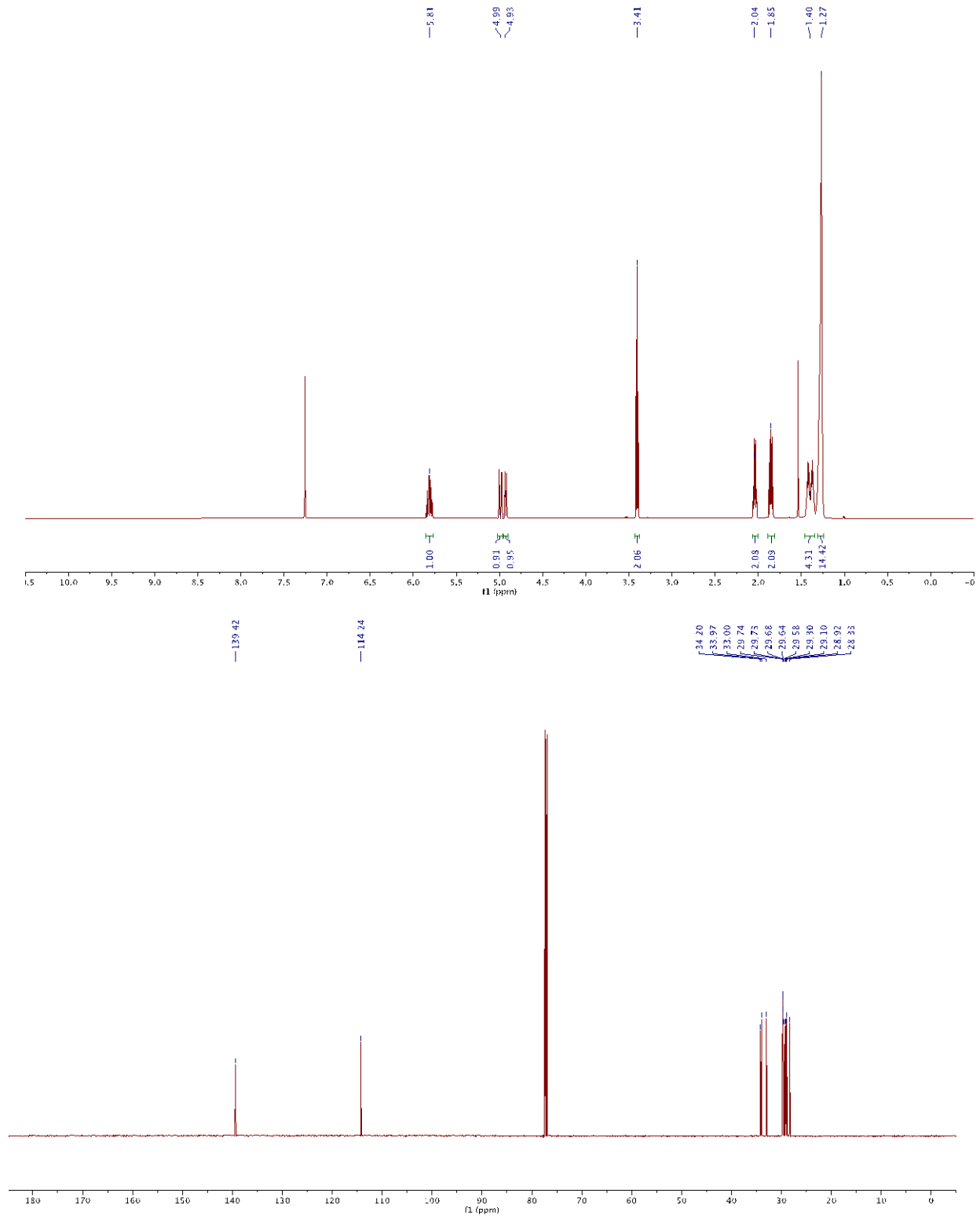
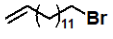


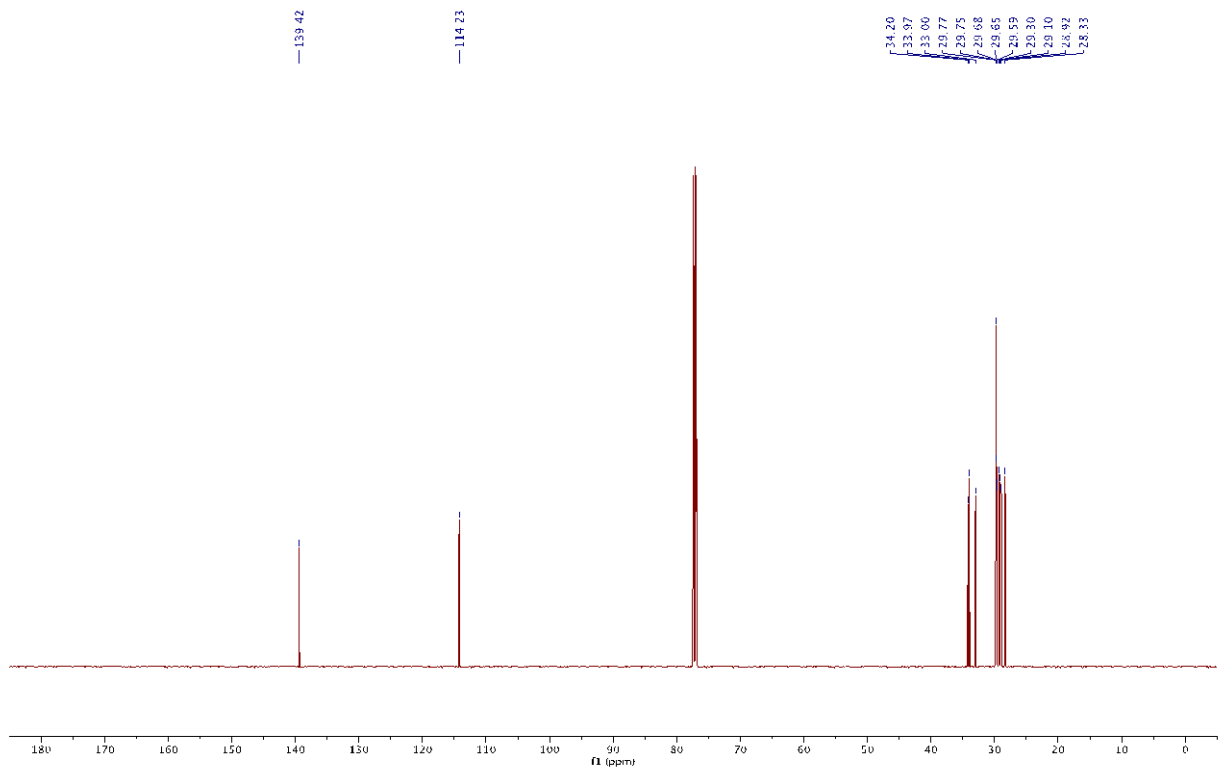
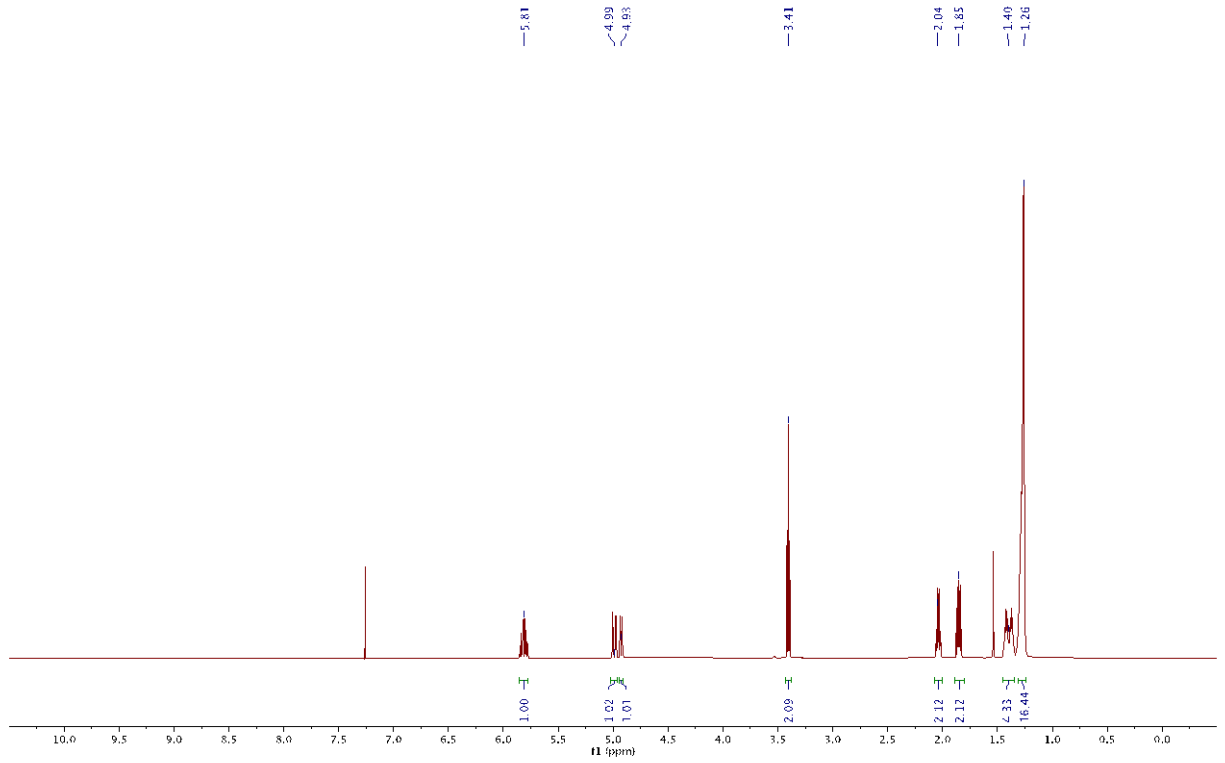
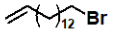


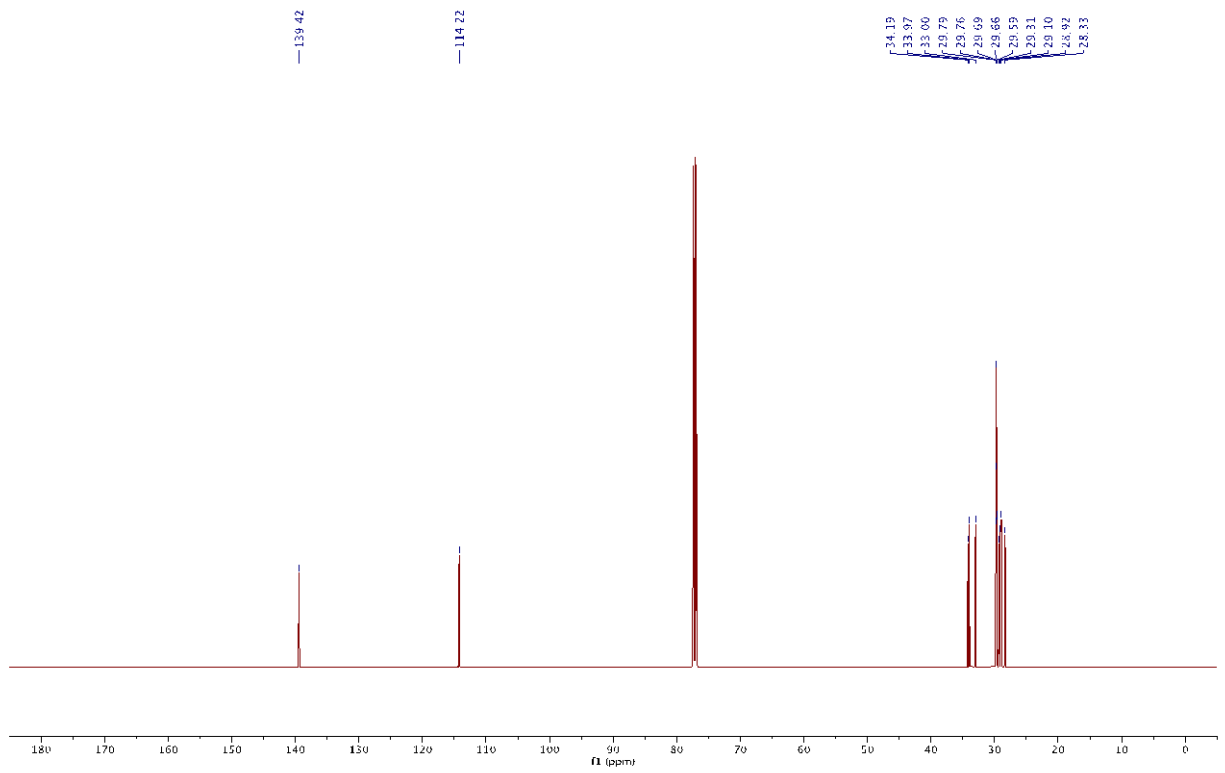
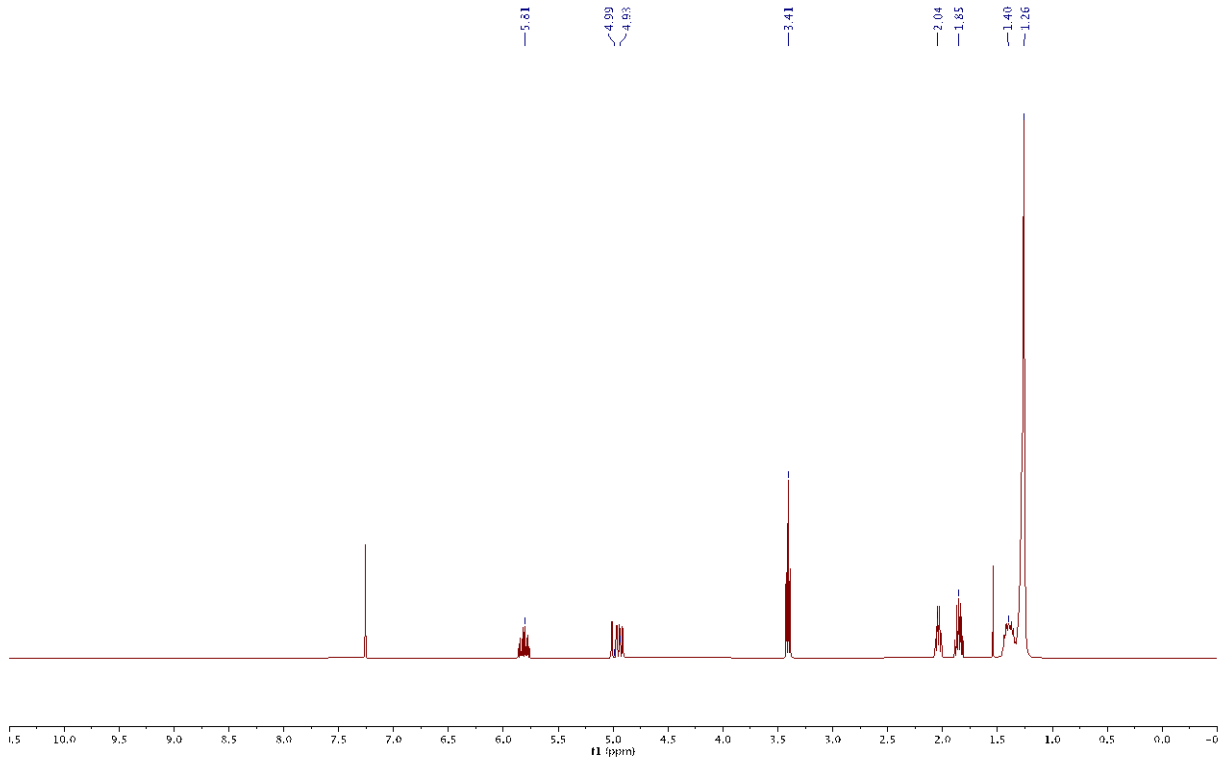
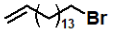


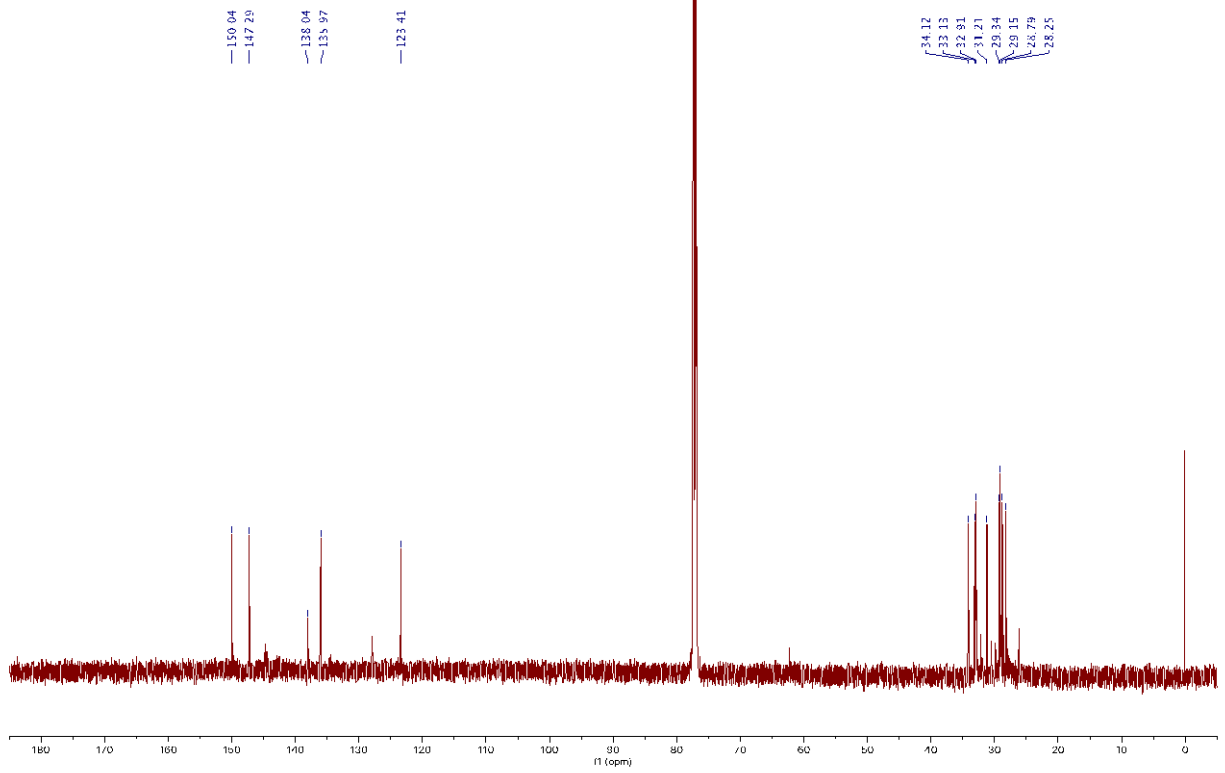
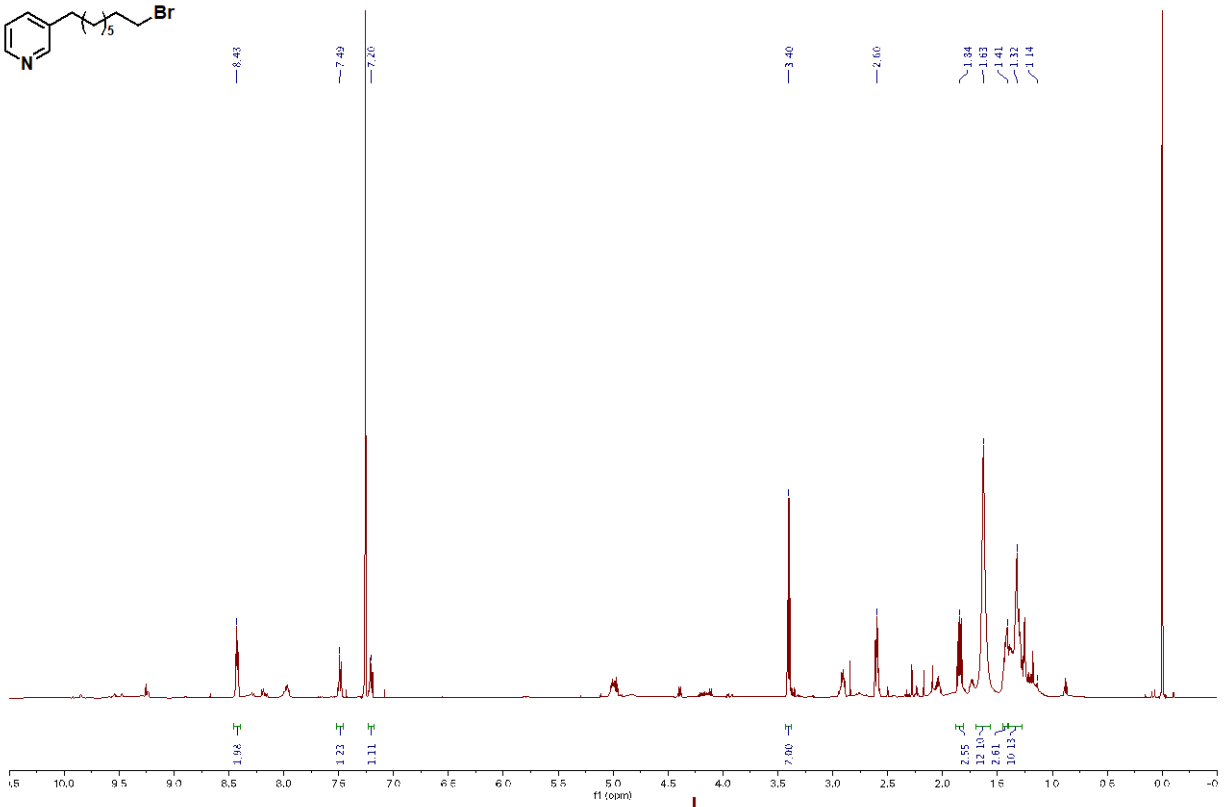
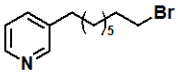
Appendix. Chapter 3

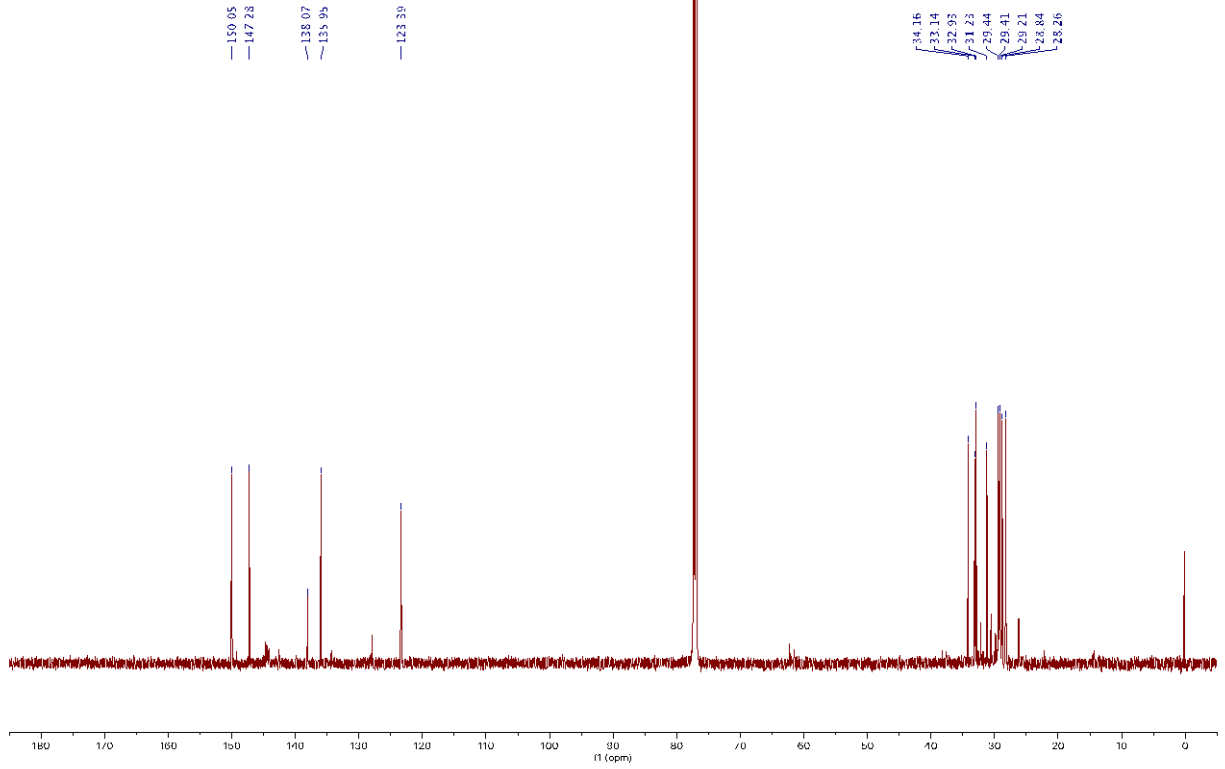
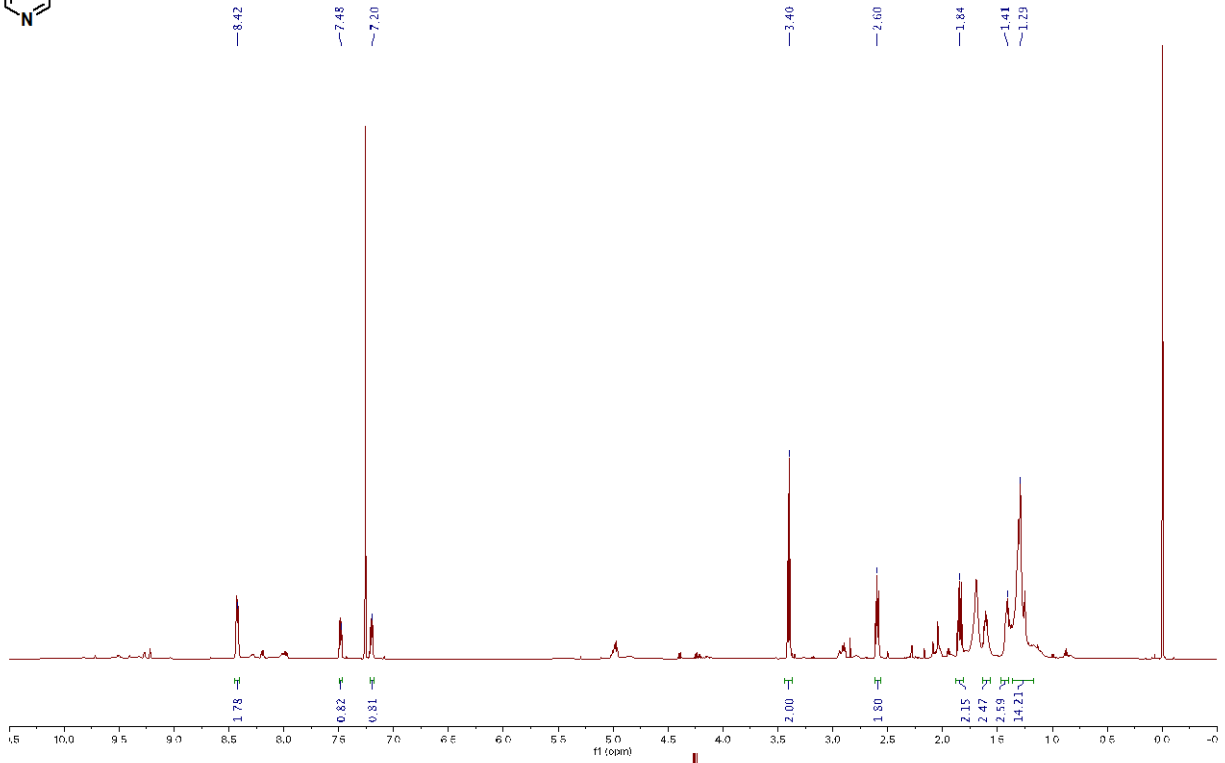
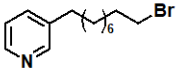


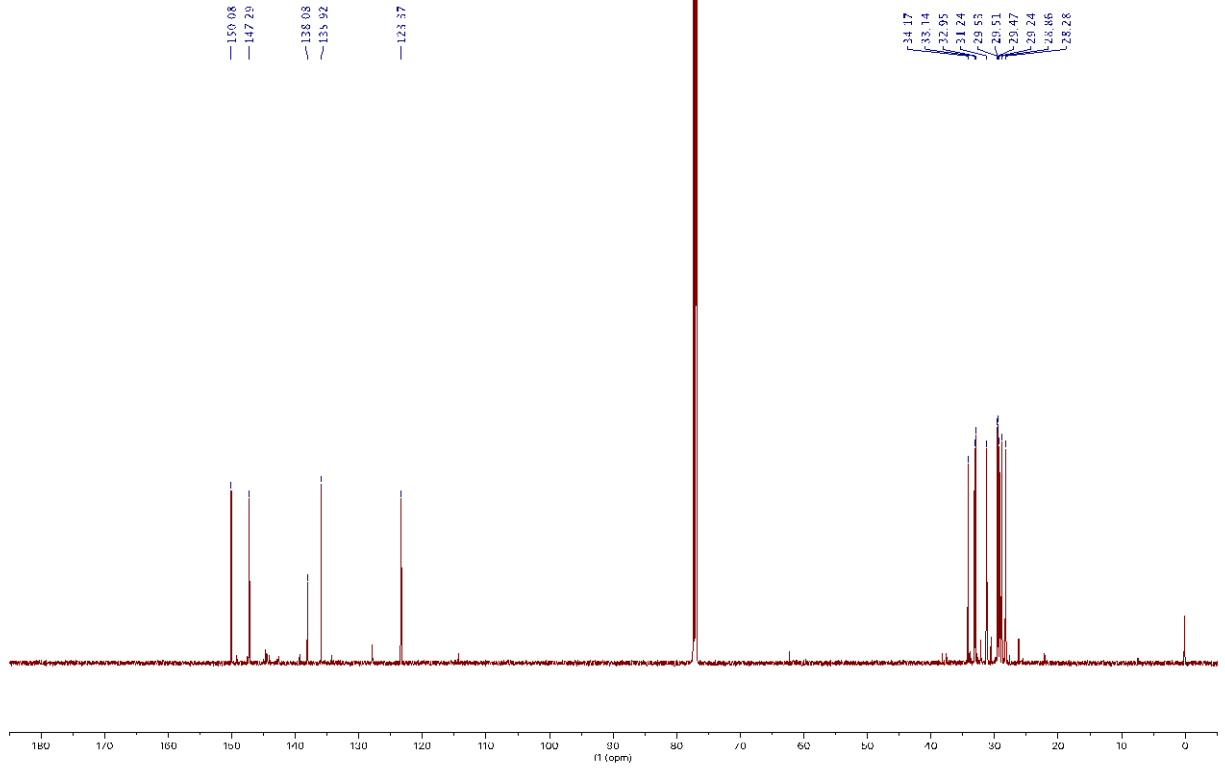
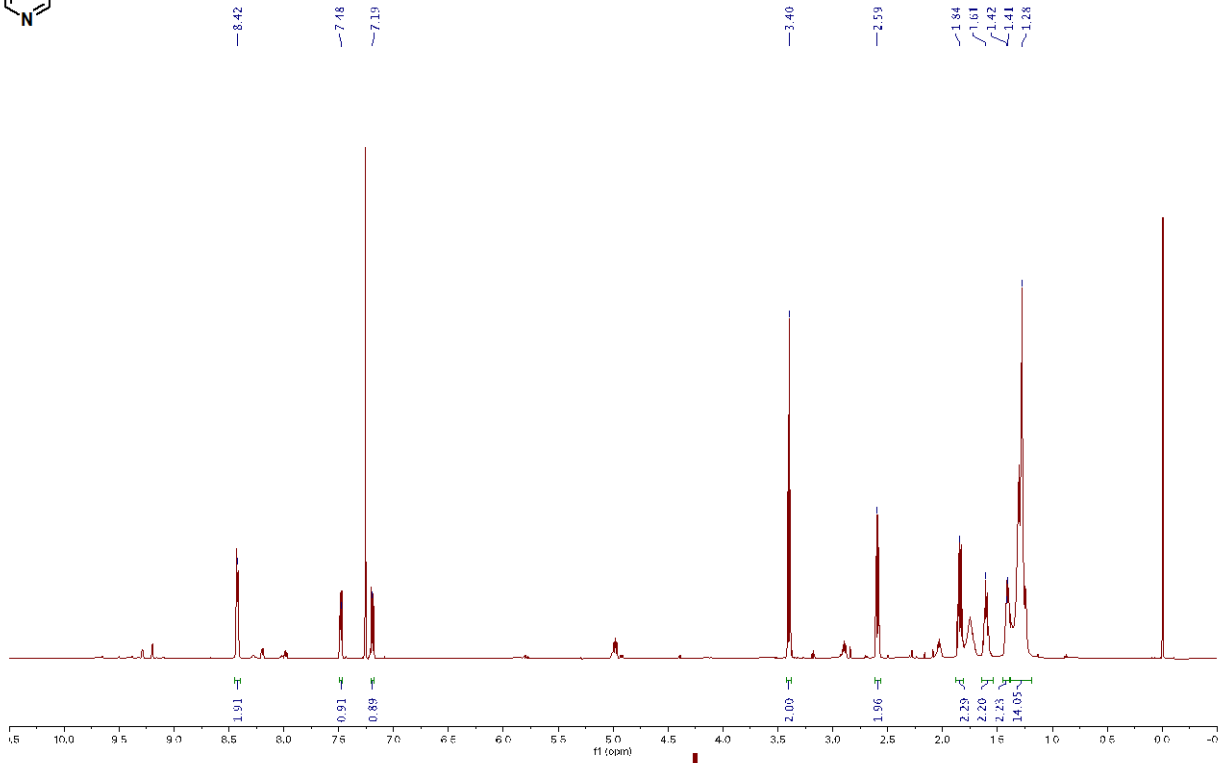
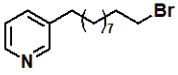


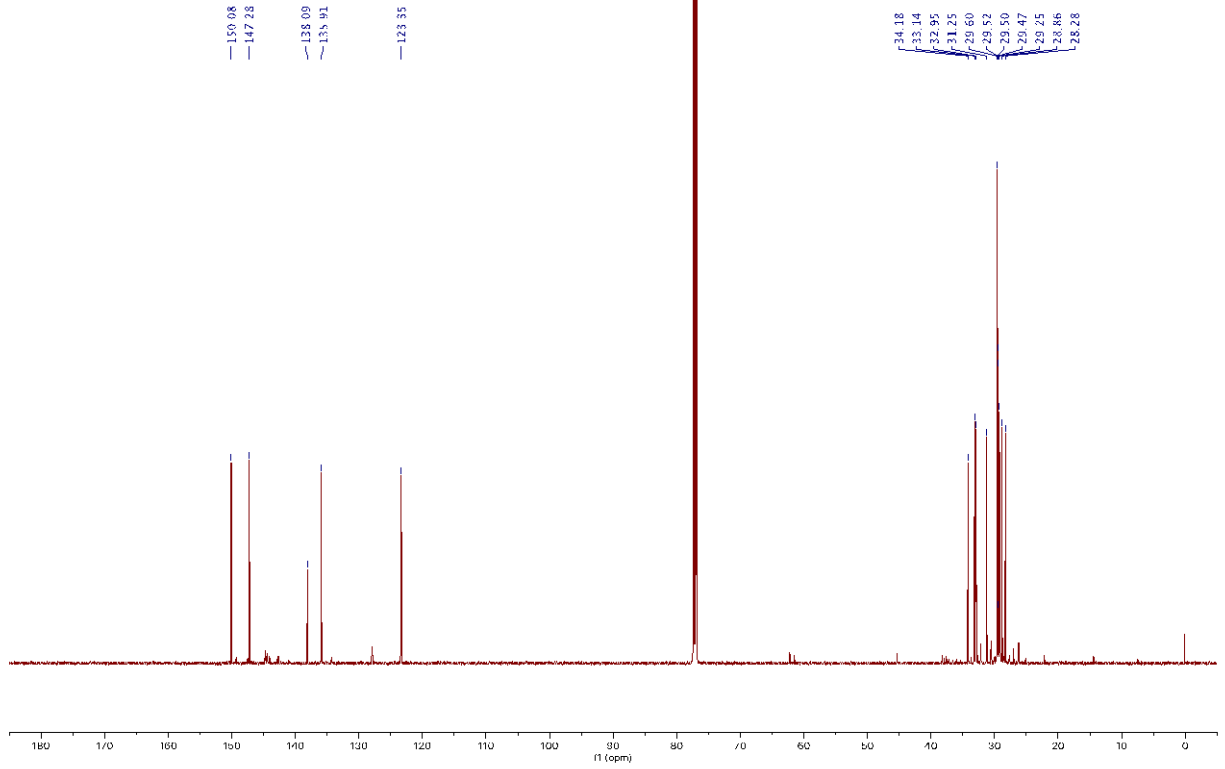
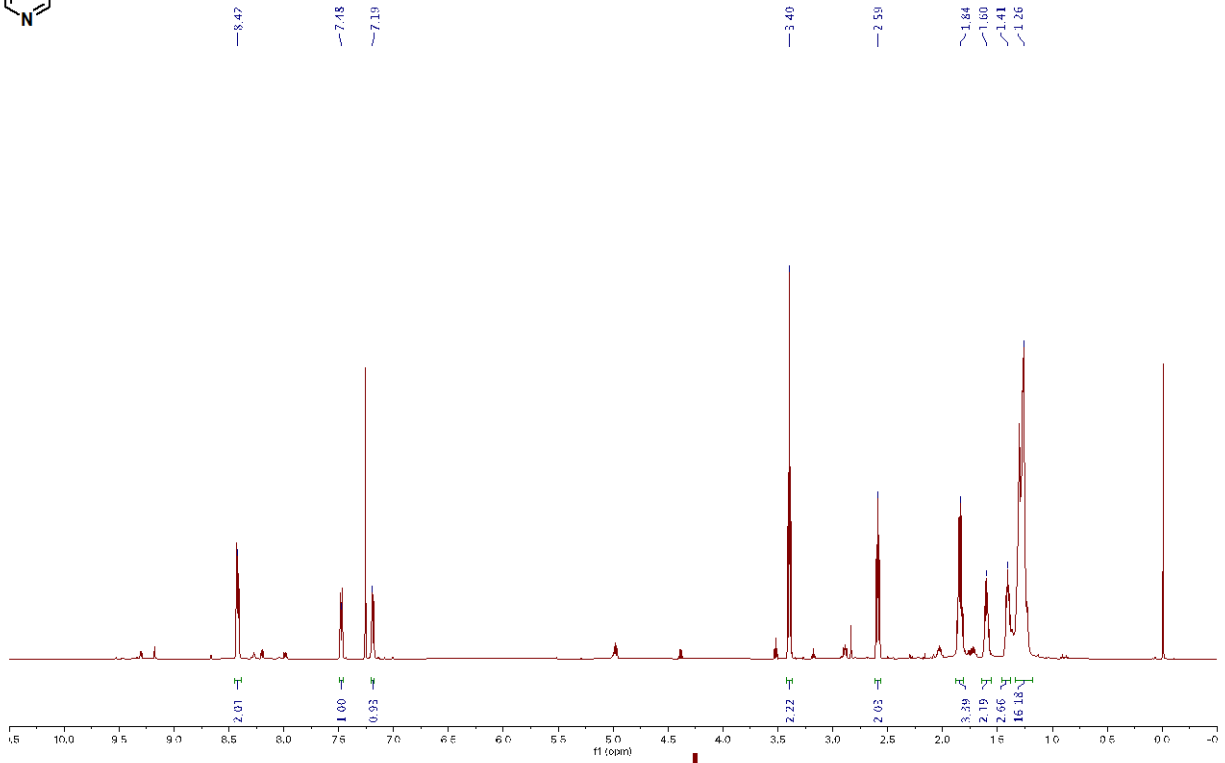
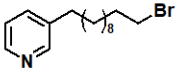


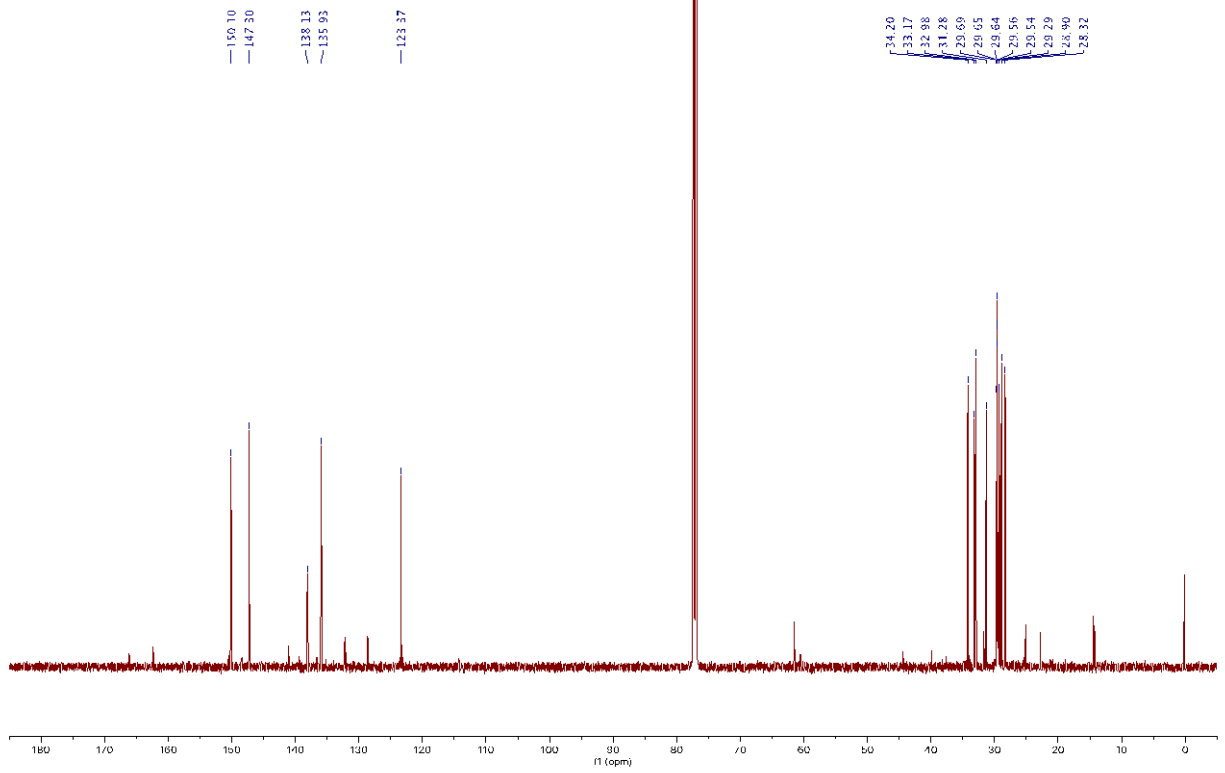
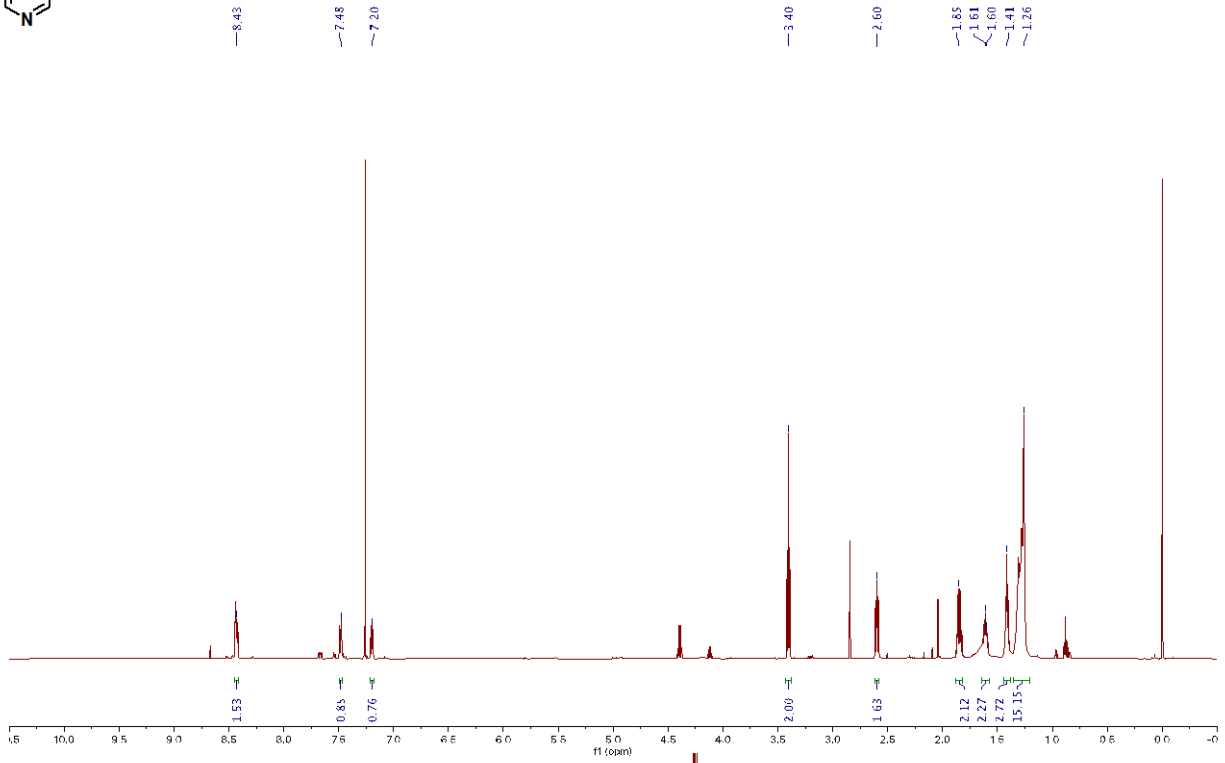
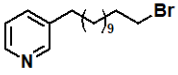


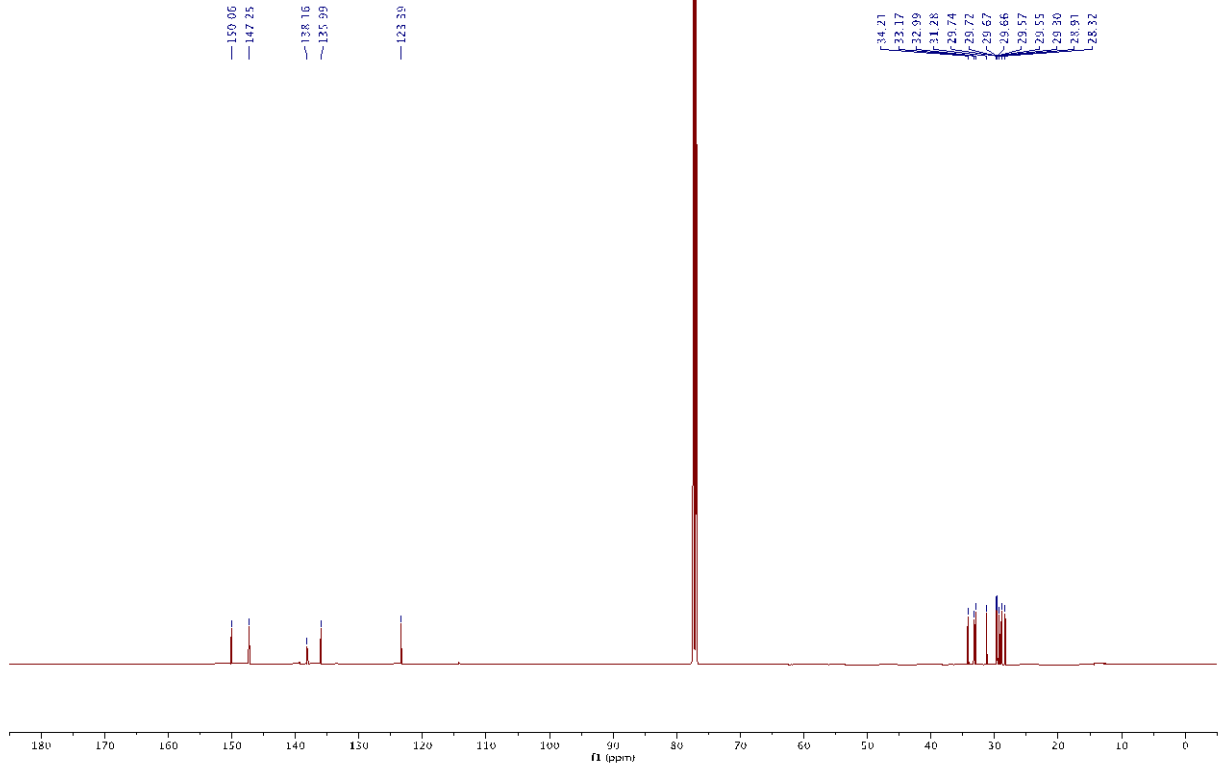
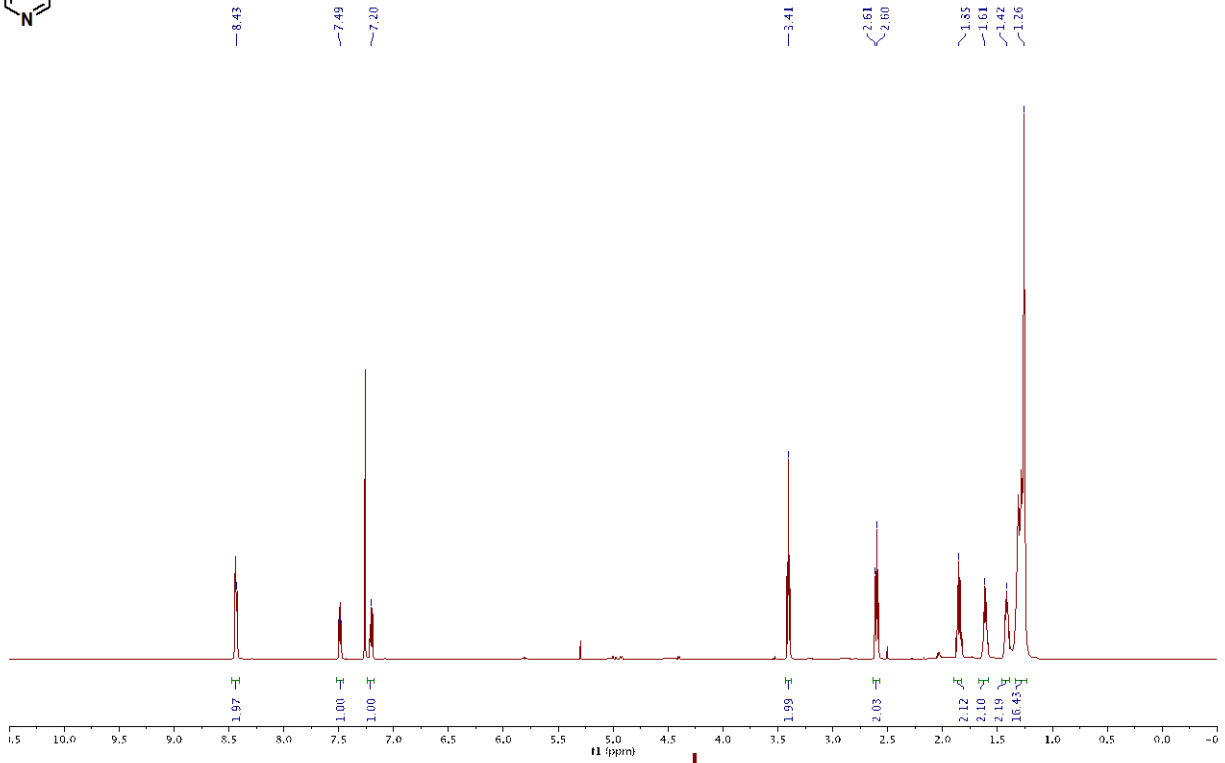
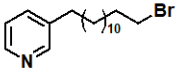


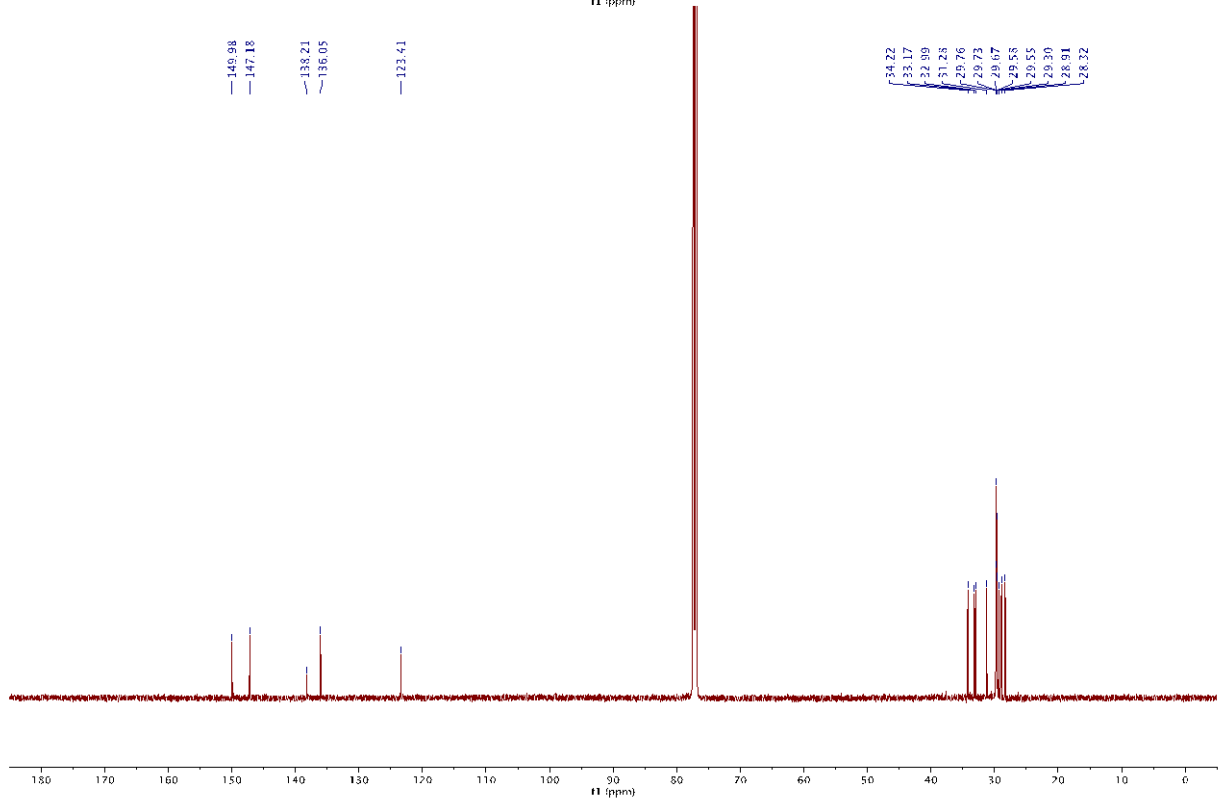
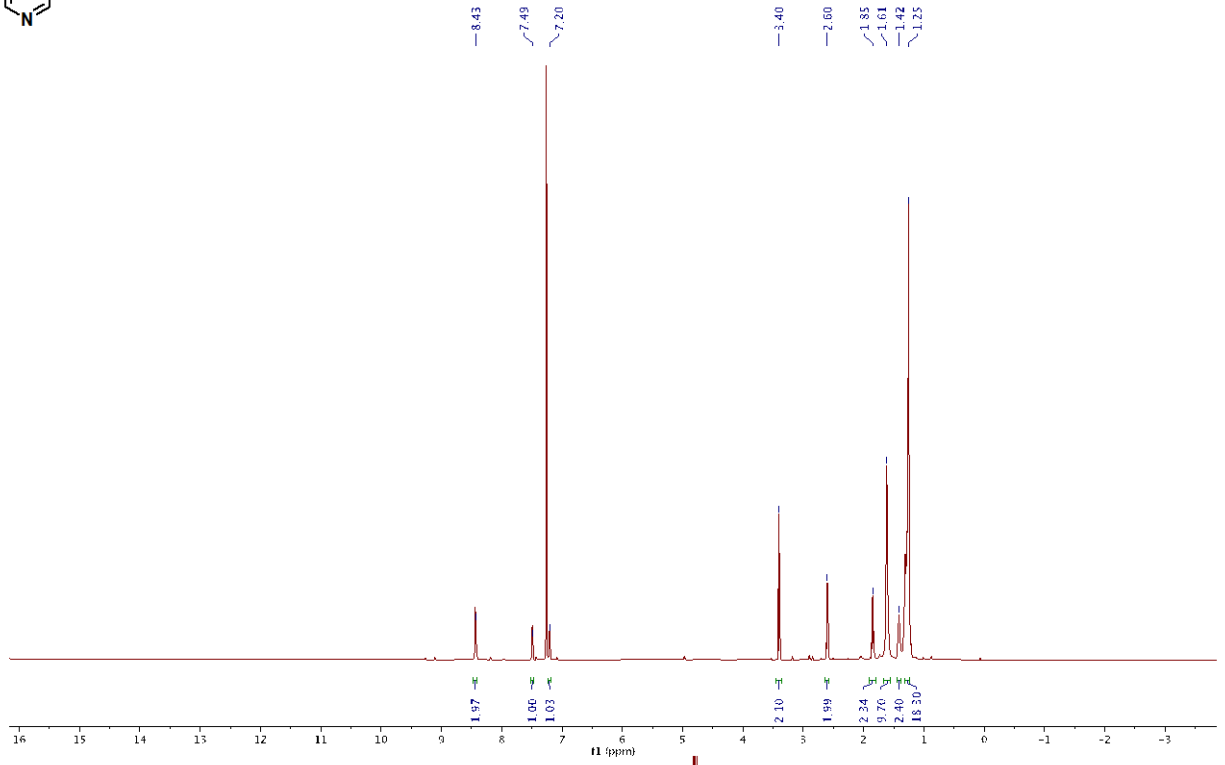
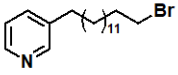


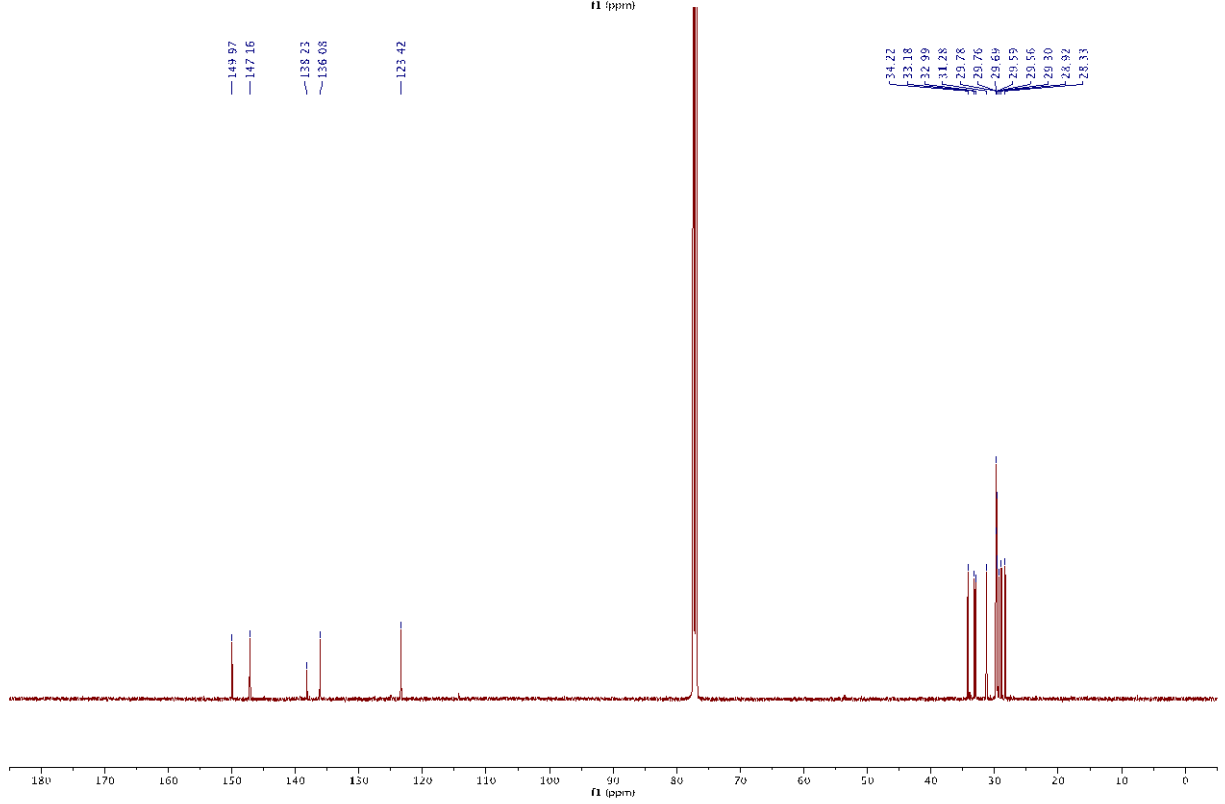
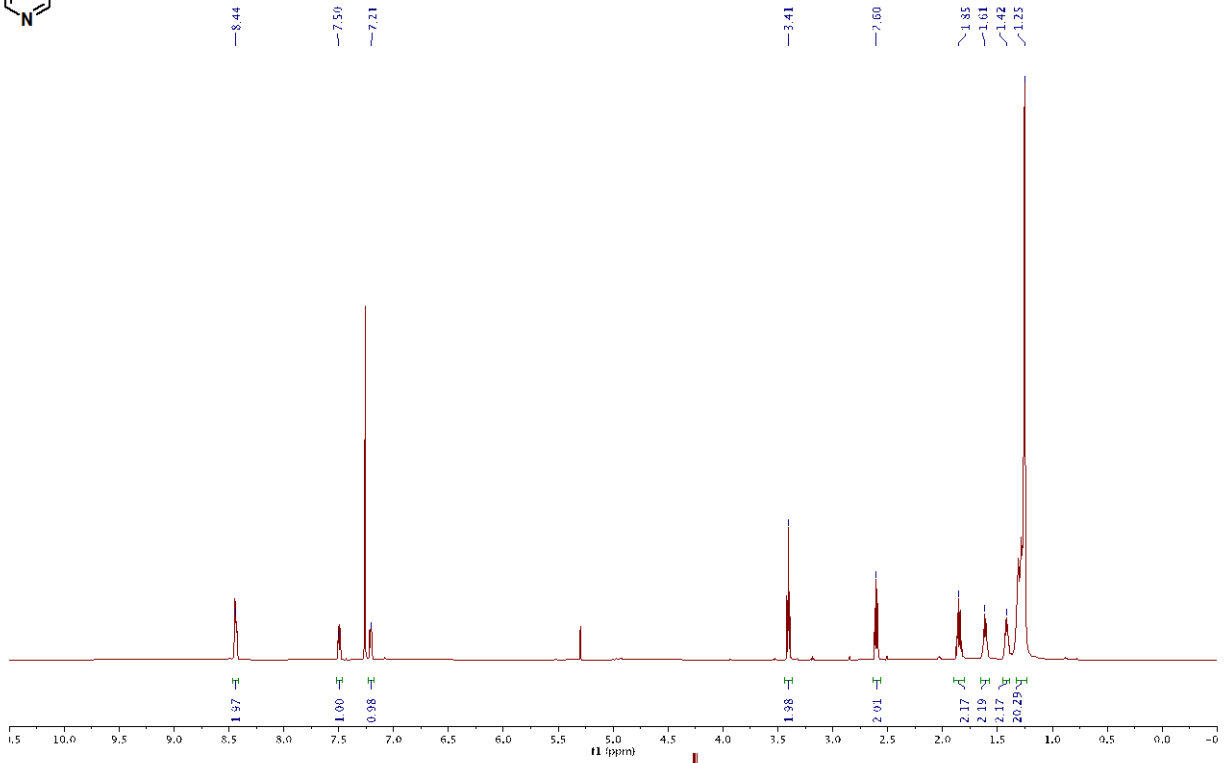
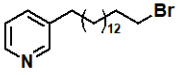


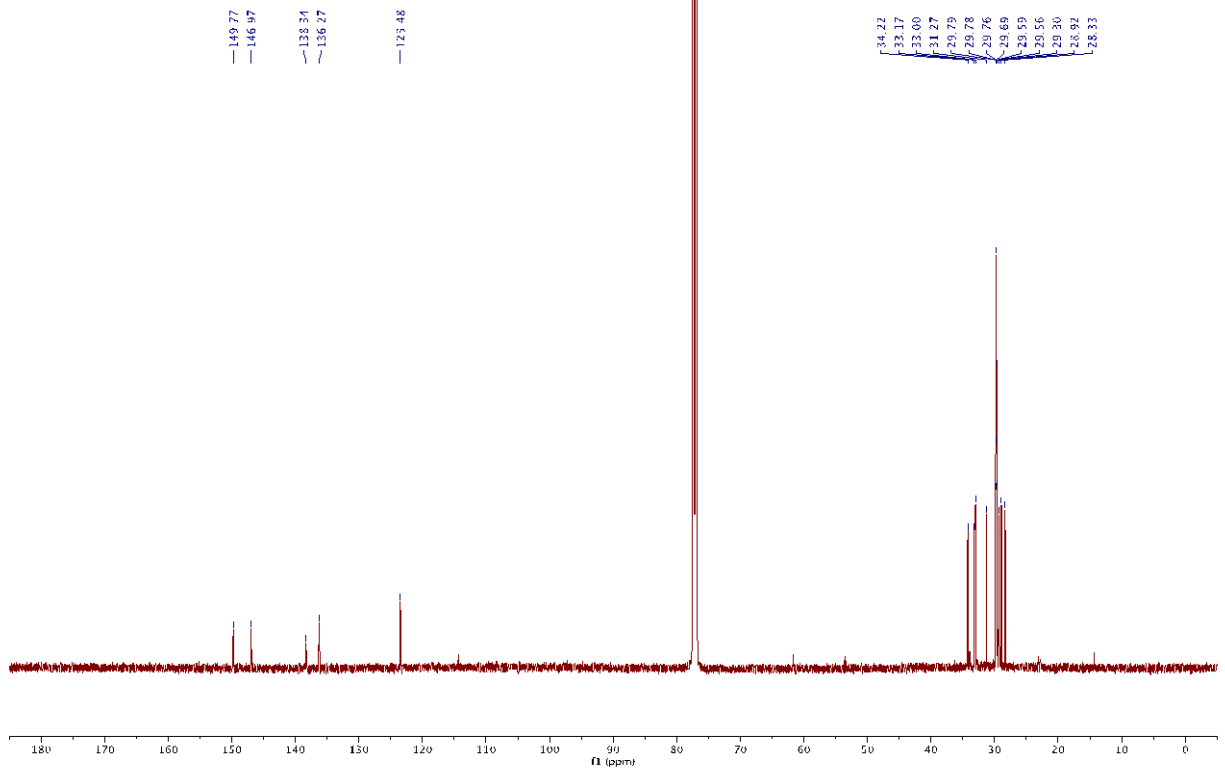
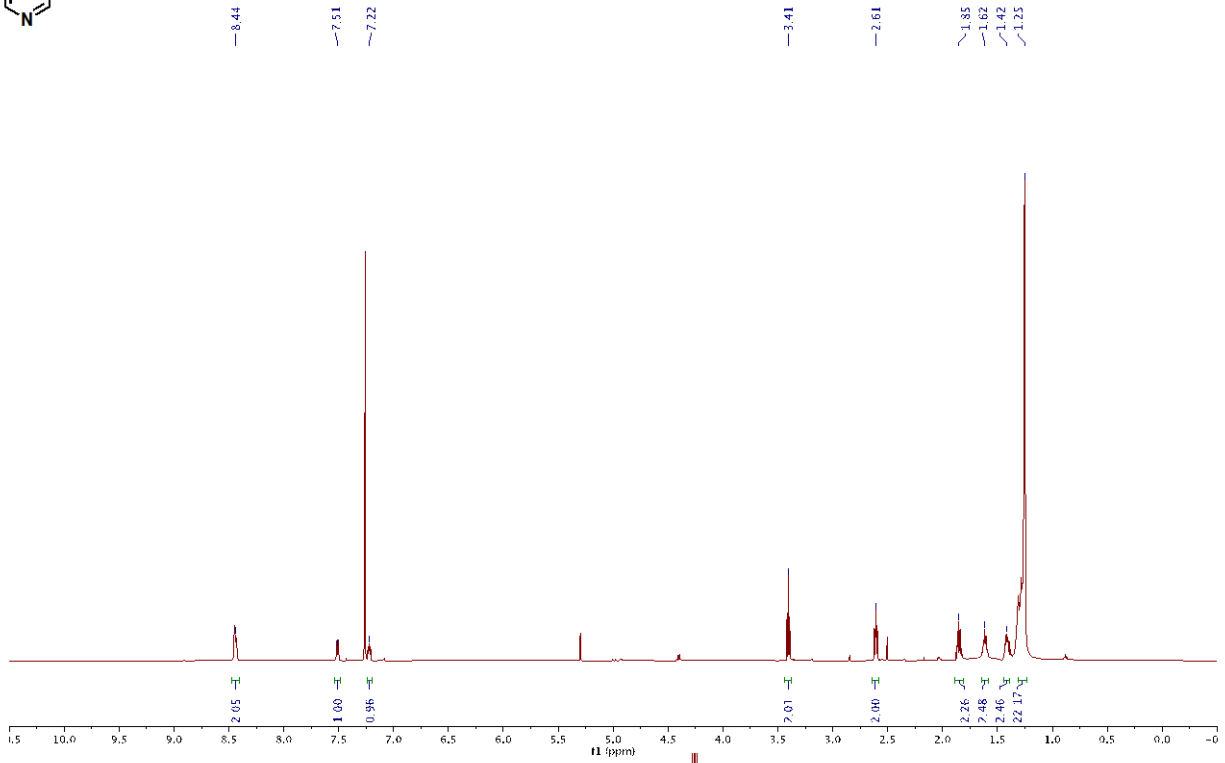
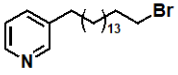


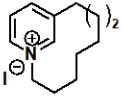




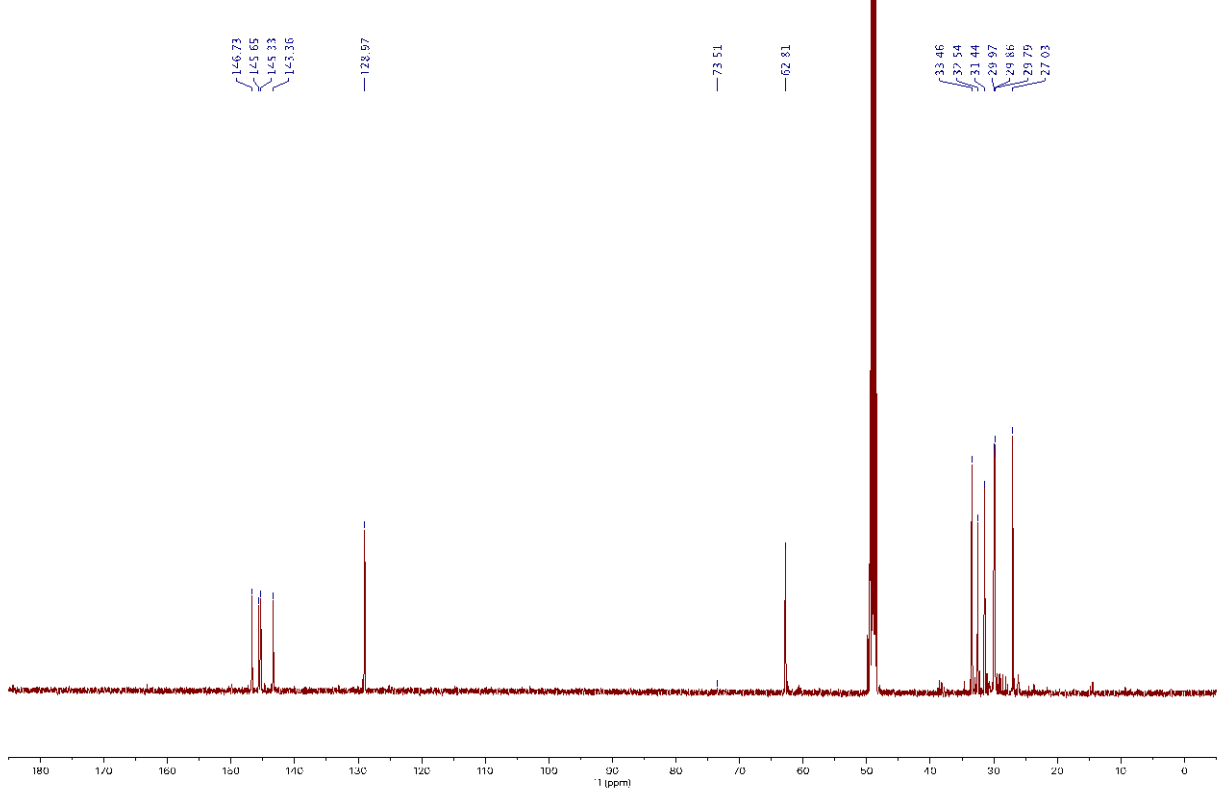
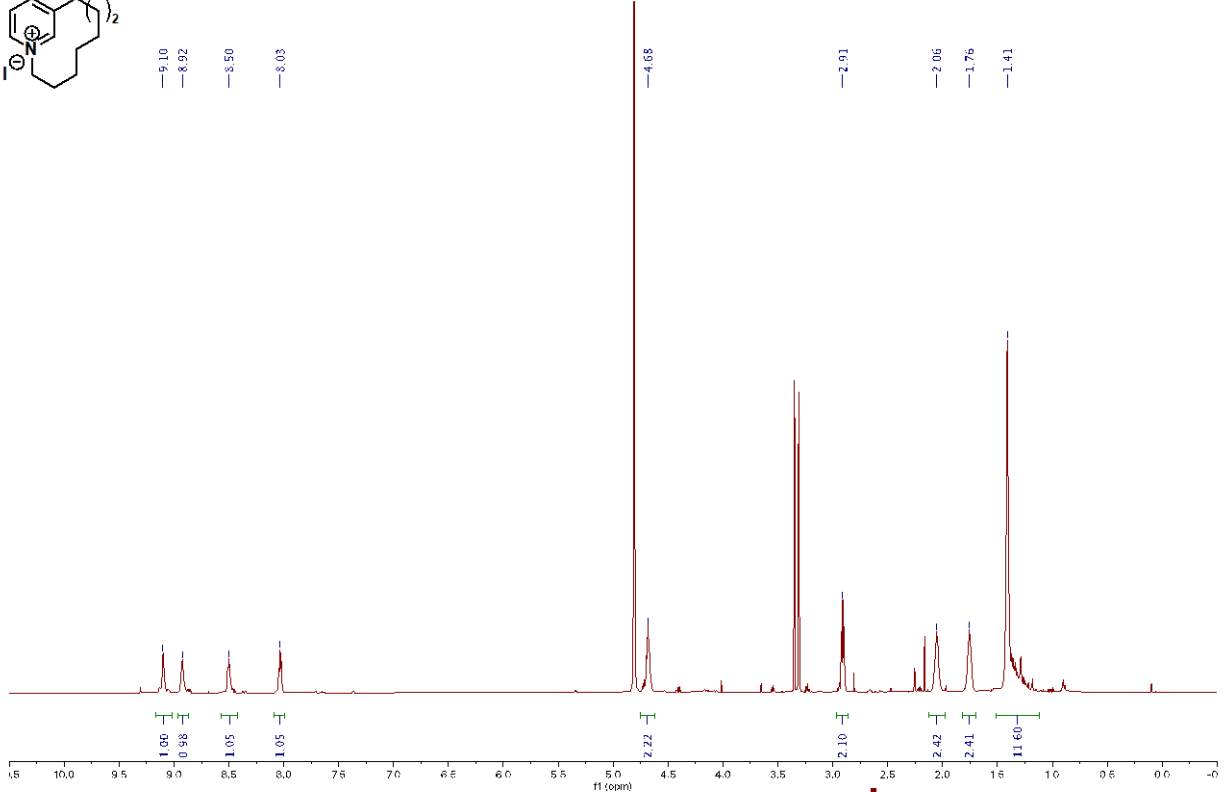


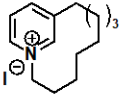




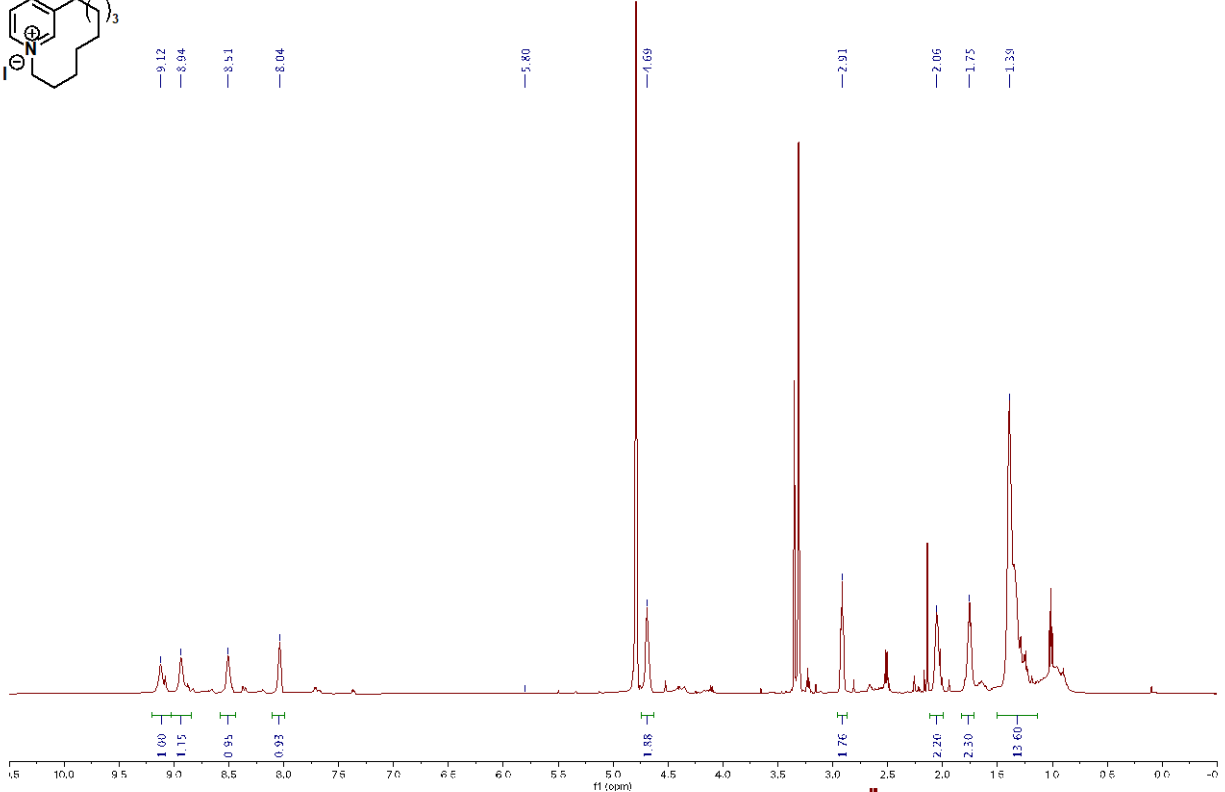


- 9.10
- 8.92
- 8.50
- 8.03





- 9.12
- 8.94
- 8.51
- 8.04

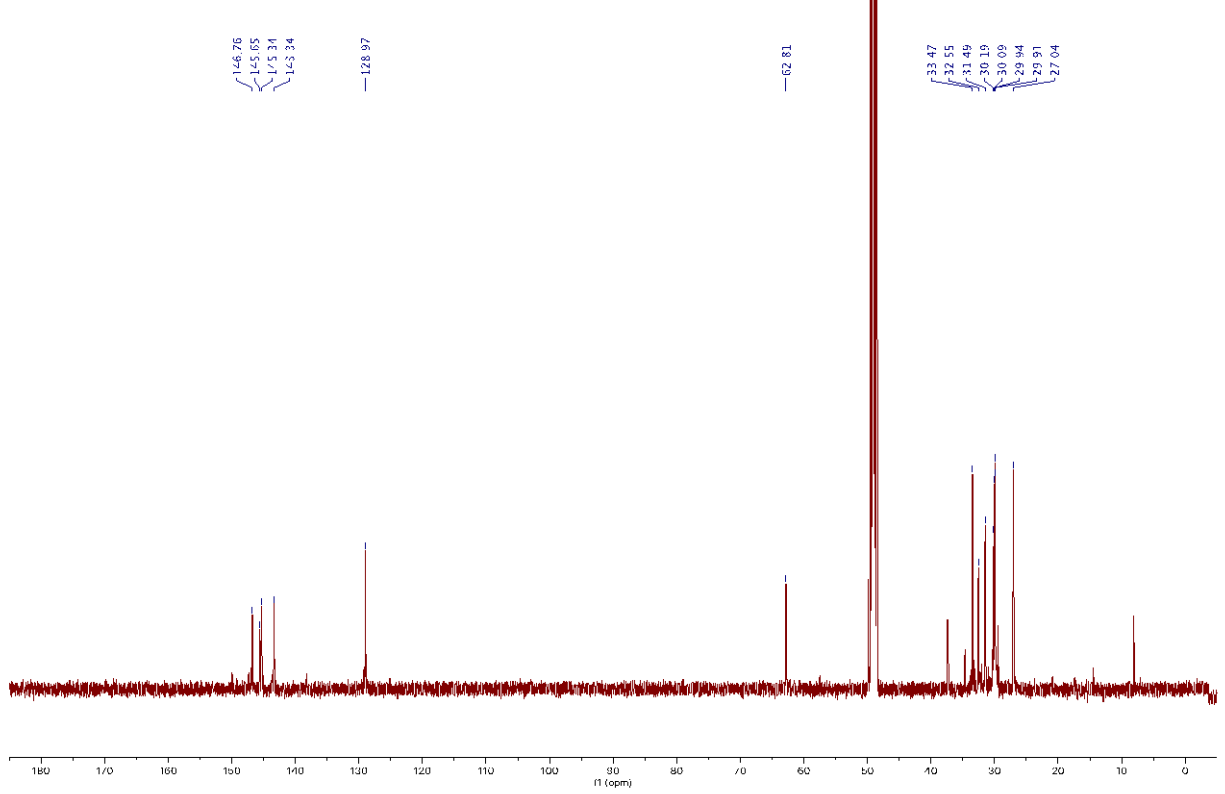


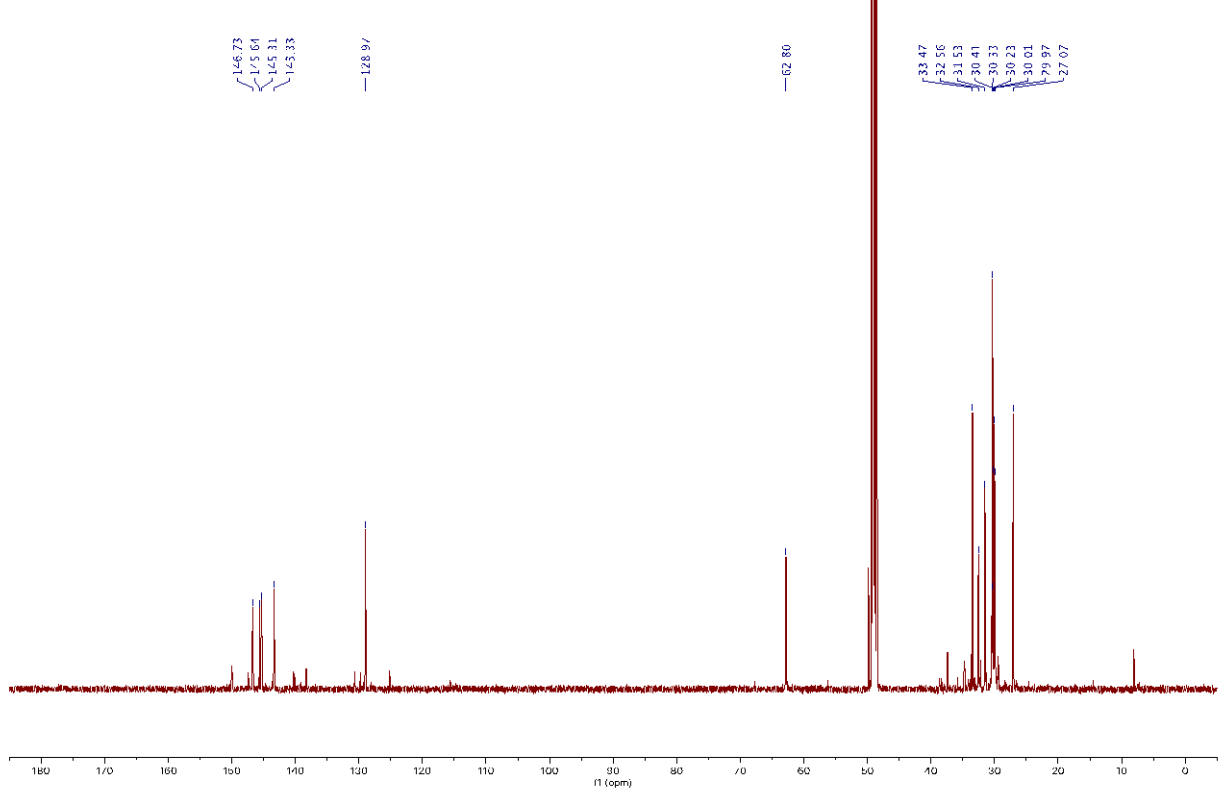
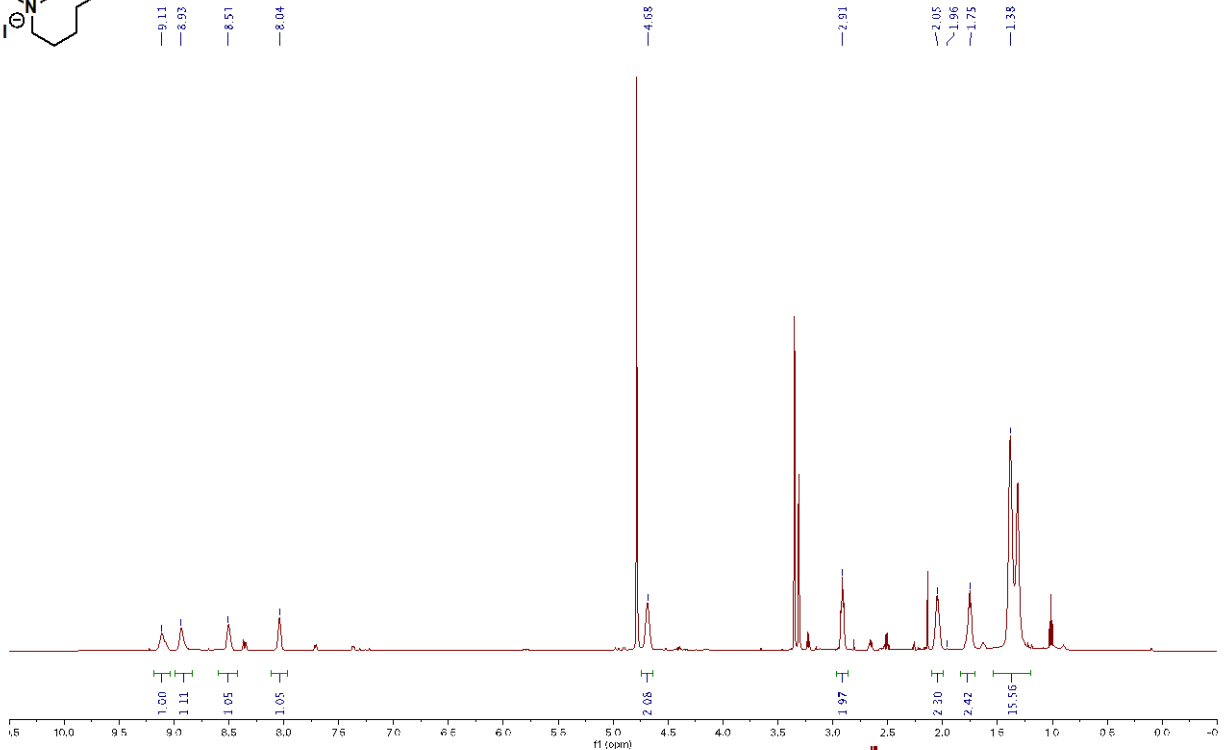
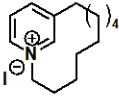
- 146.76
- 145.05
- 145.34
- 143.34

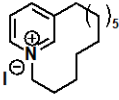
— 128.97

— 62.81

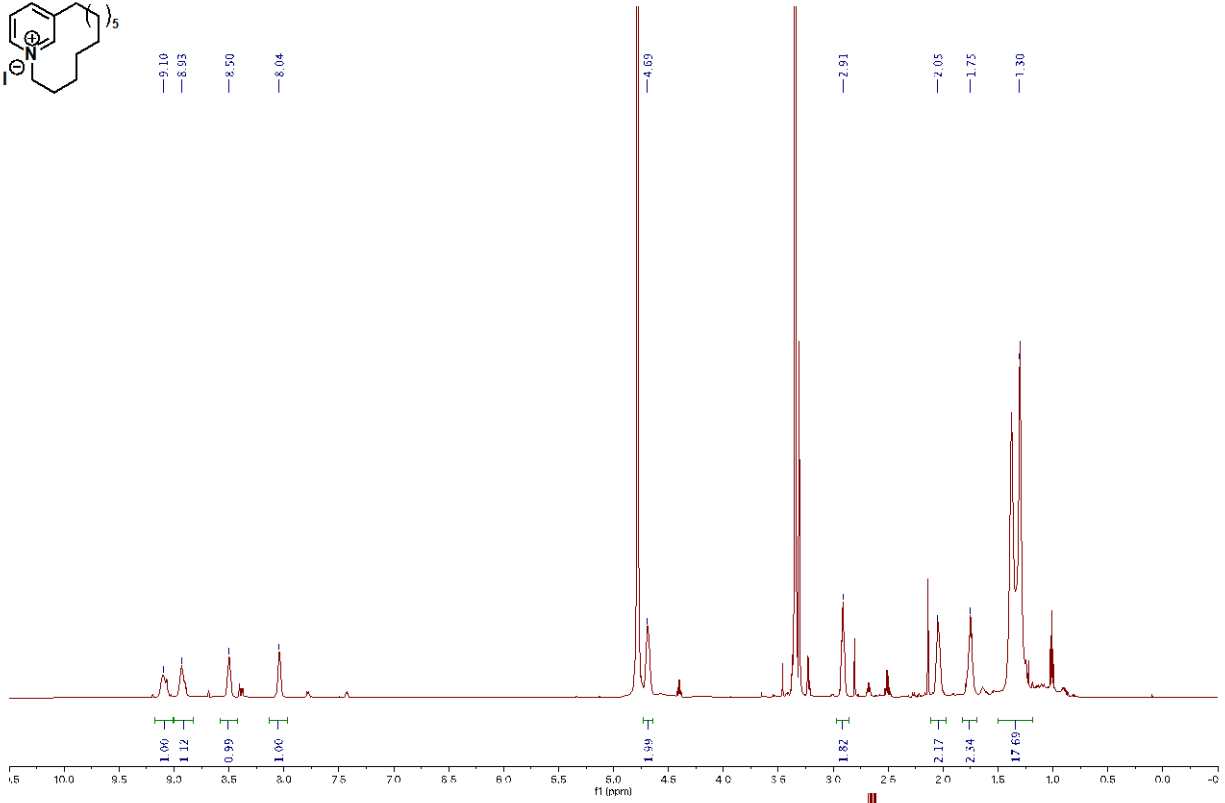
- 33.47
- 32.55
- 31.49
- 30.19
- 30.09
- 29.94
- 29.91
- 27.04







-9.10
 -8.95
 -8.50
 -8.04

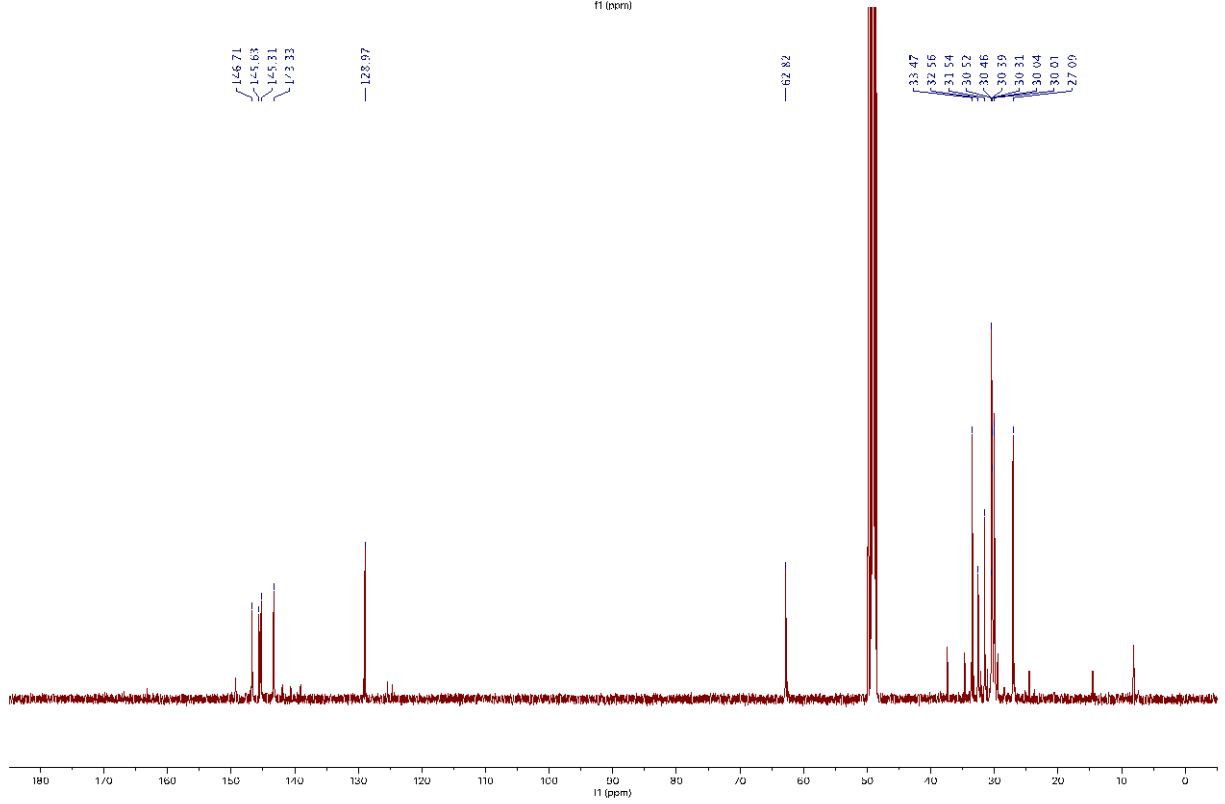


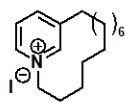
146.71
 145.63
 145.31
 133.33

128.97

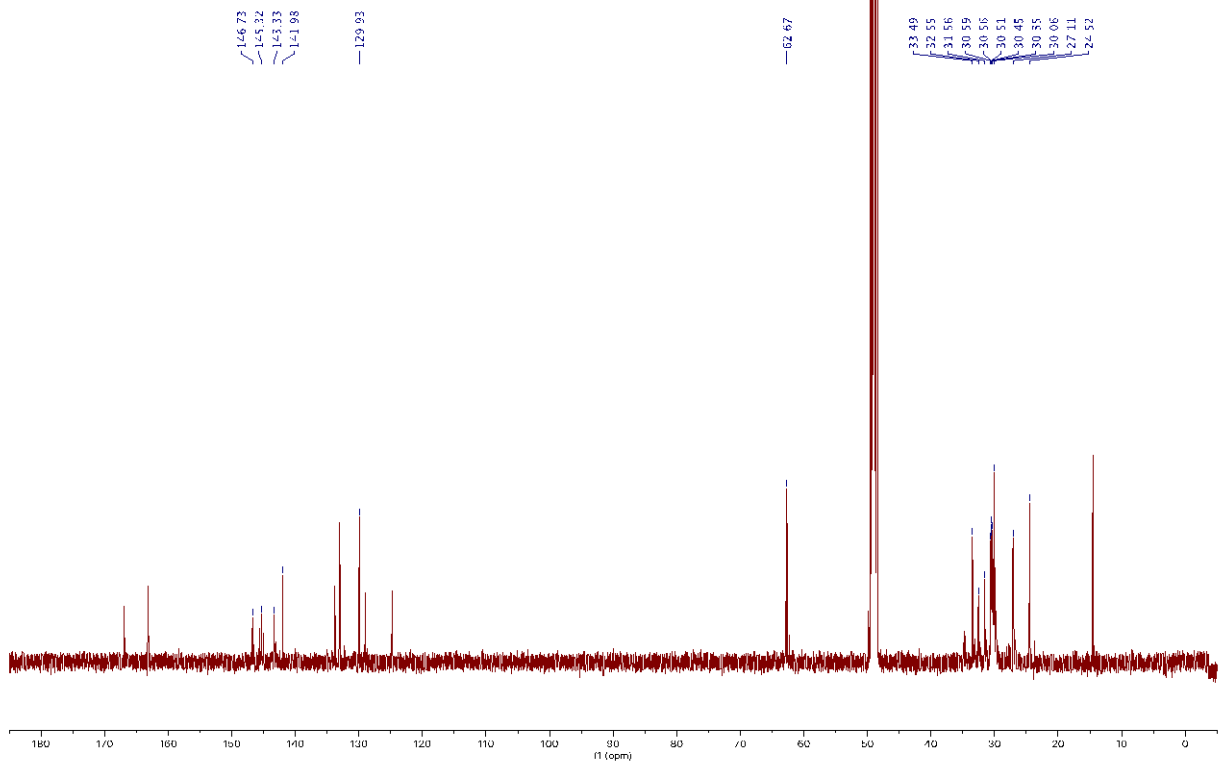
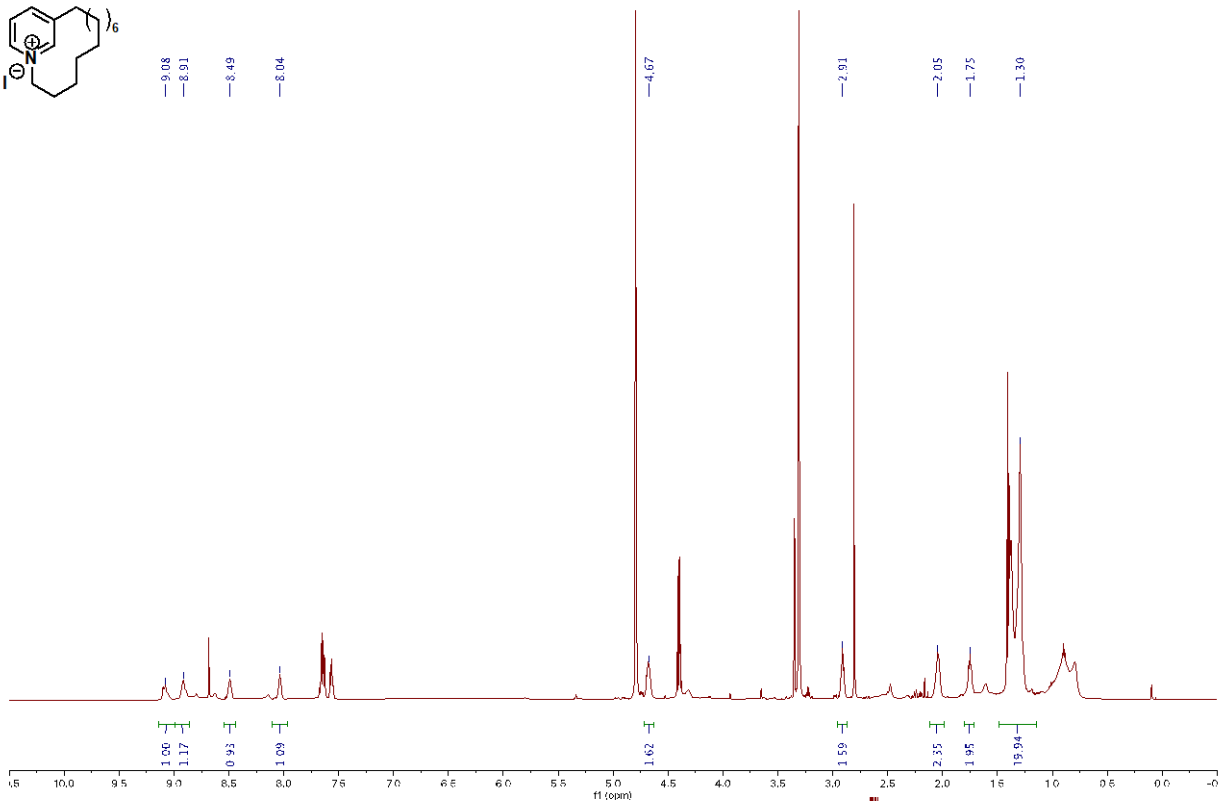
62.82

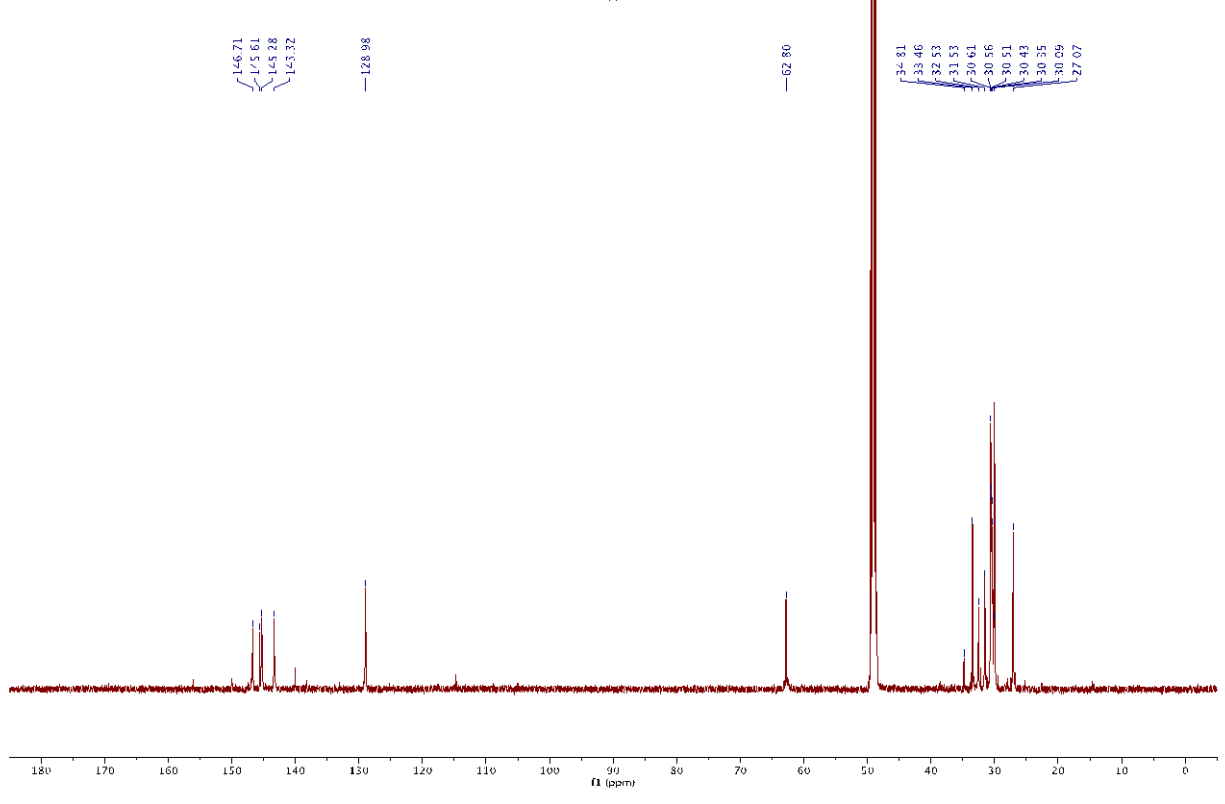
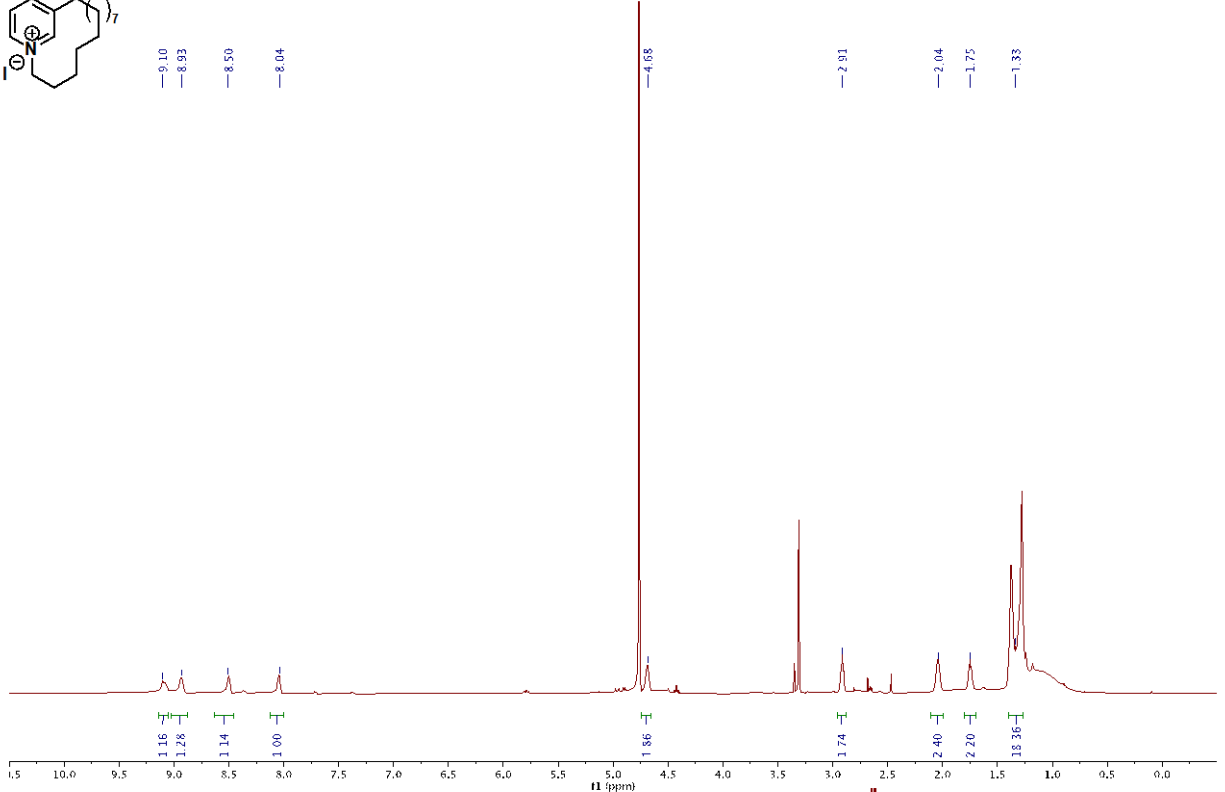
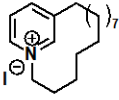
33.47
 32.56
 31.54
 30.52
 30.46
 30.39
 30.31
 30.04
 30.01
 27.09

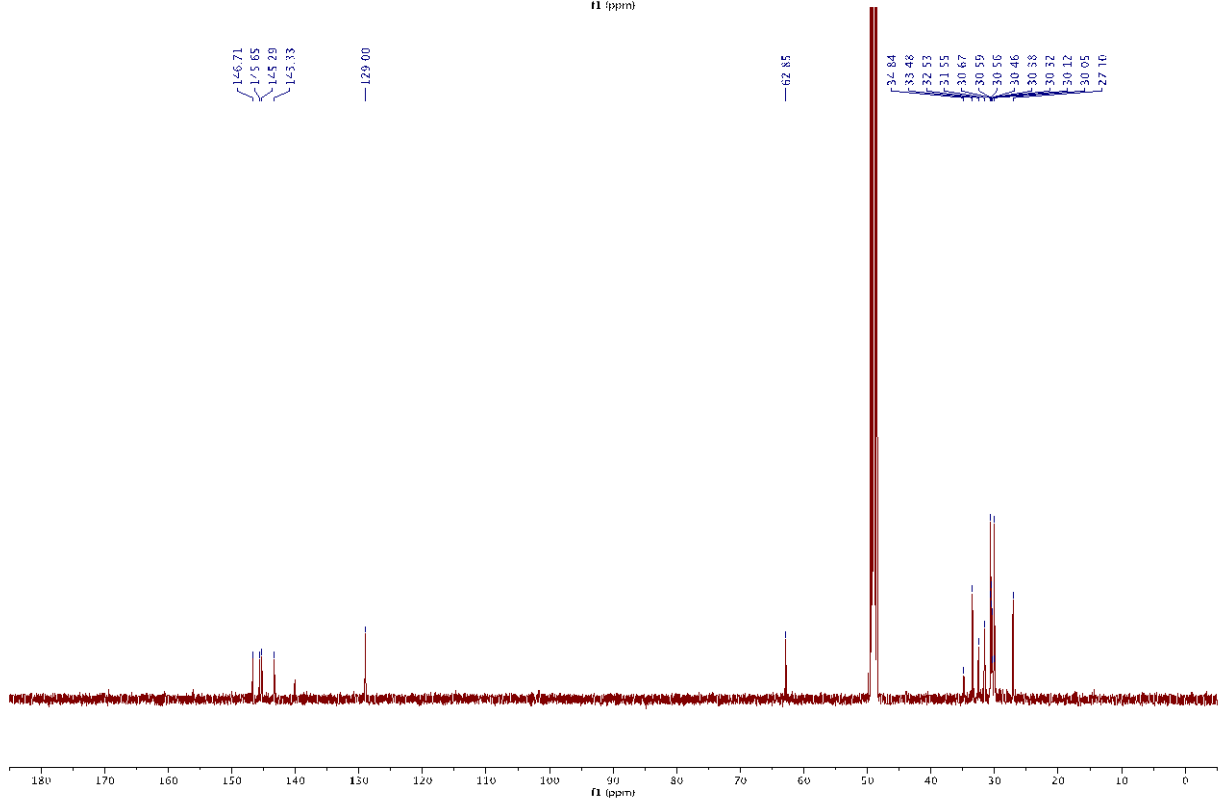
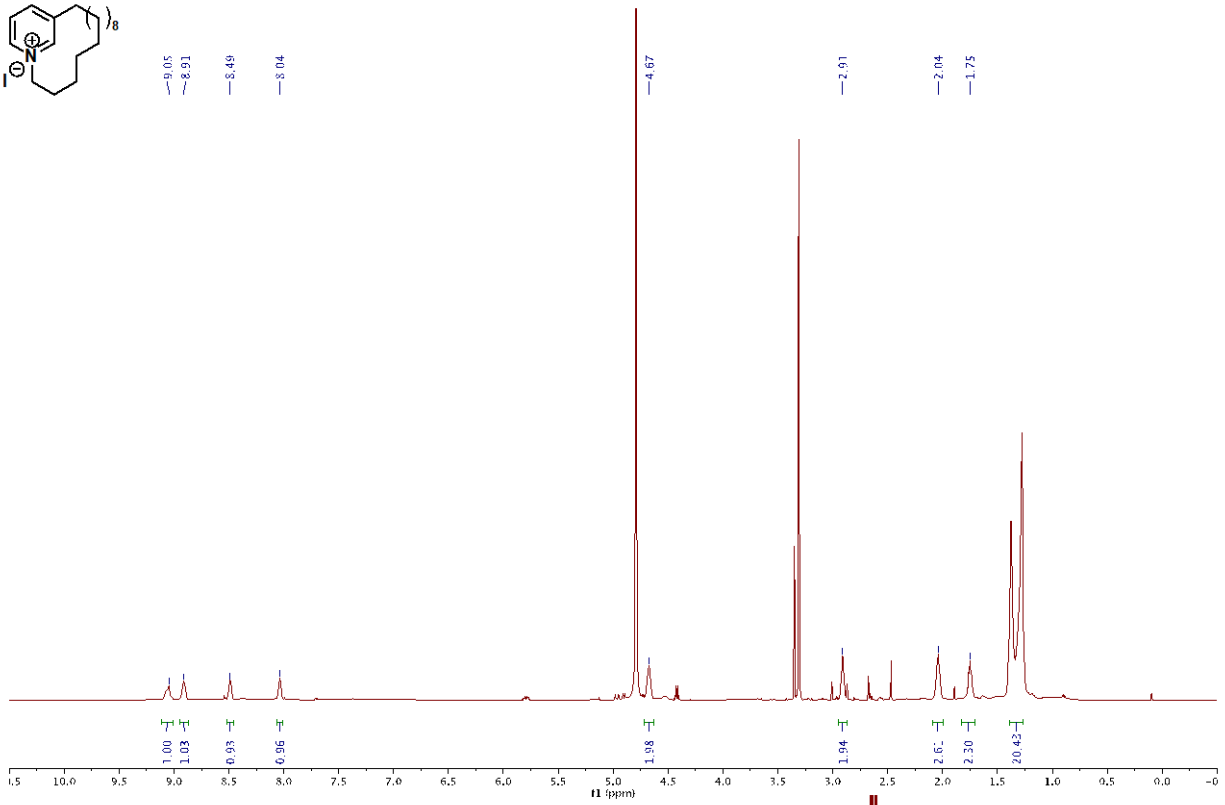
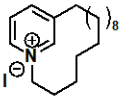


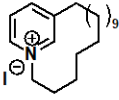


— 9.08
— 8.91
— 8.49
— 8.04

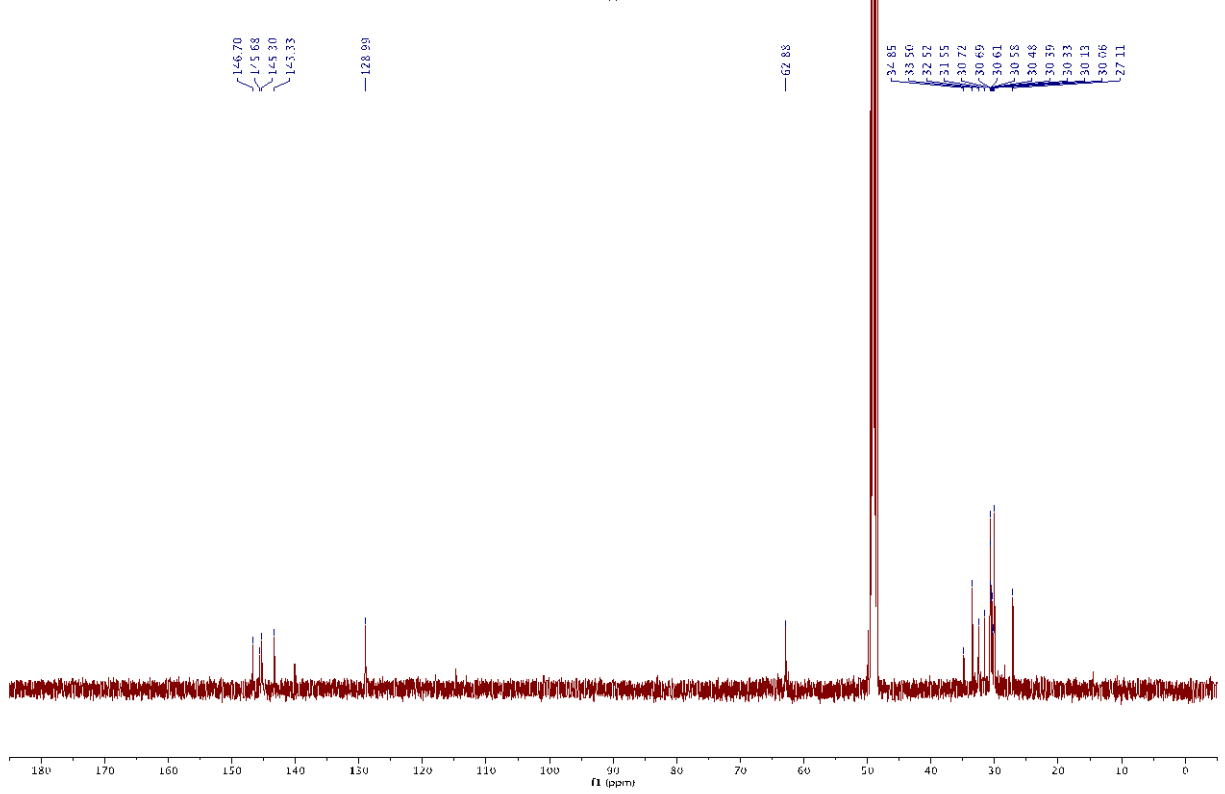
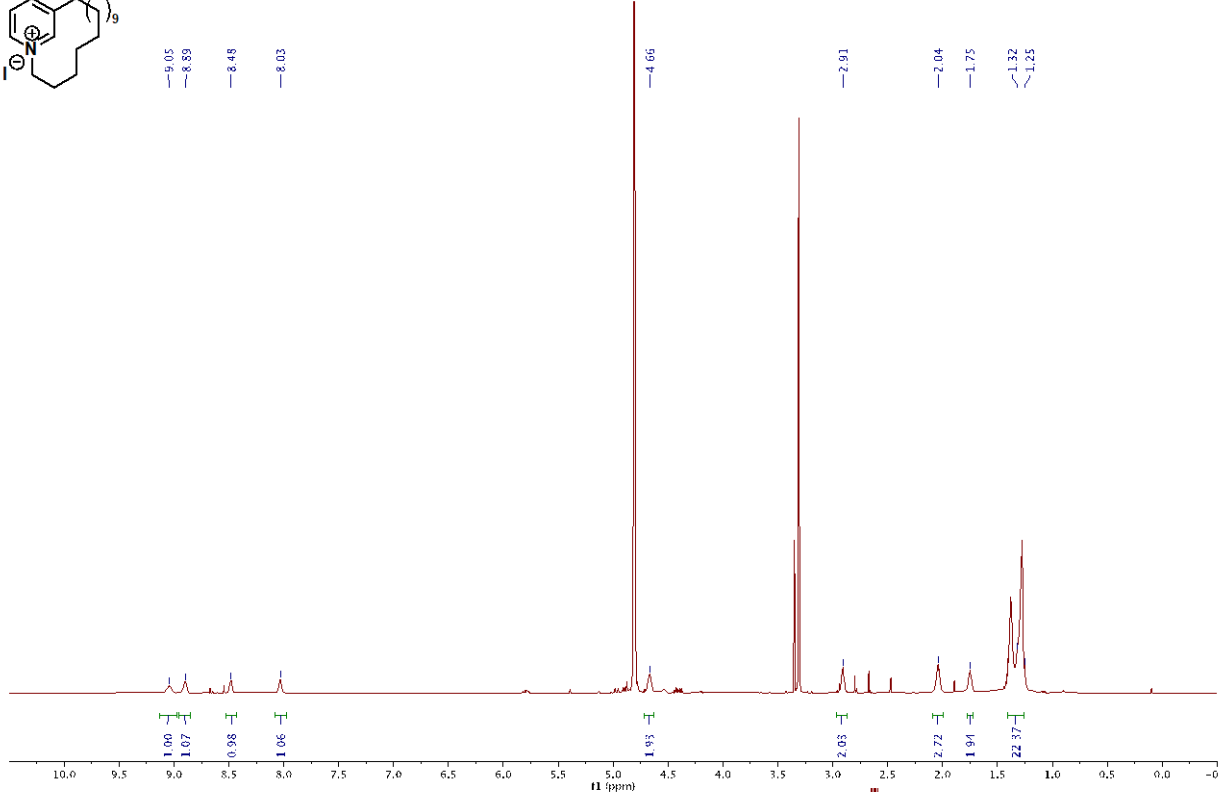


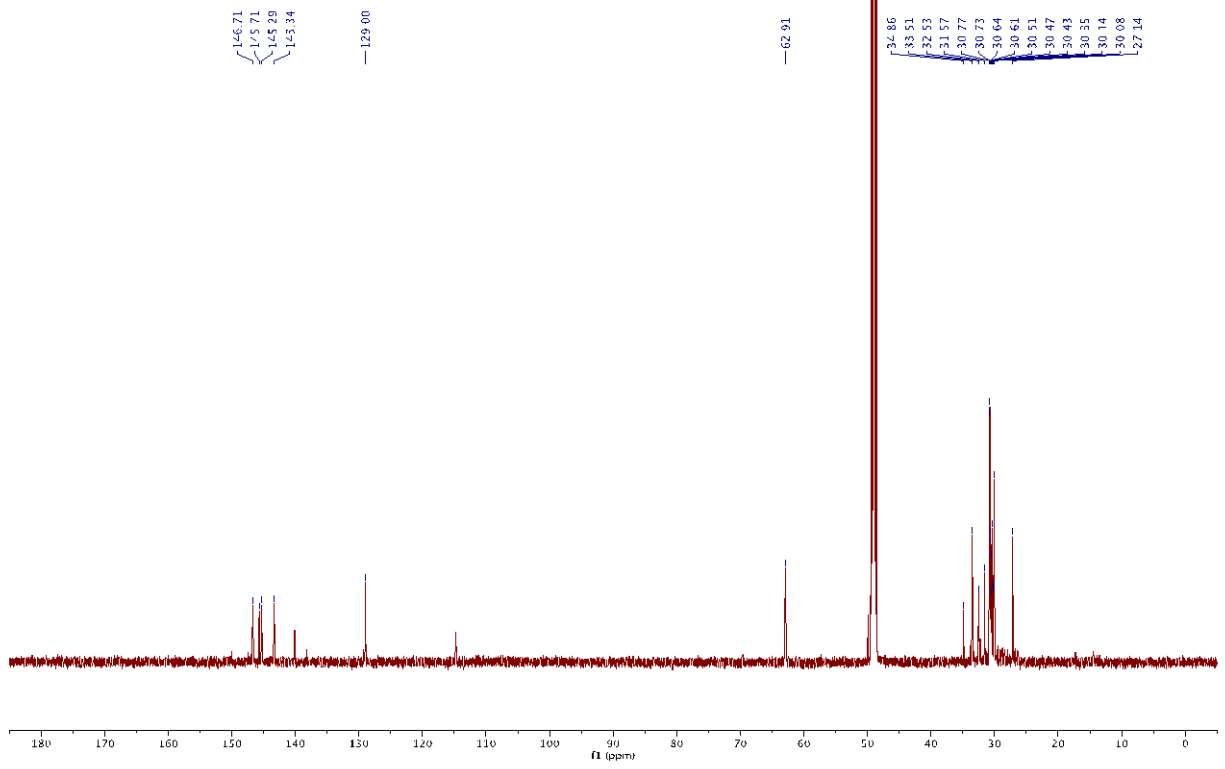
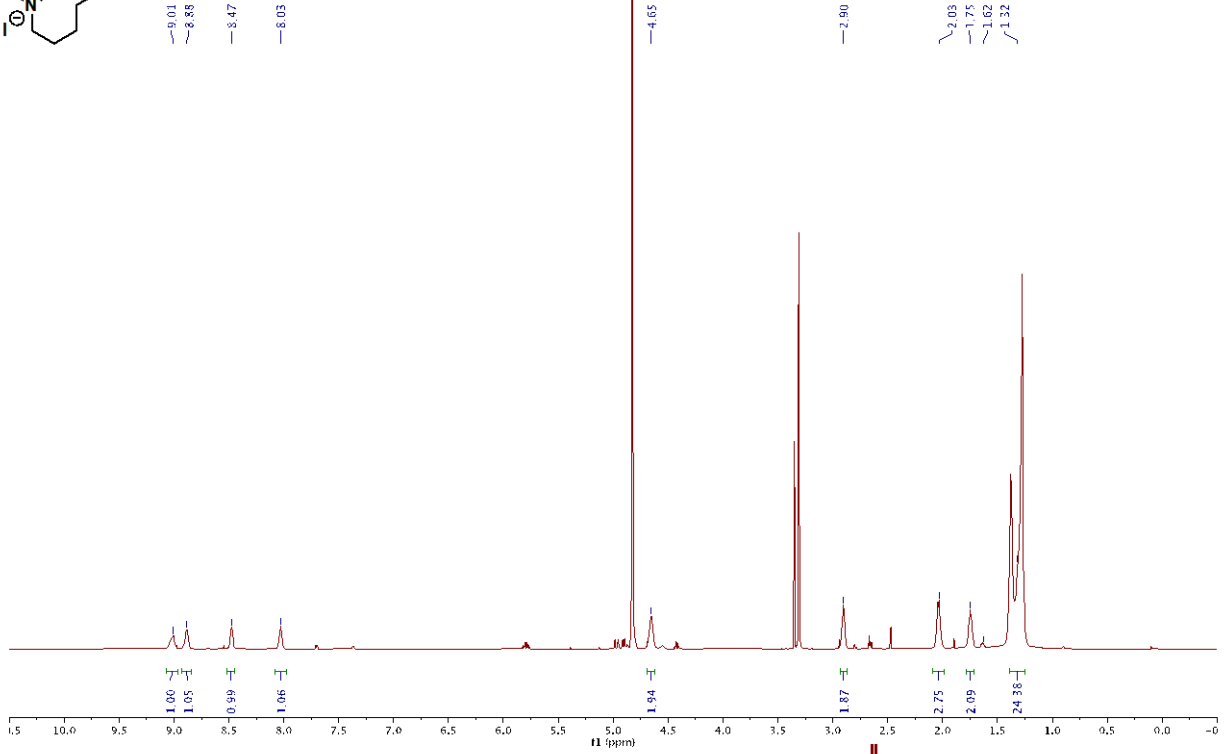
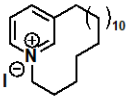






- 9.05
- 8.89
- 8.48
- 8.03





Appendix: Chapter 4

